Effect of Different Atmospheric Conditions on Optical Beam Propagation with LASER Sources of Different Wavelengths

Thesis Submitted by

Shibabrata Mukherjee

Doctor of Philosophy (Engineering)

Department of Electrical Engineering

Faculty Council of Engineering & Technology

Jadavpur University

Kolkata, India

2024

JADAVPUR UNIVERSITY
KOLKATA-700032, INDIA

INDEX NO. 215/19/E

1. Title of the thesis:

Effect of Different Atmospheric Conditions on Optical Beam Propagation with LASER Sources of Different Wavelengths

2. Name, Designation, and Institution of the Supervisor

Dr. Saswati Mazumdar

Professor,
Electrical Engineering Department
Jadavpur University
Kolkata-70032

3. List of Journal Publications:

- **Shibabrata Mukherjee,** Sujoy Paul, Saswati Mazumdar, "A cost effective FSO communication link using 808 nm laser and its performance analysis in simulated temperature conditions", ***Optical & Quantum Electronics***, Springer Nature, vol. 55, pp. 1-15, 2023.

- **Shibabrata Mukherjee,** Sujoy Paul, Saswati Mazumdar, "Experimental studies of the influence of scintillation on a FSO communication system for visible and infrared wavelengths", ***Journal of Russian Laser Research,*** Springer Nature, vol. 44, pp. 357-364, 2023.

- **Shibabrata Mukherjee,** Sujoy Paul, Saswati Mazumdar, "Effect of MIMO scheme on MWIR FSO link & comparison with SWIR wavelength in the presence of different visibility and strong turbulence circumstances", ***Journal of Optical Communication,*** De Gruyter, pp. 1-7, 2023**.**

- **Shibabrata Mukherjee,** Sujoy Paul, Saswati Mazumdar, "Experimental studies and analysis of 1550 nm laser as optical wireless communication link in simulated rainy, foggy and heating conditions according to Indian atmosphere", ***Light & Engineering,*** vol. 31, pp. 19-33, 2023.

- **Shibabrata Mukherjee,** Sujoy Paul, Saswati Mazumdar, "BER performance analysis of MWIR and SWIR FSO links utilizing aperture averaging technique considering turbulence and various visibility situations with pointing errors", ***Journal of Optical Communication,*** De Gruyter, pp. 1-12, 2023**.**

- **Shibabrata Mukherjee,** Sujoy Paul, Saswati Mazumdar, "Experimental Characterization of Optical Power attenuation of 980 nm FSO Link in Artificial Rain Induced Environment & Mitigation Strategy Using Aperture Averaging Technique", ***Indian Journal of Physics***, Springer Nature, 2023. (Accepted for Publication)

- **Shibabrata Mukherjee,** Sujoy Paul, Saswati Mazumdar, "Design of an Optical Wireless Communication link using Mid Wave Infrared Laser source & comparison with Short Wave Infrared Laser sources in different atmospheric anomalies: An analytical study", ***Nonlinear Optics, Quantum Optics: Concepts in Modern Optics***, 2023. (Accepted for Publication)

4. List of Presentations in International/National Conferences:

- **Shibabrata Mukherjee,** Sujoy Paul, Saswati Mazumdar "Experimental Studies of FSO Communication Channel Using Visible Wavelengths Coherent Optical Sources in Artificial Rainy Condition", ***IEEE Calcutta Conference (CALCON)***, pp. 98-103, 2022.

- **Shibabrata Mukherjee,** Basudeb Das, Saswati Mazumdar, "Experimental studies of Laser power attenuation of 532 nm laser at different visibility using simulated foggy conditions", ***AIP Conference Proceedings***, vol. 2640, Issue. 1, 2022.

"Statement of Originality"

I **Shibabrata Mukherjee** registered on **11th July, 2019** do hereby declare that this thesis entitled "**Effect of Different Atmospheric Conditions on Optical Beam Propagation with LASER Sources of Different Wavelengths**" contains literature survey and original research work done by the undersigned candidate as part of Doctoral studies.

All information in this thesis have been obtained and presented in accordance with existing academic rules and ethical conduct. I declare that, as required by these rules and conduct, I have fully cited and referred all materials and results that are not original to this work.

I also declare that I have checked this thesis as per the "Policy on Anti Plagiarism, Jadavpur University, 2019", and the level of similarity as checked by iThenticate software is 6 %.

Shibabrata Mukherjee 02/01/2024

Signature of Candidate

Certified by Supervisor: Saswati Mazumdar 2/1/2024

Professor
Electrical Engineering Department
Jadavpur University

Certificate from the supervisor

This is to certify that the thesis entitled "***Effect of Different Atmospheric Conditions on Optical Beam Propagation with LASER Sources of Different Wavelengths***" submitted by **Shri Shibabrata Mukherjee**, who got his name registered on 11/07/2019 for the award of Ph.D (Engg.) degree of Jadavpur University is absolutely based upon his own work under the supervision of the under signed and that neither his thesis nor any part of the thesis has been submitted for any degree/diploma or any other academic award anywhere before.

Saswati Mazumdar 2/1/2024

Signature of the Supervisor and Date
with Official Seal

Professor
Electrical Engineering Department
Jadavpur University

Acknowledgments

The author like to express his sincere gratitude and deep appreciation to his supervisor *Prof. Saswati Mazumdar* of Electrical Engineering Department, Jadavpur University for her invaluable guidance carrying out the thesis work. The author has been provided with necessary freedom during the course of the research work and at the same time the intense supervision by the supervisor has helped to enhance the quality of the research. Her moral support, amiable and amicable personality, encouragement, and profound knowledge about the subject have made the research work possible. Besides, the author is also grateful to the supervisor for providing necessary mental support during difficult times helping him to become a better individual which led to his overall professional development.

The author would like to express his sincere gratitude and deep appreciation to *Mr. Basudev Chattopadhyay*, Former-Scientist 'G', DRDO, for providing necessary advice, and support to the research work.

The author would like to acknowledge his respected teachers Prof. Biswanath Roy, Dr. Suddhasatwa Chakraborty and Mrs. Sangeeta Sahana of Illumination Engineering Section, Jadavpur University, for providing necessary advice, and support to the research work.

The author is grateful to the Head of the Department of Electrical Engineering, Jadavpur University for providing necessary departmental facilities need to carryout research work.

The author would like to acknowledge Mr. Parthasarathi Satvaya, Assistant Professor of School of Illumination Science Engineering & Design (SISED), Jadavpur University for providing some necessary instruments to carry out this research work.

The author would like to acknowledge my sincere thanks & respect to Mr. Asit Kumar Sur, Visiting Demonstrator of Illumination Engineering Section for his enormous support.

I would like to acknowledge project Free Space Laser Communication for Data & Voice (FSLCDV) sponsored by Defence Research and Development Organisation (DRDO), India, in Electrical Engineering Department, Jadavpur University for using the project stuff.

The author would like to thanks his senior, colleagues & junior Dr. Rajib Malik, Dr. Basudeb Das, Mr. Bappaditya Singa, Ms. Tishya Sarma Sarkar, Mr. Sujoy Paul for providing support in various ways and making the laboratory an interesting place in carrying out the research work.

I would like to thank all staff members Mr. Santosh Kumar Sahoo, Mr. Samir Mandi, of Illumination Engineering Laboratory of Jadavpur University for their cooperation and assistance towards completion of this work.

The author would also like to extend thanks to all existing and past graduate students of the Illumination Engineering Laboratory of Electrical Engineering Department & School of Laser Science & Engineering, Jadavpur University for making it possible to work in a homely atmosphere.

The The author would like to convey his deep love and respect towards his parents Mrs. Lila Mukherjee and Mr. Somnath Mukherjee for their never-ending support and encouragement during difficult times. Without their support, this work could never have been completed.

Finally, as it is impossible to mention everybody by name, the author would like to convey his gratitude to all who have contributed in one way or another, in making this work possible.

Shibabrata Mukherjee
02/01/2024.

Abstract

Due to its many uses in areas like as communication, medical, LIDAR, laser scanners, the military, entertainment & enjoyment, and others, LASER is immensely popular in the current world. Free space optical communication can be formed and data sent successfully using LASER sources. Free space optical (FSO) communications are a low-cost, high-bandwidth access method that are gaining popularity due to its recent commercialization. This system's dependence on the atmosphere is its fundamental flaw. The system's performance has suffered in scenarios with bad weather.

In this thesis, cost effective FSO Communication channel has been established using different wavelength Laser sources like visible (532 nm, 638 nm), IR (808 nm, 980 nm, & 1550 nm). In this study, the primary atmospheric problems including fog, rain, and scintillation are taken into account. To evaluate the system performance in the aforesaid atmospheric conditions, some artificial atmospheric chamber has been developed in the laboratory. The unique aspect of this study is that the data from the artificial atmospheric chamber were created while taking Indian atmospheric conditions into consideration. Data from Indian weather reports were utilized in this.

The performance investigation of various wavelengths of laser sources under simulated weather circumstances has been done using a number of parameters, including optical power, real-time eye patterns, Signal to Noise ratio, Bit Error Rate, etc. According to the experimental findings, the optical beam attenuation has been observed to be more attenuated in foggy weather than in other atmospheric anomalies. Another significant finding from these tests is that, in the case of scintillation and fog, the performance of the FSO communication system is wavelength dependent, however in the case of rain, the optical power attenuation for various wavelengths is practically same.

For system performance enhancement, the techniques of wavelength diversity and aperture averaging have been proposed and integrated. Aperture averaging has improved system performance in terms of SNR, BER, real-time eye patterns, and optical power attenuation in different atmospheric conditions with irrespective of wavelengths, as shown by the wavelength diversity scheme, which shows that 1550 nm Laser performs better than other considered wavelengths. Finally, a theoretical link performance study for MWIR Laser sources at 4000 nm has been presented and compared with 1550 nm Laser sources at larger link distances (4 km). These analytical findings show that 4000 nm is more successful than other wavelengths under challenging air conditions. This work might lead to new developments in the field of FSO communication.

Dedicated to my parents

Contents

Table of Content

Contents

Table of Content

List of Figures

Chapter 1

Chapter 2

Chapter 3

Chapter 4

Chapter 5

List of Tables

Chapter 2

Chapter 3

Chapter 4

Chapter 5

List of Abbreviations

AO	Adaptive Optics
APD	Avalanche Photo Diode
ARQ	Automatic Repeat Request
BER	Bit Error Rate
BNC	Bayonet Neill Concelman
BW	Bandwidth
DC	Direct Current
DFB	Distributed Feedback Laser
DPSS	Diode Pump Solid State Laser
EDRS	European Data Relay System
EGC	Equivalent Gain Converter
ESA	European Space Agency
FCAOM	Fiber Coupled Acosto Optic Modulator
FEC	Forward Error Control
FOV	Field of View
FSO	Free Space Optics
He-Ne	Helium Neon
IEC	International Electrotechnical Commission's
IoT	Internet of Things
IR	Infrared
LASER	Light Amplification by the Stimulated Emission of Radiation
LCRD	Laser Communication Relay Demonstration
LED	Light Emitting Diode
LOS	Line of Sight
LWIR	Long Wave Infrared

MIMO	Multiple Input Multiple Output
MLCD	Mars Laser Communications Demonstration
MOSFET	Metal-Oxide-Semiconductor Field-Effect Transistor
MRC	Maximum Ratio Combining
MWIR	Mid wave Infrared
MSO	Mixed Signal Oscilloscope
M2M	Machine to Machine
NASA	National Aeronautics and Space Administration
NIR	Near Infrared
NEP	Noise Equivalent Power
NRZ-OOK	Non-Return to Zero On-Off Keying
OWC	Optical Wireless Communication
PARR	Peak-to-Average Power Ratio
PAM	Pulse Amplitude Modulation
PD	Photo Detector
PIN	Positive-Intrinsic-Negative diode
PPM	Pulse Position Modulation
QAM	Quadrature Amplitude Modulation
RF	Radio Frequency
RS	Reed-Solomon
SILEX	Semiconductor Inter-Satellite Laser Experiment
SIM	Sub-carrier Intensity Modulation
SIMO	Single Input Multiple Output
SMA	Sub-Miniature version A
SNR	Signal to Noise Ratio
SWIR	Short Wave Infrared
TCM	Trellis-Coded Modulation

TTL	Transistor-to-Transistor Logic
UV	Ultra-Violet
VCSEL	Vertical Cavity Surface Emitted Laser
VLC	Visible Light Communication
VL	Visible
5G	Fifth Generation

List of Symbols

θ_I Input Beam Divergence

θ_O Output Beam Divergence

D_I Input Beam Diameter

D_O Output Beam Diameter

MP Magnification factor

D_L Laser beam diameter

L Link Distance

λ Wavelength of Laser source

α Scattering Coefficient (value depends on refractive index)

d Diameter of Particle

R Distance to the particle

θ Scattering angle

k Wave number

I_0 Initial intensity of the light.

$\alpha_m(\lambda)$ Molecular absorption coefficient

$\alpha_a(\lambda)$ Aerosol absorption coefficient

$\beta_m(\lambda)$ Molecular scattering coefficient

$\beta_a(\lambda)$ Aerosol scattering coefficient

R Rain rates in mm/hr

k Power law parameter of rain

α_1 Power law parameter of rain

V Visibility range in km

n Particle size distribution coefficient

P(T) Transmitted Optical power of Laser

P(R) Received Optical power of Lase

σ Attenuation of Fog

C_n^2 Refractive index structure parameter

A Aperture Averaging Factor

$\sigma_I^2(D_R)$ Variance of the signal fluctuations from a receiver with a D_R diameter aperture

$\sigma_I^2(0)$ Receiver with an infinitely tiny aperture

$K_{\alpha-\beta}$ (.) Second order Bessel function

Ω Large scale turbulent eddies for a spherical wave

β Small scale turbulent eddies for a spherical wave

γ Value of SNR

h_a Extinction Coefficient of different atmosphere

G Meiger-G Function

erfc(.) Complementary error function

β_0^2 Spherical wave Rytov variance

d_1 Circular aperture radius

D Receiver's aperture diameter

CHAPTER 1
INTRODUCTION

1.1. INTRODUCTION

The term **"LASER"** stands for "Light Amplification by the Stimulated Emission of Radiation", is a device that excites atoms or molecules to produce light at specific wavelengths and amplifies that light, often resulting in an extremely focused beam of radiation. Based on theoretical research by Charles H. Townes and Arthur Leonard Schawlow, Theodore Maiman created the first laser in 1960 at Hughes Research Laboratories. Lasers are unique among other light sources because of their coherence. Lasers produce focused light beams that are coherent, monochromatic, controllable, and well-aimed. Laser beams have two different focusing options: they can have a very low divergence to concentrate their power at a long distance or they can be focused to very small spots to get a very high irradiance. Lasers would therefore appear to be poor options for broad illumination based on appearances alone, yet they are excellent at focusing light in space, time, or specific wavelengths. From "light shows" to special effects in movies, lasers are used in nearly every element of these professions. Other frequent uses for lasers include barcode scanners, laser printers, and laser pointers. Even so, a lot of the significant and well-known modern-day applications are found in areas like fiber-optic communication, free space optic laser communication, laser machining and manufacturing, trace element detection, laser metrology, medical imaging, defense application, war, etc.

In the last ten years, the amount of traffic carried by telecommunications networks, especially wireless networks, has grown significantly. The need for more innovation, research, and development in the new, developing communication technologies capable of providing extremely high data rates has been driven by the steadily rising demand for broadband internet services. One of the biggest success stories in the history of technology development is the creation of wireless technologies, which made it possible for people to communicate at any time and from any place. When it comes to services, wireless data and mobile internet have replaced voice communications as the main option, replacing them with considerably richer multimedia material which anybody could have anticipated ten years ago. Already, the wireless

gadgets, applications, and services are drastically altered. There is a huge increase in demand for mobile data transmission due to the development of new bandwidth-hungry apps. By 2020, mobile data traffic is anticipated to increase by three orders of magnitude over what it did in 2010, and the available spectrum for mobile services will be almost doubled [1]. In the context of fifth-generation (5G) wireless communication, this is also known as the mobile spectrum crunch, and it is already being addressed [2-4]. The concept of the Internet of Things (IoT), which has been most closely associated with machine-to-machine (M2M) communication, expands wireless connectivity among naturally occurring and man-made object sensors, etc., in the context of understanding omnipresent machine-to-machine and machine-to-human communications. By doing so, wireless communications would become an integral part of daily life and further alter how we interact with the physical environment.

Due to radio frequency (RF) technology dominance in today's technology landscape, the term "wireless" is frequently used as a synonym for RF technologies. The radio frequency band is a portion of the electromagnetic spectrum that ranges from 30 kHz to 300 GHz, and both national and international agencies have tight regulations on its usage. Sub-bands are frequently leased solely to operators, such as mobile phone companies, television networks, and point-to-point microwave lines, among others. Due to an imbalance between the supply and demand for radio frequency wireless spectrum, a bottleneck or congestion has developed.

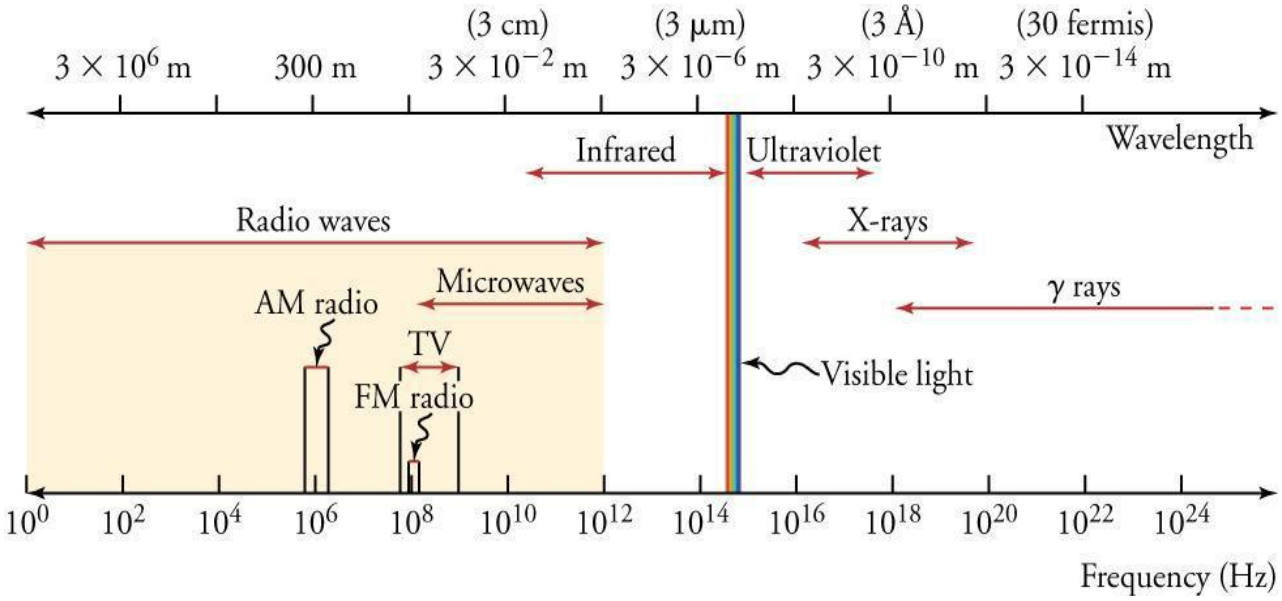

Fig. 1.1: The Electromagnetic Spectrum

The Free Space Optical Communication system (FSO) is part of optical wireless communication (OWC), which delivers virtually an enormous bandwidth (400THz) and encompasses visible (VL), infrared (IR), and ultraviolet (UV) sub-bands. So it is one of the potential complementary alternative technologies that can address and overcome these limitations. Unique prospects that have so far mostly gone untapped are presented by using these bands for communications. Fig. 1.1. shows the electromagnetic spectrum.

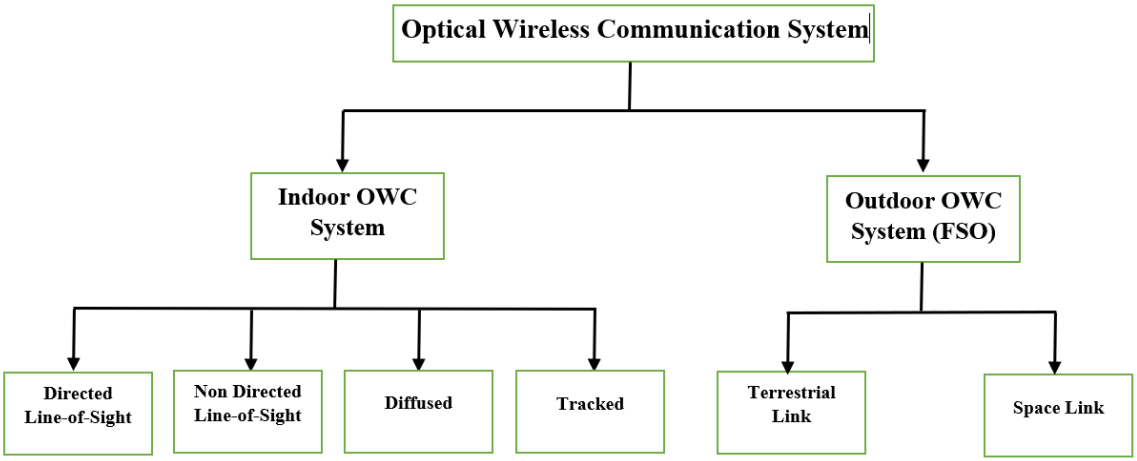

Fig. 1.2. Classification of Optical Wireless Communication (OWC) system

OWC system can be divided into two main categories: indoor and outdoor OWC systems. Four subcategories of the Indoor OWCS exist: tracked systems, diffused systems, non-direct line-of-sight systems, and directed line-of-sight systems. The term "outdoor OWCS" refers to free space optics (FSO), which may be divided into terrestrial and space connections.

Free Space Optical Communication (FSOC) [5,6] boasts superior characteristics to its radio frequency (RF) counterparts, including ultra-high bandwidth, robustness to electromagnetic interference, a high degree of spatial confinement bringing virtually unlimited frequency (or wavelength) reuse, and inherent physical security. Additionally, as FSO technologies may operate in the unlicensed spectrum, no licencing charge is necessary, making them a cost-effective choice for a variety of applications. Since there are no radios or antennae in FSO systems, modulation and demodulation are direct, making the addition of extra nodes simple because they do not cause interference like RF-based systems.

Even if its variation based on the operating wavelength or frequency may have many uses, as mentioned in the following, the term OWC refers to any optical transmission in an unguided medium. Visible light communication is the term used to describe optical wireless communication (OWC) devices that operate in the visible band (390nm–780nm) (VLC). Both laser diodes and LEDs are used in VLC systems because they can be turned on and off at extremely high speeds without having any discernible influence on the illumination output or the human eye. An ecologically sound and energy-efficient strategy that has the possibilities to alter how we use lighting in the coming future is the many uses of visible LEDs for illumination, data transfer, and indoor location. Wireless personal area networks, wireless regional area networks, and wireless connection points, and vehicle networks are just a few of the many applications that VLC for data transfer may be employed in.

On the other side, near IR frequencies are used by terrestrial point-to-point OWC systems, sometimes referred to as free space optical (FSO) systems [7]. These technologies, which commonly employ laser transmitters, enable high data speeds (10Gbps per wavelength) via cost-effective protocol-transparent links and may be able to alleviate the backhaul bottleneck [8]. There have been reports of LED-based FSO systems where the data transfer rate via VLC is constrained and greatly relies on the environment. The property that is used for rough pointing, the visible light's irradiation angle, determines the transmission span. For satellite-based combinations, low bit rate free space data transfer utilizing VLC has been accomplished without accurate pointing between the transmitter and receiver [9]. Similar to RF technology, FSO linkages in outdoor applications encounter a number of difficulties that will limit their widespread use. These difficulties are caused by atmospheric factors (such as fog, turbulence, and misalignment between transmitter & receiver), which will constantly impair the link's availability. Nevertheless, these issues can be solved by utilizing hybrid FSO and RF radio communications. Despite having a number of field applications, this technology is mostly used outside. FSO may be utilised to offer high bandwidth connection in multi-point scenarios in indoor environments (i.e., large organizations). This is a fantastic way to bridge optical fibre connectivity across a number of places in wide areas without having to make significant infrastructure adaptations. In this regard, FSO may also present the finest options for upgrading and replacing fibre optic systems in contemporary structures. It might also have a big impact on another expanding area of study, radio-over-FSO, which has many characteristics with the well-known radio-over-fiber systems.

The FSO system encounters many atmospheric anomalies such as rain, fog, dust, scintillation, smoke, snow, etc. because it is typically located outside (from a terrestrial perspective) to establish the link in regions such as building to building, hills to hills, and in many other disaster-prone areas, etc. The system performance will be reduced drastically. Beam expansion loss and misalignment are two more challenges with this method. The alignment of the transmitter and receiver (line of sight) is extremely important because this system relies on line-of-sight technology. Because the laser beam is a transmitter and it travels through free space, it is influenced by many air molecules, gases, particles, etc. As a result, the beam expands at the receiver side and a beam expansion loss occurs. To overcome the aforesaid problems, choosing of the proper optics, selection of wavelengths of the transmitter, and determination of corresponding proper receiver is necessary.

1.2. LITERATURE SURVEY

The credibility of the experiment is derived by the utilization of the knowledge absorbed by reading the following scientific journals, books, and papers about free space optical (FSO) communication, attenuation, laser, link budget, and other parameters which are colossally important for the following experiment and findings.

Midway through the 1980s, the European Space Agency (ESA) started the SILEX (Semiconductor Inter-Satellite Laser Experiment) research programme and contemplated using OWC for satellite-to-satellite links. A 50 Mbps OWC link was successfully established in 2001 between the French SPOT-4 Earth observation satellite in sun-synchronous low earth orbit and the ARTEMIS geostationary satellite [10]. Coherent modulation methods allowed for the effective achievement of data speeds on the order of Gbps [11][12][13]. A satellite system called the European Data Relay System (EDRS) is currently being developed to transmit and receive data from and to non-geostationary satellites, spacecraft, other vehicles, and fixed Earth stations. Three GEO satellites are launched, and they are outfitted with OW Cinter-satellite connections and Ka-band connectivity for space-to-ground communication. The Jet Propulsion Laboratory (JPL) of NASA (National Aeronautics and Space Administration) and the ESA have both examined the use of optical communication between Earth and a spacecraft for deep-space purposes. Particularly, the Mars Laser Communications Demonstration (MLCD) seeks to show off optical communications at data speeds between 1 and 10 Mbps from Mars to the

Earth [14]. The Laser Communication Relay Demonstration (LCRD) project, a brand-new NASA initiative, is set to debut in 2018 and aims to show how OWC lines may be deployed for deep space intersatellite transmission and deep space to Earth transmission. In addition to satellite-to-satellite and satellite-to-ground links, notable work on a terrestrial free-space optical communication connection has been going on since 1960s. In November 1962, a Hughes team conducted the first demonstration of long-distance laser transmission through the environment, covering a distance of 30 km. Following that, a collection of electro-optics systems sent voice-modulated data across a 190km distance in May 1963 from Panamint Ridge in Death Valley, California to a site in the San Gabriel mountains close to Pasadena using a 632nm laser. A team at North America Aviation claimed to have received the first TV transmission in March 1963. There was a 1.7MHz modulation bandwidth [15].

In the following five to six decades, scientists from several nations engaged in this region, and significant research advancements have been made to this day. From these, some of the significant works have been demonstrated in this section.

Muhammad Ijaz, et al. [16] demonstrated the fog and smoke effect on FSO communication channels. For those experimental studies, a 5.5 m-controlled fog chamber was created and operating wavelengths were considered visible to the NIR range (0.6 μm to 1.55 μm), the maximum visibility range has been considered 1 km. To forecast the fog and smoke attenuation operating at visible and NIR wavelengths, a novel empirical model that depends on wavelength was presented. The 0.830 μm, 0.94 μm, and 1.55 μm Laser beams produced lesser attenuation from the investigated wavelength bands (0.6 μm-1.55 μm) at the lower visibility range of 0.048 km (that is, dense fog condition). The attenuation level of these wavelengths i.e., 0.830 μm, 0.94 μm, and 1.55 μm were 360 dB/km, 354 dB/km, and 324 dB/km respectively at the visibility range of 0.048 km.

The fog influence on FSO was studied by Robin Ghalot et al [17] in Delhi and Amritsar, two states in India where the wintertime fog intensity is quite high. The FSO system was set up utilizing 8 transmitters and 1 receiver by using the 'OptiSystem' software. The system performance had been assessed using the aforementioned state visibility data. In the month of January, the visibility range decreased by about 0.064 km and 0.293 km respectively for the state of Delhi and Amritsar respectively because of dense fog. As a result, the optical power attenuation was noticed in Delhi and Amritsar in that visibility range as 61 dB/km and 13.483 dB/km respectively. According to this study, the optical power and wavelength of the Laser

have been chosen at 4 dBm & 1550 nm respectively. Using the proposed FSO system with 8 transmitters and 1 receiver, Amritsar has higher link availability than Delhi. However, the proposed methodology was unable to lessen the impact of the heavy fog in New Delhi in January. Moreover, if the link range is reduced to 750 m, the suggested model lessens the impact of dense fog and can transmit well across that distance. According to the aforementioned literature, the operating link range has been significantly decreased in the dense fog condition scenario along with the reduction in atmospheric visibility necessary for safe operation.

Another study was carried out by Aanchal Sharma, et al. [18] in the hilly region of India (Nainital & Imphal) during the winter season. According to this study, the link range of FSO was considered 9000 m, and three NIR wavelengths were considered 850 nm, 1300 nm, and 1550 nm. According to statistics from the recent five years (from 2016 to 2021), the lowest visibility during the winter season was recorded at 0.68 km in the Nainital area, and 1.57 km at Imphal. Because of this, the optical power attenuation is higher in the Nainital region (4.59 dB/km, 3.69 dB/km, and 3.37 dB/km for the wavelengths of 850 nm, 1300 nm, and 1550 nm, respectively) than in the Imphal area (1.84 dB/km, 1.38 dB/km, and 1.22 dB/km, respectively). However, 1550 nm offers the best results, and in the winter, the FSO performance in the Imphal area is superior to that in the Nainital area.

Maged Abdullah Esmail, *et al.* [19] discussed that the The main issue with the free space optics communication (FSO) technology was fog, which might be the reason for attenuation of up to hundreds of decibels per kilometre. This study's major objective was to derive a single channel attenuation model using fog measurement data collected across Europe and the United States and compare it to already-existing attenuation models. A minimum of 9 dB was attained using the suggested model, which was better than the typical RMSE (root-mean-square error). They had looked into the channel's statistical behaviour and created a probabilistic model for stochastic fog. Scientists also spoke about the signal-to-noise ratio (SNR), bit-error-rate (BER), and recommended channel capacity as performance indicators for the free space optics communication system. In communication environments with frequent fog, FSO would have been the preferred market segment. This model and result could be used to determine the switching/thresholding conditions in highly reliable hybrid FSO/radio frequency (RF) networks in future wireless fifth-generation/sixth-generation (5G/6G) networks having cell sizes that were lower than a one kilo-meter diameter.

From the aforesaid discussion, it has been inferred that fog is one of the best enemies of the FSO system, and with the increment of the wavelengths in the NIR region, the system performance has been increased and the 1550 nm Laser source provides better results, but up to some extent of visibility range, it has given better result, and dense foggy weather condition, the operation has been failed using 1550 nm Laser. For this reason, nowadays, a new optical wavelength window called 'Mid Wavelength Infrared (MWIR)' has been used. It has better fog penetration power, higher transmittance in the terrestrial region compared to 1550 nm Laser [20][21][22][23]. Different scientists and countries are immerged in this field of research. Basically, the wavelength bands used in the MWIR range lie between 3400 nm-4800 nm for the FSO communication system.

Similarly, rain is another problem for the FSO communication system. The climate in the European region is prone to fog and heavy snow, which have an immediate impact on an FSO link [24]. FSO link's availability is expected to be significantly impacted by haze and heavy rain in Malaysia, which is located in a tropical environment and does not experience snow or fog. Similar to Malaysia, Mawsynram in India is another region prone to excessive rainfall, with an average annual rainfall of about 11873 mm. As a country with a moderate climate, India experiences rain on average at a rate of 100 millimeters per hour during the monsoon season, which lasts from June to September.

Harjeevan Singh, et al. [25] discussed the performance analysis of the FSO system under rainy weather conditions for inland & coastal locations of India. For their studies, six cities of India have opted namely Mumbai, Hyderabad, Chennai, Kolkata, Pune, and Chandigarh. The maximum rain rate for Mumbai, Hyderabad, Chennai, Kolkata, Pune, and Chandigarh cities are 177.6 mm/hr, 37.7 mm/hr, 119.8 mm/hr, 52.8 mm/hr, 61.2 mm/hr and 43.3 mm/hr respectively and corresponding their specific attenuation for these rain rates are 34.6 dB/km, 12.2 dB/km, 26.6 dB/km, 15.3 dB/km, 16.9 dB/km, 13.4 dB/km respectively. Therefore, the coastal location of India (Mumbai) provides higher rain rates, whereas the inland area (Hyderabad) is given the lower rain rate. As a result, the inland regions of India have likewise provided a superior link performance than the coastal regions.

This type of research has been conducted all around the world since the rates of rainfall in different countries vary. Abu Bakar Mohammad [26] discussed the thorough applications of the free space communication systems its advantages and disadvantages of the system. The main focus of the scientific paper was to first analyze and identify the problems of free space

communication and to minimize the existing problems. The main problem identified by the paper was the problem of data attenuation which is occurred due to rain, and the effect of scintillation effect on free-space communication. To overcome this problem a unique system was developed as they have successfully managed to incorporate not only the use of one single beam of diode laser but multiple uses of the diode laser. This process was done to observe the effect which occurred due to the rainfall and other parameters of attenuation in the conduction of the experiment. The experiment was done at a distance of 1141.2 meters between two buildings. The whole experiment was conducted first with a single beam to observe the notion of the solution, then it was conducted with 4 beams in a multiplexing method. The accumulated result was very promising as the optical power was measured and the data rate of the transmission was more than the data received in case of the single beam. The basic reason behind the improvement of the data was the rate of blockage in the link which was being established in the whole process but in case of the multiple beam process, there were less chances of blockage in single, as the blockage of all 4 beams simultaneously is high unlikely thus giving more added advantages in this process. In this paper, the tracking of the last mile problem and different weather conditions which were very problematic for free space communication was also improved by the hybrid wavelength division multiplexing.

Another study has been carried out by Paramdeep Singh, et al [27], regarding the rain attenuation effect on FSO. For their study, two visible wavelengths (532 nm & 655 nm) were considered for the availability of sources and detectors in the visible spectrum and support to higher carrier frequency than infrared carriers. The overall optical link has been around 3.5 meters long. Various rain rates were artificially manufactured, with the highest rain rate taken into consideration at 3 mm per minute. This article claims that rain has a higher attenuation level at 532 nm than it does at 655 nm.

Another notable study has been carried out by Gourab Soni, et al [28], regarding the artificial rain attenuation effect on FSO. In this study, the authors used the 650 nm Laser source. The rain rates have been created from low to high in the range of 0.5 mm/min to 3 mm/min, the artificial rain chamber size being around 1.25 m. The experimentation was carried out with different rates and a maximum of 19.79 dB/km optical power decrease was found with a rain rate of 2.719 mm/hr.

Another study regarding the rain attenuation effect on FSO was studied by Gireesh G. Soni, et. al [29]. In this study, an artificial rain simulation chamber size was around 0.5x0.5x5 m^3 and a

1550 nm Laser source was used as a transmitter and a very high rain rate has been considered (210 mm/hr). According to the experiment, the received optical power remained between -24.3 dBm to -23.2 dBm for ensuring the BER range of 10^{-6} to 10^{-4} for a link distance of 15 m. From these experimental results, the authors propose a new experimental model due to rain and the value of coefficient ok k & α is around 0.63 & 0.91 respectively. The k & α is the regression parameter for rain specific attenuation model.

Another important environmental anomaly which is called turbulence can affect the FSO communication link very badly. The effect of rising ambient temperature of the surface of terrestrial region and inhomogeneous temperature effect can cause the turbulence effect. In this phenomenon, the optical beam fluctuates randomly at the receiver side and as a result, the performance has been degraded.

Hemani Kaushal, et al [30]., built a small chamber with dimensions of around 20x20x20 cm^3 to demonstrate the beam wander effect. Two visible wavelength Lasers 633 nm and 542 nm were used for this experimentation with a Laser power of 10mW. The overall length of an optical beam was 50 cm, and the temperature difference was considered 20^0 K - 100^0 K. Both sides of the chamber had 3.5 m/s of air velocity. This article [30] claims that when the temperature gradient increased, the impact of the FSO link was more pronounced.

Another noteworthy work was demonstrated by W.O. Popoola, et, al.[31], regarding the scintillation effect on the FSO system. To show the scintillation effect in a lab setting, a 140x30x30 cm^3 scintillation simulation chamber was built. According to this article [31], hot air had a temperature range of 25^0 C – 95^0 C. Air vents were used to further regulate temperature, ensuring a temperature differential between the transmitter and receiver. An 850 nm laser diode, a 1 MHz carrier signal, and intensity modulation methods were used in the experiment. The experiment was conducted with very lower scintillation regime.

Using an 830 nm laser source, the medium and lower scintillation impact on the FSO connection was demonstrated by H. Le-Minh, et al. [32]. The chamber size was 550x30x30 cm^3 and could withstand temperatures of up to 80°C. At the NRZ format with 20 Mbps data speed, lower turbulence regime, the BER value was approximately 10^{-12}, and at medium turbulence strength, the BER value was in the 10^{-8} range. In this article [32], the strong turbulence was not investigated.

Milica I. PETKOVIC *et al.* [33] observed the effectiveness of an intensity-modulated with direct detection (IM/DD) free space optical (FSO) system employing an avalanche photodiode (APD) receiver with on-off keying (OOK). Since it offered high agreement over a broad range of meteorological conditions, they employed the gamma-gamma model to characterise the influence of air turbulence. In addition, they examined the identical FSO device with equal gain combining used at the reception. The theoretical derivation of the bit error rate (BER) expression, numerical integration with previously defined relative calculation error, was carried out in this research. Monte Carlo simulations were used to show and validate the paper's findings, and they also explored how the FSO connection and receiver characteristics affected BER performance. The findings of this study show that the link distance, atmospheric turbulence intensity, and receiver temperature have a significant impact on the optimal APD gain in the minimum BER sense. The value of this optimal gain was also slightly different for applications of spatial diversity compared to single channel reception.

Yamac Dikmelik*et al.* [34] measured the inter-sub band absorption loss as mid-infrared quantum cascade lasers which actually operates on the normal function as in continuous wave at room temperature and have a high power level as it also had wall plug efficiencies. In this paper they have also calculated the waveguide loss in this paper for the two high-performance mid-infrared quantum cascade laser designs. The laser had the inter sub band absorption loss which made it very important of the waveguide loss for these structures. In this paper the main emphasis was given on the improvement of the waveguide loss as the loss of that parameter have a huge effect on the current densities as it limits the efficient extraction of generated light out of the laser cavity. The conduction band diagram for a QCL structure that is designed to have fewer voltage defects for the increase of voltage efficiency is detailed as the consequent feature in this study.

1.3. Thesis Objective & Outcomes

Nowadays, LASERS are widely used in a variety of fields, including communication, medical, LIDAR, entertainment, military use, scanners, etc. With LASER sources, it is possible to construct free space optical communication and send data successfully. The issue is recognized as one of the difficult modes in data transmission that is intended to be utilized in 5G and 6G and satellite communication. As part of the work, a new approach to environment simulation is used. It was additionally determined that the best operating frequency is 1550 nm in wavelength.

Free Space Optical (FSO) communication is a low-cost, high-bandwidth access method that is gaining popularity due to its recent commercialization. The performance of this system suffers bad weather conditions, so the fundamental flaw of this system is its dependence on the surrounding atmosphere. The objective and scope of this project is to establish free space optical communication in a given (rain, fog, scintillation) environmental condition and with improvements of factors like signal to noise ratio and bit error rate.

In this thesis, cost effective FSO Communication channel has been established using different wavelength Laser sources like visible (532 nm, 638 nm) sources and IR (808 nm, 980 nm, & 1550 nm) sources. In this study, the primary atmospheric problems including fog, rain, and scintillation are taken into account. To evaluate the system performance in the aforesaid atmospheric conditions, some artificial atmospheric chambers have been developed in the laboratory. The unique aspect of this study is that the data from the artificial atmospheric chamber were created while taking Indian atmospheric conditions into consideration. Data from Indian weather reports were utilized in this experimental studies.

The performance investigation of various wavelengths of laser sources under simulated weather circumstances have been done using a number of parameters, including optical power, real-time eye patterns, Signal to Noise ratio (SNR), Bit Error Rate (BER), etc. According to the experimental findings, the optical beam attenuation has been observed to be more attenuated in foggy weather than in other atmospheric anomalies. Another significant finding from these tests is that, in case of scintillation and fog, the performance of the FSO communication system is wavelength dependent, however in case of rain, the optical power attenuation for various wavelengths is practically same.

For system performance enhancement, the techniques of wavelength diversity and aperture averaging have been proposed and integrated. Aperture averaging has improved system performance in terms of SNR, BER, real-time eye patterns, and optical power attenuation in different atmospheric conditions with all types of LASER wavelengths. It is clear that 1550 nm Laser performs better than other considered wavelengths. Finally, a theoretical link performance study for Mid-Wave Infrared (MWIR) Laser sources at 4000 nm has been presented and compared with 1550 nm Laser sources at larger link distances (4 km). These analytical findings show that 4000 nm is more successful than other wavelengths under challenging air conditions. This work might lead to new developments in the field of FSO communication.

1.4. Outline of Thesis

In **Chapter 1**, a general overview of LASER and its applications for mankind are presented, along with a review of the relevant literature regarding the thesis work.

The Free Space Optics (FSO) communication system, its components, benefits, drawbacks, and applications in different fields are covered in **Chapter 2**.

The development of an artificial simulation setup for rising ambient temperature, fog, and rain is covered in **Chapter 3** along with the detailed design of the developed FSO system. In this chapter, the hardware for an FSO data communication link using several laser sources with varying wavelengths has also been covered.

The system's experimental findings are presented in **Chapter 4.** This chapter is divided into two sections: the first discusses optical power attenuation, and the second discusses channel attenuation caused by various weather anomalies, such as rain, fog, and rising ambient temperatures.

Some strategies for reducing the impact of the atmosphere on the FSO system have been described in **Chapter 5**. Again, this chapter is broken into two parts: The first is a theoretical approach, whereas the second is a practical simulation approach.

The conclusion and the thesis's future scopes are covered in **Chapter 6.**

CHAPTER 2
THEORETICAL BACKGROUND OF FSO SYSTEM

2.1. INTRODUCTION

In general, the FSO system comprises of three parts- transmitter unit, receiver unit, and free space channel. Laser sources of different wavelengths are used as transmitter; according to the wavelength band of the Laser source, the receiver (photodetector) is chosen. The sensitivity of detector materials are not same for different wavelengths of the Laser source. In FSO communication system, the optical beam passes through the free air channel as an unguided communication process, no guided material like fiber is not required. Therefore, optical beam faces different atmospheric anomalies like rain, fog, temperature, dust, etc. These anomalies degrade the system performance. In this chapter, the brief description of optics, transmitter, receiver, and atmospheric effect on free space channel have been given.

2.2. TRANSMITTER SIDE

Generally, a transmitter unit comprises of an LASER source, modulator unit, an optical amplifier and beam forming optics. At first data bits or voice signal which is transmitted from the information source encoded and then modulated. Then the modulated optical beam is fed to the optical amplifier which boosts up the optical intensity. This optical beam is fed to the beam forming optics to refocus the beam. Certain wavelengths near infrared range can penetrate the eye to damage the retina. In case of greater than 1400 nm Laser source, absorption coefficient of the front part of the eye is large. For this reason, 1550 nm Laser source is most popular wavelength source because of fifty times more power is transmitted than near infrared wavelength (850 nm) optical source [35,36]. Visible wavelengths are also used in the FSO system for its cost-effectiveness and are commercially available in the market. These are used in different FSO's applications, with alignment purposes (pilot Laser) for NIR wavelengths. Different types of Lasers, their wavelength, and different features which is used in terrestrial-based FSO systems are discussed in Table 2.1

Table 2.1 Several types of Lasers used in terrestrial-based FSO system

Sl. No.	Type of Optical Source	Wavelength (nm)	Features
1.	Vertical Cavity Surface Emitted Laser (VCSEL)[37,38]	750-1064	Inexpensive, reliable at high data rates (10 Gbps), average life span, lower power density.
2.	Fabry-Perot[39]	1400-1600	Longer Life span, high data rates (40 Gbps), 50 times more power is transmitted than previous wavelength range for same eye safety issue, useful in atmospheric hazardous conditions like fog, snow etc., attached properly with optical amplifier.
3.	Distributed Feedback Laser (DFB)[40]	1300/1500	Reliable at high data rates (40 Gbps), small temperature dependence, highly appreciable at long distance communication application, connected properly with optical amplifier .
4.	Quantum Cascade Laser (QCL)[41][42]	Mid Wavelength IR- Far Wavelength IR	Emission is produced by use of inter-subband transitions in a repeated stack of semiconductor superlattices, highly sensitive, very high cost, very fast, relevant components are not readily available, better fog penetration characteristics.
5.	Solid State Laser[40]	1064	High power in infrared region, very good coherence, Laser gain dependent on polarization.
6.	Diode Pump Solid State Laser (DPSS)[41]	450-1064 nm	Different wavelengths (450 nm-1064 nm) are easily available, cheap, moderate life, energy efficient, etc.

7.	Fiber Laser[42]	UV-MWIR	Different wavelengths from UV to MWIR are available, high cost, high power, longer life, etc.

2.3. RECEIVER SIDE

When transmitter transmits the modulated data through atmospheric channel, the data should be demodulated at receiver section and this work is primarily done by photo detector. Receiver of the terrestrial based FSO system comprises of photo-detector, optical band pass filter, receiver optics and decision circuit (amplifier, signal processor).

The solid state photo-detector can be a PIN photo-diode (P-i-N) or APD (avalanche) photo-diode. PIN diodes are mainly used for FSO system with a link range up to few kilometers. Due to large thermal noise, the performance of PIN type photo detector is reduced. This is the most important drawback of using PIN type photo detector. APDs, which offer a current gain owing to the process of impact ionisation, are frequently employed for long distance communications. APDs' disadvantage is the excessive noise at their output, which simulates the random phenomena underlying the production of secondary photo-electrons [43]. Table 2.2 shows the different photo detector material and their different properties are given below:

Table 2.2. Different FSO photo detector[44]

Sl No.	**Material**	**Dark Current**	**Speed**	**Sensitive Wavelength (nm)**	**Cost**
1.	Silicon (Si)	Low	High	400-1000	Low
2.	Gallium Phosphide (GaP)	Low	High	150-550	Medium
3.	Germanium (Ge)	High	Low	900-1600	Low
4.	Indium Gallium Arsenide (InGaAs)	Low	High	800-1800	Medium
5.	Quantum-well and Quantum-dot detectors	Low	High	~10,000	High
6.	Heterostructural thermally cooled HgCdTe	-	High	3000-17000	High

2.4. OPTICS

For reliable, rugged and proper terrestrial based free space communication, different accessories are also required with above mentioned three parts, like lens, filter, beam expander etc. which is cumulatively known as optics[45]. Different main parts of optics are described below:

2.4.1. BEAM EXPANDER

Beam expander is a combination of convex and concave lens. Beam expander is used to increase the diffraction aperture. The main function of the beam expander to decrease the beam divergence angle and expand the laser beam waist, such that the system's total beam divergence loss is kept to a minimum [46,47]. Fig 2.1. shows the beam expander.

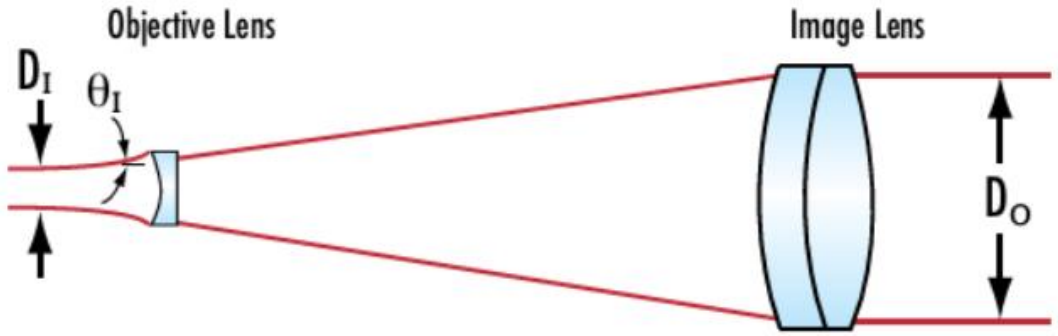

Fig.2.1. Beam Expander

As the output beam divergence (θ_0) declines, the output beam diameter (D_0) increases, and vice versa, according to the interpretation of Equations 2.1, 2.2 and 2.3. As a result, when a beam expander is used to reduce the beam, its diameter will drop but the laser's divergence will increase.

It's also critical to be able to figure out the output beam diameter at a particular operating distance (L). The input beam diameter and the beam divergence after a particular working distance (L) determine the output beam diameter (which is depicted in Figure 2.1. (a)).

$$\frac{\text{Input Beam Divergence}(\theta_I)}{\text{Output Beam Divergence }(\theta_0)} = \frac{\text{Output Beam Diameter}(D_0)}{\text{Input Beam Diameter }(D_I)} \qquad 2.1.$$

The beam divergences or beam diameters can now be used to represent the magnifying power (MP) which is depicted by equation 2.2 & 2.3.

$$MP = \frac{\theta_I}{\theta_0} \qquad 2.2.$$

$$MP = \frac{D_0}{D_I} \qquad 2.3$$

By the Magnifying Power, a beam expander will reduce the input divergence and enlarge the input beam. This can be represented by the equation 2.4.

$$D_L = (MPxD_I) + L.\tan\left(\frac{2\theta_I}{MP}\right) \qquad 2.4.$$

D_L = Laser beam diameter, L = Link distance

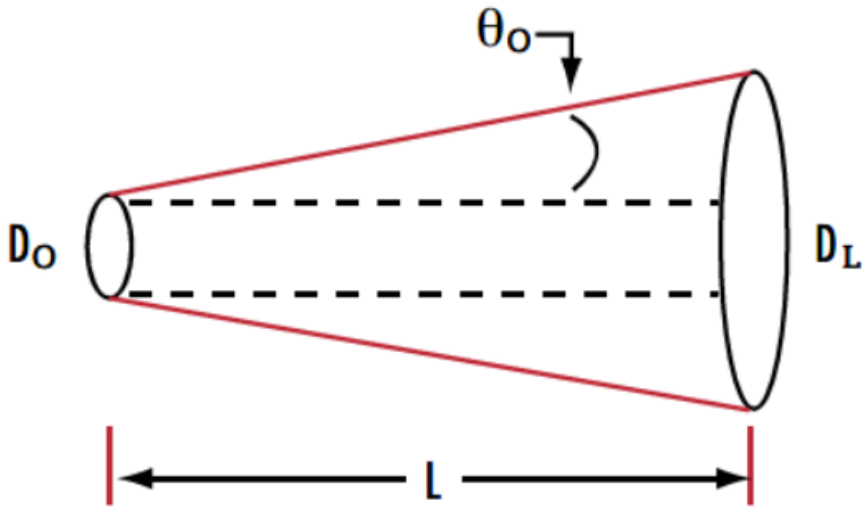

Fig.2.1. (a). The output beam diameter at a particular operating distance may be calculated using the input beam diameter and divergence of a laser

2.4.2. OPTICAL LENS

The optical lens is chosen depending upon the line of sight (LOS) distance of communication so that the Laser beam is well concentrated and collimated properly at the receiver side. Plano-Convex or Biconvex lens is appropriate for focusing into photo-detector. It is preferable to have a large receiver lens size since it gathers several indistinguishable radiations and focusses their average on the photo-detector [48]. Fig 2.2. shows the plano convex and biconvex lens.

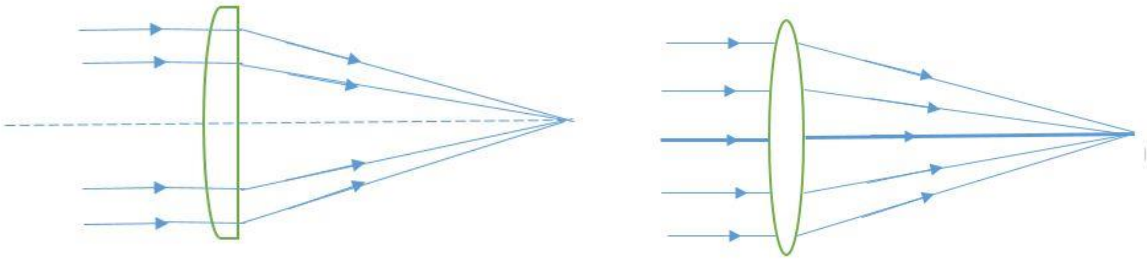

Fig 2.2. Plano-convex & Biconvex lens

2.4.3. OPTICAL FILTER

Optical filter is used at the receiver side after the collimating optical lens. This is used to transmit the selective or desired wavelength and reject the unwanted wavelengths. Background radiation can be reduced by this component. As a result, only selective wavelength which is desired fall on the photo-detector[49]. Fig. 2.3 shows the optical filter.

Fig. 2.3. Different wavelengths optical filter

2.5. ATMOSPHERIC CHANNEL

Attenuating factors for the signal-carrying laser beam include fog, rain, temperature, dust, snow, smoke, and other aerosol particulate matter. To some extent, this attenuation can be compensated for by raising the signal gain. By choosing the right optical wavelength, one may reduce molecule absorption. On the other hand, optical turbulence caused by random variations in the atmosphere's refractive index always leads to higher bit error rates in the system, particularly for propagation pathways that pass over extended segments of the Earth's atmosphere near horizontally. There is no wavelength "window" where these effects may be avoided, however longer wavelengths do better. Additionally, because optical turbulence-induced signal losses rise with increasing transmitter to receiver distance, improving signal

gain does not necessarily translate into a higher laser beam quality. In many situations of practical consequence, the constant presence of optical turbulence in the air channel is the limiting factor for reliable wireless optical communication connection performance. With the goal of equipping the reader with the skills needed to assess and forecast the expected performance of laser communication systems, in this chapter, we try to explain the fundamental principles underpinning optical extinction and optical turbulence-induced signal losses. We start with a summary of the fundamental physics concepts behind the mechanisms that molecules and aerosol particles utilise to absorb and scatter light, which create optical extinction. We review the models that best predict signal loss for molecular and aerosol extinction. The creation of optical turbulence and its relationship to atmospheric characteristics are then covered. To enable the estimate of optical turbulence strength at various atmospheric levels, a complete collection of optical turbulence models is offered. The behaviour of the signal beam as it propagates in optical turbulence is explored, and this discussion results in equations for calculating bit error rates in optical communication systems as functions of both communication system and optical turbulence characteristics. It is possible to compute projected system performance for ground-to-ground, ground-to-air/air-to-ground, and satellite uplink/downlink optical communication scenarios with the use of the information supplied, which is suitable for both system designers and users.

2.5.1. SCATTERING OF LIGHT

Due to the non-uniformities in the medium, certain radiation forms diverge from their intended course. Scattering is the name for this deviation process.

One of the most significant phenomena we see every day is light scattering. Everyone has witnessed these phenomena since they were little, just like they did with the colour of the rainbow and the blue sky. In contrast to reflection and refraction, light dispersion is a totally separate phenomenon. Light travels in a straight line when it is reflected, however when it is dispersed, the medium it is travelling through scatters the light in many directions.

The scattering of light, which we refer to as an optical phenomenon like the sky's blue colour, is a result of the process by which microscopic particles in the atmosphere cause the light to go in different directions.

As an illustration, when light strikes airborne particles, some of the light is absorbed and the remainder is radiated in all directions other than the one from which it originated. The term

"scattering of light" describes this. The light's wavelength and the size of the particle that dispersed it both have a role in determining how strong the scattering is.

For instance, when the sun's rays hit airborne particles on Earth, they are impacted. In addition to being scattered in all directions, some of these photons are absorbed by the particles. The provided figure shows how this is. In light of this, it may be claimed that particles, imperfections, or interference between the two mediums might cause light to be diverted off its incident path. As a result, dispersion is increased by light with shorter wavelengths and higher frequencies.

Similar to how light scatters when it interacts with raindrops, light's physical origin is light colliding with moisture. But when droplet size shrinks, scattering changes in both kind and quantity. Greater scatter is produced by smaller droplets, particularly more backscatter from headlights, which is also bigger and causes more loss of contrast. The use of high beam when driving in fog is discouraged for this reason.

Based on a dimensionless size parameter, light scattering models may be separated into three domains, α which is defined as equation 2.5

$\alpha = \Pi d/\lambda$……. (2.5)

where Πd is the circumference of a particle and λ is the wavelength of incident radiation. Based on the value of α, scattering can be classified as

$\alpha << 1$: Rayleigh scattering (small particle compared to wavelength of light);

$\alpha \approx 1$: Mie scattering (particle about the same size as wavelength of light, valid only for spheres);

$\alpha >> 1$: Geometric scattering (particle much larger than wavelength of light).

As the object is scattering in fog. So, the discussion will be about Rayleigh scattering and Mie scattering [50].

2.5.1.1. RAYLEIGH SCATTERING

Electric and magnetic field vectors serve as the defining features of light as an electromagnetic wave. For the sake of simplicity, it is assumed that the incident wave is a plane wave that is linearly polarised and hits a tiny spherical particle. About 0.5 m is the wavelength of light in the visible spectrum. The local electric field created by the wave is roughly homogeneous at any given time for particles much smaller than the wavelength. A dipole is created in the particle by the applied electric field. The induced dipole also oscillates in response to the electric field, and in accordance with classical theory, the dipole radiates in all directions. The term "Rayleigh scattering" refers to this kind of scattering.

The dipole moment “P” induced in the particle is proportional to the instantaneous electric field vector as equation 2.6.

$P=\alpha E$…… (2.6)

Polarization is described in this statement, which is a scalar for every isotropic spherical particle and has the dimension of volume. It is possible to get an expression for the intensity of scattered radiation as equation 2.7 from the energy of electric field generated by the oscillating dipole.

$I=(1+\cos 2\theta).k^4.\alpha.22.R^2/I_0$…….. (2.7)

R= Distance to the particle;

θ= *Scattering angle;*

α= scalar (value depends on refractive index);

k= wave number = 2π/λ;

I_0= Initial intensity of the light.

With equal peaks and minima in the forward and backward directions, as well as a minimum at a right angle, the scattering is symmetrical with regard to the direction of the incident beam. Blue light (with a short wavelength) scatters more often than red light, and the intensity of the scattered light decreases inversely with the fourth power of the wavelength [51].

2.5.1.2. MIE SCATTERING

The generalised solution, known as the Mie scattering theory, illustrates how an electromagnetic wave might be scattered by a homogeneous, spherical material with a different RI than the medium the wave is travelling through. The fact that Mie scattering is not a stand-alone physical event should be emphasised once more. Due to the electric polarisation of the molecules in the scattering particles, the Maxwell's equations for multipole radiation can only be solved definitively when an electromagnetic wave strikes the system. It provides scattering solutions where the phase of the input signal may even fluctuate noticeably within the scattering particle's diameter. As a result, it differs from Rayleigh scattering in that it does not need that the $2\pi d/\lambda \ll 1$ requirement be satisfied. Following the Mie solution, frequent scattering factors for waves that are propagating include dust, smoke, and raindrop particles.

The Mie solution is a multipole polarisation expansion that occurs infinitely many times as a result of an incoming wave in a spherical media. Infinite series, with each member denoting the contribution of a certain order of multipole expansion, is another way to depict the electric and magnetic field of such polarisation. Now, keep in mind that you may estimate the power

spread in any direction from the vector pointing in that direction. The pointing vector may also be determined, just like we did for Rayleigh scattering, if the formula for the fields E and H is well understood. As a result, the cross section may likewise be determined by using these formulae for any specific direction once the expressions for E and H are known. For finding the Mie solution, there are several effective methods available today (Hergert and Wriedt, 2012). The book isn't intended to address how to find the Mie solutions, though. We won't examine the aspects of the solution here; instead, we'll just state the formulas for the scattering cross sections that were derived.

For big particles, the square of the particle diameter determines the Mie scattering intensity. The light beam turned toward the direction the incident light ray was coming from after being scattered by a particle. Dust particles exhibit the majority of this form of scattering. Even still, this form of scattering is less common in fog because of the abundance of tiny water droplets in the sky. Rayleigh and Mie scattering are shown in Fig. 2.4.

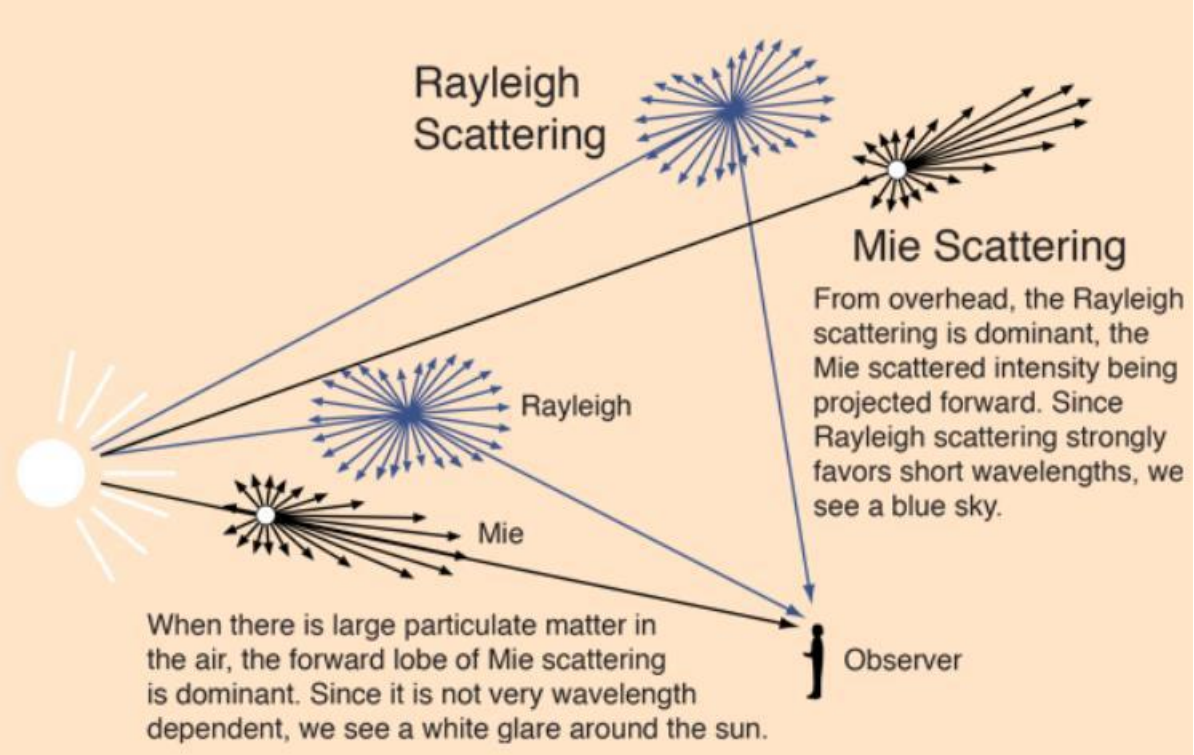

Fig. 2.4. Rayleigh & Mie Scattering

The square of the particle diameter determines the Mie scattering intensity for significant particles. After being scattered by a particle, the light beam shifted to face the incident light ray's direction. The bulk of this scattering is shown by dust particles. Due to the amount of microscopic water droplets in the sky, this type of dispersion is still less frequent in fog.

When air particle become very small, the situation is more complicated because not all wavelength is affected equally. Air molecules, for example, scatter short wavelength (blue) more [50].

2.5.1.3. GEOMETRIC SCATTERING

This is a phenomenon that occurs when photons collide with the structure of a particle in free space, but because airborne particles behave differently than those that are scattered above, this sort of scattering will be unique as well.

Geometric scattering is the term for the sort of scattering that occurs when a suspended particle has a size greater than the visible light spectrum, which has a wavelength of around 400–780 nm. Because the scattering becomes directed and unpredictable as a result of the particle size exceeding the light's wavelength, the pattern of the scattering is substantially altered. A lob-like shape with a predominance of scattering in the forward direction characterises the new kind of scattering. As in Rayleigh's scattering, the pattern is very directional, which aids in understanding that in the case of rain, which falls under this type of scattering. However, unlike Rayleigh's scattering, where the scattering is uniform in all directions due to the particles' extreme smallness in relation to the wavelength of light. Although photons are scattered via raindrops in many directions and the size of the droplets makes an assumption about the scattering, most of the scattering is facade. Fig. 2.5. shows the scattering pattern of geometrical scattering.

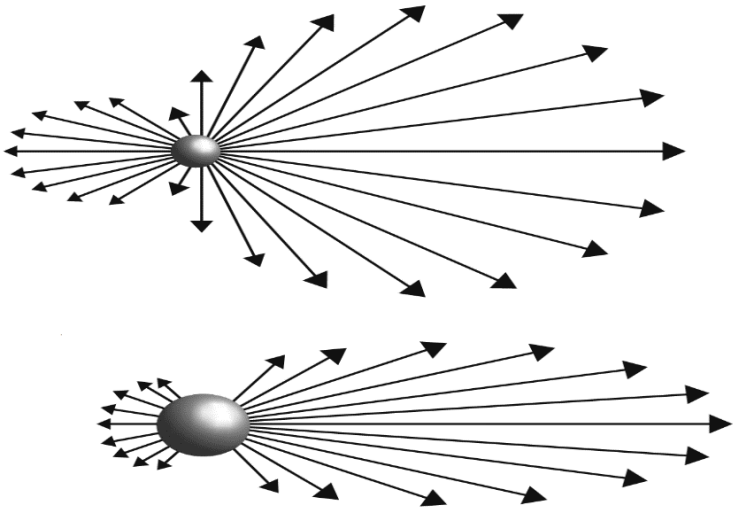

Fig. 2.5. Geometrical Scattering

2.5.2. SCATTERING & ABSORPTION OF LASER BEAM DUE TO DIFFERENT ENVIRONMENTAL ANOMALIES

Absorption and scattering process affect the FSO system severely. The main atmospheric absorber ingredients are molecules of water, carbon dioxide, ozone etc. which are main absorber of visible and infrared wavelength[52]. The attenuation coefficient due to absorption and scattering from aerosols and molecular ingredient is given below in equation 2.8.[5] [92]

$$\gamma(\lambda) = \alpha_m(\lambda) + \alpha_a(\lambda) + \beta_m(\lambda) + \beta_a(\lambda) \quad \text{.....(2.8)}$$

Where $\alpha_m(\lambda)$ is molecular absorption coefficient, $\alpha_a(\lambda)$ is aerosol absorption coefficient, $\beta_m(\lambda)$ is molecular scattering coefficient, $\beta_a(\lambda)$ is aerosol scattering coefficient.

Generally, the absorption coefficient for different wavelengths of laser sources are very low compared to scattering coefficients, so the absorption coefficients are ignored. So the equation 2.4 can be written as in equation 2.9.

$$\gamma(\lambda) = \beta_m(\lambda) + \beta_a(\lambda) \quad \text{.....(2.9)}$$

The optical channel contains air particles of various sizes. and corresponding different scattering process is given in Table 2.3

Table 2.3. The optical channel contains air particles of varying sizes, which result in various scattering processes [53]

Sl. No.	Type	Radius	Scattering process
1.	Air molecules	0.0001	Rayleigh
2.	Haze particle	0.01-1	Rayleigh-Mie
3.	Fog droplet	1-20	Mie-Geometrical
4.	Rain	100-10000	Geometrical
5.	Snow	1000-5000	Geometrical
6.	Hail	5000-50000	Geometrical

2.5.2.1.RAIN

Rain is another important ingredient to attenuate the terrestrial based FSO system. In general, high rain rate (>100 mm/hr) can produce low visibility which also impair the FSO performance. Table 2.4. indicates[54,55] the different rain intensity types, their diameter size (mm), rates (mm/hr) and corresponding visibility in km.

Table 2.4. Different rain intensity types and their parameters

Sl. No.	Rain Intensity	Drizzle	Light Rain	Medium Rain	Heavy Rain	Cloud-burst
1.	Diameter (mm)	< 0.8	0.8-1.2	1.2-2.0	2.0-3.5	>3.5
2.	Rates (mm/hr)	0.25	2.5	12.5	25	100
3.	Visibility (km)	18.1	5.9	2.8	1.9	0.770

The sizable rain droplets can produce non selective or geometrical scattering because there is independent of attenuation coefficient on laser wavelength. The specific attenuation (dB/km) due to rain[56] may be evaluated from the given equation 2.10.

$A_{rain} = k\,(R^{\alpha}{}_{1})$ (dB/km) ……..(2.10)

Where R stands for rain rates in mm/hr, k and α_1 is power law parameter which depend upon rain drop size, rain temperature, frequency and polarization. Table 2.5. shows the different attenuation model used for the measuring the specific attenuation (dB/km) due to rain.

Table 2.5 Different attenuation model with different value of k and α [87][90][91]

Sl No	Model Name	Rain Rate (r) (mm/hr)/Region	Rain Model
1.	Japan Model [60]	Temperate	$1.58r^{0.63}$
2.	Charbonneau (France) [59]	Temperate	$1.076r^{0.67}$
3.	Laws & Parson [61]	-	$0.543r^{0.87}$
4.	Malaysia [59]	Tropical	$2.03r^{0.74}$

Table 2.6 shows the Attenuation (dB/km) due to different rain rates (mm/hr) for different models.

Table 2.6. Attenuation (dB/km) due to different rain rates (mm/hr) for different models

RAIN RATE	LOSS DUE TO CHARBONNEAU MODEL	LOSS DUE TO JAPAN MODEL	LOSS DUE TO LAWS & PARSON MODEL	LOSS DUE TO MALAYSIA MODEL
1	1.076	1.58	0.543	2.03
5	3.16	4.35	2.2	6.68
10	5.03	6.74	4.02	11.15
20	8	10.43	7.35	18.63
30	10.5	13.46	10.46	25.15
40	12.74	16.41	13.44	31.11
50	14.79	18.57	16.32	36.7
60	16.71	20.84	19.13	42
70	18.53	22.96	21.88	47.08
80	20.73	24.98	24.57	51.97
90	21.93	26.9	27.22	56.70
100	23.54	28.75	29.84	61.3
120	26.6	32.25	34.97	70.16
140	29.5	35.54	39.988	78.63
150	30.88	37.11	42.461	82.75
170	33.6	40.16	47.34	90.78
180	34.9	41.63	49.76	94.71
190	36.2	43.07	52.15	98.57
200	37.45	44.49	54.53	102.39

From the aforesaid table, it has been shown that at higher rain rate, the optical power attenuation is huge. From different attenuation models, it has been shown that in the tropical country, where the rain rates are very much higher compared to temperate countries, as a result, the attenuation is also high compared to others models.

Figure 2.6. shows the different model used for measuring of specific attenuation (dB/km) due to rain versus rain rate (mm/hr). During heavy rain rate, a huge amount power to be loss, so that's why a high power laser must be employed and for the FSO system's most prevalent link availability, it is necessary to achieve and maintain sufficient link margin higher than 30 dB [57].

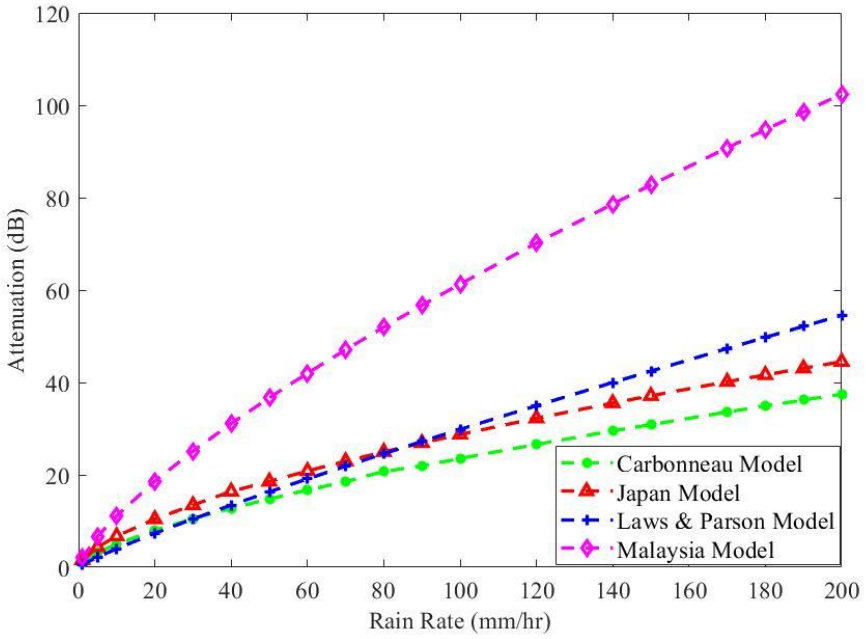

Fig. 2.6. Specific attenuation (dB/km) for different rain rates (mm/hr) of different models

2.5.2.2 FOG

The main enemy of the terrestrial FSO system is fog. During dense fog, the visibility may be reduced to few meters (20-50 m), that time the attenuation also is more (greater than 250 dB/km). As a result, the communication link range has been reduced, the link performance has been reduced. Different fog events can be classified by their visibility ranges like dense fog situation (when the visibility around 20 m), thick fog (visibility around 100 m), moderate fog (visibility around 250 m), light fog (500 m), haze (visibility around 2 km)[82] [95].

The specific attenuation due to fog can be measured from the equation (2.11) which is mentioned in below [81]:

$\Upsilon_{fog}(\lambda) = 17/V\,(550/\lambda)^{n}$ …….(2.11)

Where V is the visibility range in km, λ is the operating wavelength in nm and n is the size distribution coefficient of scattering. The comparative value of n according to Kim model and Kruse model is given in the table 2.7.

Table 2.7. Kruse Model and Kim Model for determine the value of n [62][86]

Sl. No.	Visibility (km)	Kruse Model	Kim Model
1.	V>50	1.6	1.6
2.	6<V<50	1.3	1.3
3.	1<V<6	$0.585V^{(1/3)}$	0.16V + 0.34
4.	0.5<V<1	$0.585V^{(1/3)}$	V-0.5
5.	V<0.5	$0.585V^{(1/3)}$	0

From the aforesaid table, it has been shown that when the visibility range is V < 0.5 km, the attenuation due to fog is wavelength independent in case of KIM model whereas according to Kruse model, when the visibility range is V < 0.5 km, the attenuation due to fog is wavelength dependant. The transmittance or extinction coefficient due to different visibility for a particular link range (L) can be predicted from the equation (2.12)[62]

$$\tau\,(Z) = P(R)/P(T) = e^{-\sigma L} \quad \ldots\ldots\ldots\ldots\ldots\ldots\ldots\ldots\ldots\ldots\ldots\ldots\ldots\ldots(2.12)$$

Table 2.8 shows attenuation (dB/km) due to different visibility for different models (KIM & KRUSE models).

Table. 2.8. Attenuation (dB/km) due to different visibility for different models

Visibility (m)	LOSS DUE TO KIM MODEL 532 nm	LOSS DUE TO KRUSE MODEL 532 nm	LOSS DUE TO KIM MODEL 638 nm	LOSS DUE TO KRUSE MODEL 638 nm	LOSS DUE TO KIM MODEL 808 nm	LOSS DUE TO KRUSE MODEL 808 nm	LOSS DUE TO KIM MODEL 980 nm	LOSS DUE TO KRUSE MODEL 980 nm	LOSS DUE TO KIM MODEL 1550 nm	LOSS DUE TO KRUSE MODEL 1550 nm
50	340.11	342.45	340.11	329.06	340.11	312.92	340.11	300.16	340.11	271.9
150	113.33	114.51	113.33	108.11	113.33	100.55	113.33	94.69	113.33	82.11
300	56.66	57.41	56.66	53.40	56.66	48.74	56.66	45.19	56.66	37.76
600	28.42	28.8	27.90	26.29	27.26	23.43	26.74	21.30	25.54	16.99
1200	14.42	14.46	13.07	12.89	11.54	11.15	10.42	9.89	8.163	7.44
2500	6.97	6.982	6.078	6.03	5.115	5.01	4.434	4.29	3.158	2.987
5000	3.53	3.515	2.86	2.921	2.193	2.314	1.759	1.908	1.043	1.206
10000	1.775	1.775	1.396	1.396	1.031	1.031	0.801	0.801	0.442	0.442
25000	0.710	0.710	0.5584	0.5584	0.412	0.412	0.321	0.321	0.176	0.176
50000	0.358	0.358	0.266	0.266	0.183	0.183	0.135	0.135	0.064	0.064

From the table, it has been shown that at the higher visibility conditions scenario like (V > 50 km and 6 km <V < 50 km), the attenuation level is same for both the models, but the lower visibility range, a small deviation has been noticed. At very lower visibility condition (V <500 m), KIM model is wavelengths independent, whereas KRUSE model is wavelength dependent.

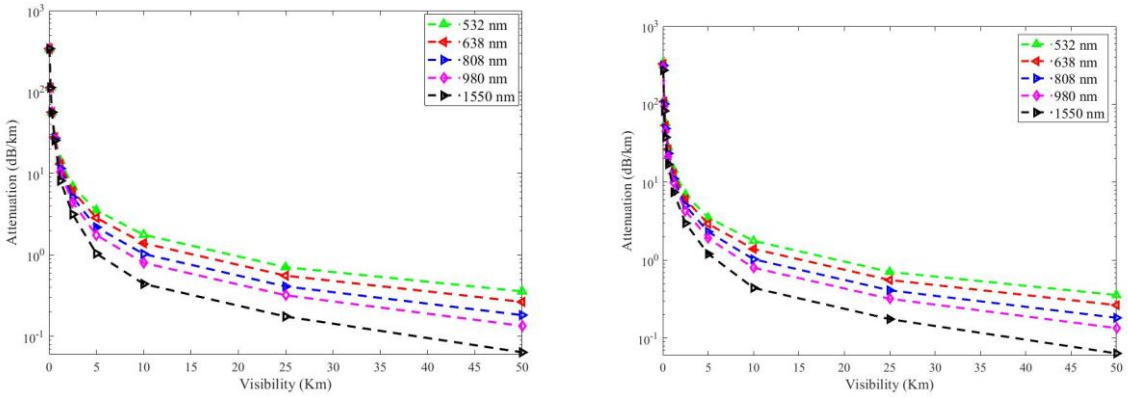

(a) (b)

Fig 2.7. Attenuation for different visibility due to (a) KIM & (b) Kruse Model

Fig.2.7 shows the attenuation for different visibility due to different models like KIM & KRUSE. As the visibility increases from low to high, the optical attenuation is high to low for both the models (dB/km). At higher wavelengths, the attenuation is lower compared to lower wavelengths optical source.

Table 2.9. shows transmittance due to different visibility for different models with different wavelengths laser sources.

Table 2.9. Transmittance due to different visibility for different models

Visibility (m)	**TRANS-MITTA-NCE KIM MODEL 532 nm**	**TRANS-MITTA-NCE KRUSE MODEL 532 nm**	**TRANS-MITTA-NCE KIM MODEL 638 nm**	**TRANSMI-TTANCE KRUSE MODEL 638 nm**	**TRANS-MITTA-NCE KIM MODEL 808 nm**	**TRANSMI-TTANCE KRUSE MODEL 808 nm**	**TRANS-MITTA-NCE KIM MODEL 980 nm**	**TRANS-MITTA-NCE KRUSE MODEL 980 nm**	**TRANSMI-TTANCE KIM MODEL 1550 nm**	**TRANSMI TTANCE KRUSE MODEL 1550 nm**
50	$1.9x10^{-148}$	$1.8x10^{-149}$	$1.9x10^{-148}$	$1.2x10^{-143}$	$1.9x10^{-148}$	$1.2x10^{-136}$	$1.9x10^{-148}$	$4.4x10^{-131}$	$1.9x10^{-148}$	$8.2x10^{-119}$
150	$6x10^{-50}$	$1.84x10^{-50}$	$6x10^{-50}$	$1.1x10^{-47}$	$6x10^{-50}$	$2.1x10^{-44}$	$6x10^{-50}$	$7.5x10^{-42}$	$6x10^{-50}$	$2.1x10^{-36}$

300	$2.4x10^{-41}$	$1.16x10^{-25}$	$2.4x10^{-41}$	$6.4x10^{-24}$	$2.4x10^{-41}$	$6.8x10^{-22}$	$2.4x10^{-41}$	$2.3x10^{-20}$	$2.4x10^{-41}$	$4x10^{-17}$
600	$4.5x10^{-13}$	$3.1x10^{-13}$	$7.6x10^{-13}$	$3.8x10^{-12}$	$1.4x10^{-12}$	$6.6x10^{-11}$	$2.4x10^{-12}$	$5.6x10^{-10}$	$8.1x10^{-12}$	$4.1x10^{-8}$
1200	$5.4x10^{-7}$	$5.25x10^{-7}$	$2.1x10^{-6}$	$2.5x10^{-6}$	$9.7x10^{-6}$	$1.4x10^{-5}$	$2.98x10^{-5}$	$5.06x10^{-5}$	0.00028	0.0005
2500	0.0009	0.00093	0.0023	0.0024	0.006	0.0066	0.012	0.0137	0.042	0.05
5000	0.029	0.0297	0.057	0.054	0.111	0.0988	0.17	0.148	0.352	0.3
10000	0.169	0.169	0.247	0.247	0.356	0.356	0.448	0.448	0.642	0.642
25000	0.491	0.491	0.572	0.572	0.662	0.662	0.725	0.725	0.838	0.838
50000	0.7	0.7	0.766	0.766	0.832	0.832	0.873	0.873	0.938	0.938

Similarly, at lower visibility range, the transmittance is very poor for all of the wavelengths and both the models. In case of higher visibility range, the transmittance is good for all the wavelengths with both the models, and higher wavelength exhibits better transmittance property than lower wavelength optical source.

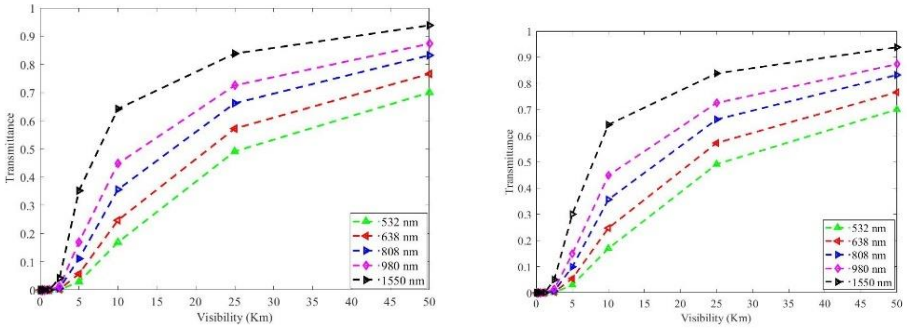

(a) (b)

Fig. 2.8. Transmittance for different visibility due to (a) KIM & (b) Kruse Model

Fig.2.8 shows transmittance for different visibility due to different models like KIM & KRUSE. As the visibility increases from low to high, the transmittance is low to high for both the models (dB/km). At higher wavelengths, the transmittance is higher compared to lower wavelengths optical source.

Apart from the above mentioned two model, some of the empirical models are used for evaluation of fog attenuation which is given in table 2.10.

Table 2.10: Fog attenuation models

Sl. No.	Model	Formula	Wavelength range (nm)	Visibility range (km)
1.	Al Naboulsi Convection[58]	$A_F = 4.343\ (\frac{0.11478\lambda + 3.8367}{V})$	690-1550	0.05-1
2.	Al Naboulsi Advection[58]	$A_F = 4.343\ (\frac{0.18126\lambda^2 + 0.13709\lambda + 3.7502}{V})$	690-1550	0.05-1
3.	Ijaz [16]	$A_F = \left(\frac{17}{V}\right)(\frac{\lambda}{0.55})^{-q(\lambda)}$ $q(\lambda) = 0.1428\lambda - 0.0947$	600-1600	0.015-1

The aforesaid contemporary fog attenuation models (table 2.10) have some drawbacks in terms of usage of wavelengths and measurement of visibility range. From the table, it has been shown that wavelength range in between 690 nm -1550 nm for Al Naboulsi Convection and Al Naboulsi Advection method and 600 nm -1600 nm for Ijaz method respectively. When measured the below this range wavelengths like (532 nm, 450 nm, etc.) and measured above this range wavelengths like (2000 nm, 4000 nm, 10000 nm, etc.), these methods are not applicable. Other shortcomings of these methods are in terms of visibility measurements. The range of applicable visibility of these models are between 0.05 km -1 km and 0.015 km – 1 km for Al Naboulsi Convection, Al Naboulsi Advection and Ijaz respectively. When the visibility range is grater than 1000 m, then these models are not worked.

2.5.2.3 EFFECT OF TEMPERATURE

When the optical beam is propagated through the terrestrial free space, due to fluctuation of atmospheric temperature and pressure is affected along the propagated path adversely. As a result, turbulent cell is generated which also called turbulent eddies of different sizes and different refractive indices. When the atmospheric turbulence affected on the optical propagation path, received signal fades and performance of the FSO communication system degrades [93,94].

'C_n^2' is the important parameter called refractive index parameter structure which is function of scintillation index. The resilience of the turbulence of the atmosphere may be predicted by the C_n^2 parameter. Varying the time of day, geographical location and height, C_n^2 also varying. Different strength of turbulence and their values are given in table 2.11.

Table 2.11. Different strength of turbulence and their value[63,64,66]

Sl. No.	Different strength of Turbulence	Weak Turbulence	Moderate Turbulence	Strong Turbulence
1.	Value	10^{-15} - 10^{-17} $m^{-2/3}$	10^{-14} $m^{-2/3}$	10^{-12} - 10^{-13} $m^{-2/3}$

The attenuation due to scintillation σ^2_{Scin} (dB) at different turbulent strength can be determined by the equation (2.13) [83] [88] [89]:

$$\sigma^2_{Scin} = 2 * \sqrt{23.17 * \left(\frac{2\pi * 10^9}{\lambda}\right)^{\frac{7}{6}} * Cn^2 * L^{\frac{11}{6}}} \quad \text{.....(2.13)}$$

Where λ is wavelength (nm), C_n^2 is the refractive index structure parameter ($m^{-2/3}$), and L is the link length (m).

Table 2.12 depicts attenuation for different range of scintillation with different wavelengths.

Table 2.12. Attenuation (dB) for different range of scintillation with different wavelengths

SCINTILLATION RANGE ($m^{-2/3}$)	LOSS DUE TO 532 nm	LOSS DUE TO 638 nm	LOSS DUE TO 808 nm	LOSS DUE TO 980 nm	LOSS DUE TO 1550 nm
10^{-12}	104.62	95.53	84.89	77.08	61.293
10^{-13}	33.08	30.21	26.84	24.37	19.38
10^{-14}	10.46	9.55	8.48	7.708	6.13
10^{-15}	3.31	3.02	2.68	2.43	1.938
10^{-16}	1.046	0.95	0.8489	0.77	0.613
10^{-17}	0.33	0.302	0.268	0.24	0.1938

From the table, it has been shown that at the higher scintillation conditions scenario like (10^{-12}-10^{-13} $m^{-2/3}$), the attenuation level is higher. When the scintillation range is lower, the attenuation level is low.

Fig. 2.9. shows attenuation (dB) level for different scintillation range for different wavelengths

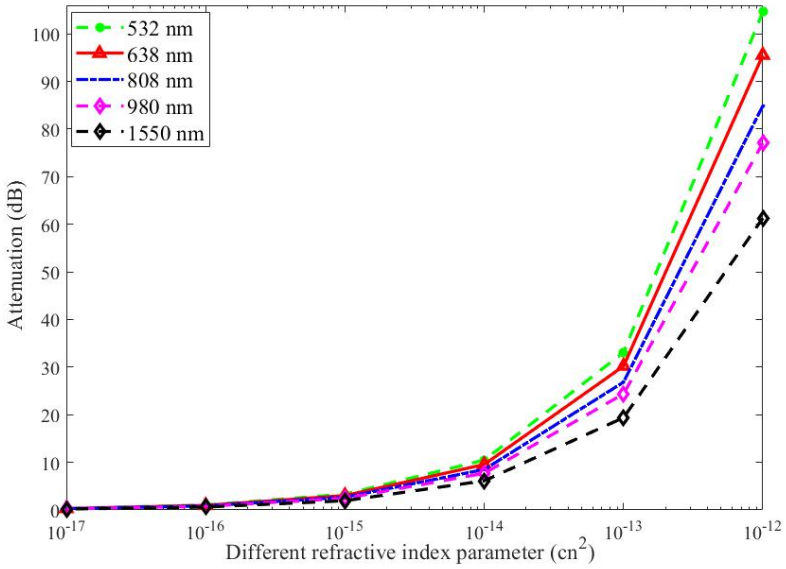

Fig 2.9. Attenuation for different scintillation range for different wavelengths

From the figure, it has been depicted that attenuation due to scintillation is a wavelength dependent phenomenon. At the higher wavelength, the attenuation is lower compared to lower wavelength with same scintillation range.

2.6. SNR & BER MEASUREMENTS

Signal to Noise Ratio (SNR) and Bit Error Rate (BER) are two important parameters to predict the quality of a optical signal at the receiver side. As the SNR is higher, the BER is low. The SNR of a signal can be predicted from the equation (2.14) [65]

$$SNR = \frac{P(R)}{NEP \times \sqrt{BW}} \qquad (2.14)$$

Where, BW = Bandwidth of the Photo detector, NEP = Noise equivalent power of the photo detector.The Noise Equivalent Power (NEP) is the noise of the photo detector which is included the dark current noise, thermal noise, shot noise, f-noise etc.

The Bit Error Rate (BER) of the NRZ-OOK can be computed from the equation (2.15) [65],

$$BER = \left(\frac{1}{2}\right) erfc\left(\frac{1}{2\sqrt{2}}\sqrt{SNR}\right) \qquad (2.15)$$

2.7. APPLICATIONS OF FSO

For high-speed communication across lengths of up to several kilometres between two fixed sites, FSO systems are employed. The FSO link's extremely high accessible optical bandwidth allows for significantly greater data speeds as compared to RF equivalents. Systems for FSO utilise extremely thin laser beams. The high reuse factor, built-in security, and electromagnetic interference resistance of this spatial confinement are all advantages. Additionally, the frequency that the FSO technology uses is over 300 GHz, which is globally unlicensed. As a result, no licence costs are needed for FSO systems [67]. Deploying and reinstalling FSO systems is extremely simple and doesn't require a separate fibre optic connection, which saves money. Fig. 2.10 shows FSO optical connection link.

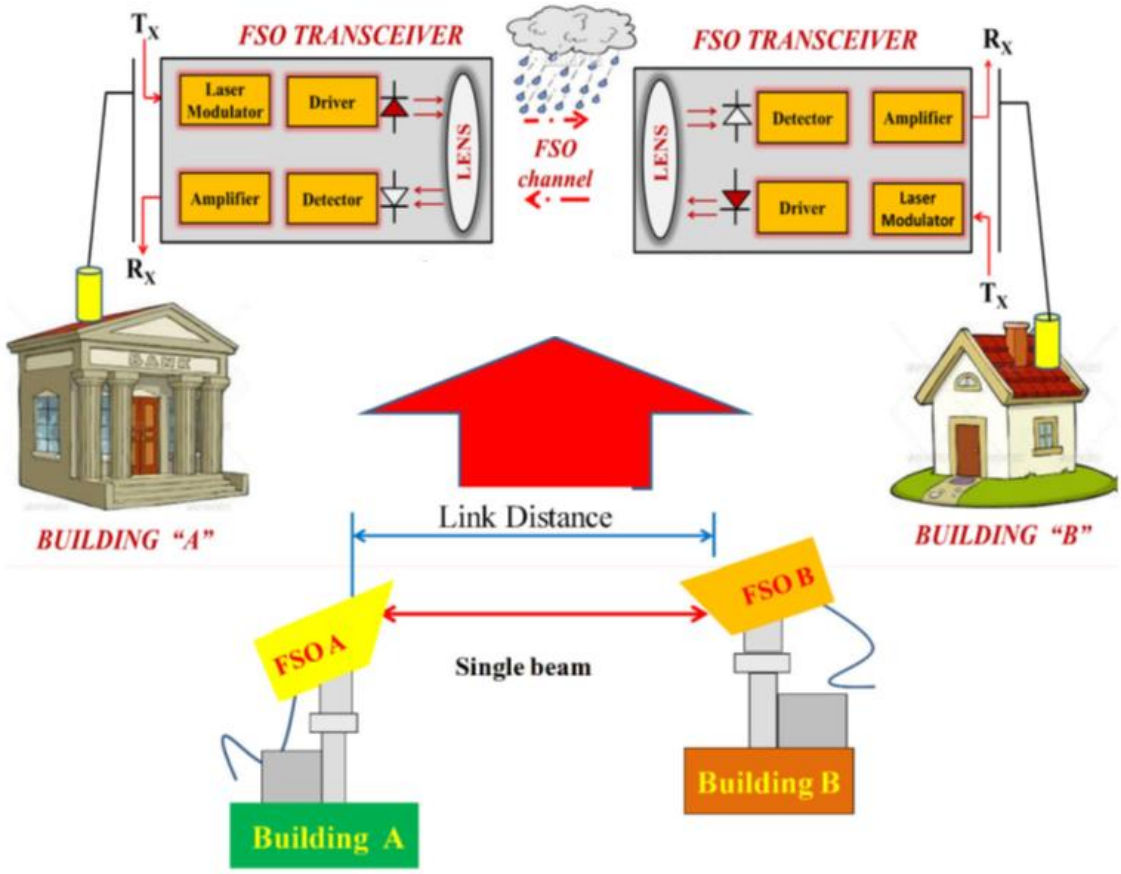

Fig. 2.10. FSO optical communication link [68]

2.7.1. ENTERPRISE/CAMPUS CONNECTIVITY

The conventional connections are being overwhelmed by the varied network traffic that is currently being experienced by businesses and college/university campuses (i.e., phone, data, fax, and multimedia traffic). Corporate and campus networks that enable ultra-high speeds can

connect several buildings with FSO systems without having to pay for separate fibre optic connections. Fig.2.11. shows campus/enterprise connectivity [68].

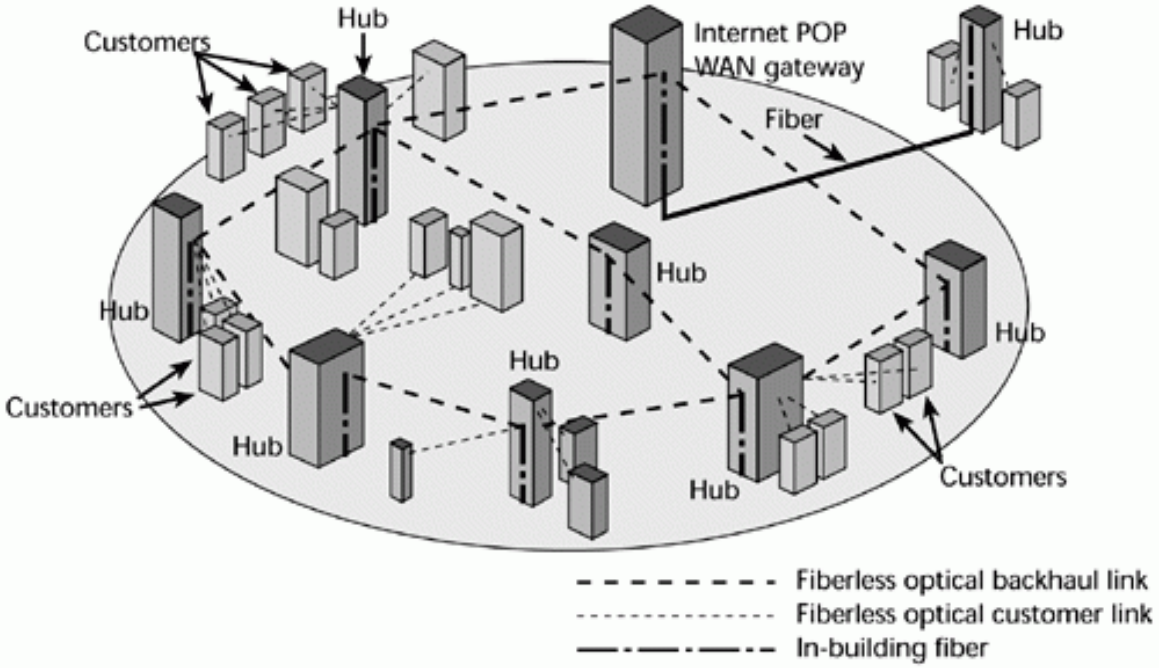

Fig. 2.11. Campus/enterprise connectivity [84]

2.7.2. VIDEO SURVEILLANCE AND MONITORING

In commercial, law enforcement, public safety, and military purposes, surveillance cameras are frequently used. Although wireless video is quick and simple to set up, traditional wireless technologies fall short of meeting the high throughput requirements for video broadcasts. An effective solution to enable high quality video transmission is FSO technology[68].

2.7.3. BACK-HAUL FOR CELLULAR SYSTEMS

In a cellular system, wire line connections, such as T1/E1 leased lines and microwave links, are frequently used between the base stations and the mobile switching centre. It is now necessary to implement technologies like FSO that allow for substantially higher throughput due to the increase in the number of bandwidth-intensive mobile phone services[69].

2.7.4. REDUNDANT LINK AND DISASTER RECOVERY

Emergency circumstances, terrorist assaults, and natural calamities all call for adaptable and creative solutions. In such catastrophic circumstances when local infrastructure may be destroyed or unreliable, temporary FSO linkages can be easily installed within hours. The

efficacy of the FSO deployment as a redundant connection was tragically demonstrated in the wake of the 9/11 terrorist attacks in New York City. For the financial corporations that were left behind without landlines, FSO linkages were swiftly implemented in this area [70].

2.7.5. SECURITY

The advent of quantum computers, for instance, would render electronic money suddenly useless because current cryptosystems can only provide computational security within the bounds of available conventional computing power. Quantum cryptography, which is based on the unchanging principles of physics, offers an entirely new approach to encryption and ensures complete security. Usually, fibre optic infrastructure is taken into account in combination with quantum cryptography systems. In situations where the deployment of fibre optics is expensive and/or impractical, FSO linkages offer a flexible substitute [70].

2.7.6. BROADCASTING

To broadcast live events like sports and ceremonies, as well as television reporting from far-flung areas and combat zones, signals from the camera (or cameras) must be transferred to the broadcasting truck, which is linked to a central office via satellite uplink. A FSO link may be used to transmit data at the needed high quality between the cameras and the vehicle. High definition television (HDTV) broadcasting applications currently have throughput requirements that can be met even by FSO lines. For instance, the UK TV station BBC used FSO lines for the 2010 FIFA World Cup to carry high quality footage between temporary studio facilities built up in Cape Town, South Africa, using Ethernet.

Several businesses, including Canon (Japan), Cassidian (Germany), fSONA (Canada), GeoDesy (Hungary), Laser ITC (Russia), Light Pointe Communications (USA), MRV (USA), Northern Hi-Tec (UK), Novasol (USA), Omnitek (Turkey), Plain tree Systems (Canada), and Wireless Excellence (UK), among others, are currently developing and manufacturing FSO systems as outdoor wireless transmission solutions [71].

2.8. DISADVANTAGES OF FSO CHANNEL

Before it reaches the receiver, the optical power released from the transmitter is impacted by a number of things. These include ambient noise, system loss, geometric loss, misalignment loss, atmospheric loss, and fading caused by air turbulence. The design parameters, which are

typically supplied by the manufacturers, have a significant impact on the system loss. The next paragraphs address losses that are included into the FSO channel.

2.8.1. GEOMETRIC AND MISALIGNMENT LOSSES

The geometric loss is brought on by the beam's divergence during atmospheric propagation. Given the divergence angle, link length, and receiver lens aperture size, it may be determined. The optical wave propagation model is a crucial component in determining the geometric loss. A useful approximation for horizontal FSO broadcasts is to think of the beam intensity as having a Gaussian profile [72]. A Gaussian beam's statistical characteristics resemble those of a point source when the divergence is reasonably big [73][83].

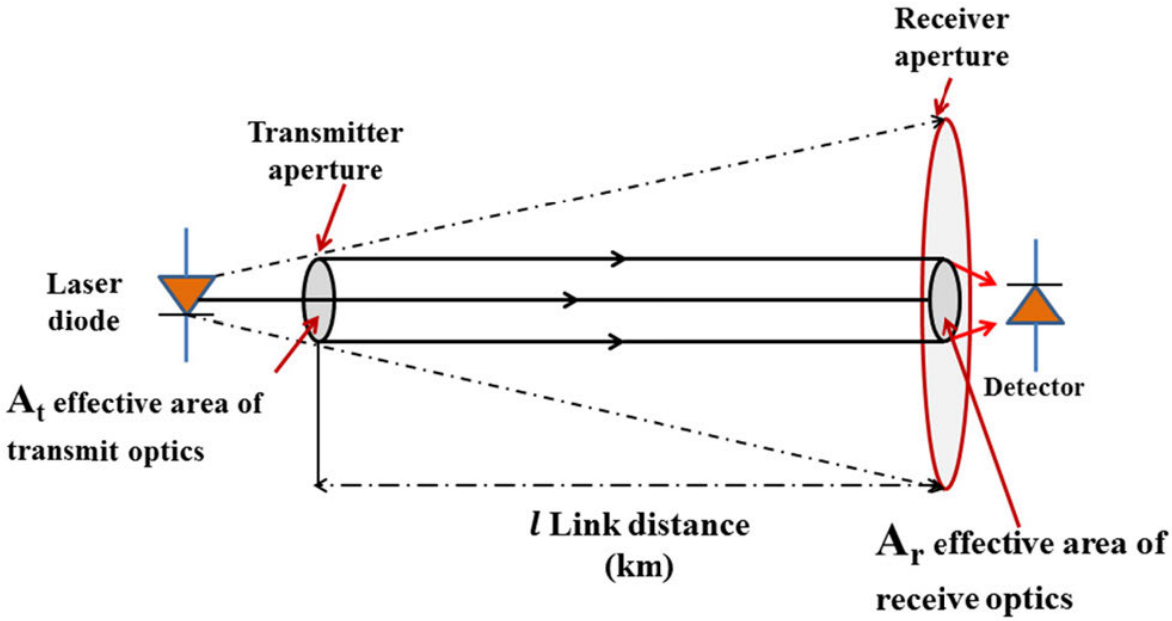

Fig. 2.12. Expanding the broadcast beam of an FSO system across open space between the transmitter and receiver [63][85]

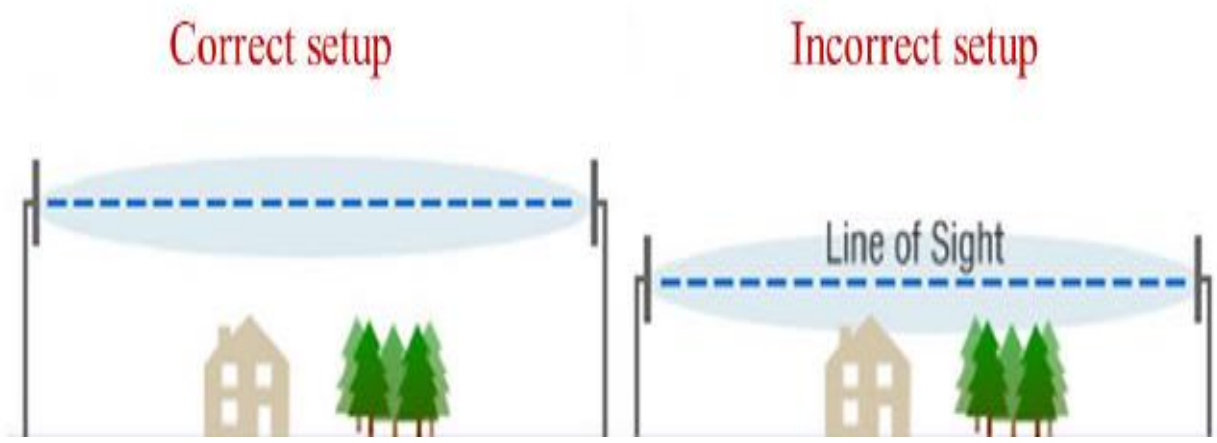

Fig. 2.13. Illustrations of how wireless antennas should and shouldn't be installed on towers [74]

The approximations of a plane wave or spherical wave can be employed successfully in this situation. The alignment of the transmitter and receiver as well as beam tracking at the reception are both impacted by the level of beam divergence misalignment happens in real life most often as a result of beam wander, structural issues with structures, or tracking system mistakes. Large-scale, non-homogeneous air eddies cause the optical beam to randomly deflect, which causes the beam to deviate from its intended path. This is known as beam wander [75,76]. For long distance routes, this phenomenon is very significant. In contrast, building sway is caused by a number of variables, such as thermal expansion, wind loads, minor earthquakes, and vibrations [77]. Building sway has the potential to effectively stop communication due to the narrow transmission beam and often short receiver field of vision (FOV). The use of automated pointing and tracking at the receiver becomes important over long distances (i.e., one kilometre or more), since a narrower beam should be employed to avoid suffering from a significant geometric loss, in order to eliminate or limit the consequences of pointing mistakes. Fig. 2.12. shows expanding the broadcast beam of an FSO system across open space between the transmitter and receiver. Fig. 2.13 depicts an illustrations of how wireless antennas should and shouldn't be installed on towers. Fig .2. 14 reveals the building swaying effect towards an FSO system.

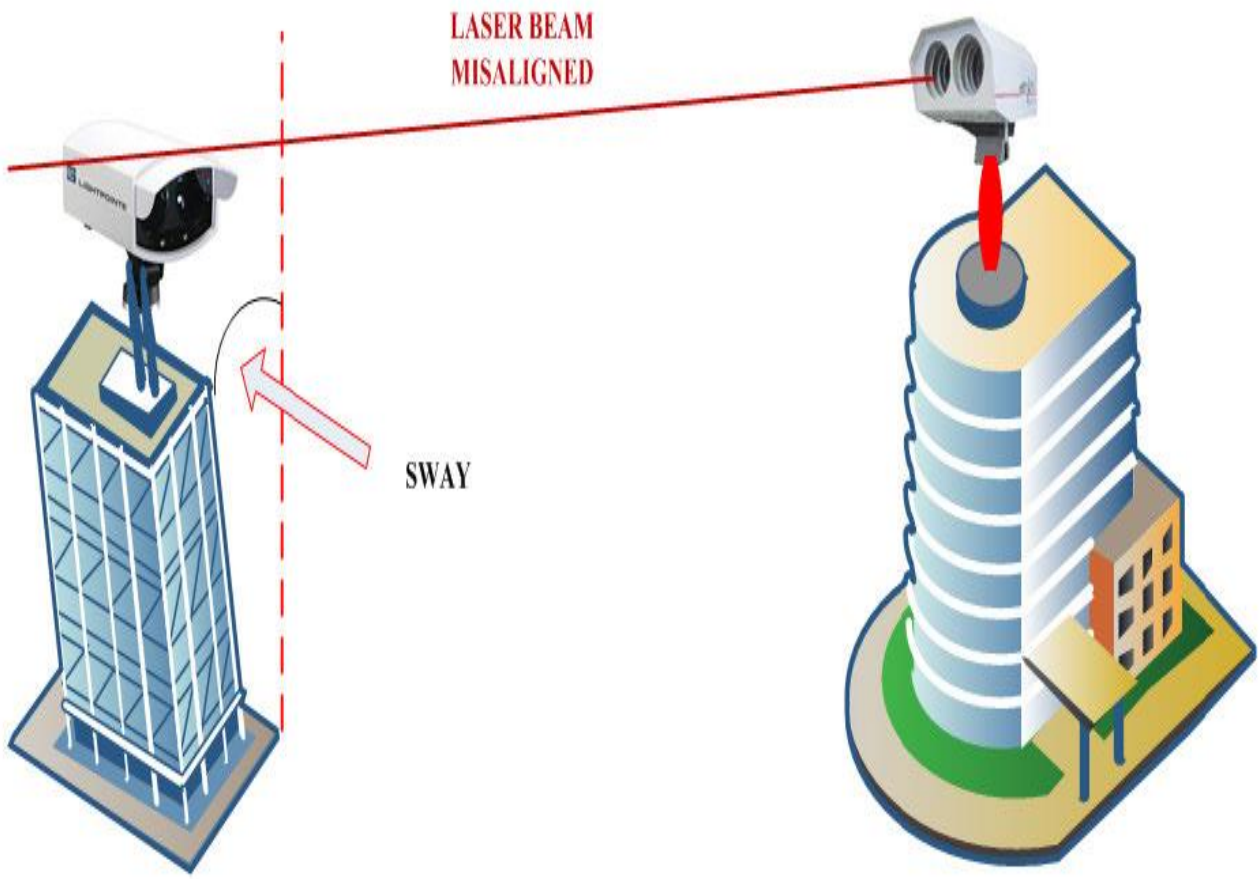

Fig. 2.14. Building swaying effect towards a FSO system [77].

2.8.2. ATMOSPHERIC & OBSTRUCTION LOSS

In the visible and near-IR wavelength ranges, the physics and transmission characteristics of the radiation penetrating the atmosphere are extremely similar. As a result, visibility may also be used to describe particles that scatter or absorb near-IR radiation. Rain, snow, and fog are examples of the particles that can reduce visibility, but they also include pollution, dust, aerosols, smoking, etc. They partially absorb the energy of the laser light, which reduces the optical power. Water vapour plays a major role in near-IR absorption [78].

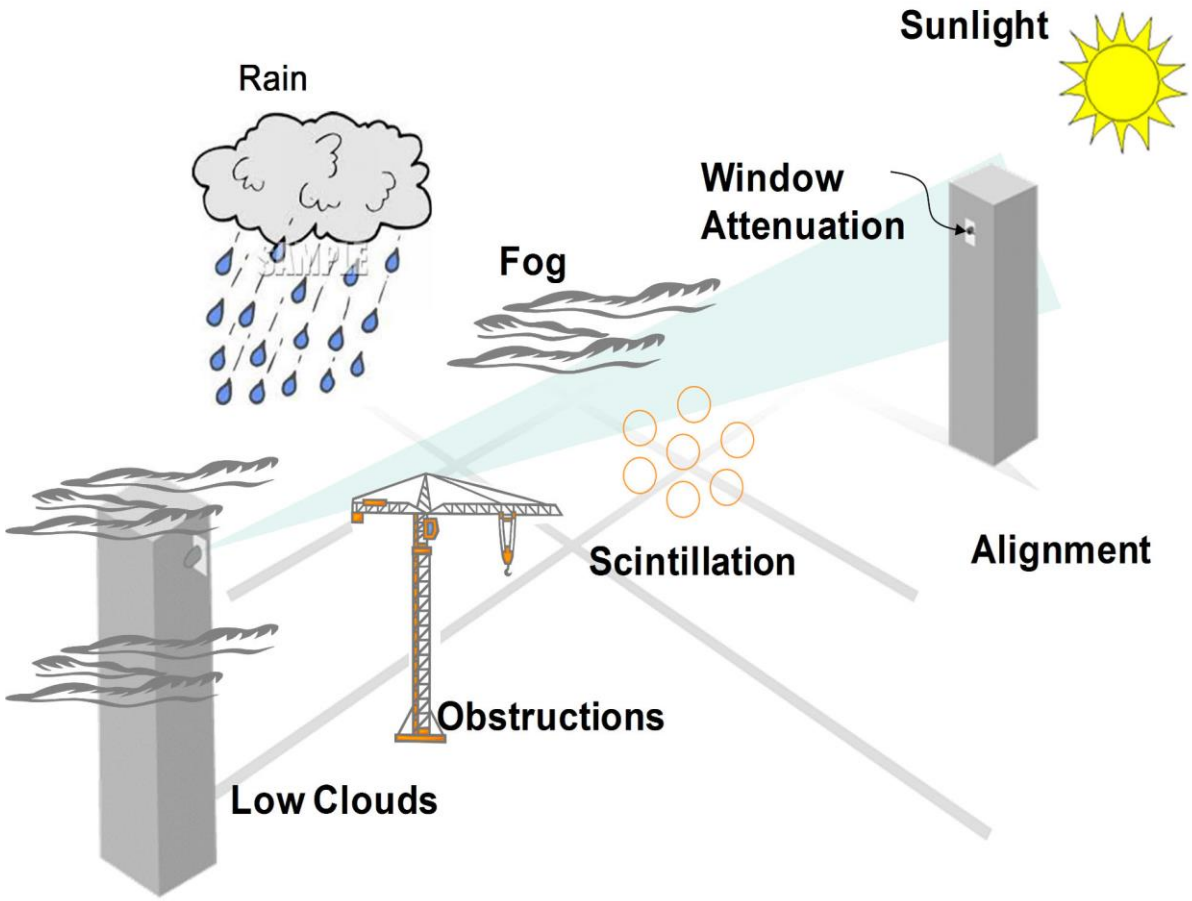

Fig. 2.15. Different physical and weather condition effect on FSO link [79,80]

They produce spatial, angular, and temporal dispersion by inducing light scattering, which is the deflection of incoming light from its initial direction. Any obstruction between the transmitter and receiver is also harmful for the system. Fig 2.15. shows the different physical and weather condition effect on FSO link.

2.9. CONCLUSION

It is very obvious from this chapter that a sound theoretical foundation has been offered. The principle of the FSO technology as well as its specific construction are both presented in this chapter. This chapter also discusses the system's drawbacks, benefits, and potential uses. With the help of this chapter, a rudimentary theoretical understanding of the optical power attenuation level of the FSO communication system under various atmospheric anomalies has been gained.

CHAPTER 3
EXPERIMENTAL SETUP

3.1. INTRODUCTION

To evaluate the performance of different wavelengths for FSO system in the different atmospheric conditions, artificial atmospheric simulation chambers have been developed in Illumination Engineering Laboratory of Electrical Engineering Department. The most hazardous and common natural elements to affect FSO system are rain, fog, temperature rise, snow, dust, etc. Here, effect of rain, temperature rise, and fog have been tested. Fig. 3.1. depicts the classification of artificial atmospheric simulation setup.

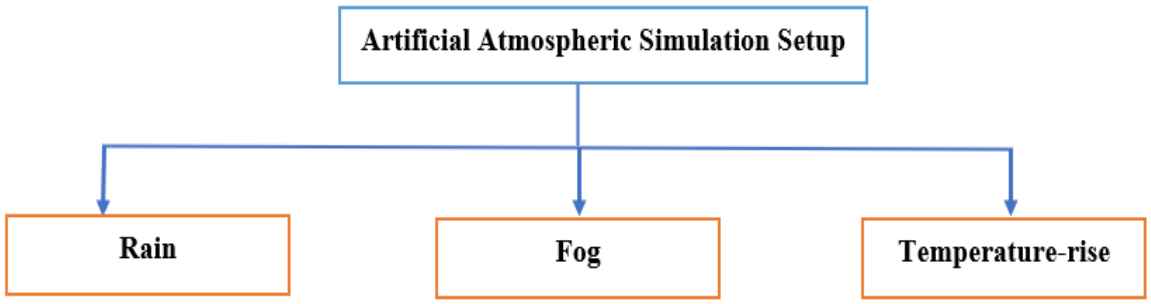

Fig .3.1. Classification of artificial atmospheric simulation setup

Similarly, set up of artificial atmospheric simulation chamber has been developed to test the Free Space Optical (FSO) Communication channel through. For FSO channel establishment, two essential parts have been developed that is transmitter section and receiver section. The classification of the FSO channel parts is given in the Fig. 3.2.

Fig.3.2. Classification of FSO channel parts

3.2. RAIN SIMULATION CHAMBER

This developed artificial rain simulation set up has been established on the roof of the Electrical Engineering department, thus the entire experiment is conducted outside, exposed to the sky. The construction is composed of 6 mm diameter pure iron rods and is shaped like a rectangular hollow box with a length of 20 ft., a width of 3.5 ft., and a height of 10 ft. Three 20 ft. long PVC pipes are installed to the rod at the top of the iron structure. For the experimental

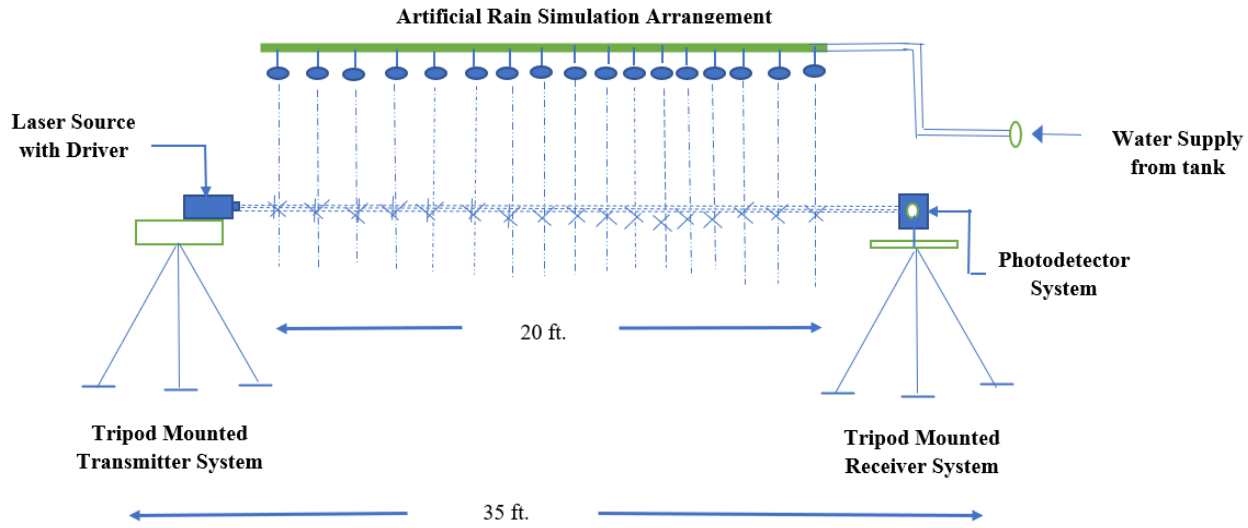

Fig. 3.3. A schematic layout of rain simulation setup

purpose each pipe is drilled with the help of the drill machine. Each pipe has a different diameter of the holes made by the drill machine. As a result, different types of rain rates can be obtained through this arrangement There are gardening nozzles installed at a distance of 1 ft. and each nozzle provides water from two directions. Fig 3.3 shows the schematic layout of rain simulation setup.

Fig. 3.4. Artificial Rain Simulation setup

The PVC pipelines and nozzle pipelines are well fixed with iron structure with the help of cable tie. Through the use of a motor-pump, water was delivered to the pipe from a tank. Fig. 3.4. shows the actual artificial Rain Simulation setup. The transmitter and receiver are placed 7.5 ft. from the artificial rain setup, so as to primary protect the laser and its module and other instruments which are used in this experiment. Different rain rates (low to high) are created by this arrangement like 6 mm/hr to 180 mm/hr. Rain rates are measured by a standard rain gauge.

3.3. FOG SIMULATION CHAMBER

The proposed fog chamber has been made up of plywood of thickness 0.5 inch. The dimension of each chamber is around 1.5 ft. in height and 3.3 ft. in length. Initially, six chambers have been connected serially with above mentioned dimension that means; 20 ft. length is achieved whose height is 1.5 ft. Each section of the chamber has three small windows, two window attach on both side and one window attach top of the chamber of each section. The dimension of each window is around 1 ft. length and 0.5 ft. in height. Each window is made up with glass. Each section of the chamber is attached with gasket, as a result no air or fog is leaked from the chamber. Fig. 3.5 shows the schematic layout of fog simulation setup.

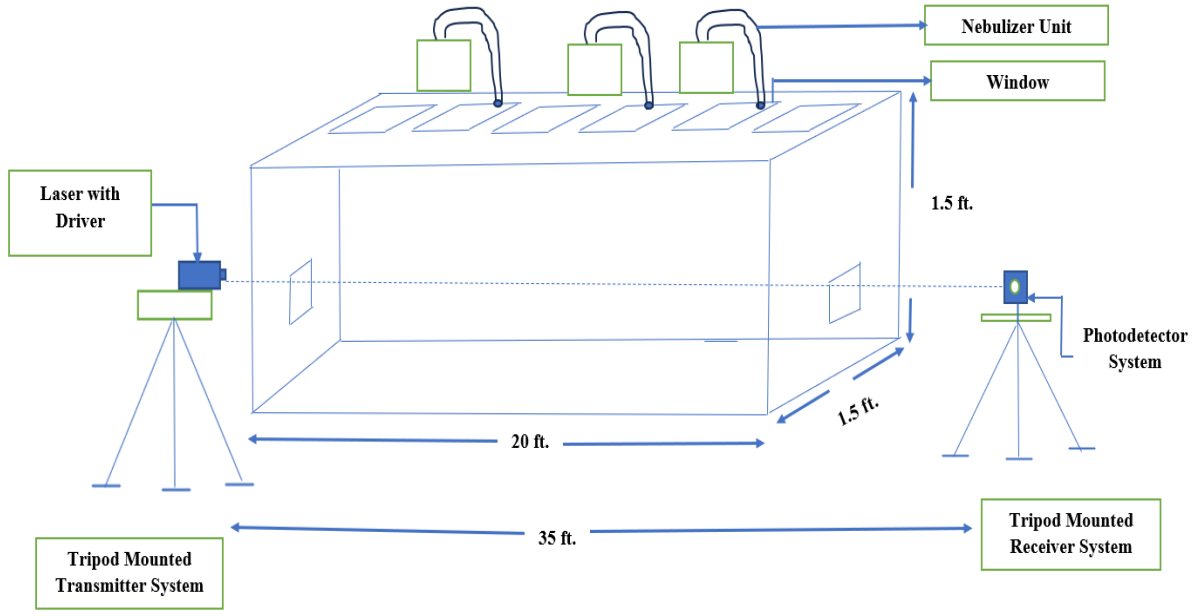

Fig. 3.5. A schematic layout of fog simulation setup

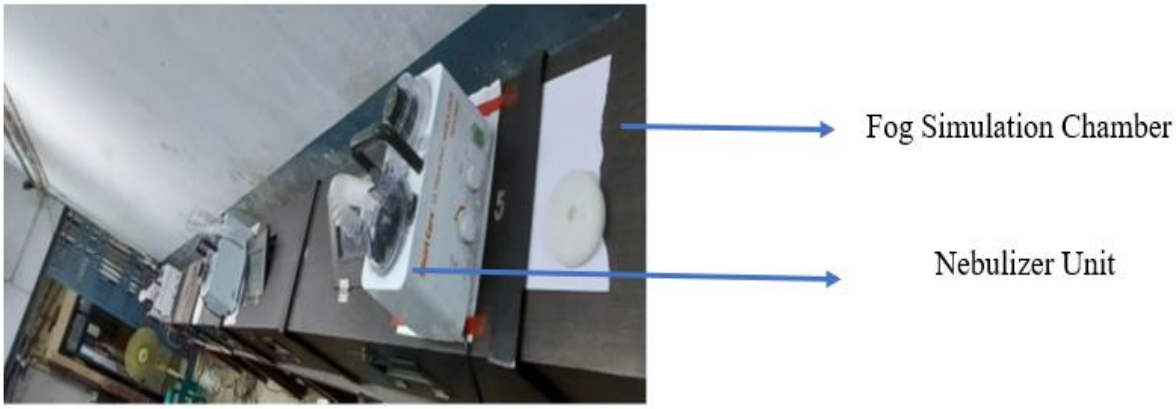

Fig3.6. Artificial fog simulation chamber

Fig.3.6. shows the artificial fog simulation chamber. Three nebulizers are installed on top side of the wooden box. To simulate the natural fog, Nebulizer is used. With the help of the speed controlling button of the nebulizer, the amount of fog for the experiment is changed. Different types of fog like thin fog, light fog, moderate fog, light haze, haze, thick fog and dense fog are produced with the help of the speed controlling button of the nebulizer. A nebulizer uses normal water to produce the fog, natural fog had been produced because particle of the fog was made with water.

(a) (b)

Fig.3.7. Different visibility conditions inside the chamber (a) lower & (b) dense visibility

Fig. 3.7. shows the different visibility conditions inside the chamber at lower and dense visibility conditions.

3.4. TEMPERATURE SIMULATION CHAMBER

For this setup six hollow wooden boxes were made. Each of the six boxes is 3.3 feet in length, 1.5 feet in width and 1.5 feet in height. Out of six boxes this design has been made for the four boxes in the middle which are completely open two sides and other three sides out of four sides have one glass window on each side. Remaining one side of the wooden box is completely closed because that side is placed on the wooden bench. Each glass window are 1 feet in length, 0.5 feet in width and 0.25 feet distance from edge to edge of three sides. The other two boxes on the extreme side have the same design, one side of the box is completely open and the exact opposite side has a square shape glass window of which each side has 0.25 feet. When all the boxes are merged, then these two windows of the two sides work as inward and for outward way of Laser rays. Each small box is numbered for the convenience of the experiment. Outside of every small box is coated with sun-mica and inside of the box is painted with heat-resistant black color to prevent any unexpected stray light incidents during the experiment as well as glass to these windows also resist the heat. Each small box is completely attached as well as aligned to the other box and in order to prevent the movement of the air through the sticking parts, the boxes are fully air sealed by using gas blocking strip. As a result, the outside weather cannot affect during the experiment. For this system setup we obtained the results of our experiment with more accuracy. Three coils with the power rating of 1500W each were used. Fig. 3.8. shows the schematic layout of rising temperature simulation setup.

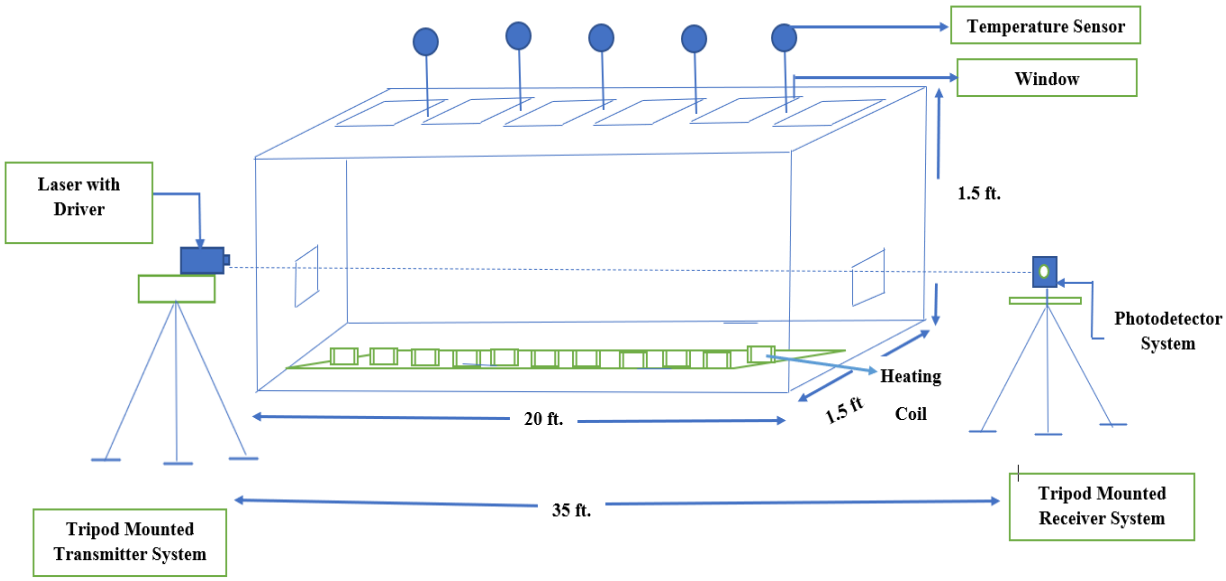

Fig.3.8. A schematic layout of rising temperature simulation setup

The end terminals of each of the coils were connected with separate AC Voltage source and a separate variac. Due to flow of the current, heat was produced in the coils as per the Joule's law. Temperature difference between the two ends of the wooden box was made by using two different combinations of coils. At one end two coils were connected in series and at the other end one separate coil was placed. This temperature difference results the variation in refracting index of the air inside the box along vertical direction. Generally, the refractive index parameter structure (c_n^2) value remains between 10^{-12} to10^{-15} inside the chamber. A digital thermometer was installed in the top side glass window of each box. The temperature of the main core focused region was optimized for the experiment by increasing or decreasing the voltage with the help of the variac by observing the temperature of the digital temperature. Fig 3.9. shows the artificial temperature simulation chamber.

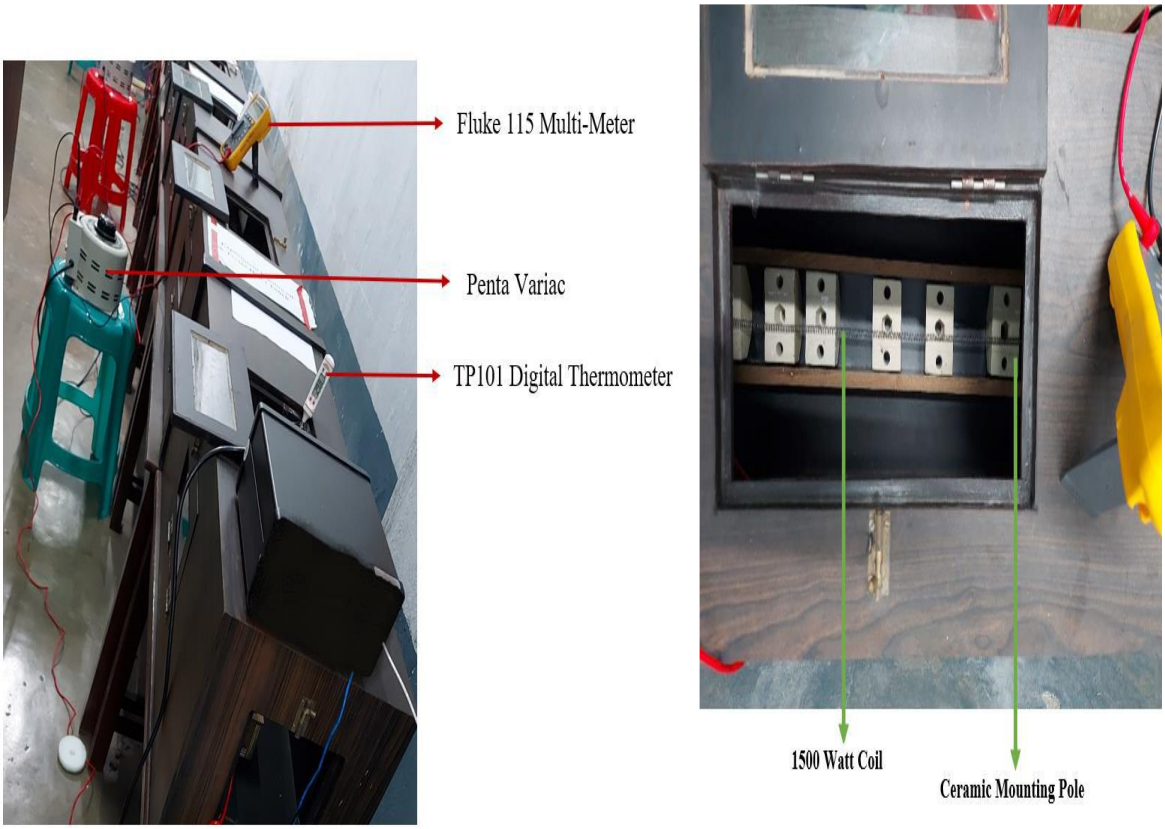

Fig. 3.9. Artificial temperature simulation chamber

3.5. FSO COMMUNICATION CHANNEL SETUP

In general, Laser beam can be modulated by two techniques, Direct modulation, and external modulation. Fig. 3.10 shows the classification of modulation techniques.

Fig. 3.10. Classification of Modulation techniques

3.5.1. DIRECT MODULATION

Direct modulation is a type of modulation used in optical communications where the optical power output of a source is changed depending on some property of the modulating signal. The modulating signal is often recovered by direct detection.

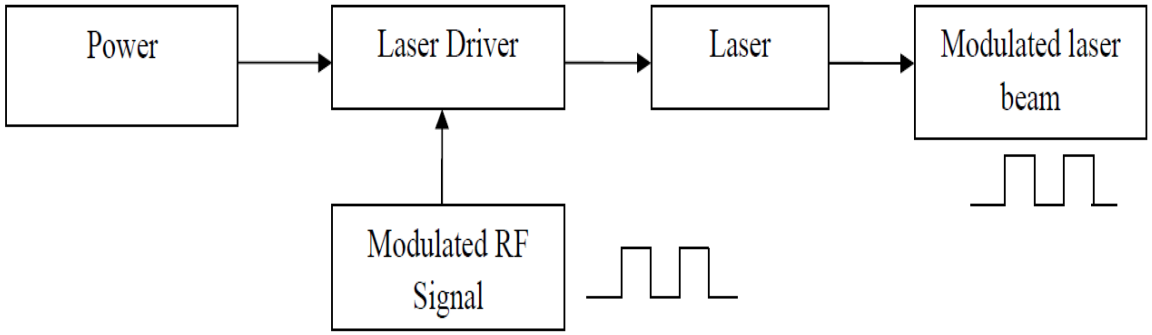

Fig. 3.11. Schematic of direct modulation technique

However, a proper dc power supply is given to Laser driver to drive Laser source. A modulated RF signal is also fed to the Laser driver. According to this Modulated signal, the laser beam is also varied. Here Laser beam acts as a carrier. This modulated Laser beam is propagated through free space to the photo detector. Fig 3.11. shows the block diagram of direct modulation of Laser communication.

3.5.2. ESTABLISHMENT OF DIRECT MODULATION TECHNIQUE

The Laser driver switches the DPSS Laser in accordance with the incoming TTL signal using the modulated TTL output from the Arbitrary waveform generator. The Laser driver comprises of MOSFET driver and a MOSFET unit which is used the switching the Laser module. Fig. 3.12. shows block diagram of FSO Data Communication Channel.

As the AWG is provided the TTL signal to the MOSFET Driver and the MOSFET is connected according to the MOSFET driver, as a result the MOSFET is on off, according to the TTL input signal. Mainly, Intensity Modulation has been done by this process. The modulated Laser beam is transmitted through a beam expander. The main functioning of the beam expander is reduced the optical beam expansion at the receiver side according to its magnification factor.

Through this conduit, the optical beam can reach the appropriately positioned photo detection equipment. The Trans-impedance amplifier stage comes after the photo detector system and amplifies as well as transforms the input current level from the photo detector to the appropriate voltage level, whose operating frequency and slew rate are selected in accordance with the frequency of the signal. A convex lens should be used for the longer range operation to reduce the beam expansion loss and collimate the laser beam accordingly.

The collimated Laser beam is fall into the photodetector unit and signal is processed as per block diagram and finally, the output signal has been captured from the comparator and transimpedance side through a Mixed Signal Oscilloscope (MSO), model no. MSOS054A, Keysight. The optical signal power has been measured by an Optical power meter, Ophir, Vega.

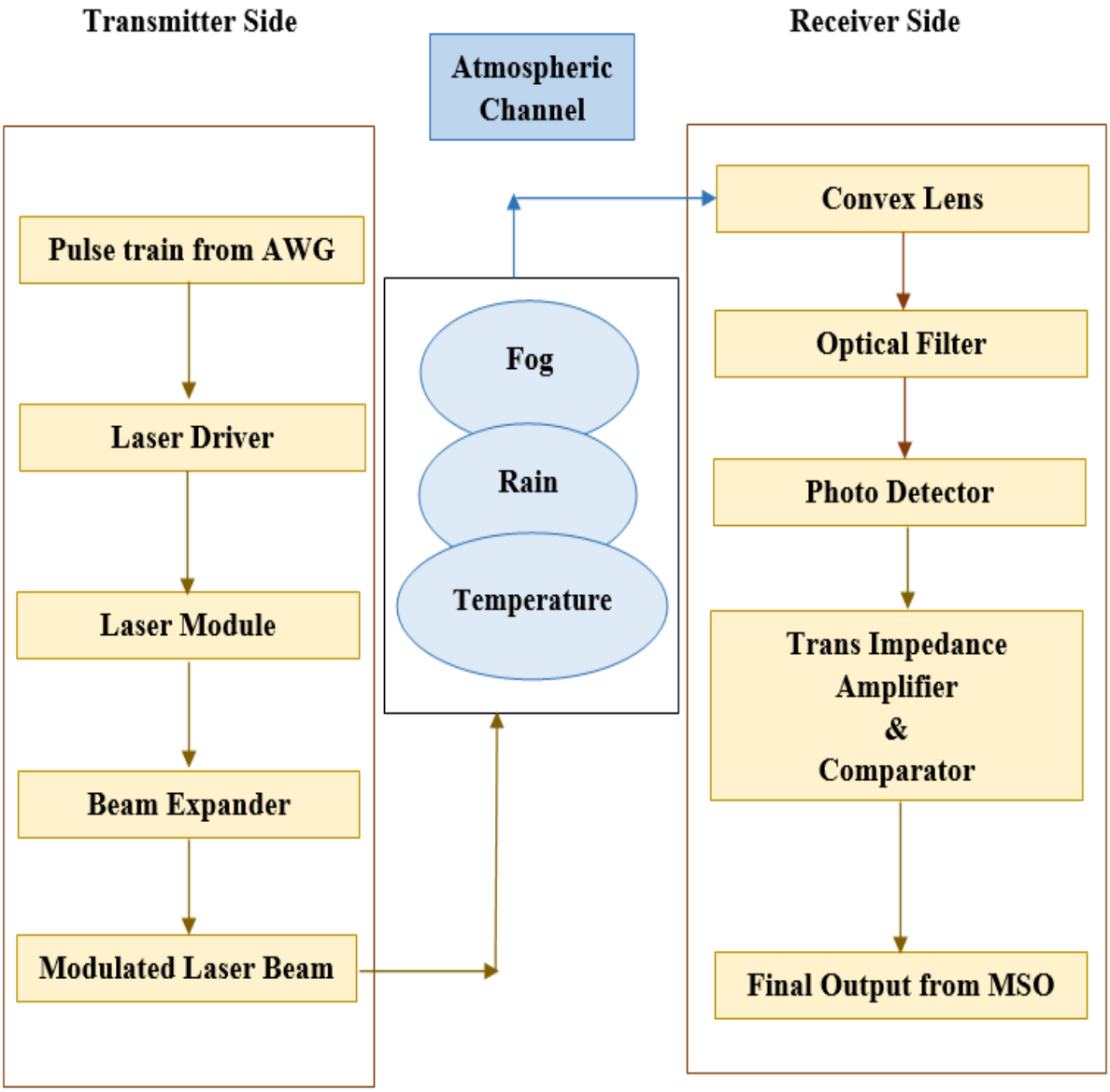

Fig. 3.12. Block diagram of transmitter and receiver side with direct modulation technique

3.5.2.1 TRANSMITTER UNIT OF DIRECT MODULATION TECHNIQUE

The 5 V supply is provided to the MOSFET driver circuit and a TTL signal is provided as a input to the MOSFET driver (through a BNC connector BN1) with respect to ground, the output of the driver (TTL Pulses) is provided to the gate of the MOSFET through a resistor. The source of the MOSFET is grounded and the output from the drain is connected to the one pin of the two pin connector (CN2) unit. Another pin (CN2) is connected to the 5V supply.

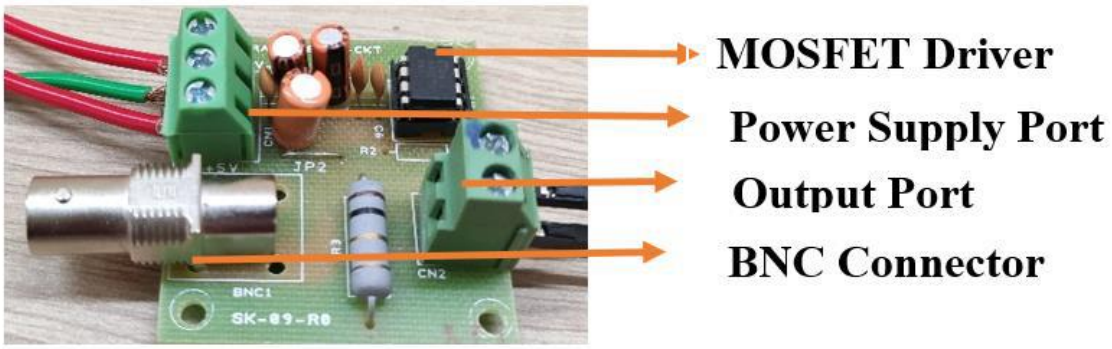

Fig. 3.13. MOSFET driver circuit for direct modulation technique

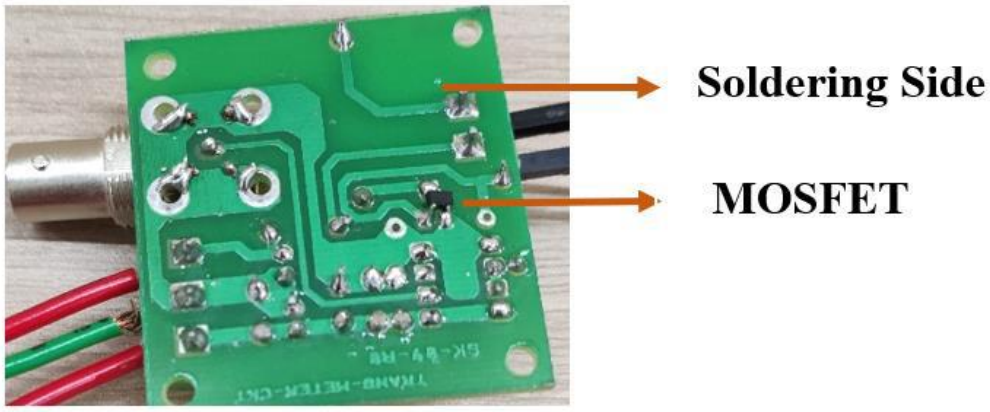

Fig. 3.14. Soldering part of the MOSFET driver circuit

According to the TTL pulses is coming from the MOSFET driver, the MOSFET works accordingly. The output has been tapped from two port connector (CN2) which is fed to the LASER module. According to the output, the LASER is switched on off accordingly. Fig.3.13. and Fig. 3.14 show the transmitter side MOSFET driver circuit and soldering part of the circuit. Fig.3.15. (a) shows the schematic layout of MOSFET driver circuit (Laser Driver).

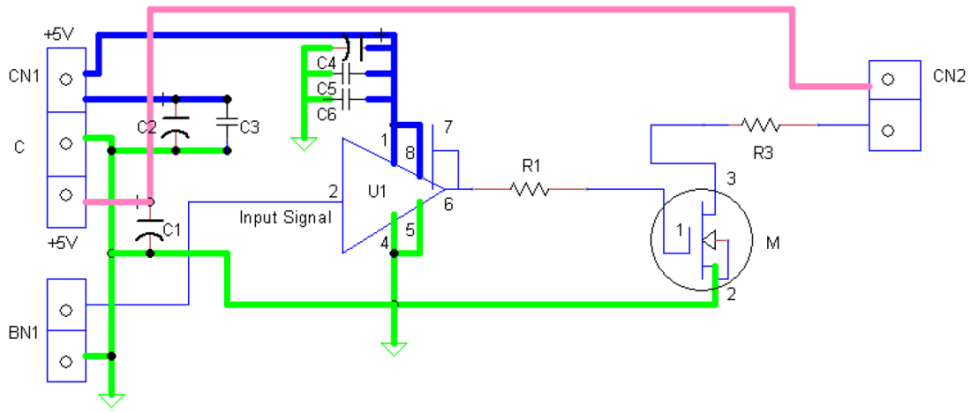

Fig. 3.15.(a) Schematic layout of MOSFET driver circuit (Laser Driver)

The experimental setup of the transmitter using 532 nm and 638 nm has been demonstrated in the Fig. 3.15 (b), Fig. 3.15. (c) respectively.

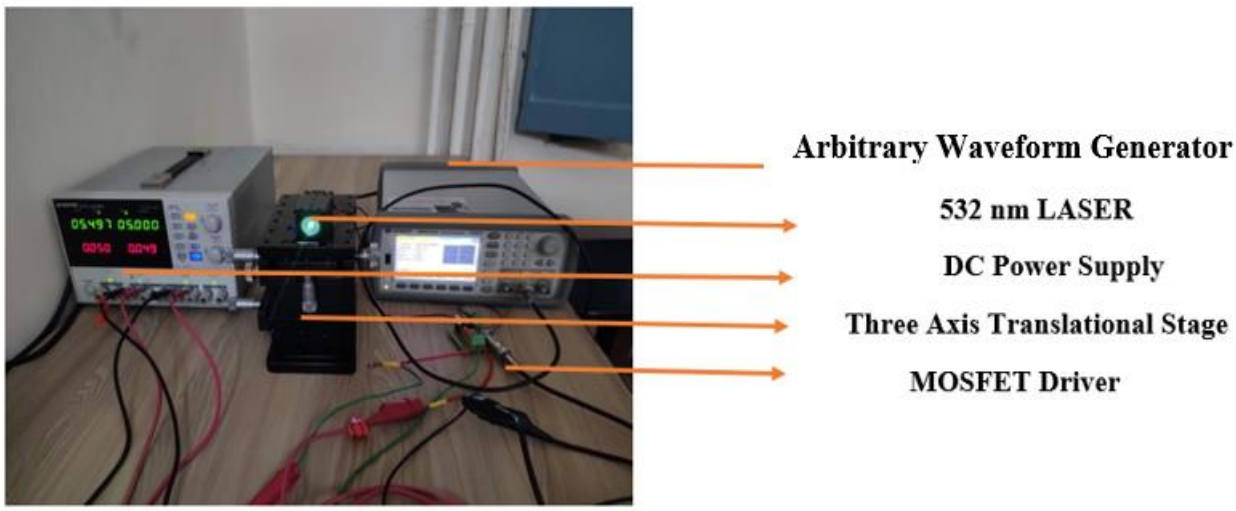

Fig. 3.15.(b) Transmitter side using 532 nm LASER source

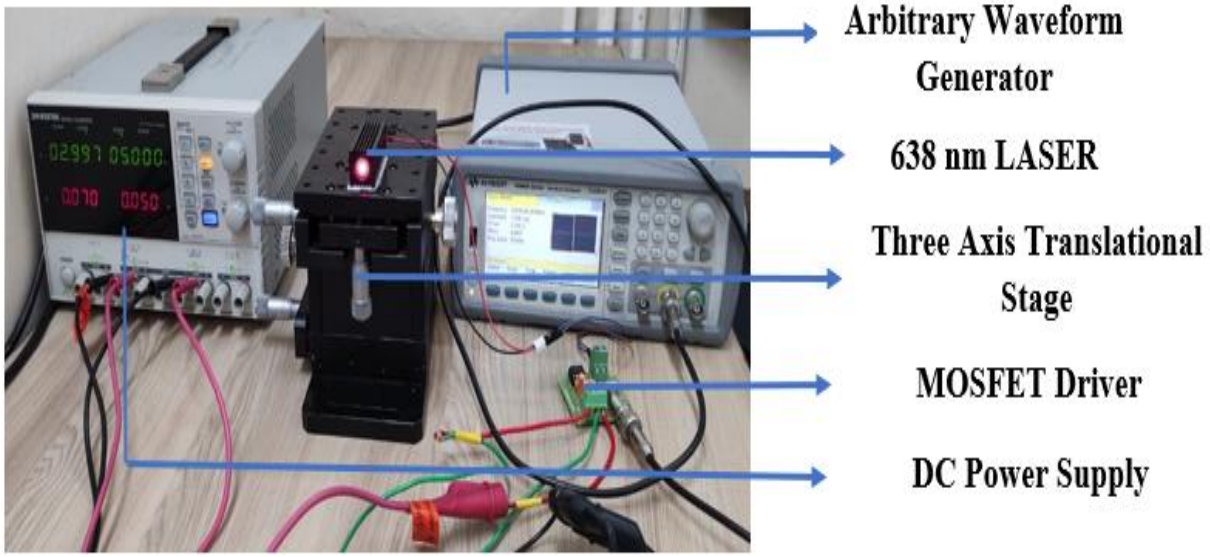

Fig. 3.15.(c) Transmitter side using 638 nm LASER source

The experimental setup of the transmitter using 808 nm and 980 nm has been demonstrated in the Fig. 3.15 (d), Fig. 3.15 (e) respectively.

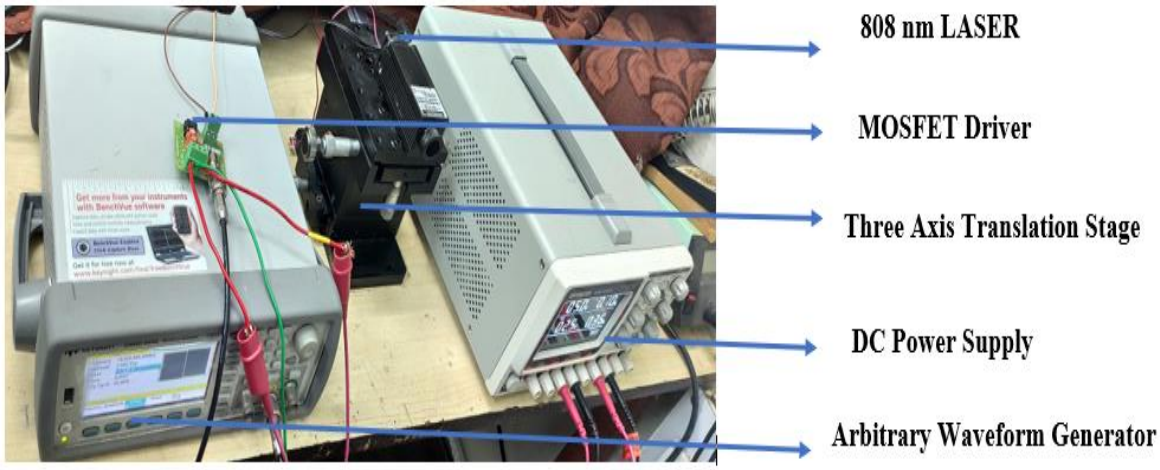

Fig. 3.15.(d) Transmitter side using 808 nm LASER source

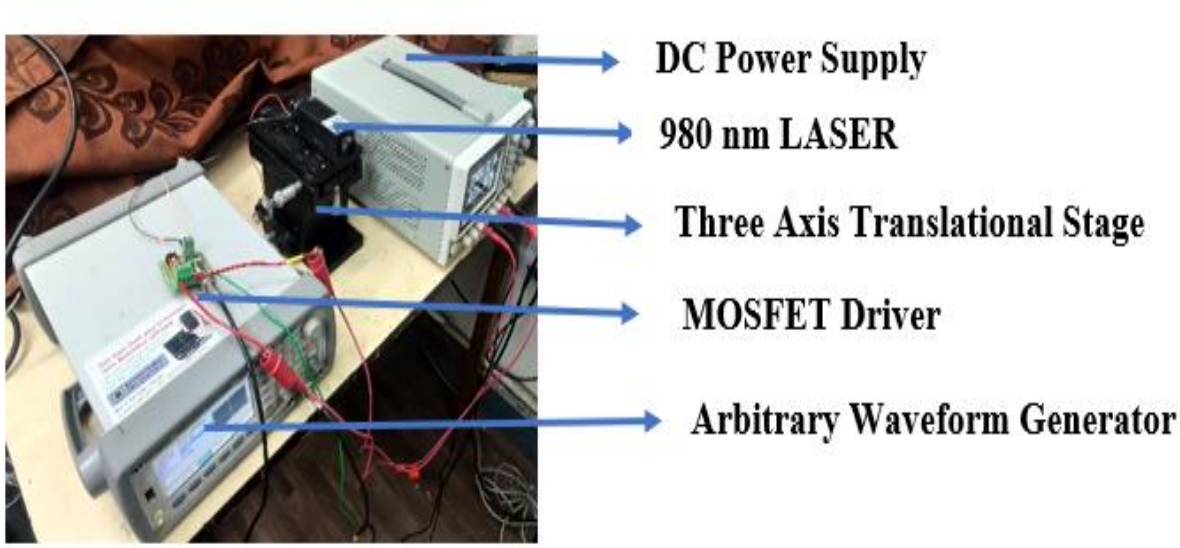

Fig. 3.15.(e) Transmitter side using 980 nm LASER source

3.5.2.2. RECEIVER UNIT OF INTERNAL MODULATION TECHNIQUE

The trans-impedance amplifier is used for amplify the captured photodetector signal and convert the photodetector current signal into voltage signal. The photodetector signal (PD IN) is fed to the inverter terminal of the U1A which is a high speed op-amp. The value of R3 and C10 has been chosen according to the bandwidth requirement of the system. As the

photodetector signal is fed to the inverting terminal of U1A, the signal is inverted. This inverted signal is not comparable with comparator unit, so, this signal is inverted in another stage (U1B), as a result this amplified signal is similar of photodetector signal (PD IN) which was not the amplified signal. The second stage has been configured as a unity gain. This signal is fed to the high speed comparator (U2) non inverting side, and a minimum threshold value is set for the accurate operation of the comparator. Two voltage regulator has been used U3 and U4 for positive supply regulator and negative supply regulator respectively for proper functioning of the U1A, U1B, U2 respectively. Fig.3.18. shows Schematic layout of the trans-impedance amplifier and fig.3.16. shows Trans-impedance and comparator unit and fig.3.17 shows soldering part of transimpedance with comparator circuit.

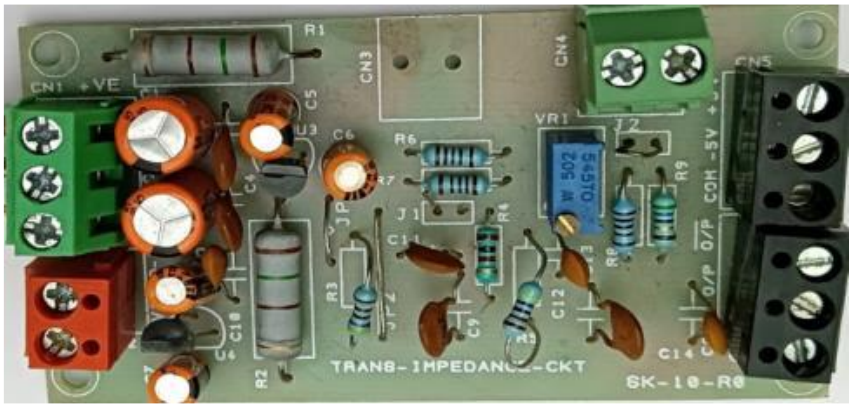

Fig. 3.16. Transimpedance with comparator circuit

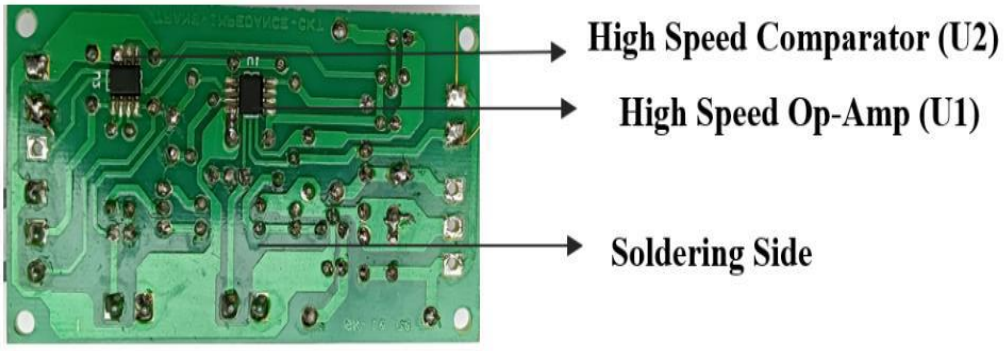

Fig.3.17. Soldering part of trans-impedance with comparator circuit

Fig. 3.18.(a) shows the schematic layout of the trans-impedance amplifier with a comparator circuit. Similarly, Fig. 3.18.(b), Fig. 3.18. (c), & Fig. 3.18. (d) show the receiver side unit of 532 nm, 638 nm, 808 nm & 980 nm respectively.

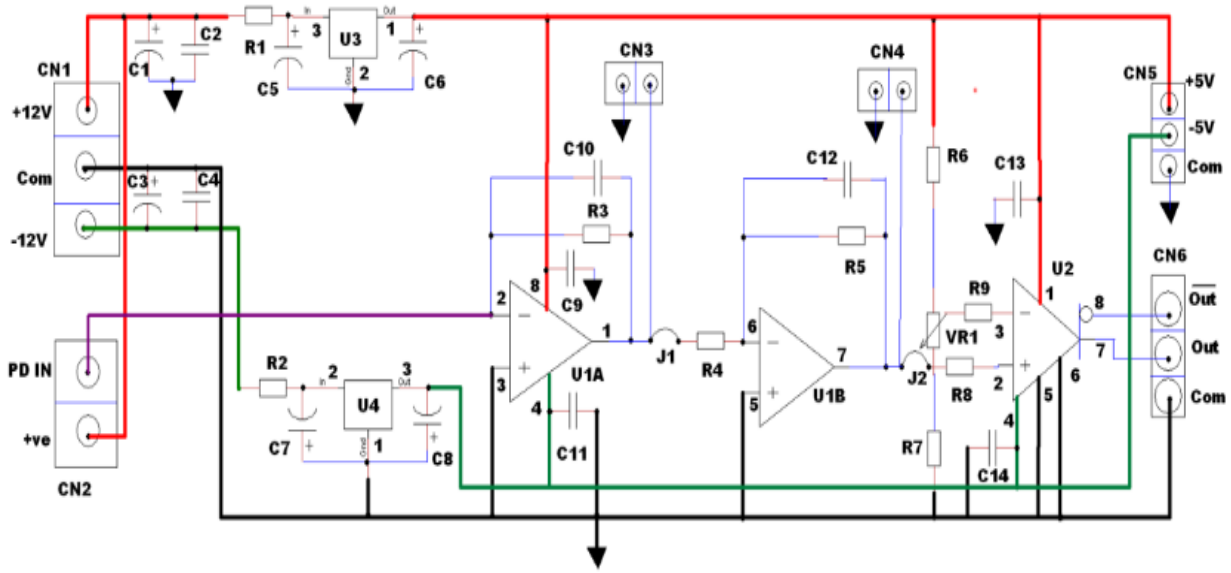

Fig. 3.18. (a) Schematic layout of transimpedance with comparator circuit

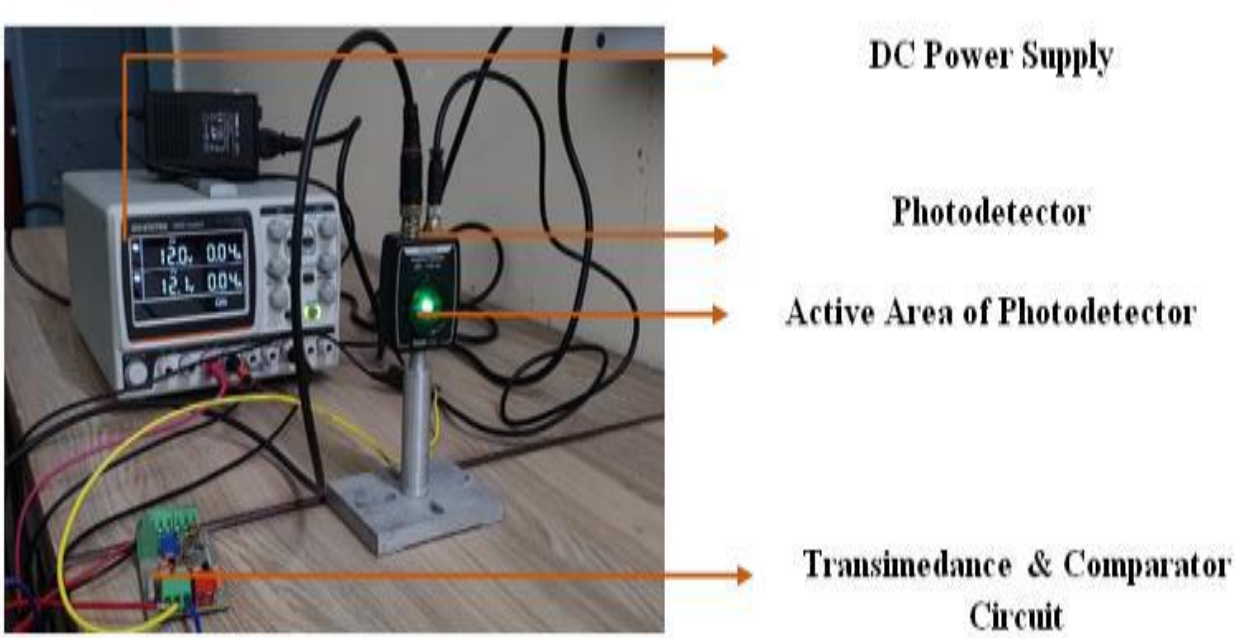

Fig. 3.18.(b) Receiver side for 532 nm LASER

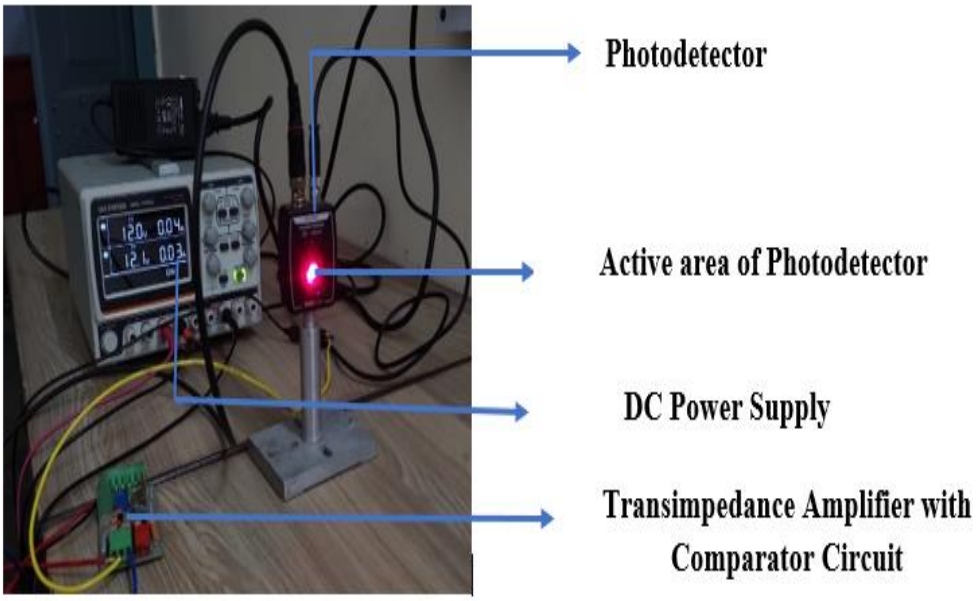

Fig. 3.18.(c) Receiver side for 638 nm LASER

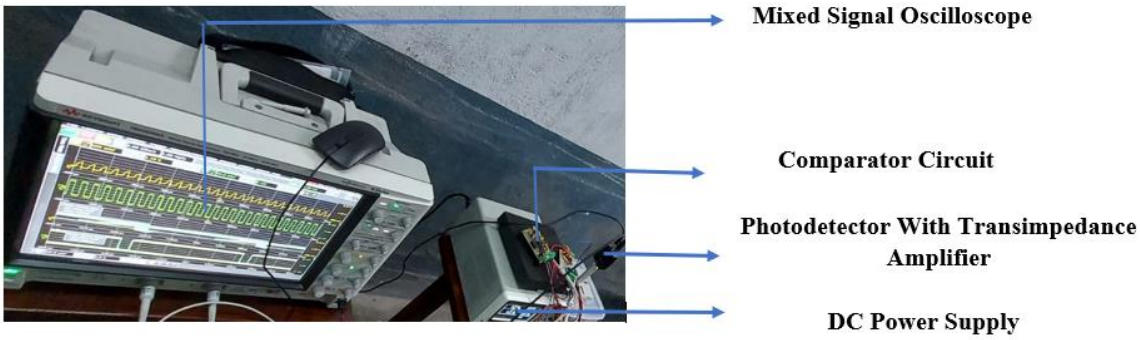

Fig. 3.18. (d) Receiver side for 808 nm & 980 nm LASER

3.6. EXTERNAL MODULATION

In general, three types of external modulator are observed, that is Acousto Optic Modulator, Electro Optic modulator, and Electro-absorption modulators. Different external modulator units and their features are given in the Table 3.1.

Table 3.1. Different External modulator units and their features

Sl. No.	Name of External Modulator Unit	Features
1.	Mach-Zehnder interferometer / Electro Optic Modulator	Fiber-coupled mode and free space, both modes are available, Insertion loss generally high, typically 4-5 dB, modulation bandwidth generally very high 100 Gbps, optical power handling capability low [61,62,63].
2.	Acousto-Optic (AO) Modulator/ Bragg Cell	Two types of mode are available: fiber-coupled mode or free space mode (without fiber-coupled), insertion loss is typically 3 dB, handle relatively high optical power, bandwidth generally 1 Gbps [64,65].
3.	Electro-Absorption Modulator's	Low drive voltage required (typically 2V), it provides higher data rates (50 GHz) with the low noise level and from the large quantity of production point of view, it is very cost-effective.[62]

However, a proper dc power supply is given to Laser driver to drive Laser source. This Laser source gives the continuous laser beam output. But this Laser beam must be modulated for data communication.

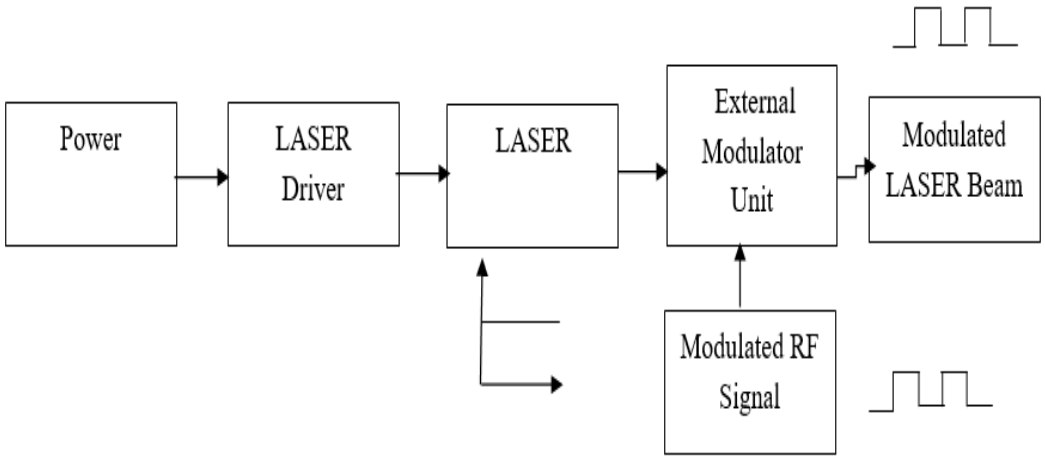

Fig. 3.19. Block diagram of the external modulation schemes

This continuous beam is fed to the external modulator unit which is a signal-controlled element is used to modulate a beam of laser light. In this way Laser beam is modulated externally. Fig. 3.19. shows the block diagram of external modulation of Laser communication.

3.6.1. ESTABLISHMENT OF EXTERNAL MODULATION TECHNIQUE

The total link establishment setup is shown in Fig. 3.20 with transmitter and receiver part for external modulation scheme.

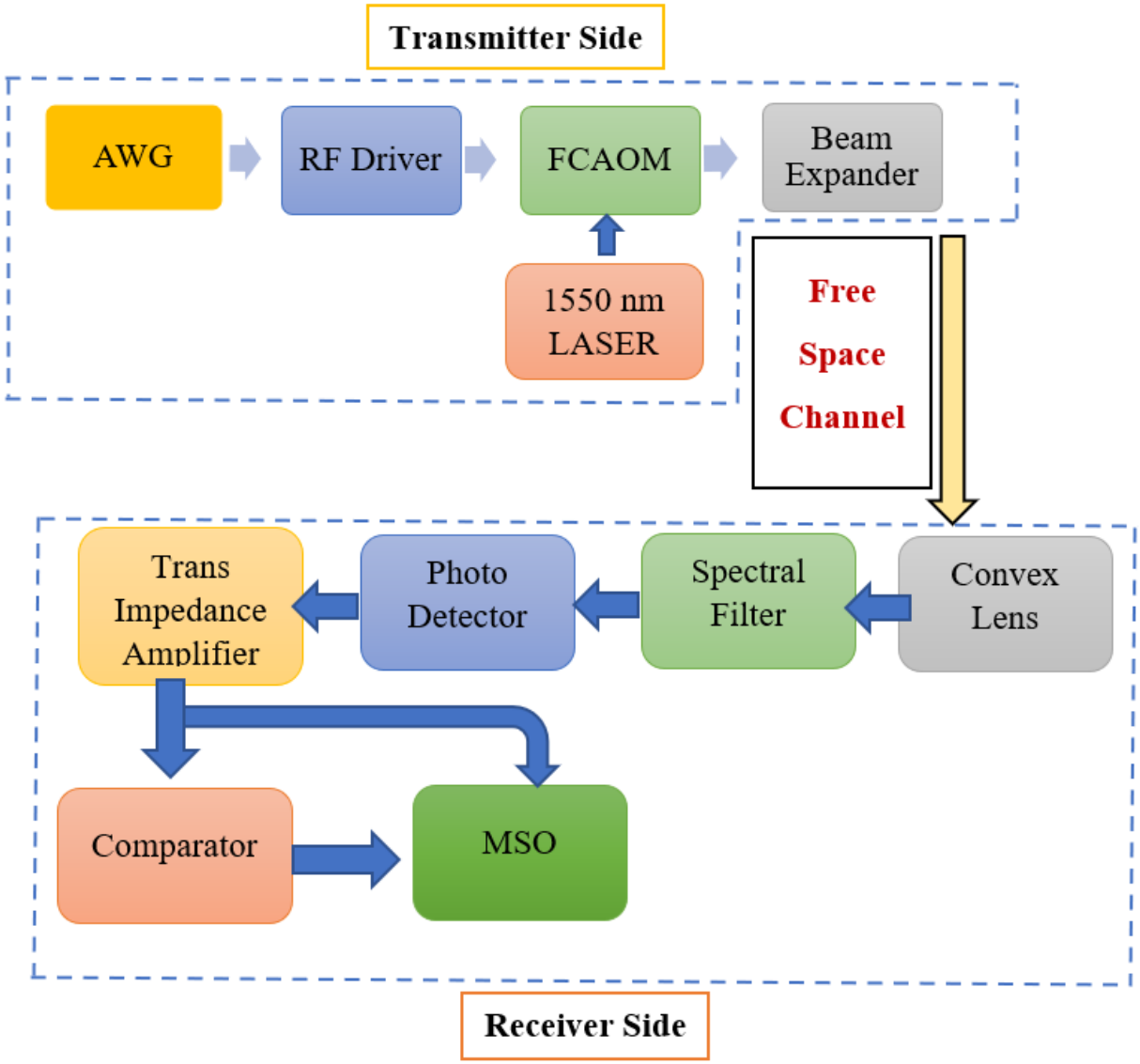

Fig.3.20. Block diagram of the transmitter and receiver part of external modulation scheme

3.6.1.1. TRANSMITTER SIDE OF EXTERNAL MODULATION TECHNIQUE

In order to establish the FSO link a transmitter and a receiver is required. The main components of the transmitter side comprise of an Arbitrary Waveform Generator (AWG), a Radio Frequency (RF) driver, a FCAOM, a beam expander and a 1550 nm fiber Laser. Message signal produced by AWG is modulated with carrier wave in the RF driver. Then the modulated signal is fed to the FCAOM for switching the LASER beam accordingly. The FC/APC to FC/APC connector is used to connect the output of the fiber Laser and Input of the FCAOM.

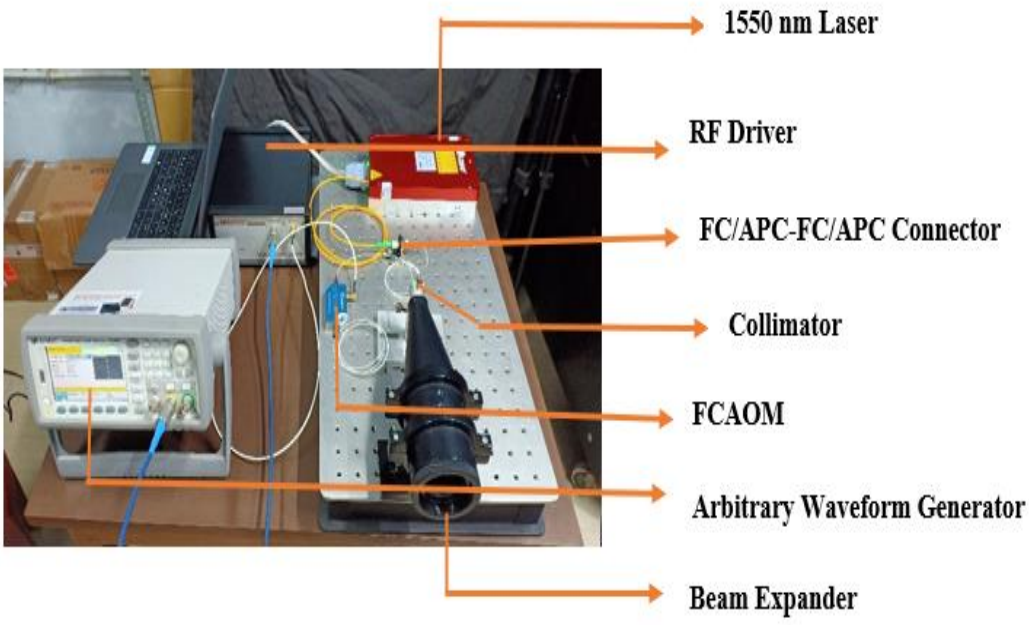

Fig. 3.21. Transmitter Unit of the FSO system

The switched LASER beam emits from the LASER outlet through a Collimeter. Collimeter is required at the outlet of the LASER to direct the LASER beam in a straight direction. A beam expander is also being used to prevent the spreading of the emitted LASER beam in larger amount in a longer distance. The magnification factor of the beam expander is 10x and exit and entrance aperture is 50 mm and 5 mm respectively, and the transmittance is around 98 %. Fiber coupled Acousto Optic Modulator is used which has 10 MHz digital bandwidth, type of fiber is used SMF 28 and insertion loss is around 2-3 dB. The RF Driver which is the necessary part of the FCAOM, has TTL voltage of 0-5 V and impedance of around 330 ohms, and RF connector is SubMiniature version A (SMA) . Fig. 3.21. depicts the Transmitter Unit of the FSO system.

3.6.1.2. RECEIVER SIDE OF EXTERNAL MODULATION TECHNIQUE

In the receiving end, the emitted LASER beam is collected in a Photo detector through a convex lens and a spectral filter respectively. Convex lens is used to converge the incoming LASER beam into a focal point and the spectral filter is used to prevent any beam other than 1550nm to fall into the photo detector. The photo detector turns the light source into equivalent current, which turns into equivalent voltage through a trans-impedance amplifier and amplifies the signal also. The output from trans-impedance amplifier is fed to a comparator, which fed and observed in a mixed signal oscilloscope (MSO), model no. Keysight. Real time eye diagram is also being observed at the same time. The optical power has been measured by the Laser power meter, Ophir, Vega model. Fig. 3.22. shows the receiver unit of FSO system.

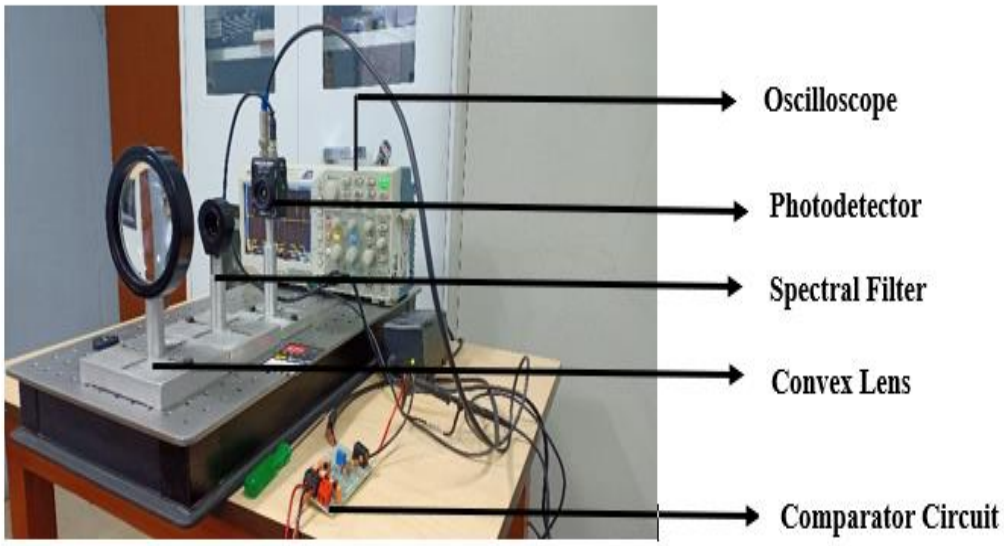

Fig. 3.22. Receiver Unit of FSO system

3.7. CONCLUSION

The designed cost-effective FSO communication channel system employing various wavelength Laser sources has been found to be thoroughly described in this chapter. The designed transmitter and receiver circuits of the FSO system were conceptualised from this chapter. The developed artificial climatic simulation chambers, such as the rain simulation setup, increasing temperature simulation chamber, and fog simulation setup, have also been adequately explained in this chapter.

CHAPTER 4
EXPERIMENTAL RESULTS & ANALYSIS

4.1. INTRODUCTION

In this chapter, the experimental results and their analysis have been demonstrated. Basically, total five wavelengths of LASERs are used for the experimentation purposes. The wavelengths are 532 nm, 638 nm, 808 nm, 980 nm and 1550 nm. An optical communication channel has been established using these wavelengths. The channel bandwidth is around 5 MHz. The total optical channel distance (distance between transmitter and receiver) is around 35 ft. has been considered. These optical channels have been tested in different atmospheric conditions which are created artificially which are discussed in the previous chapter (3). Basically, three atmospheric conditions are established like rain, temperature, and fog. In general, the total experimentation has been carried out in the two ways. At first, the optical channel has been established using different wavelengths and the optical power has been measured in the free atmospheric condition (no hazards present in the atmosphere) after that different atmospheric condition has been created and these condition scenarios, the optical power attenuation has been measured for different wavelengths. Similarly, the channel reliability or performance in different atmospheric condition has been measured on terms of eye diagram of the received signal, Signal to Noise Ratio (SNR) and Bit Error Rate (BER) conditions. Finally, an analysis has been done using these obtained results.

4.2. SPECIFICATIONS OF LASERS & PHOTODETECTORS SYSTEM

Different wavelengths Laser sources are used as a transmitter of the system. To obtain the better result, proper photodetector should be chosen at the receiver side. The visible wavelengths (532 nm & 638 nm) Laser sources technical specifications are given in the table 4.1.

Table 4.1. Technical Specifications of 532 nm & 638 nm Laser sources

Optical Power	Operating Life	Beam Waist	Divergence Angle
Variable (Upto 400 mW)	>5000 hours	3 mm	2.5 mrad

Similarly, the technical specification of the photodetector for the wavelengths of 532 nm and 638 nm is given the table 4.2.

Table 4.2. Technical Specifications of 532 nm & 638 nm Photodetector

Operating Wavelength	**Bandwidth**	**Responsivity**	**Noise Equivalent Power (NEP)**	**Material**
200-1100 nm	150 MHz	0.44 A/W	$5.5x10^{-10}$ $W/Hz^{0.5}$	Si

The responsivity curve for different wavelengths is shown in the Fig 4.1. The operating temperature of the detector is 10^0 C- 50^0 C. The responsivity of 532 nm is around 0.29 A/W and 638 nm is around 0.39 A/W respectively.

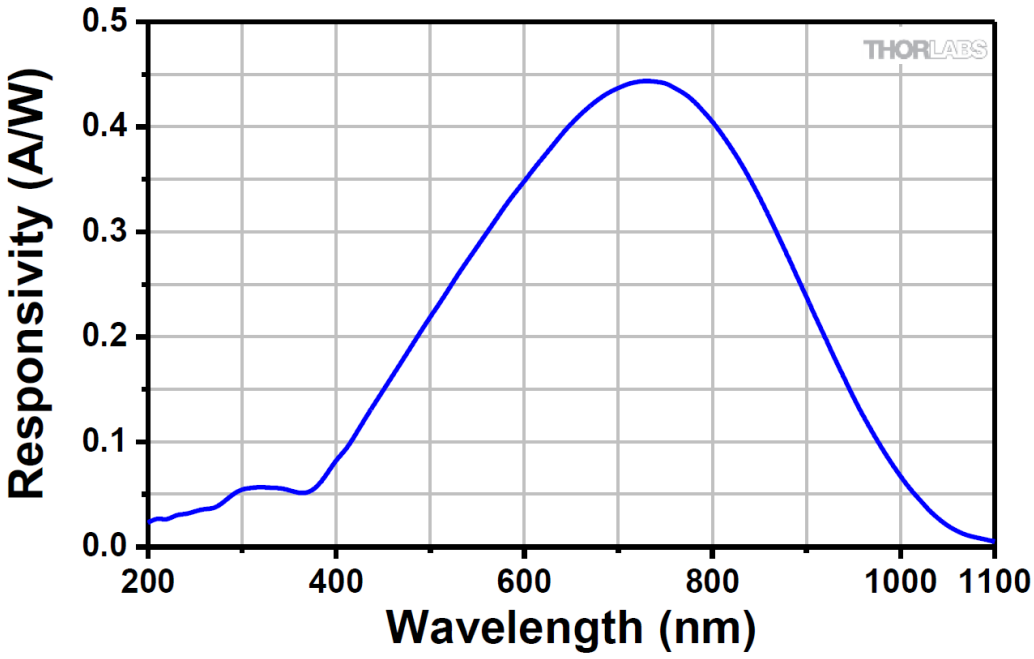

Fig. 4.1. Responsivity (A/W) vs wavelength curve

The technical specification for 808 nm Laser and 980 nm Laser are given in the table 4.3.

Table 4.3. Technical Specifications of 808 nm & 980 nm Laser sources

Optical Power	**Operating Life**	**Beam Waist**	**Divergence Angle**
Variable (Upto 400 mW)	>5000 hours	3.5 mm	3.0 mrad

Similarly, the technical specification of the photodetector for the wavelengths of 808 nm and 980 nm is given the table 4.4.

Table 4.4. Technical Specifications of 808 nm & 980 nm Photodetector

Operating Wavelength	**Bandwidth**	**Responsivity**	**Noise Equivalent Power (NEP)**	**Material**
400-1100 nm	150 MHz	1.0 A/W	5.25×10^{-10} W/Hz$^{0.5}$	Si

The responsivity curve for different wavelengths is shown in the Fig 4.2. The operating temperature of the detector is -40^0 C- 125^0 C. The responsivity of 808 nm is around 0.85 A/W and 980 nm is around 0.89 A/W respectively.

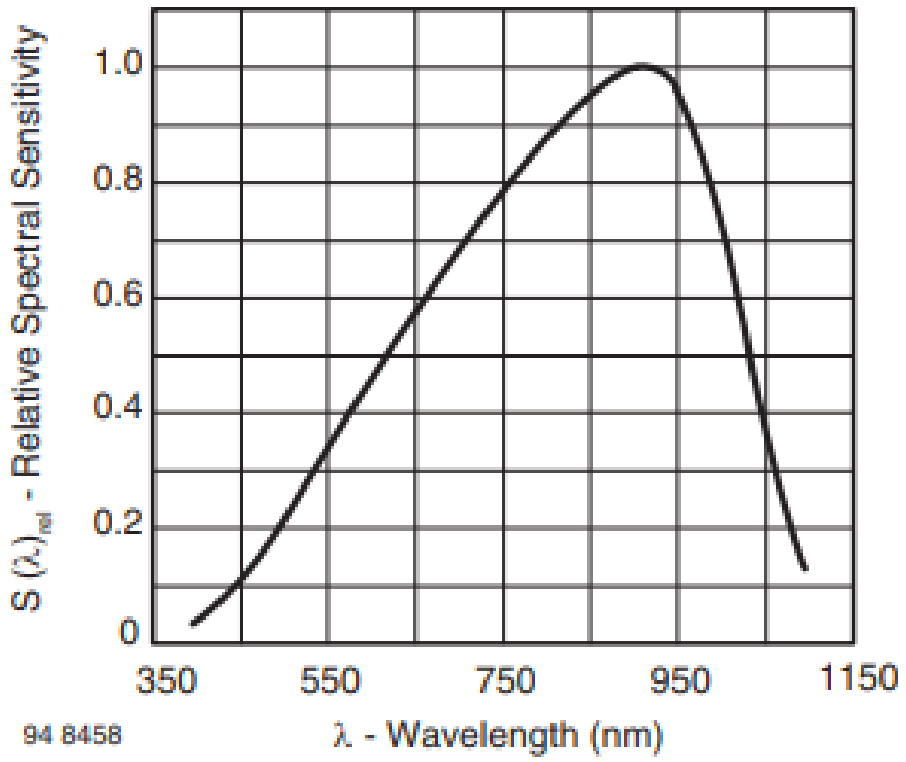

Fig. 4.2. Responsivity (A/W) vs wavelength curve

The physical shape & dimension of the photodetector (808 nm & 980 nm) has been depicted in the Fig. 4.3.

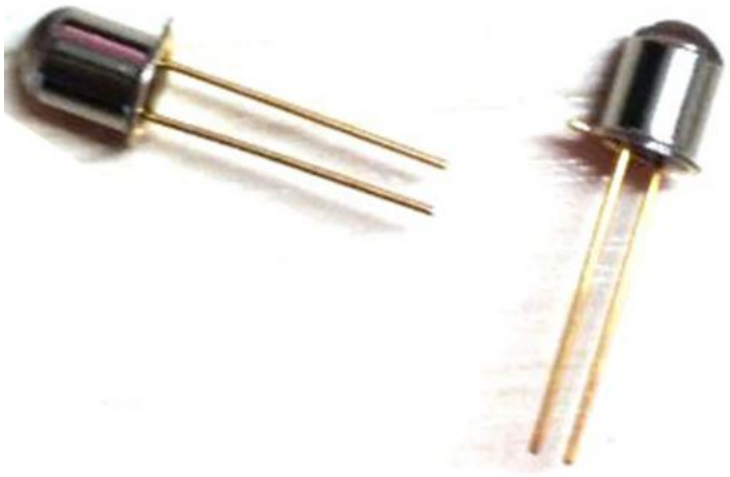

Fig. 4.3. Photodetector for 808 nm & 980 nm

The technical specification for 1550 nm Laser is given in the table 4.5.

Table 4.5. Technical Specifications of 1550 nm Laser sources

Optical Power	**Operating Life**	**Beam Waist**	**Divergence Angle**
Variable (Upto 1000 mW)	>5000 hours	2.0 mm	1.1 mrad

Similarly, the technical specification of the photodetector for the wavelength of 1550 nm is given the table 4.6.

Table 4.6. Technical Specifications of 1550 nm Photodetector

Operating Wavelength	**Bandwidth**	**Responsivity**	**Noise Equivalent Power (NEP)**	**Material**
800-1700 nm	150 MHz	1.0 A/W	$4x10^{-10}$ $W/Hz^{0.5}$	InGaAs

The responsivity curve for different wavelengths is shown in Fig 4.4. The operating temperature of the detector is 10^0 C- 50^0 C. The responsivity of 1550 nm is around 1 A/W.

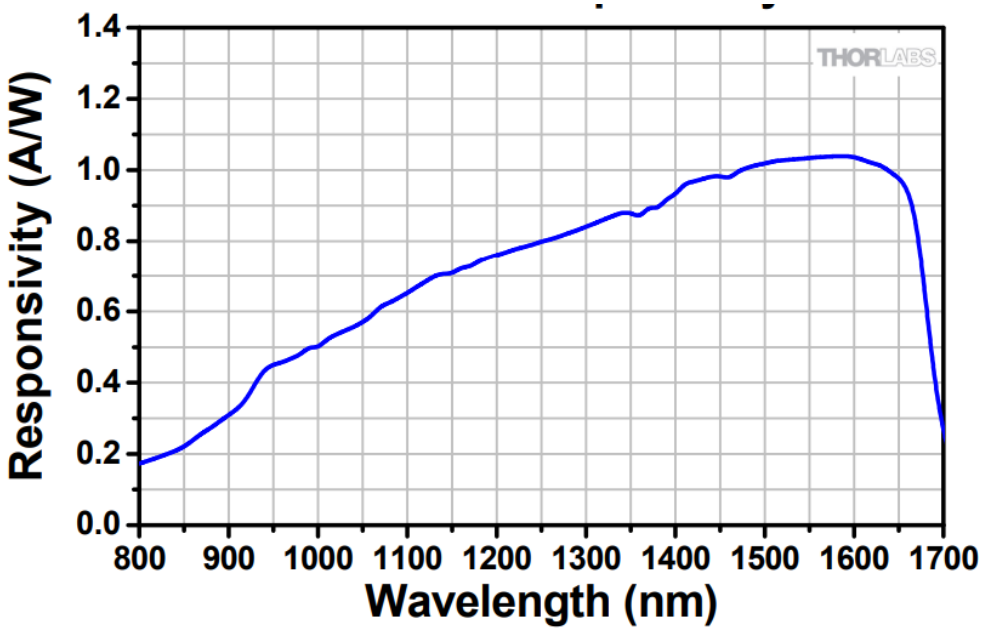

Fig. 4.4. Responsivity (A/W) vs wavelength curve

The beam divergence angle is an important parameter. At the longer link distance, the beam divergence loss is higher. To obtained smaller beam divergence loss, the beam divergence should be smaller. The beam divergence loss can be predicted from the equation 4.1.

$$\text{Beam Divergence loss} = \frac{D_R}{D_o} \qquad (4.1)$$

Where D_R = Received laser beam diameter at a particular propagation path, D_o = Receiver optics diameter.

The diameter of the Laser beam at the receiver side for a particular link distance can be achieved by the equation 4.2.

$$D_R = \theta \times L + D_L \qquad (4.2)$$

Where, θ = Beam divergence angle (mrad), L = Distance between transmitter and receiver, D_L = Laser aperture diameter (mm).

The optical beam diameter at the receiver side for the wavelength 532 nm and 638 nm is around 0.028 m for a distance of 35 ft., the optical beam diameter at the receiver side for the wavelength 808 nm and 980 nm is around 0.033 m for a distance of 35 ft., and the optical beam diameter at the receiver side for the wavelength 1550 nm is around 0.015 m for a distance of 35 ft.. The diameter of optical power meter (D_o) sensor is around 0.06 m. The beam divergence loss is negligible at this distance for all the Laser sources.

The total experimentation has been classified by the two sets, one is optical power attenuation and another one is optical communication channel attenuation measurement due to different atmospheric conditions scenario like rain, temperature, and fog Fig. 4.5. shows the classification of the total experimentation process.

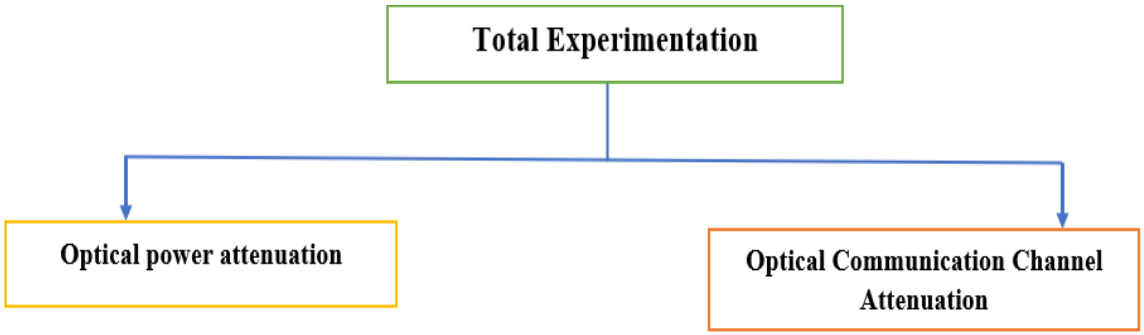

Fig.4.5. Classification of total experimentation process

4.3. OPTICAL POWER ATTENUATION

The optical power attenuation due to different atmospheric conditions like rain, temperature, fog for different wavelengths have been shown in this section.

4.3.1. OPTICAL POWER ATTENUATION DUE TO RAIN

The optical power attenuation due to different rain rates are demonstrated in this section Fig. 4.6 shows the optical power attenuation for rain rate of 7 mm/hr for all the considered wavelengths for 35 ft. link distance,

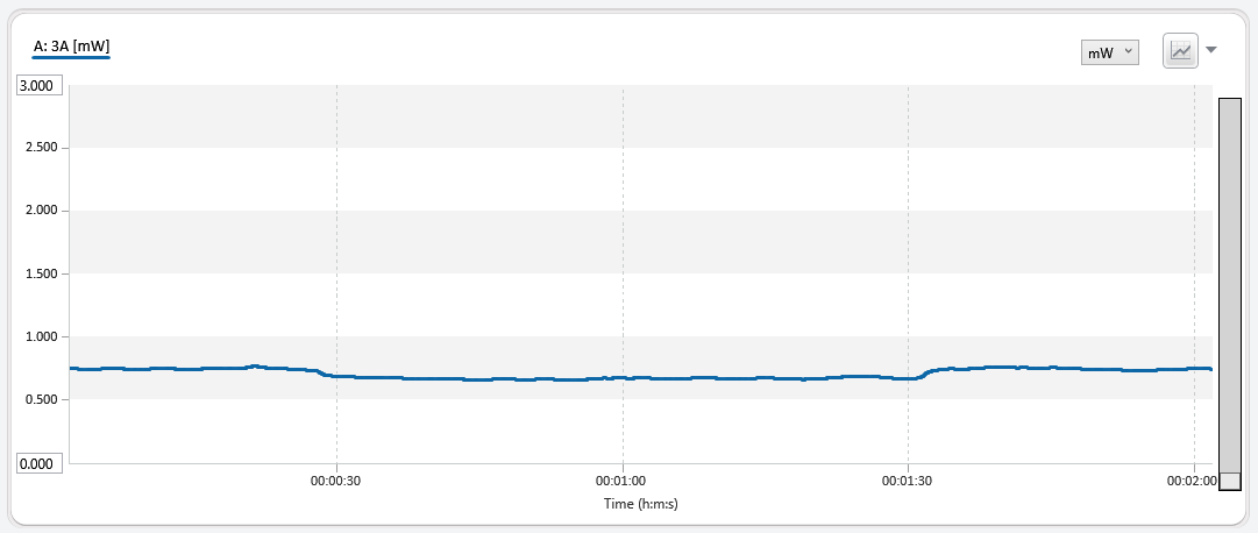

Fig.4.6. Optical power attenuation for rain rate 7 mm/hr

From this figure, it has been shown that initially 0.70 mW optical power has been received. The first 30 second optical power are remaining same that is 0.70 mW, in this duration, the weather is clear, after 30 second, the 7 mm/hr rain rate has been started and the rain is continued for 1 min more, after that the rain is stopped, as a result, the optical power came returned to the previous value that is 0.70 mW. Therefore, during the total raining time of 1 second, the optical power attenuation occurred and that has been measured.

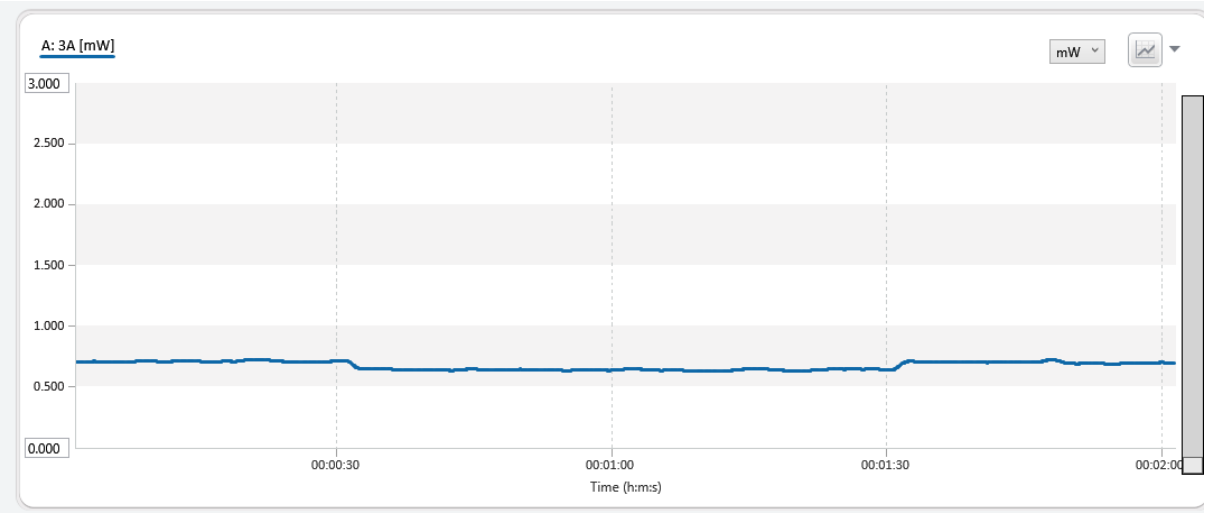

Fig.4.7. Optical power attenuation for rain rate 28 mm/hr

Similarly, optical power attenuation has been measured for different rain rates like 28 mm/hr, 69 mm/hr, 121 mm/hr, 180 mm/hr etc. Fig. 4.7, Fig. 4.8, Fig. 4.9, Fig. 4.10 show the optical power attenuation due to 28 mm/hr, 69 mm/hr, 121 mm/hr, 180 mm/hr rain rates respectively.

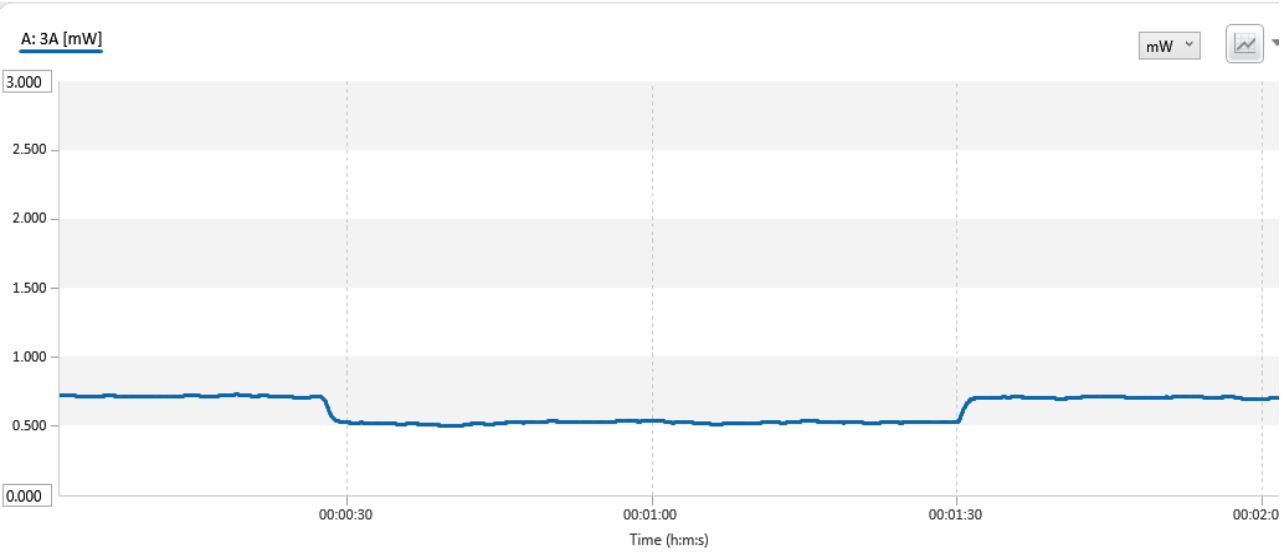

Fig.4.8. Optical power attenuation for rain rate 69 mm/hr

The optical power attenuation profile is almost same for all the wavelengths. The optical power attenuation due to rain is wavelength independent phenomenon.

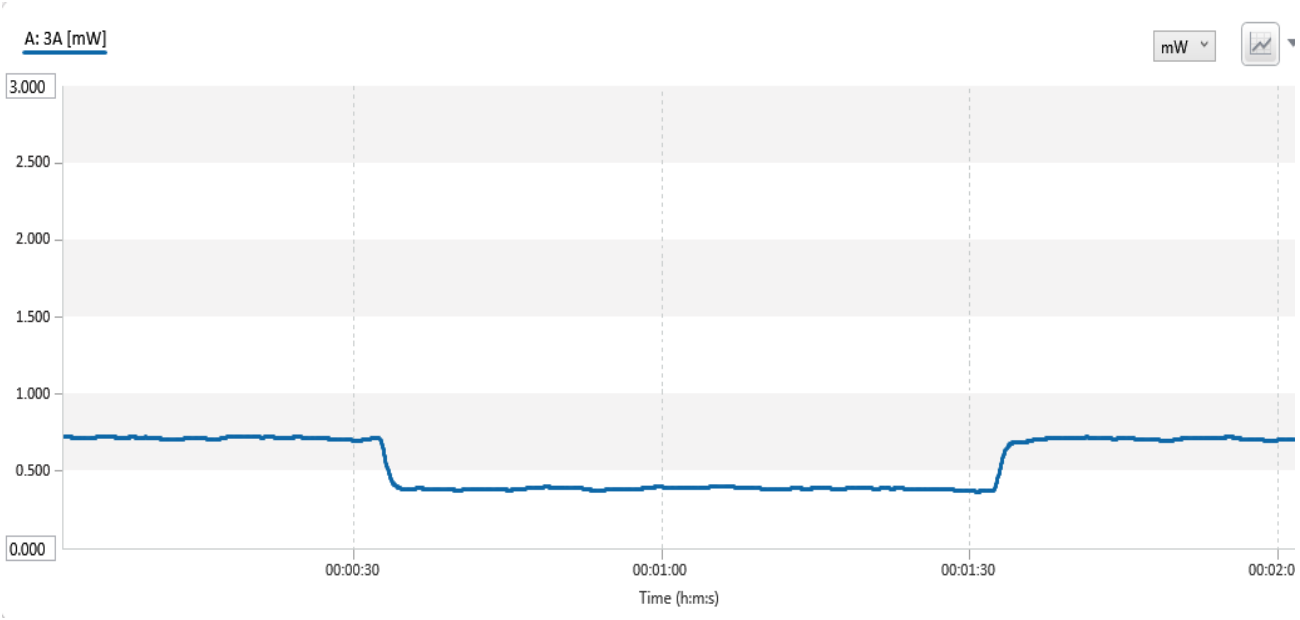

Fig.4.9. Optical power attenuation for rain rate 121 mm/hr

As the rain rates is increased, the optical power attenuation also increased, and at the 180 mm/hr rain rate condition, the optical power attenuation is highest observed.

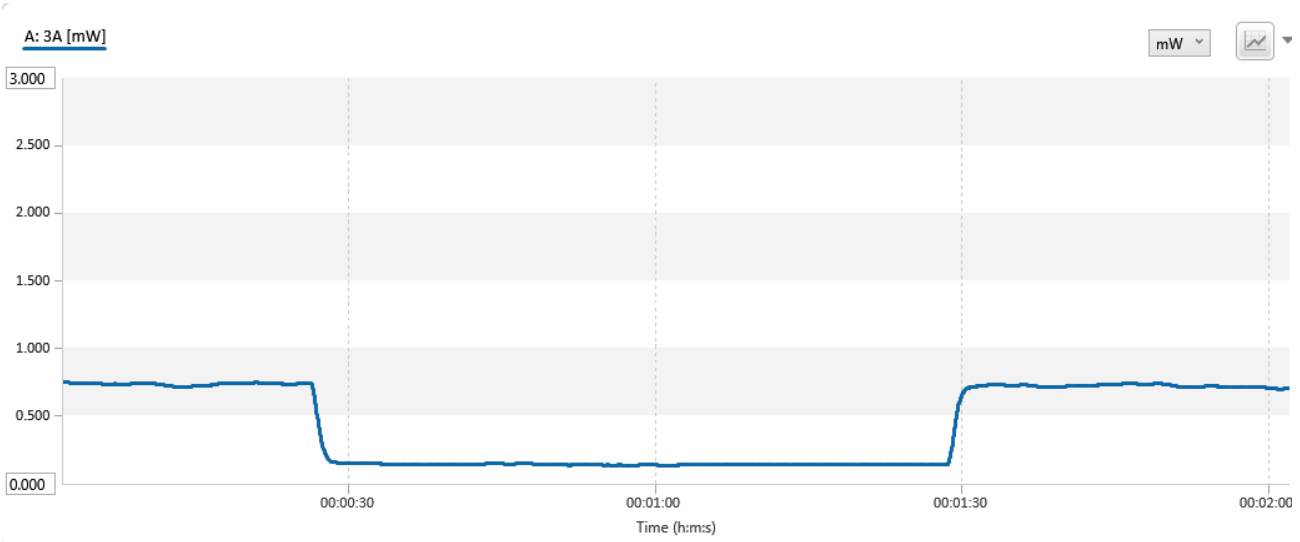

Fig.4.10. Optical power attenuation for rain rate 180 mm/hr

Table 4.7. shows the optical power attenuation for different rain rates (mm/hr) for the link range of 35 ft.

Table 4.7. Optical power loss for different rain rates (mm/hr) using different wavelengths at link distance of 35 ft.

Rain Rates (mm/hr)	Transmitted optical power (mW)	Optical power loss for 532 nm (dB)	Optical power loss for 638 nm (dB)	Optical power loss for 808 nm (dB)	Optical power loss for 980 nm (dB)	Optical power loss for 1550 nm (dB)
7	0.70	0.09741	0.09738	0.09736	0.09736	0.09728
28	0.70	0.2375	0.2372	0.2371	0.237	0.237
69	0.70	0.425	0.4248	0.4243	0.424	0.4238
121	0.70	0.6112	0.611	0.61	0.608	0.606
153	0.70	0.709	0.7084	0.7081	0.708	0.7078
180	0.70	0.791	0.7906	0.7902	0.7902	0.79

The optical power attenuation for different rain rates for different wavelengths are shown in Fig. 4.11.

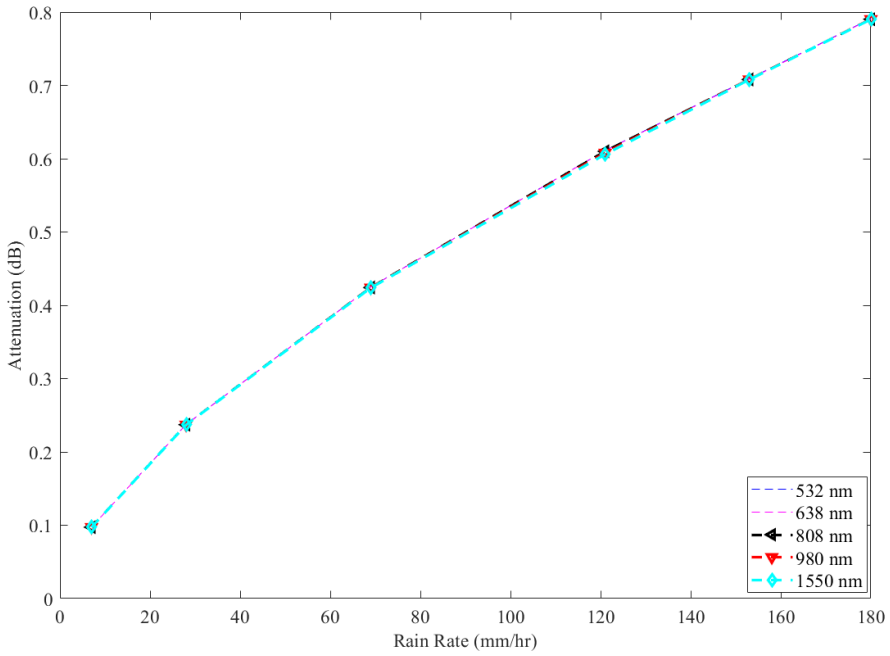

Fig. 4.11. Optical power attenuation vs different rain rates for different wavelengths

From this figure and aforesaid table, it has been shown that at different rain rates (mm/hr), the optical power attenuation is almost same for different wavelengths. These values are converted to the dB/km range and as a result, with these values, different models are compared and finally a model has been proposed from these obtained values.

Table 4.8. Optical power attenuation (dB/km) for different rain rates (mm/hr) using 532 nm wavelength and compared with different models

Rain Rates (mm/hr)	**Measured Optical power loss for 532 nm (dB/km)**	**Optical power loss for CHARBONNEAU MODEL for 532 nm (dB/km)**	**Optical power loss for Japan Model for 532 nm (dB/km)**	**Optical power loss for Laws & Parson Model for 532 nm (dB/km)**	**Optical power loss for Malaysia Model for 532 nm (dB/km)**
7	6.088	3.963	5.38355	2.951	8.56778
28	14.84375	10.032476	12.8933	9.8588	23.89973
69	26.5625	18.358667	22.7579	21.6072	46.5848
121	38.2	26.747	32.42	35.2227	70.5922
153	44.3125	31.3	37.585	43.199764	83.9784
180	49.4375	34.901	41.63	49.7607	94.7104

Table 4.9. Optical power attenuation (dB/km) for different rain rates (mm/hr) using 638 nm wavelength and compared with different models

Rain Rates (mm/hr)	**Measured Optical power loss for 638 nm (dB/km)**	**Optical power loss for CHARBONNEAU MODEL for 638 nm (dB/km)**	**Optical power loss for Japan Model for 638 nm (dB/km)**	**Optical power loss for Laws & Parson Model for 638 nm (dB/km)**	**Optical power loss for Malaysia Model for 638 nm (dB/km)**
7	6.087	3.963	5.38355	2.951	8.56778
28	14.8437	10.032476	12.8933	9.8588	23.89973

69	26.5621	18.358667	22.7579	21.6072	46.5848
121	38.16	26.747	32.42	35.2227	70.5922
153	44.3123	31.3	37.585	43.199764	83.9784
180	49.43754	34.901	41.63	49.7607	94.7104

Table 4.10. Optical power attenuation (dB/km) for different rain rates (mm/hr) using 808 nm wavelength and compared with different models.

Rain Rates (mm/hr)	**Measured Optical power loss for 808 nm (dB/km)**	**Optical power loss for CHARBONNEAU MODEL for 808 nm (dB/km)**	**Optical power loss for Japan Model for 808 nm (dB/km)**	**Optical power loss for Laws & Parson Model for 808 nm (dB/km)**	**Optical power loss for Malaysia Model for 808 nm (dB/km)**
7	6.085	3.963	5.38355	2.951	8.56778
28	14.8437	10.032476	12.8933	9.8588	23.89973
69	26.5622	18.358667	22.7579	21.6072	46.5848
121	38.181	26.747	32.42	35.2227	70.5922
153	44.3124	31.3	37.585	43.199764	83.9784
180	49.4372	34.901	41.63	49.7607	94.7104

Table 4.11. Optical power attenuation (dB/km) for different rain rates (mm/hr) using 980 nm wavelength and compared with different models

Rain Rates (mm/hr)	**Measured Optical power loss for 980 nm (dB/km)**	**Optical power loss for CHARBONNEAU MODEL for 980 nm (dB/km)**	**Optical power loss for Japan Model for 532 nm (dB/km)**	**Optical power loss for Laws & Parson Model for 980 nm (dB/km)**	**Optical power loss for Malaysia Model for 980 nm (dB/km)**
7	6.082	3.963	5.38355	2.951	8.56778

28	14.8437	10.032476	12.8933	9.8588	23.89973
69	26.562	18.358667	22.7579	21.6072	46.5848
121	38.20014	26.747	32.42	35.2227	70.5922
153	44.312	31.3	37.585	43.199764	83.9784
180	49.43738	34.901	41.63	49.7607	94.7104

Table 4.12. (a) Optical power attenuation (dB/km) for different rain rates (mm/hr) using 1550 nm wavelength and compared with different models

Rain Rates (mm/hr)	**Measured Optical power loss for 1550 nm (dB/km)**	**Optical power loss for CHARBONNEAU MODEL for 1550 nm (dB/km)**	**Optical power loss for Japan Model for 1550 nm (dB/km)**	**Optical power loss for Laws & Parson Model for 1550 nm (dB/km)**	**Optical power loss for Malaysia Model for 1550 nm (dB/km)**
7	6.082	3.963	5.38355	2.951	8.56778
28	14.8437	10.032476	12.8933	9.8588	23.89973
69	26.56214	18.358667	22.7579	21.6072	46.5848
121	38.14	26.747	32.42	35.2227	70.5922
153	44.3118	31.3	37.585	43.199764	83.9784
180	49.43732	34.901	41.63	49.7607	94.7104

Optical power attenuation (dB/km) for different rain rates (mm/hr) using different wavelengths like 532 nm, 638 nm, 808 nm, 980 nm, 1550 nm have been depicted in the Table 4.8, Table 4.9, Table 4.10, Table 4.11, Table 4.12.(a) respectively and compared with different models like Charbonneau, Japan, Laws & Parson & Malaysia Model.

A table has been drawn which is given below (Table 4.12.b). In this table, the error/ deviation has been depicted between measured and existing models. From this table, it has been clearly

depicted that at lower rain rate (7 mm/hr-69mm/hr) condition, the error has been lower for Japan model, when the rain rates gradually increased (greater than 69 mm/hr to 180 mm/hr), lower deviation has noticed in Laws & Parson Models. A huge error was observed in both the models with Malaysia & Carbonneau models.

Table 4.12.(b) Error noticed between measured value with different existing model with different rain rates

Rain Rates (mm/hr)	**Error with Carbonneau Model**	**Error with Japan Model**	**Error with Laws & Parson Model**	**Error with Malaysia Model**
7	0.536209942	0.13085	1.063029482	0.289431
28	0.479569949	0.15128	0.50563456	0.378916
69	0.446864307	0.16718	0.229335592	0.429803
121	0.428197555	0.17829	0.084527875	0.458864
153	0.415734824	0.17899	0.025757918	0.472335
180	-0.41650669	-0.18755	0.006495085	0.478014

Fig. 4.12 shows the Measured optical power attenuation (dB/km) for different rain rates and for different models. From this graph, it has been shown that the highest optical attenuation for different rain rates (mm/hr) have been observed in Malaysia Model and lowest has been observed in Charbonneau model. These models are developed in the different countries according to those countries' rain rate conditions. Malaysia is a tropical country and, in that place, the rain rate is very high (around 250 mm/hr). Whereas Charbonneau model has been developed in France which is an European country, and the rain rate (35 mm/hr) there is very low. In the temperate region like India, the rain rate is moderate level (100 mm/hr-150 mm/hr), so the optical power attenuation is generally moderate in level. The measured optical power attenuation due to artificial rain rates (mm/hr) are between the highest and lower optical power attenuation model like Japan and laws and Parson models. The Japan and Laws and Parson model has been developed for temperate region.

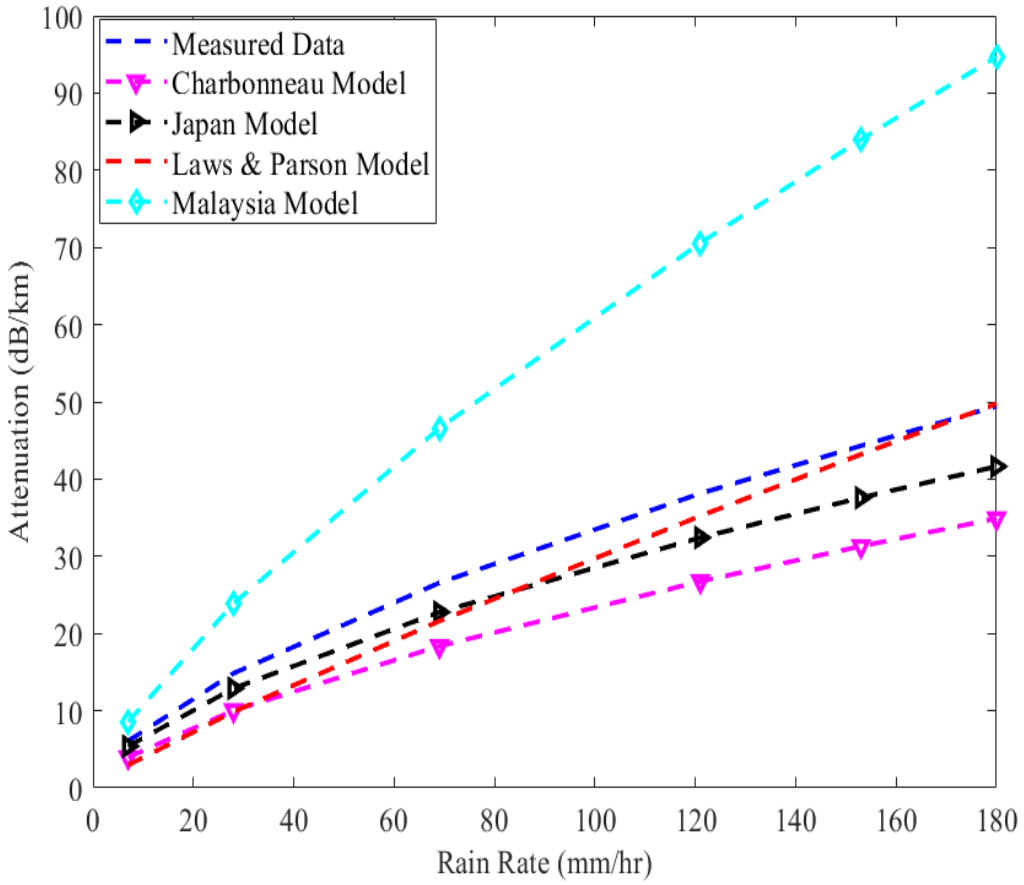

Fig. 4.12. Measured optical power attenuation (dB/km) for different rain rates and compared with others model

From the obtained optical power attenuation values in different rain rates, a rain attenuation model is proposed. The proposed optical power attenuation due to rain has been given in the equation 4.3.

$$Attenuation = 1.724R^{0.6455} \text{ dB/km} \qquad 4.3$$

Where R = Rain Rate (mm/hr)

The above-mentioned equation is based on the Power Law and the previous developed models were also developed by the Power Law of the equation. The obtained power law fitted curve using different rain rates with optical power attenuation has been depicted in Fig. 4.13.

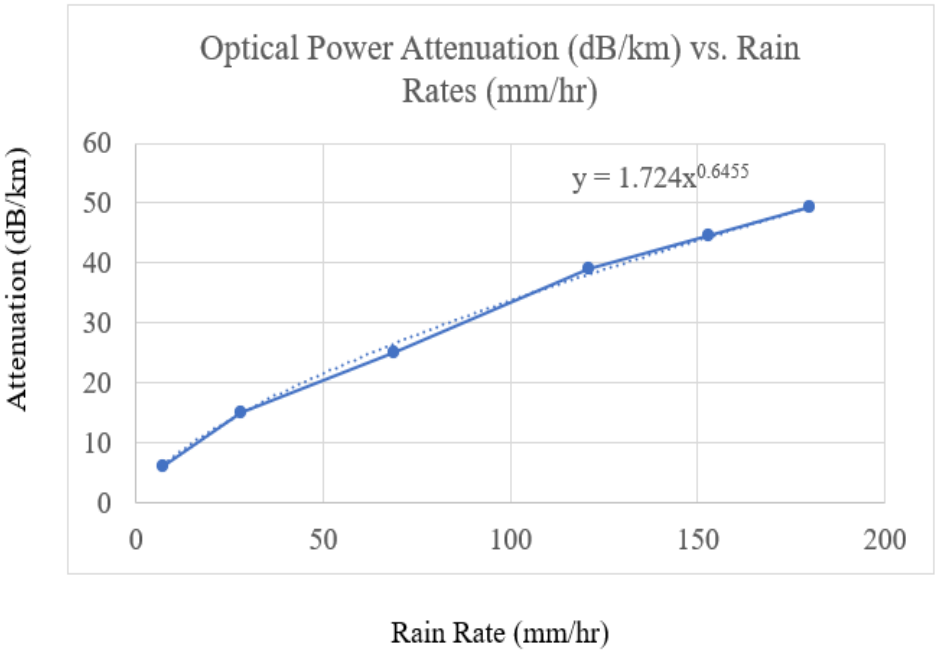

Fig. 4.13. Different rain rates (mm/hr) with measured optical power attenuation (dB/km) fitted curve

4.3.2. OPTICAL POWER ATTENUATION DUE TO TEMPERATURE

The optical power attenuation due to different temperature effects has been depicted in this section. The scintillation effect has been observed in the terrestrial space due to non-uniform effect of temperature of the terrestrial surface. As a result, the temperature fluctuation has been observed and the fluctuation has been increased with the increment of strength of the scintillation, as a result, the optical power also fluctuates for this scintillation events.

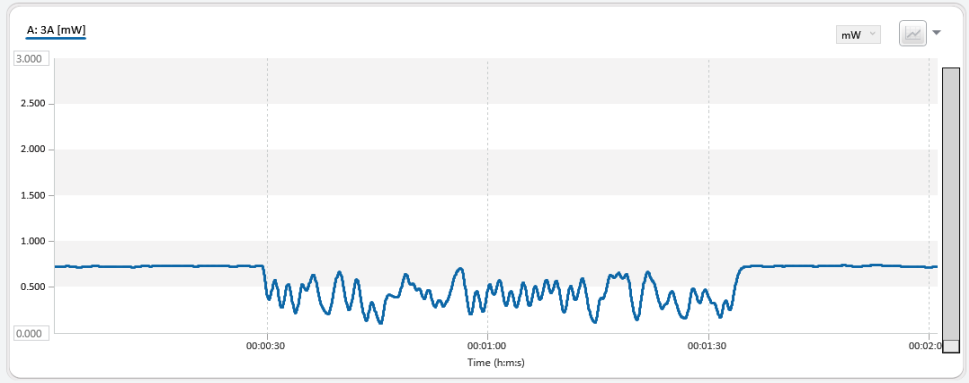

Fig. 4.14. The optical power fluctuation for the scintillation range $2.5x10^{-13}$ $m^{-2/3}$ using wavelength 532 nm Laser

To demonstrate this type of phenomenon, a scintillation simulation chamber is developed, description of this chamber is given in the previous chapter. When the temperature difference is around 2.5^0 K, 16^0 K, 28^0 K, 42^0 K, the C_n^2 value is around 10^{-16} $m^{-2/3}$, $3.5x10^{-15}$ $m^{-2/3}$, 10^{-14} $m^{-2/3}$, $2.5x10^{-13}$ $m^{-2/3}$ respectively.

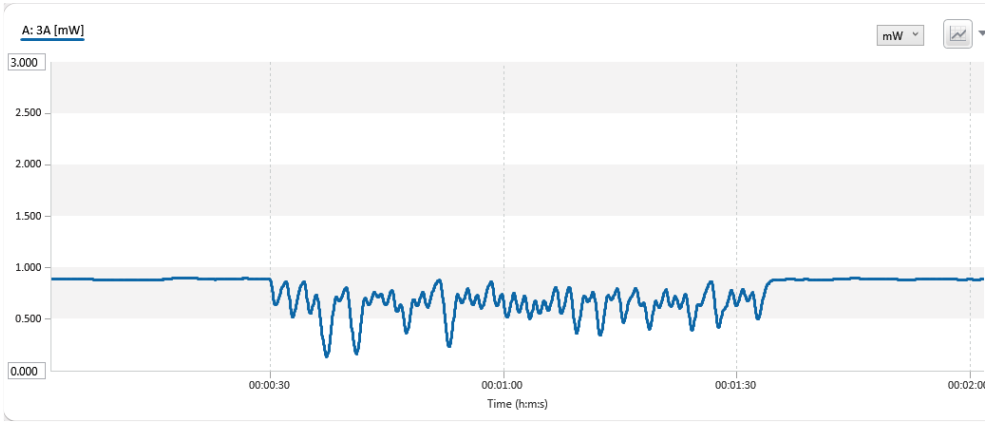

Fig. 4.15. The optical power fluctuation for the scintillation range $2.5x10^{-13}$ $m^{-2/3}$ using 638 nm Laser

As the temperature difference is increased, the optical power fluctuation also increased, the optical power attenuation experimentation has been carried out during 2 minutes.

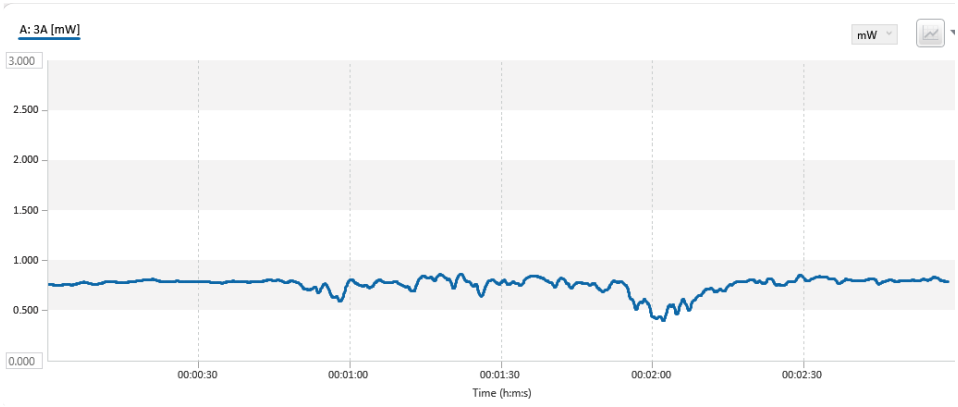

Fig. 4.16. The optical power fluctuation for the scintillation range $2.5x10^{-13}$ $m^{-2/3}$ using 808 nm Laser

From Fig. 4.14, it has been shown that for first 30 second duration, the received optical power remain almost constant, after 30 second, the temperature difference has been created, as a result the optical power fluctuation has been observed and this is continued with 1 minute duration, after that the temperature difference is put off as a result, the optical power returns back to the previous value.

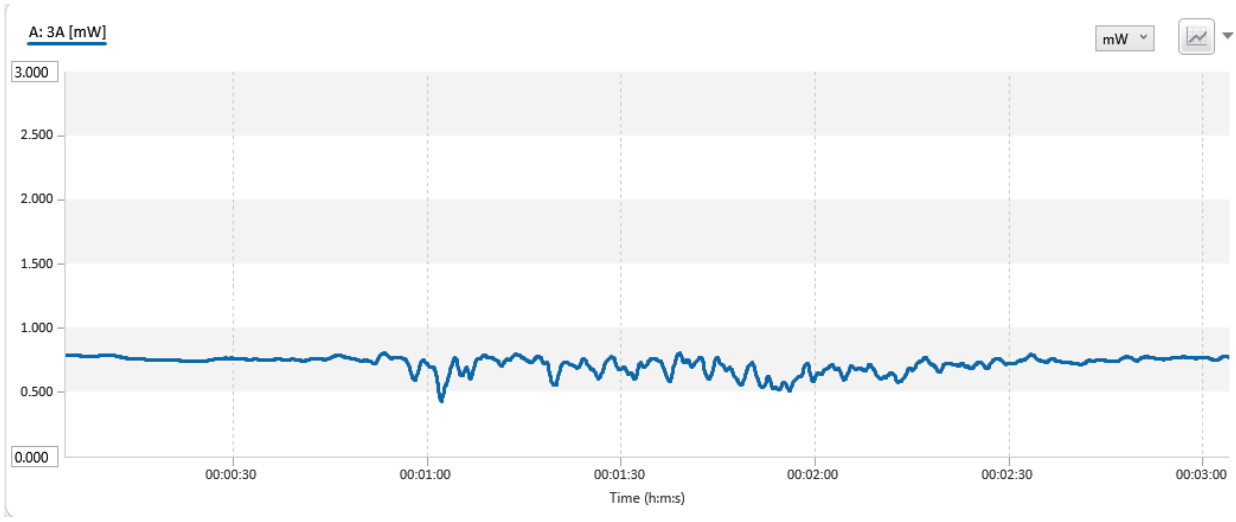

Fig. 4.17. The optical power fluctuation for the scintillation range $2.5x10^{-13}$ $m^{-2/3}$ using 980 nm Laser

The same operation has been repeated for the others wavelength and the optical power attenuation for the same scintillation range has been measured.

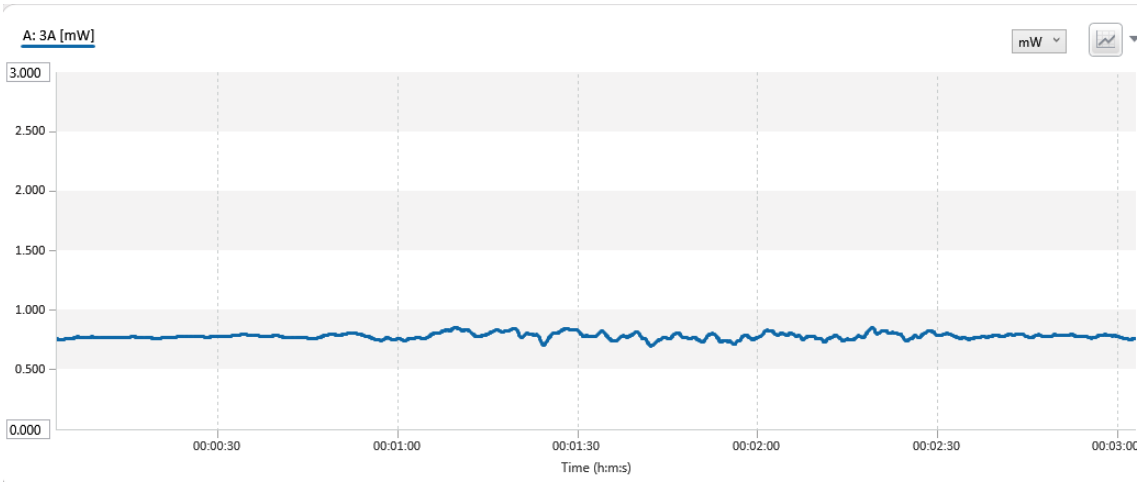

Fig. 4.18. The optical power fluctuation for the scintillation range $2.5x10^{-13}$ $m^{-2/3}$ using 1550 nm Laser

In Fig. 4.15, Fig. 4.16, Fig. 4.17, Fig 4.18, the optical power attenuation due to scintillation strength of $2.5x10^{-13}$ $m^{-2/3}$ using 532 nm, 638 nm, 808 nm, 980 nm, 1550 nm respectively have been shown.

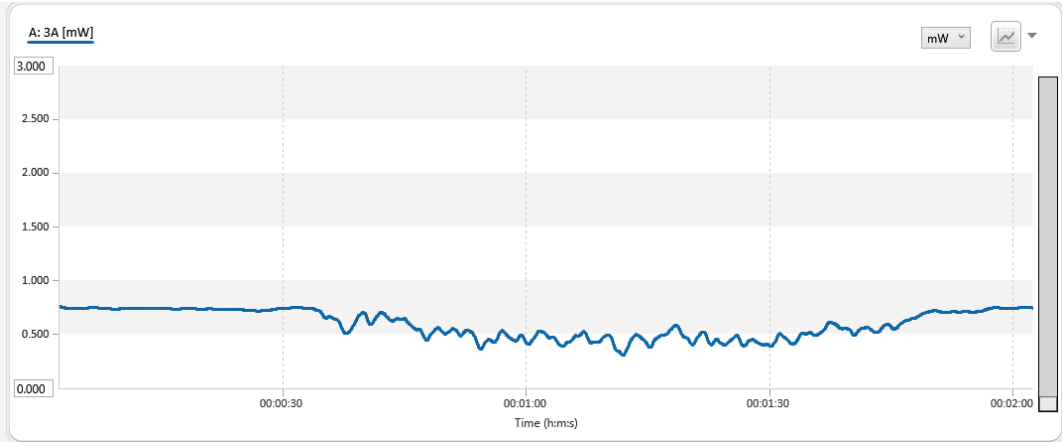

Fig. 4.19. The optical power fluctuation for the scintillation range $3.5x10^{-15}$ $m^{-2/3}$ using 532 nm Laser

From these figures, it has been shown that the optical power fluctuations are less, when increasing the value of wavelengths. The highest optical power attenuation has been noticed in 532 nm and lowest optical power attenuation has been noticed for 1550 nm wavelengths.

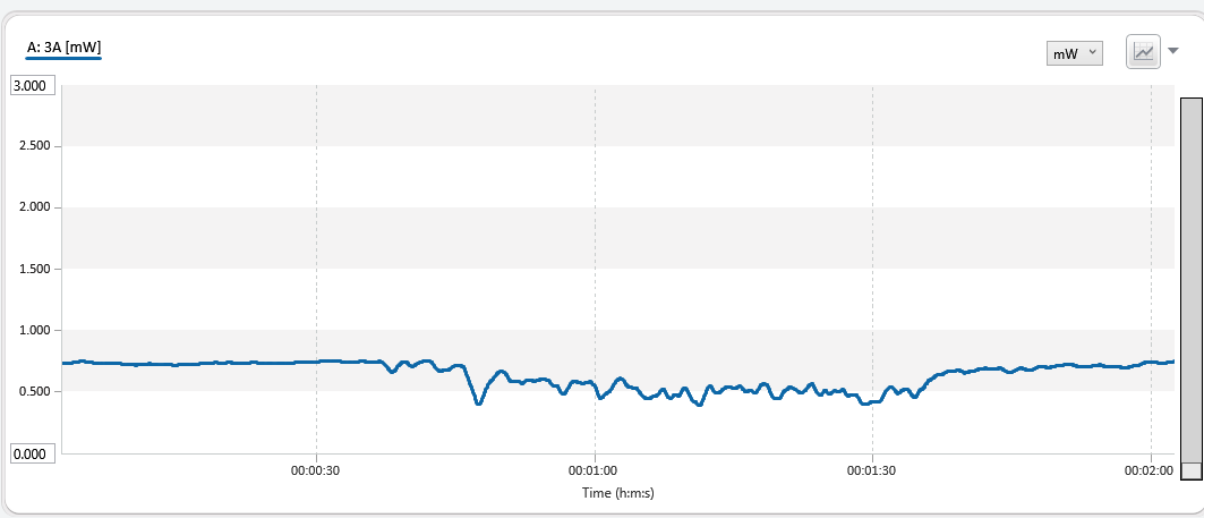

Fig. 4.20. The optical power fluctuation for the scintillation range $3.5x10^{-15}$ $m^{-2/3}$ using 638 nm Laser

Similarly, when the scintillation is lower e.g., $3.5x10^{-15}$ $m^{-2/3}$, the optical power fluctuation is again lowest for 1550 nm and highest for 532 nm Laser source. Therefore, from these attenuation trends, it has been predicted that scintillation process is a wavelength dependent phenomenon.

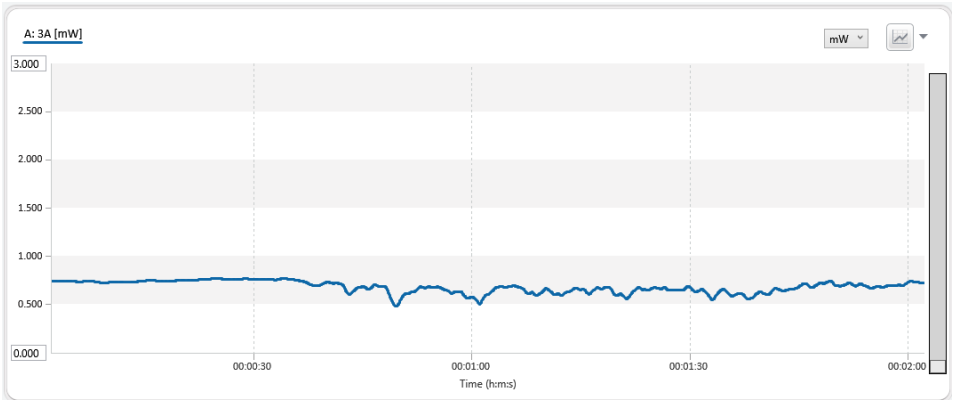

Fig. 4.21. The optical power fluctuation for the scintillation range $3.5x10^{-15}$ $m^{-2/3}$ using 808 nm Laser

In Fig. 4.19, Fig.4.20, Fig. 4.21, Fig. 4.22, Fig. 4.23, the optical power attenuation for the scintillation range $3.5x10^{-15}$ $m^{-2/3}$ using 532 nm, 638 nm, 808 nm, 980 nm and 1550 nm have been shown respectively.

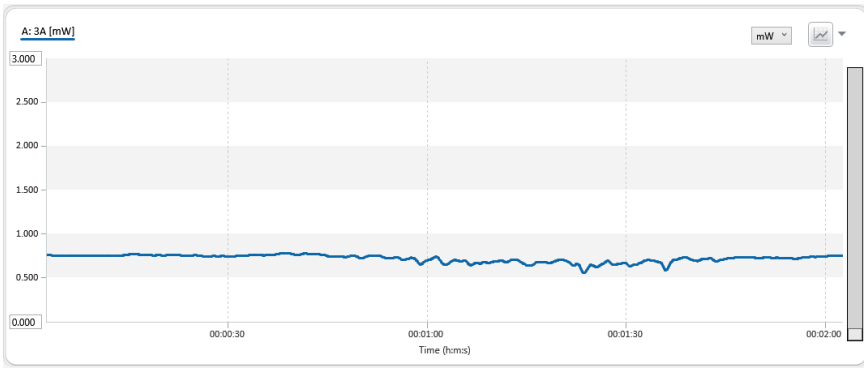

Fig.4.22. The optical power fluctuation for the scintillation range $3.5x10^{-15}$ $m^{-2/3}$ using 980 nm Laser

Table 4.13 and Table 4.14 show the theoretical and measured values of optical power attenuation for different wavelengths and different scintillation ranges respectively.

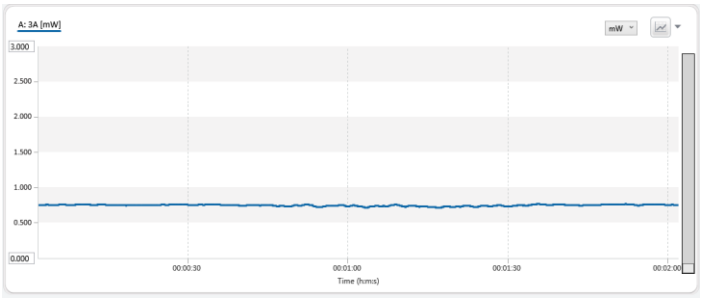

Fig. 4.23. The optical power fluctuation for the scintillation range $3.5x10^{-15}$ $m^{-2/3}$ using 1550 nm Laser

From these tables, a similar trend has been observed that when the scintillation strength is increased, the optical power attenuation is increased.

Table 4.13. Theoretical values of optical power attenuation for different wavelengths and different scintillation ranges

532 nm		638 nm		808 nm		980 nm		1550 nm	
C_n^2 ($m^{-2/3}$)	**Loss (dB)**	**C_n^2 ($m^{-2/3}$)**	**Loss (dB)**	**C_n^2 ($m^{-2/3}$)**	**Loss (dB)**	**C_n^2 ($m^{-2/3}$)**	**Loss (dB)**	**C_n^2 ($m^{-2/3}$)**	**Loss (dB)**
$2.5x10^{-13}$	0.907	**$2.5x10^{-13}$**	0.829	**$2.5x10^{-13}$**	0.7363	**$2.5x10^{-13}$**	0.668	**$2.5x10^{-13}$**	0.53166
10^{-14}	0.181	**10^{-14}**	0.1657	**10^{-14}**	0.1473	**10^{-14}**	0.133	**10^{-14}**	0.106
$3.5x10^{-15}$	0.107	**$3.5x10^{-15}$**	0.0981	**$3.5x10^{-15}$**	0.087	**$3.5x10^{-15}$**	0.0791	**$3.5x10^{-15}$**	0.063
10^{-16}	0.018	**10^{-16}**	0.0165	**10^{-16}**	0.015	**10^{-16}**	0.0106	**10^{-16}**	0.0106

Another trend is observed that when the wavelength is increased, the optical power attenuation is decreased. Table 4.14. (a) shows the measured values of optical power attenuation for different wavelengths and different scintillation ranges. Table 4.14.(b) shows the error / deviation between measured & Theoretical value of optical power attenuation for different wavelengths and different scintillation ranges

Table 4.14.(a) Measured values of optical power attenuation for different wavelengths and different scintillation ranges

532 nm		638 nm		808 nm		980 nm		1550 nm	
C_n^2 ($m^{-2/3}$)	**Loss (dB)**	**C_n^2 ($m^{-2/3}$)**	**Loss (dB)**	**C_n^2 ($m^{-2/3}$)**	**Loss (dB)**	**C_n^2 ($m^{-2/3}$)**	**Loss (dB)**	**C_n^2 ($m^{-2/3}$)**	**Loss (dB)**
$2.5x10^{-13}$	1.14	**$2.5x10^{-13}$**	1.04	**$2.5x10^{-13}$**	0.925	**$2.5x10^{-13}$**	0.74	**$2.5x10^{-13}$**	0.66
10^{-14}	0.23	**10^{-14}**	0.208	**10^{-14}**	0.185	**10^{-14}**	0.168	**10^{-14}**	0.133
$3.5x10^{-15}$	0.135	**$3.5x10^{-15}$**	0.123	**$3.5x10^{-15}$**	0.109	**$3.5x10^{-15}$**	0.099	**$3.5x10^{-15}$**	0.079
10^{-16}	0.023	**10^{-16}**	0.02	**10^{-16}**	0.018	**10^{-16}**	0.0168	**10^{-16}**	0.0133

Table 4.14.(b) Error / Deviation between measured & Theoretical value of optical power attenuation for different wavelengths and different scintillation ranges

532 nm		638 nm		808 nm		980 nm		1550 nm	
C_n^2 ($m^{-2/3}$)	**Error**	**C_n^2 ($m^{-2/3}$)**	**Error**	**C_n^2 ($m^{-2/3}$)**	**Error**	**C_n^2 ($m^{-2/3}$)**	**Error**	**C_n^2 ($m^{-2/3}$)**	**Error**
$2.5x10^{-13}$	0.257	**$2.5x10^{-13}$**	0.254	**$2.5x10^{-13}$**	0.256	**$2.5x10^{-13}$**	0.075	**$2.5x10^{-13}$**	0.241
10^{-14}	0.271	**10^{-14}**	0.255	**10^{-14}**	0.256	**10^{-14}**	0.25	**10^{-14}**	0.254
$3.5x10^{-15}$	0.262	**$3.5x10^{-15}$**	0.254	**$3.5x10^{-15}$**	0.253	**$3.5x10^{-15}$**	0.25	**$3.5x10^{-15}$**	0.254
10^{-16}	0.277	**10^{-16}**	0.212	**10^{-16}**	0.2	**10^{-16}**	0.54	**10^{-16}**	0.255

From the aforesaid table, it has been depicted that a constant error level has been noticed, and another point has been noted that the error variation is more at lower scintillation level compared to higher scintillation level irrespective of wavelengths.

Fig. 4.24 shows the optical power attenuation (dB) due to different scintillation range using 532 nm, 638 nm, 808 nm, 980 nm, 1550 nm respectively.

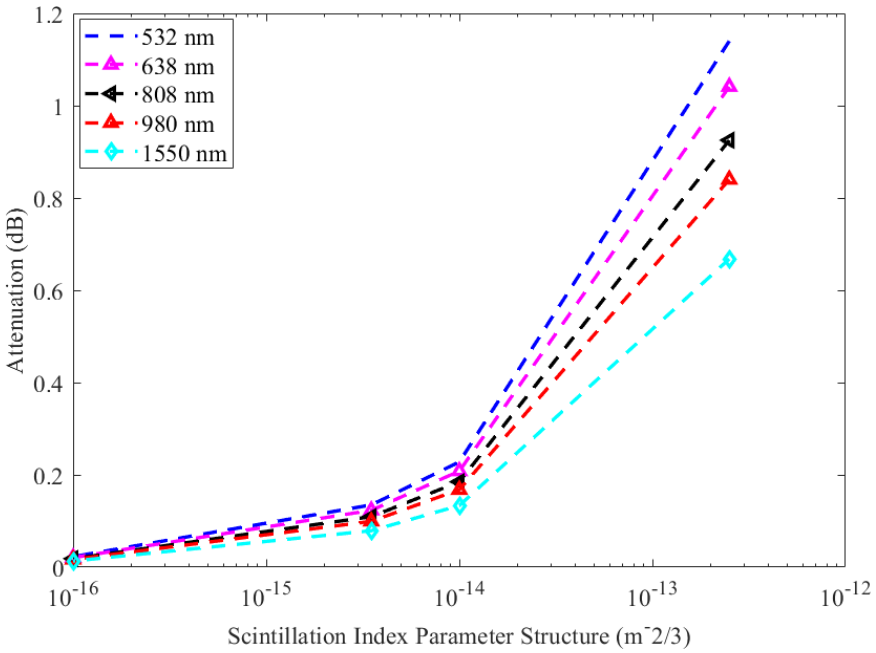

Fig. 4.24. Optical power attenuation (dB) due to different scintillation range ($m^{-2/3}$) using different wavelengths

4.3.3. OPTICAL POWER ATTENUATION DUE TO FOG

Finally, the optical power attenuation due to artificial foggy conditions has been measured and presented in this section. In the foggy weather conditions scenario, the visibility is an important parameter and this term associated with the foggy condition. According to the visibility range values, the fog can be defined as very dense fog, dense fog, moderate fog, light fog, haze etc. At the very dense fog condition, visibility is very low (about 50 m) and at light fog and haze condition (2-3 km), the visibility is higher compared to dense condition. This type of visibility has been created in the artificial fog chamber. Primarily, in clear condition, a particular optical power has been set. After that artificial fog was entered to the chamber with different densities. With respect to the different density condition, the received optical power has been measured with different time. The visibility (attenuated received power with respect to transmitted power) has been measured using KIM law. Similarly, previous weather condition scenarios, in this foggy weather condition scenario also, five wavelengths have been considered that is 532 nm, 638 nm, 808 nm, 980 nm and 1550 nm.

From the figure of optical power attenuation due to fog (Fig. 4.25), it has been revealed that initially (for first 30 second duration), the received optical power remains almost constant that is no fog was entered to the chamber. After 30 second, the fog has been entered into the chamber, as a result, the optical power has been attenuated and this was continued with 7 minute 30 second, after that fog was evacuated as a result, optical power returns back to the previous value. In this 7 minute 30 second time duration different fog visibility has been created. The same operation has been repeated for the others wavelengths and the optical power attenuation for the same visibility has been measured.

Fig. 4.25. & Fig. 4.26 show the optical power attenuation due to foggy weather condition for the wavelengths of 532 nm and 638 nm Laser with respect to different visibility and different time condition. With compared fig 4.25 and fig. 4.26, it has been shown that a time difference has been noticed.

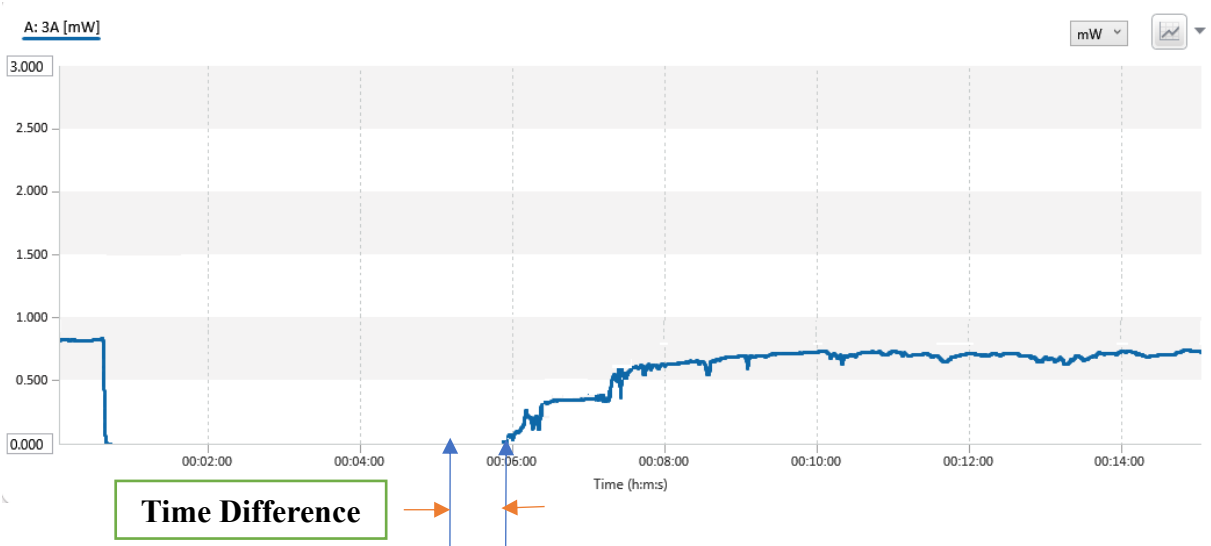

Fig. 4.25. Optical power attenuation of 532 nm Laser in different visibility with respective time

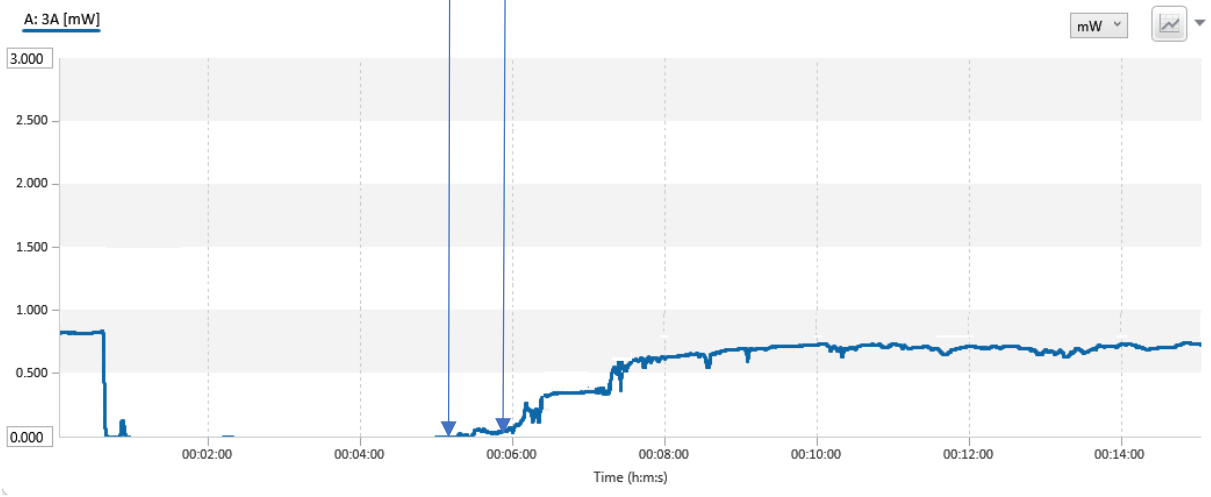

Fig. 4.26. Optical power attenuation of 638 nm Laser in different visibility with respective time

For the same amount of fog was entered in the chamber, but the 532 nm wavelength is more attenuated compared to 638 nm, this can be revealed by time difference of the optical power attenuation graph (Fig. 4.25 & Fig. 4.26). From the figures, it has been at 6-minute time duration, 532 nm received less optical power compared to 638 nm Laser. Therefore, for the same time duration with same visibility condition, 638 nm is less attenuated compared to 532 nm Laser.

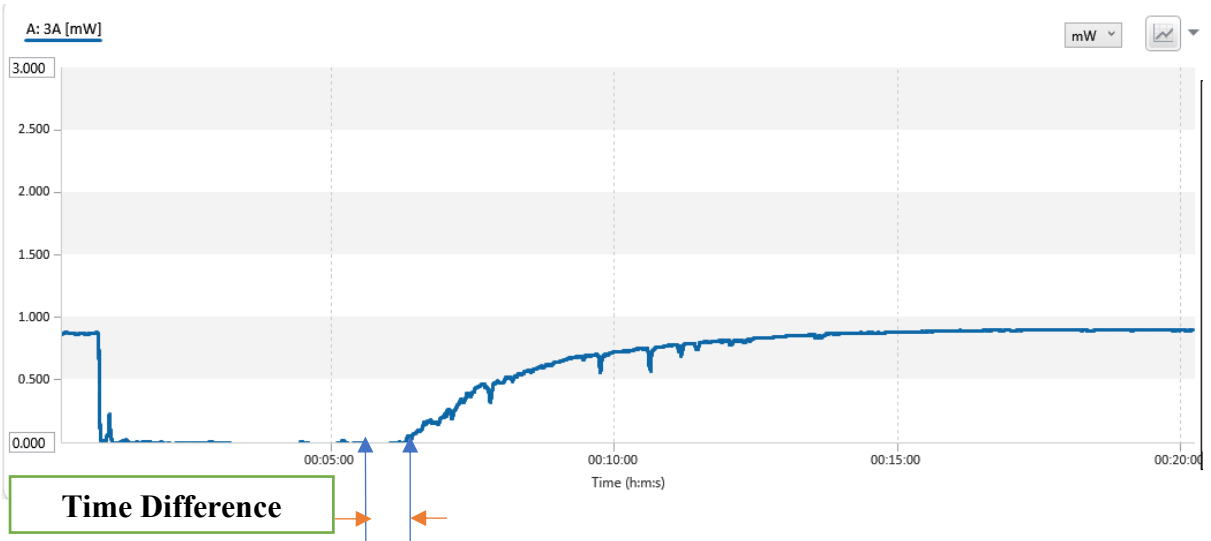

Fig. 4.27. Optical power attenuation of 808 nm Laser in different visibility with respective time

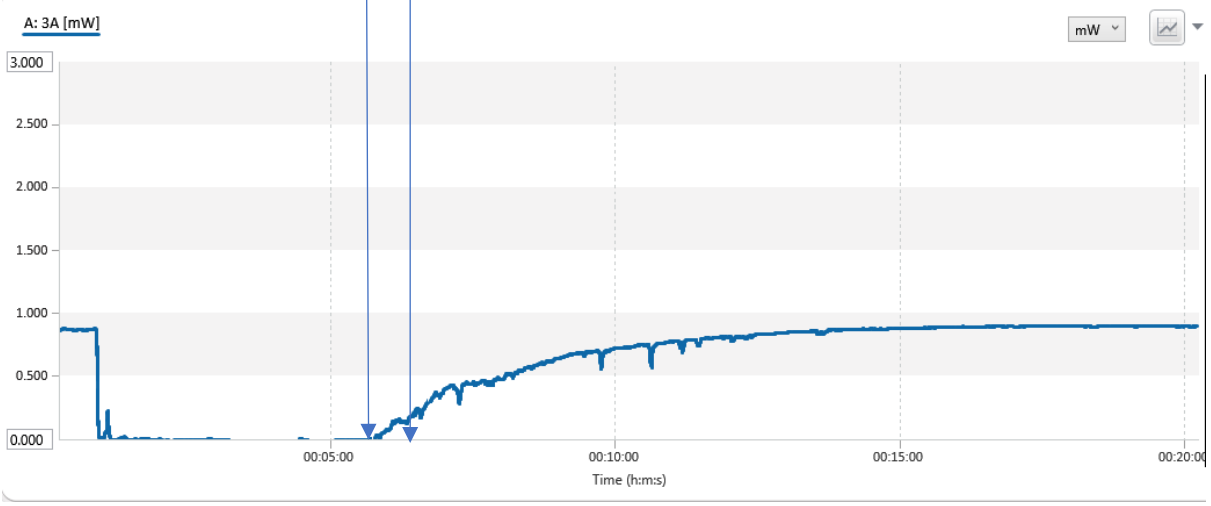

Fig. 4.28. Optical power attenuation of 980 nm Laser in different visibility with respective time

Similarly, Fig. 4.27. & Fig. 4.28 show the optical power attenuation due to foggy weather condition for the wavelengths of 808 nm and 980 nm Laser with respect to different visibility and different time condition. With compared fig 4.27 and fig. 4.28, it has been shown that a time difference has been noticed. For the same amount of fog was entered in the chamber, but the 808 nm wavelength is more attenuated compared to 980 nm, this can be revealed by time difference of the optical power attenuation graph (Fig. 4.27 & Fig. 4.27). From the figures, it has been at 5 minute 30 second time duration, 808 nm received less optical power compared to

980 nm Laser. Therefore, for the same time duration with same visibility condition, 980 nm is less attenuated compared to 808 nm Laser.

Fig. 4.29. shows the optical power attenuation of 1550 nm Laser in different visibility with respective time. The optical power attenuation lower for this wavelength compared to others wavelength. The same fog density, the optical power risen too early (before 5 minutes) compared to others wavelengths.

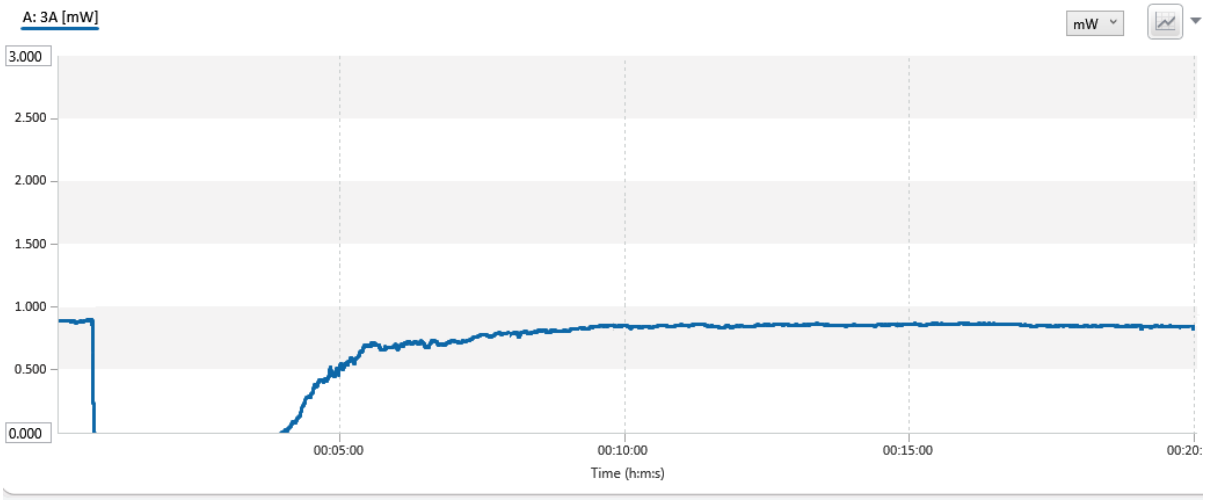

Fig. 4.29. Optical power attenuation of 1550 nm Laser in different visibility with respective time

From these aforesaid figures, the different visibility conditions have been derived from the same time duration for the different wavelengths. Fig.4.30 shows the different visibility condition with respective time duration.

In the case of foggy atmospheric condition scenario, due to lack of visibility meter instrument, the visibility measurement did not perform. As a result, the KIM model has been taken into consideration for the measurement. Other models have been discussed in the chapter 2, like Ijaz Model, Al- Naboulsi models. But these models are valid for above or equal to 690 nm wavelength and up to 1550 nm wavelength. But, in this thesis the 532 nm & 638 nm Wavelength Laser sources have been considered. Another point is that the aforesaid models (Ijaz Model, Al- Naboulsi models), the visibility range is constrained to 0.015 km to 0.9 km, these models are not valid for higher visibility range. As a result, these models are not valid for this thesis evaluation. Only KIM models are valid for these wavelengths evaluation, as these models are valid for all the considered wavelengths.

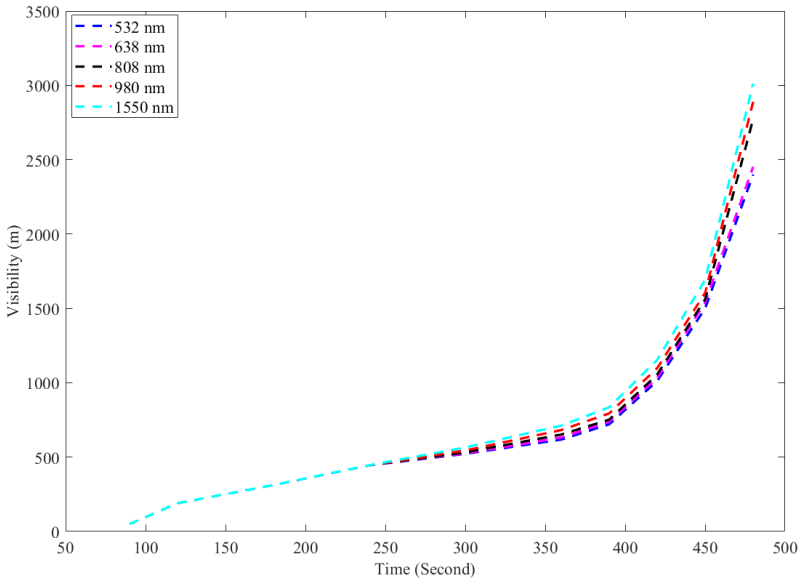

Fig.4.30. Different visibility with respect to time

From this figure, it has been shown that for the higher time duration (like 300 second - 450 second), the 1550 nm achieved more visibility compared to others wavelength and for lower time duration (less than 250 second), almost same visibility has been achieved irrespective of wavelengths.

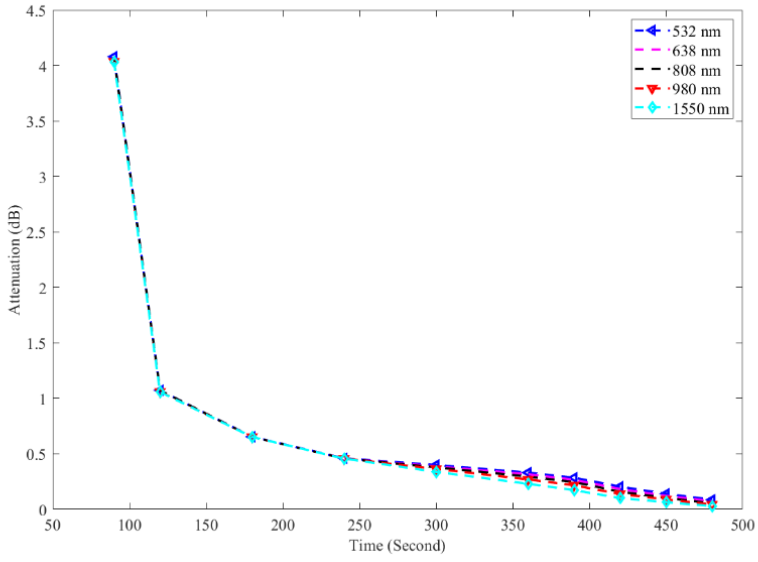

Fig.4.31. Measured optical power attenuation (dB) due to different visibility condition with respect to time

Similarly, Fig. 4.31 shows the optical power attenuation (dB) due to different visibility condition with respect to time. From the previous curve, it has been shown that at the higher visibility condition, the 1550 nm achieved greater visibility compared to other wavelengths, therefore, the optical power attenuation is lower compared to others wavelength. The attenuation level is higher for lower wavelength and with increment of wavelengths the optical power attenuation is low.

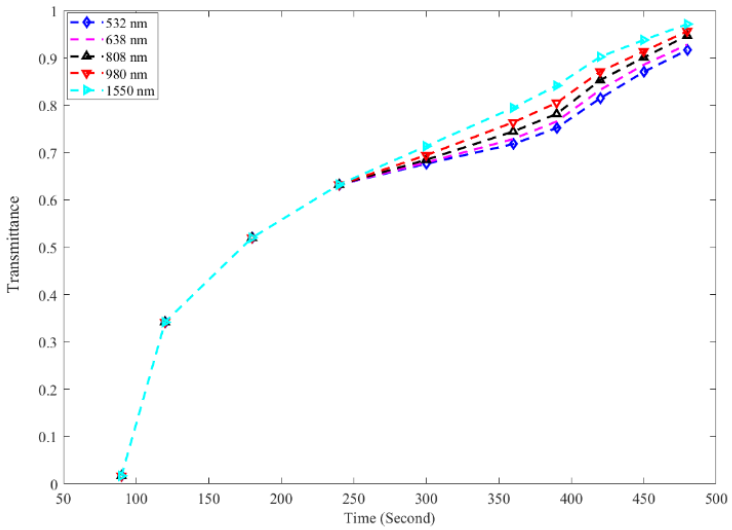

Fig.4.32. Measured transmittance due to different visibility condition with respect to time

Similarly, Fig.4.32 shows the measured transmittance due to different visibility condition with respect to time. As from the previous figure, it has been shown that the optical power attenuation is lower for 1550 nm laser, so a higher transmittance has been observed for 1550 nm Laser compared to lower wavelengths. With increment of wavelengths, the transmittance also increased.

Table. 4.14.1. shows the measured values of optical power attenuation for different wavelengths and different visibility range. As the visibility is decreased in the table, the attenuation is increased irrespective of wavelengths.

Table. 4.14.1. Measured values of optical power attenuation for different wavelengths and different visibility range

532 nm		638 nm		808 nm		980 nm		1550 nm	
Visibility (m)	Attenuation (dB)	Visibility (m)	Attenuation (dB)	Visibility (m)	Attenuation (dB)	Visibility (m)	Attenuation (dB)	Visibility (m)	Attenuation (dB)
190	1.073	190	1.0725	190	1.07244	190	1.05954	190	1.05
312	0.654	312	0.6528	312	0.6526	312	0.65248	312	0.6524
445	0.46	445	0.4584	445	0.45781	445	0.457512	445	0.4575
522	0.4	522	0.39	522	0.3875	522	0.3858	522	0.382
618	0.331	618	0.3234	618	0.3154	618	0.30888	618	0.2921
721	0.285	721	0.2924	721	0.25988	721	0.249	721	0.225
1012	0.205	1012	0.1871	1012	0.1662	1012	0.151	1012	0.11984
1500	0.14	1500	0.136	1500	0.1088	1500	0.0973	1500	0.0745
2400	0.087	2400	0.0763	2400	0.06434	2400	0.056	2400	0.0401
3012	0.0696	3012	0.044	3012	0.05	3012	0.0422	3012	0.0289

From these aforesaid figures, the optical power attenuation in different visibility conditions is predicted, with a link distance of 35 ft. Fig. 4.33 shows the optical power attenuation with different visibility condition for different wavelengths of Laser source.

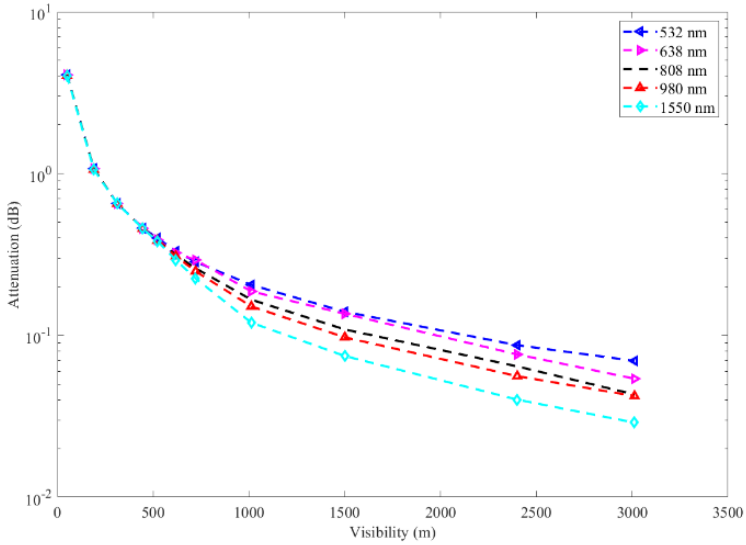

Fig. 4.33. Optical power attenuation with different visibility (m) for different visibility

From this figure, it has been shown that 1550 nm attenuates less compared to others wavelengths and attenuation increasing with decreasing the wavelengths for the same visibility conditions. When the visibility less than 500 m, the attenuation is almost same for all the considered wavelengths.

4.4. PERFORMANCE ON COMMUNICATION CHANNEL

In this section, different atmospheric conditions like rain, temperature, fog effect on optical communication channel has been determined in terms of eye diagram, Signal to Noise Ratio (SNR), Bit Error Rate (BER).

4.4.1. RAIN EFFECT ON COMMUNICATION CHANNEL

The amplified photodetector signal, comparator output signal, and corresponding eye patterns are shown in Fig. 4.34 during clear weather. Because of the comparator's high threshold limit, a clean eye pattern is produced when the amplified signal is clear, which is around 1.2 V.

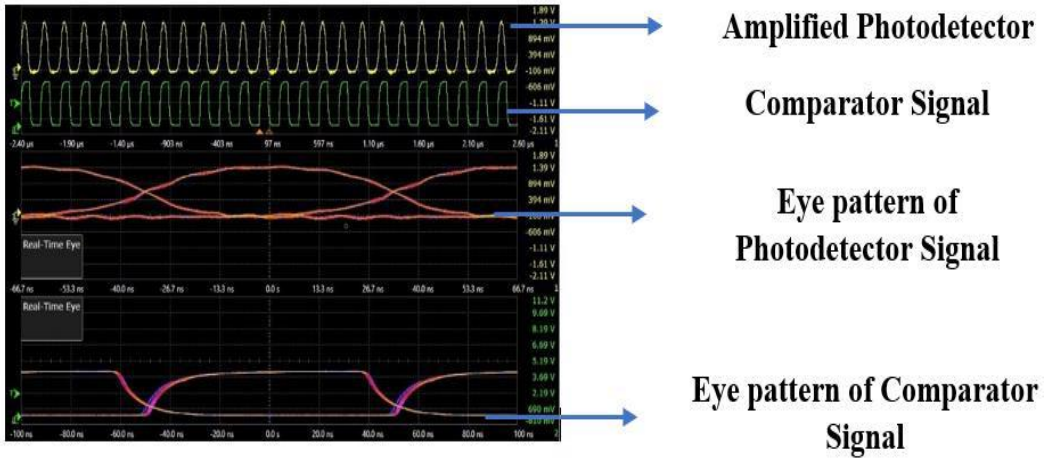

Fig 4.34. At clear weather condition, Comparator & Amplified photodetector signal and corresponding their eye patterns

When the 7 mm/hr rain rate has been applied to the system, the eye pattern of the photodetector signal and corresponding comparator eye pattern are illustrated in Fig. 4.35. Due to the optical power attenuation being relatively modest for the rain rate of 7 mm/hr, the eye height is still high but lower than in clear weather. Since comparator's threshold limit is high, the output of the comparator produces a clear signal.

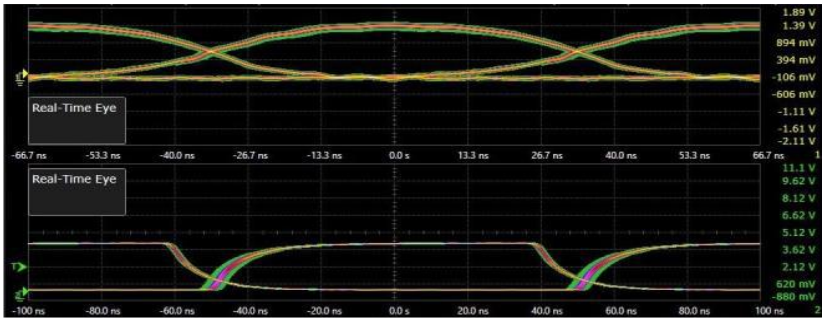

Fig 4.35. At 7 mm/hr rain rate condition, Comparator & Amplified photodetector signal and corresponding their eye patterns

Similar to this, at rain rates between 69 and 121 mm/hr, the photodetector signal's eye height decreases as the rain rate rises, but the comparator signal stays clear since the threshold value is still high up to 121 mm/hr.

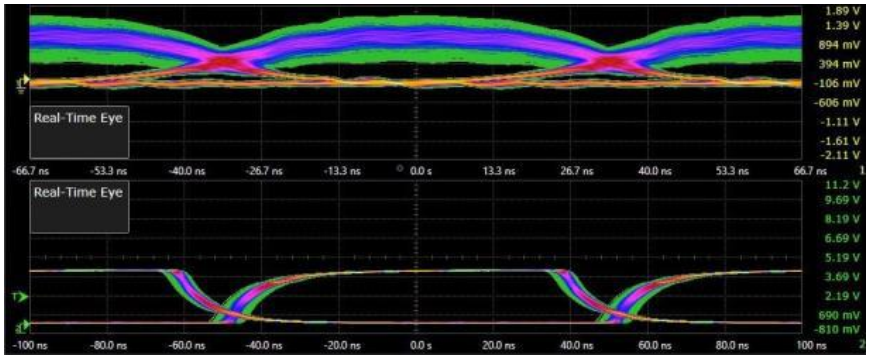

Fig. 4.36. At 69 mm/hr rain rate condition, Comparator & Amplified photodetector signal and corresponding their eye patterns

For rain rates of 69 mm/hr and 121 mm/hr, respectively, the photodetector signal and corresponding comparator eye pattern are shown in Fig. 4.36 & Fig. 4.37.

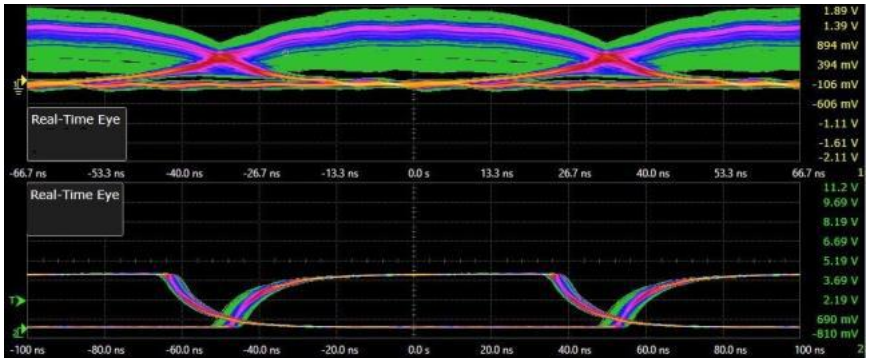

Fig. 4.37. At 121 mm/hr rain rate condition, Comparator & Amplified photodetector signal and corresponding their eye patterns

Because the comparator's threshold limit (150 mV) is lower for 180 mm/hr, the optical power is also degraded, the comparator is malfunctioning, and as a result, the communication link is not effectively created at the specific rain rates. The photodetector and comparator signal's eye pattern at a 180 millimetres per hour rain rate is depicted in Fig. 4.38.

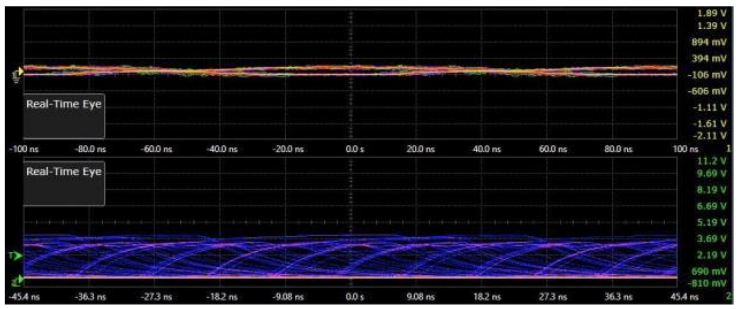

Fig. 4.38. At 180 mm/hr rain rate condition, Comparator & Amplified photodetector signal and corresponding their eye patterns

Since the optical power attenuation for different wavelengths are the same, the signal level at the receiver end is also the same, which causes the eye pattern there to be practically identical for different wavelengths.

4.4.2. SNR & BER MEASUREMENT FOR DIFFERENT RAIN RATES

The two key factors that determine the performance of a communication channel are SNR and BER. As the SNR is higher the BER is lower and vice versa. A communication channel's lower BER is a desirable feature for the receiver end. The SNR and BER measurement for different rain rates and different wavelengths are demonstrated in this section. Table 4.15 shows the SNR (dB) values for different rain rates (mm/hr) with different wavelengths.

Table. 4.15. SNR (dB) values for different rain rates (mm/hr) with different wavelengths

Rain Rates (mm/hr)	SNR for 532 nm (dB)	SNR for 638 nm (dB)	SNR for 808 nm (dB)	SNR for 980 nm (dB)	SNR for 1550 nm (dB)
7	22.59	22.59	22.63	22.63	22.98
28	20.81	20.81	20.88	20.89	21.15
69	17.894	17.893	17.9988	17.9988	18.216
121	14.002	14.001	14.1125	14.1128	14.567
153	12.886	12.886	12.984	12.984	13.1007
180	9.38	9.37	9.41	9.41	9.893

In general, the Signal to Noise Ratio (SNR) depends on the received optical power at the receiver side, Noise Equivalent Power (NEP) of the receiver system, etc.

As the received optical power for different wavelengths for a particular rain rate are same (wavelength independent phenomenon), so the SNR values should be practically same. But a small difference has been observed due to its small difference of NEP values of the used different photodetectors in the experimentation. Fig. 4.39. shows the SNR (dB) values for different rain rates with different wavelengths.

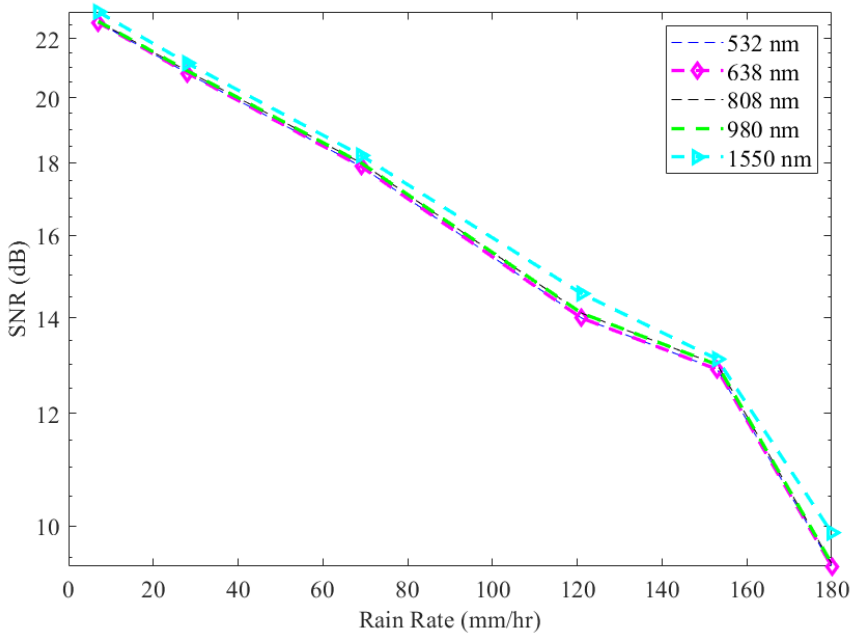

Fig. 4.39. SNR (dB) values for different rain rates with different wavelengths

As the rain rates increases gradually, the SNR values are decreasing in nature, as the optical power attenuation is more for higher rain rates. These trends are followed by all the considered wavelengths.

Table. 4.16. BER values for different rain rates (mm/hr) with different wavelengths

Rain Rates (mm/hr)	**BER for 532 nm**	**BER for 638 nm**	**BER for 808 nm**	**BER for 980 nm**	**BER for 1550 nm**
7	8.6891×10^{-12}	8.689×10^{-12}	7.016×10^{-12}	7.016×10^{-12}	9.933×10^{-13}
28	2.1252×10^{-8}	2.125×10^{-8}	1.6525×10^{-8}	1.593×10^{-8}	6.029×10^{-9}

69	4.4768×10^{-5}	4.485×10^{-5}	3.6716×10^{-5}	3.671×10^{-5}	2.398×10^{-5}
121	0.006164	0.006169	0.00562	0.005626	0.00378
153	0.013873	0.013873	0.01301	0.0130131	0.01203
180	0.07079	0.071022	0.07010	0.070107	0.059458

Table 4.16 depicts the BER values for different rain rates with different wavelengths. As the a little bit amount of change of SNR has been observed for different wavelengths, therefore a little bit amount of change of BER has been observed. Fig. 4.40. shows the BER values for different rain rates with different wavelengths.

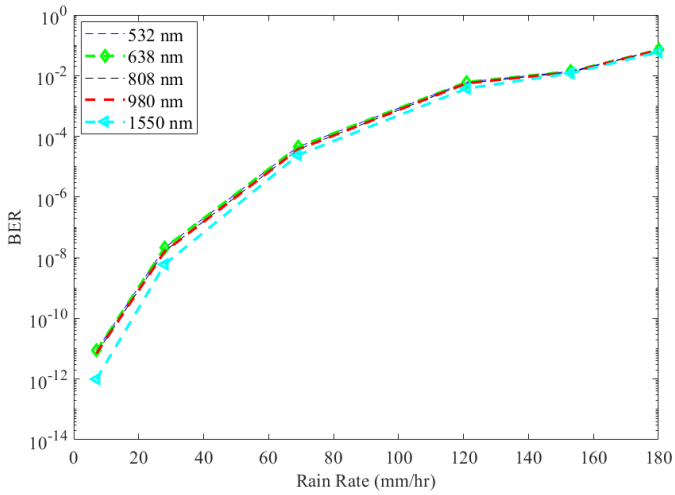

Fig. 4.40. BER values for different rain rates with different wavelengths

As the rain rates are increased gradually, the BER is increased and the same trend is observed for all the considered wavelengths.

4.4.3. TEMPERATURE EFFECT ON COMMUNICATION CHANNEL

The temperature difference between two points of a place can create the scintillation effects. In this section two ranges like higher and lower has been depicted. At higher ranges scintillation values, that is 2.5×10^{-13} $m^{-2/3}$, the 532 nm & 638 nm wavelengths are not worked as shown in the Fig. 4.41 and Fig. 4.42.

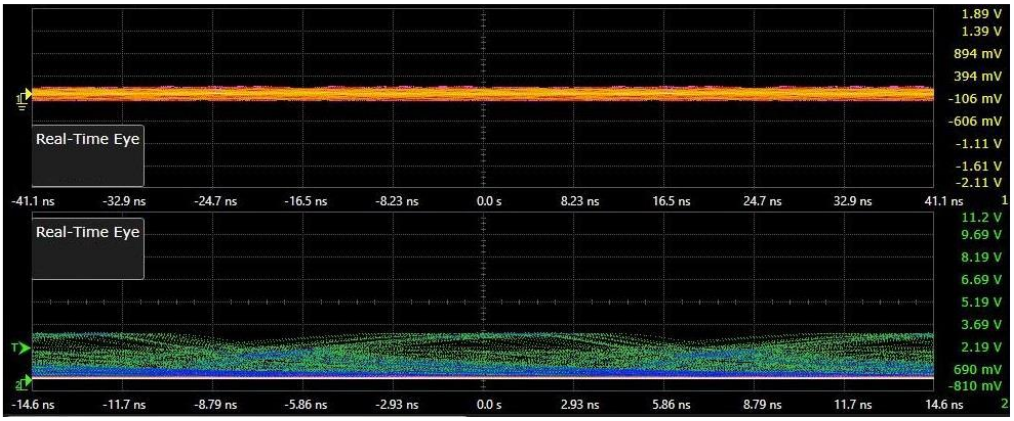

Fig. 4.41. Comparator & Amplified photodetector signal and corresponding their eye patterns for the scintillation range $2.5x10^{-13}$ $m^{-2/3}$ using wavelength 532 nm, 638 nm

As the optical power attenuation is more in the higher scintillation range for 532 nm and 638 nm, as a result, the comparator threshold limit is well below for these two wavelengths. So, in this scintillation range, these wavelengths are not worked.

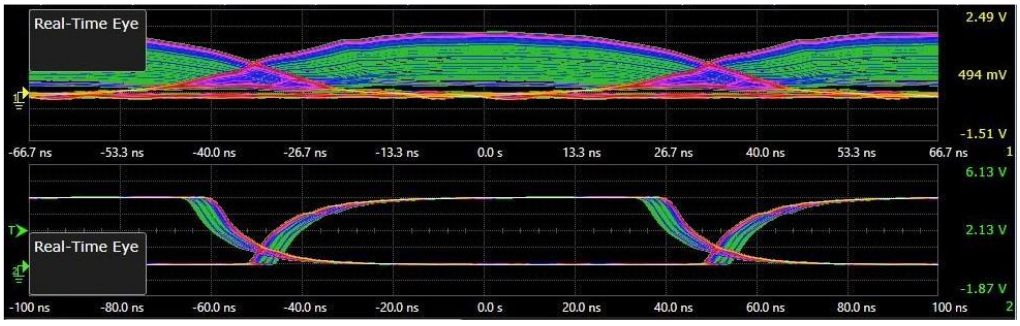

Fig. 4.42. Comparator & Amplified photodetector signal and corresponding their eye patterns for the scintillation range $2.5x10^{-13}$ $m^{-2/3}$ using wavelength 808 nm

Again, Fig. 4.43 and Fig.4.44 show the Comparator & Amplified photodetector signal and corresponding their eye patterns for the scintillation range $2.5x10^{-13}$ $m^{-2/3}$ using wavelength 808 nm and 980 nm respectively. The optical power attenuation is more compared to 638 nm for these two wavelengths, as a result, the comparator threshold limit is high enough, consequently, in this range, 808 nm and 980 nm is worked.

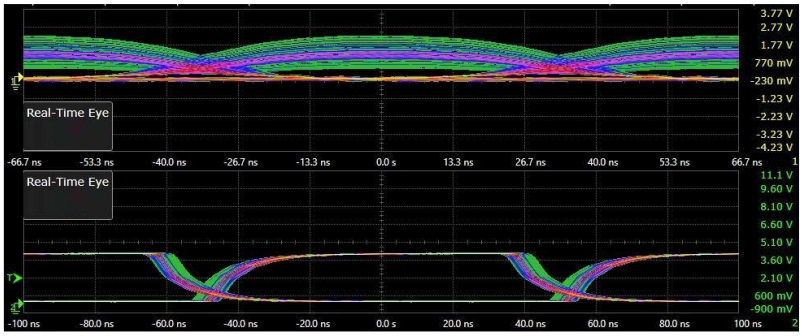

Fig. 4.43. Comparator & Amplified photodetector signal and corresponding their eye patterns for the scintillation range $2.5x10^{-13}$ $m^{-2/3}$ using wavelength 980 nm

Similarly, Fig. 4.44 shows the comparator & amplified photodetector signal and corresponding their eye patterns for the scintillation range $2.5x10^{-13}$ $m^{-2/3}$ using wavelength 1550 nm. As the optical power attenuation is lower compared to others wavelength, the comparator worked properly.

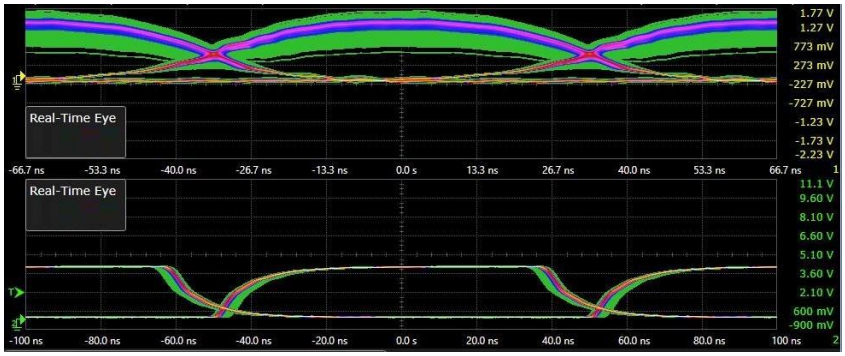

Fig. 4.44. Comparator & Amplified photodetector signal and corresponding their eye patterns for the scintillation range $2.5x10^{-13}$ $m^{-2/3}$ using wavelength 1550 nm

Fig. 4.45, Fig. 4.46, Fig. 4.47, Fig. 4.48 and Fig. 4.49 show the comparator & amplified photodetector signal and corresponding their eye patterns for the scintillation range $3.5x10^{-15}$ $m^{-2/3}$ using wavelength 532 nm, 638 nm, 808 nm, 980 nm, and 1550 nm respectively.

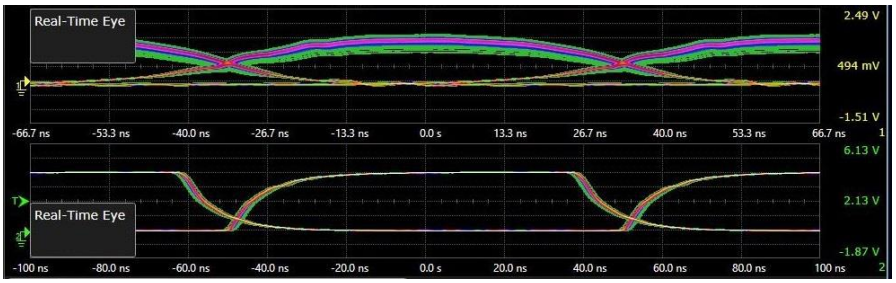

Fig. 4.45. Comparator & Amplified photodetector signal and corresponding their eye patterns for the scintillation range $3.5x10^{-15}$ $m^{-2/3}$ using wavelength 532 nm

As the optical power attenuation is increasing with decreasing the optical wavelength, the eye height is decreasing, in the lower scintillation range ($3x10^{-15}$ $m^{-2/3}$).

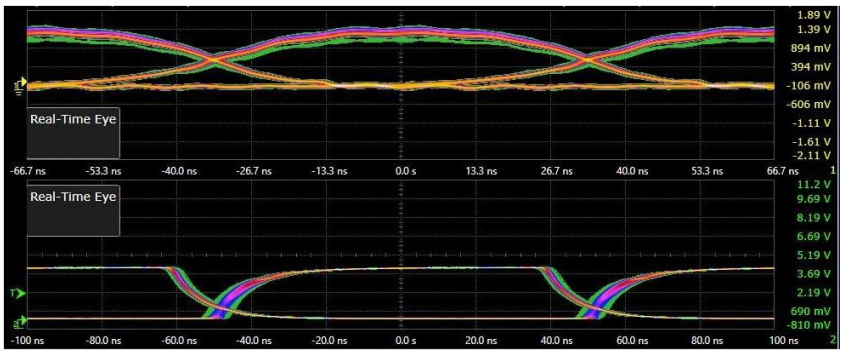

Fig. 4.46. Comparator & Amplified photodetector signal and corresponding their eye patterns for the scintillation range $3.5x10^{-15}$ $m^{-2/3}$ using wavelength 638 nm

In this lower scintillation range, the optical power attenuation is low for all the considered wavelengths and the threshold limit for the comparator is high for all the wavelength, as a result, all the wavelengths are worked properly in this scintillation range.

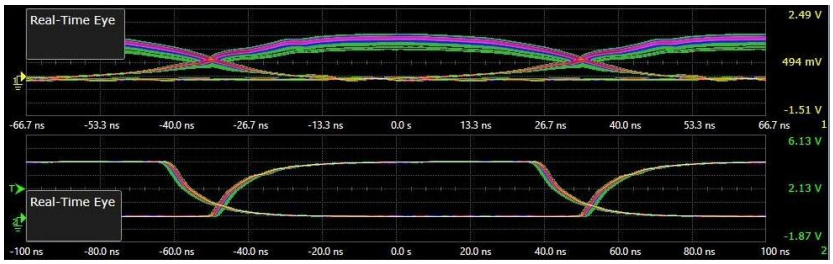

Fig. 4.47. Comparator & Amplified photodetector signal and corresponding their eye patterns for the scintillation range $3.5x10^{-15}$ $m^{-2/3}$ using wavelength 808 nm

Though optical power attenuation is low in this scintillation range, among all the considered wavelengths 532 nm provides grater optical attenuation and 1550 nm provides the lower optical power attenuation.

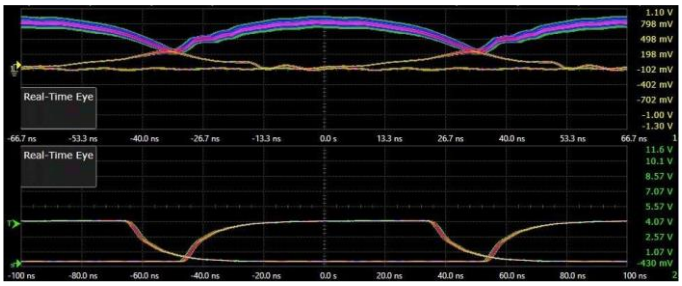

Fig. 4.48. Comparator & Amplified photodetector signal and corresponding their eye patterns for the scintillation range $3.5x10^{-15}$ $m^{-2/3}$ using wavelength 980 nm

Consequently, the eye height is lower compared to others wavelength and 1550 nm provide higher eye height in the same scintillation range.

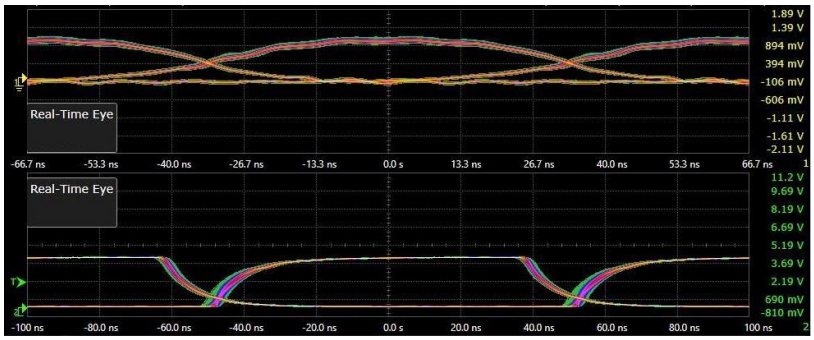

Fig. 4.49. Comparator & Amplified photodetector signal and corresponding their eye patterns for the scintillation range $3.5x10^{-15}$ $m^{-2/3}$ using wavelength 1550 nm

4.4.4. SNR & BER MEASUREMENT FOR DIFFERENT SCINTILLATION RANGE

The SNR & BER performance due to different scintillation ranges are depicted in this section. Table 4.17 shows the SNR values for different scintillation range ($m^{-2/3}$) with different wavelengths.

Table. 4.17. SNR (dB) values for different scintillation range ($m^{-2/3}$) with different wavelengths

532 nm		**638 nm**		**808 nm**		**980 nm**		**1550 nm**	
C_n^2 ($m^{-2/3}$)	**SNR (dB)**	**C_n^2 ($m^{-2/3}$)**	**SNR (dB)**	**C_n^2 ($m^{-2/3}$)**	**SNR (dB)**	**C_n^2 ($m^{-2/3}$)**	**SNR (dB)**	**C_n^2 ($m^{-2/3}$)**	**SNR (dB)**
$2.5x10^{-13}$	9.01	**$2.5x10^{-13}$**	9.16	**$2.5x10^{-13}$**	9.87	**$2.5x10^{-13}$**	10.546	**$2.5x10^{-13}$**	11.214
10^{-14}	16.43	**10^{-14}**	16.714	**10^{-14}**	17.042	**10^{-14}**	17.621	**10^{-14}**	18.004
$3.5x10^{-15}$	20.22	**$3.5x10^{-15}$**	20.76	**$3.5x10^{-15}$**	21.02	**$3.5x10^{-15}$**	21.92	**$3.5x10^{-15}$**	22.02
10^{-16}	23.33	**10^{-16}**	23.91	**10^{-16}**	24.12	**10^{-16}**	24.961	**10^{-16}**	25.914

As the optical power attenuation is decreased as increased with wavelengths, the SNR values are better for higher wavelengths. As the SNR values are dependent on received optical power and NEP of the photodetector system, 1550 nm wavelength provides higher SNR (dB) values compared to others wavelengths for all the scintillation ranges, because, 1550 nm provides lower optical power attenuation at all the scintillation ranges and NEP value of the photodetector which is used for 1550 nm wavelength is lower.

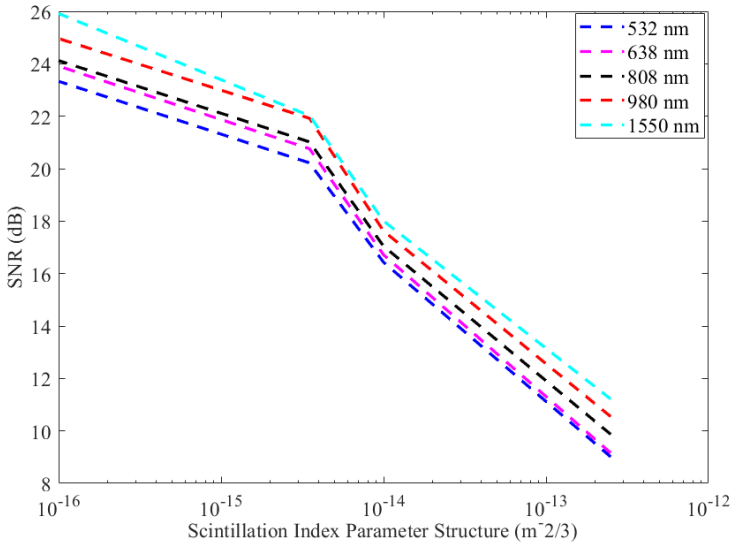

Fig. 4.50. SNR (dB) values for different scintillation ranges with different wavelengths

Fig. 4.50 shows the SNR values for different scintillation ranges with different wavelengths. Similarly, Table 4.18 depicts the BER values for different scintillation range with different wavelengths.

Table. 4.18. BER values for different scintillation range ($m^{-2/3}$) with different wavelengths

532 nm		**638 nm**		**808 nm**		**980 nm**		**1550 nm**	
C_n^2 ($m^{-2/3}$)	**BER**	**C_n^2 ($m^{-2/3}$)**	**BER**	**C_n^2 ($m^{-2/3}$)**	**BER**	**C_n^2 ($m^{-2/3}$)**	**BER**	**C_n^2 ($m^{-2/3}$)**	**BER**
2.5×10^{-13}	0.098	**2.5×10^{-13}**	0.081	**2.5×10^{-13}**	0.026	**2.5×10^{-13}**	0.00075	**2.5×10^{-13}**	0.00014
10^{-14}	0.00046	**10^{-14}**	0.00031	**10^{-14}**	0.00019	**10^{-14}**	7.35×10^{-5}	**10^{-14}**	2.64×10^{-5}
3.5×10^{-15}	1.5×10^{-7}	**3.5×10^{-15}**	2.5×10^{-8}	**3.5×10^{-15}**	9.8×10^{-9}	**3.5×10^{-15}**	2.3×10^{-10}	**3.5×10^{-15}**	1.05×10^{-11}
10^{-16}	1.2×10^{-13}	**10^{-16}**	2.4×10^{-15}	**10^{-16}**	5.2×10^{-16}	**10^{-16}**	4.9×10^{-19}	**10^{-16}**	3.02×10^{-23}

As the received SNR is higher for 1550 nm Laser source compared to others considered wavelengths, 1550 nm provides better BER values compared to others wavelengths in the different scintillation regimes.

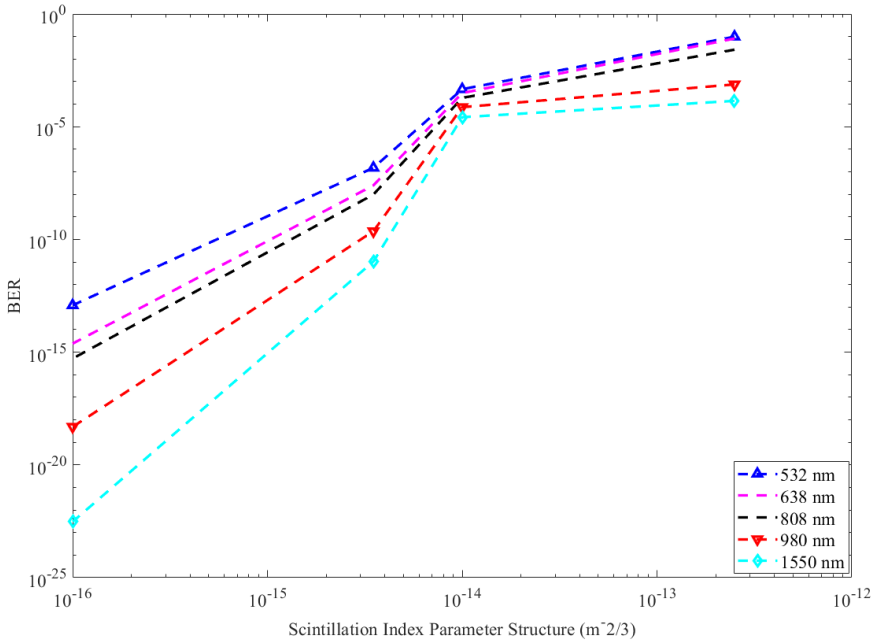

Fig. 4.51. BER values for different scintillation ranges with different wavelengths

However, at the lower wavelengths or visible wavelengths condition (532 nm & 638 nm), the BER is highest at all the scintillation regimes. But, the 638 nm performs better than 532 nm wavelength at all the scintillation regimes.

Similarly, at the NIR wavelengths scenario, that is 808 nm and 980 nm wavelengths, the 980 nm provides lower BER values than 808 nm Laser source. Moreover, from this discussion it has been shown that at higher wavelength condition, the effect of scintillation is lower. Fig. 4.51 shows the BER values for different scintillation ranges with different wavelengths.

4.4.5. FOG EFFECT ON COMMUNICATION CHANNEL

In this section, the effect of fog on communication channel has been depicted. Fig. 4.52, Fig 4.53, Fig. 4.54, Fig. 4.55 and Fig. 4.56 show the Comparator & Amplified photodetector signal and corresponding their eye patterns for the visibility of 721 m using wavelength 532 nm, 638 nm, 808 nm, 980 nm and 1550 nm respectively.

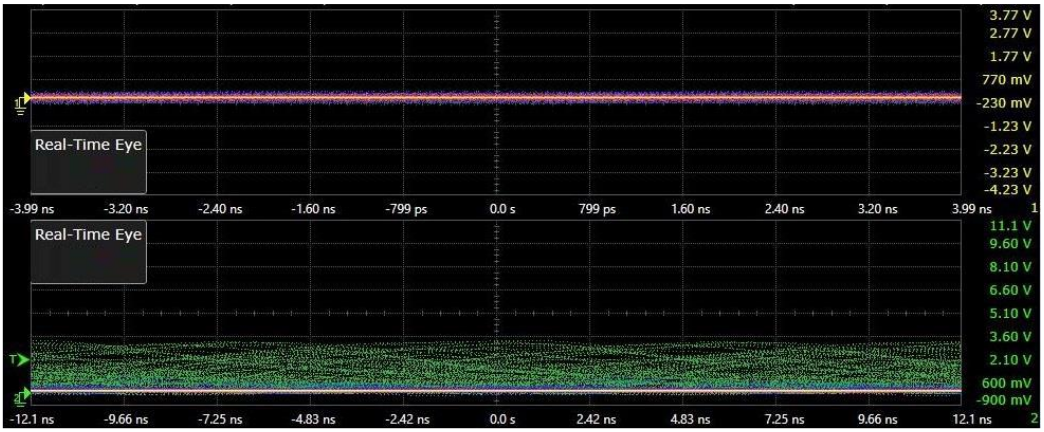

Fig. 4.52. Comparator & Amplified photodetector signal and corresponding their eye patterns for the visibility of 721 m using wavelength 532 nm

From these figures, it has been shown that at 721 m visibility range, the visible wavelengths (532 nm & 638 nm) are not worked. As the optical power attenuation in this visibility range is higher for these wavelengths, so the threshold limit of the comparator is low, so these wavelengths are not worked in this visibility condition.

However, comparing with 808 nm and 980 nm wavelength, the optical power attenuation is lower than visible wavelengths, but 980 nm provides better result than 808 nm. As a result, the eye height of amplified photodetector signal of the 980 nm wavelength is higher compared to 808 nm wavelength.

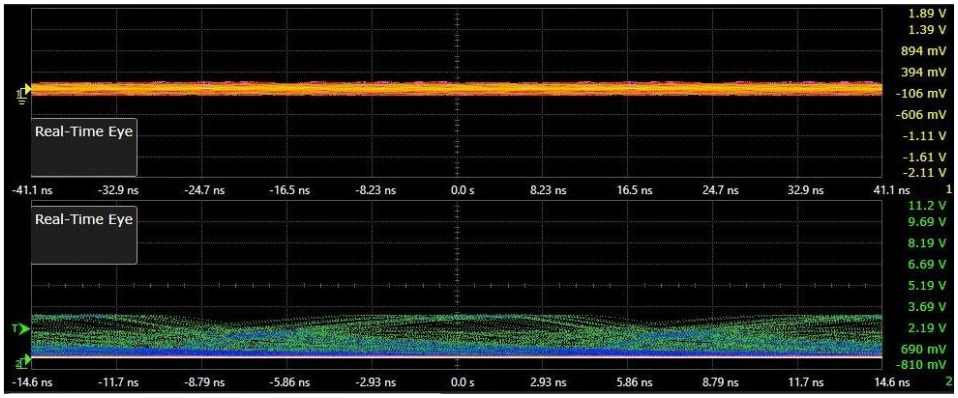

Fig. 4.53. Comparator & Amplified photodetector signal and corresponding their eye patterns for the visibility of 721 m using wavelength 638 nm

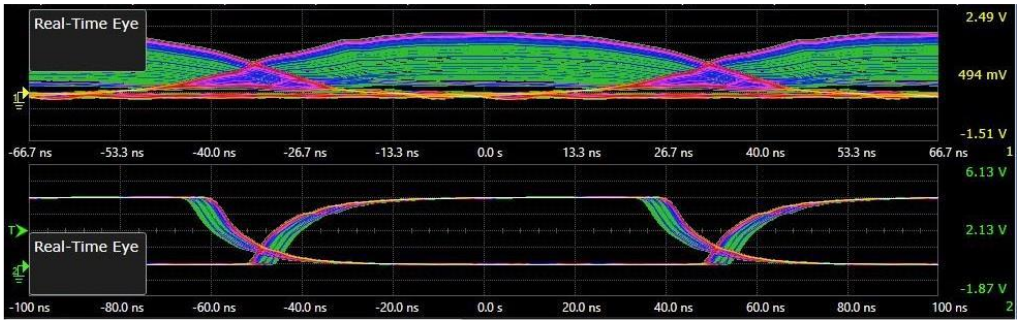

Fig. 4.54. Comparator & Amplified photodetector signal and corresponding their eye patterns for the visibility of 721 m using wavelength 808 nm

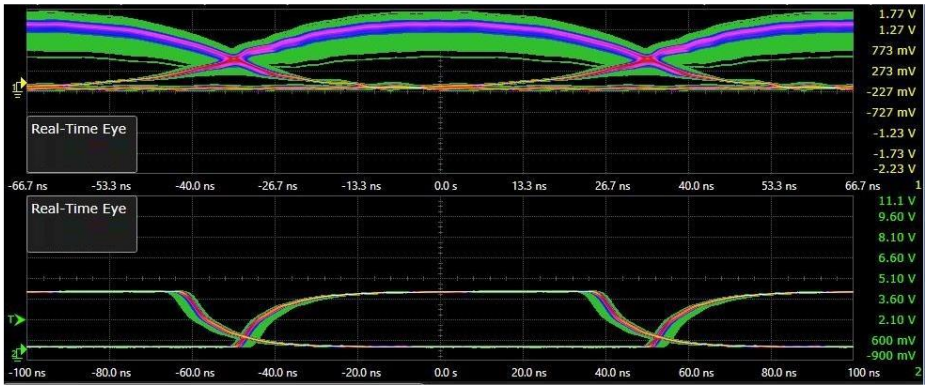

Fig. 4.55. Comparator & Amplified photodetector signal and corresponding their eye patterns for the visibility of 721 m using wavelength 980 nm

Finally, 1550 nm provides lower optical power attenuation among all the considered wavelengths. Therefore, 1550 nm provides better result in this visibility condition and the eye height of this wavelength is more compared to otters considered wavelength.

When considering the higher visibility range (1500 m), similar type of trends is observed. At higher wavelength, the communication performance is better than lower wavelength for the same visibility condition.

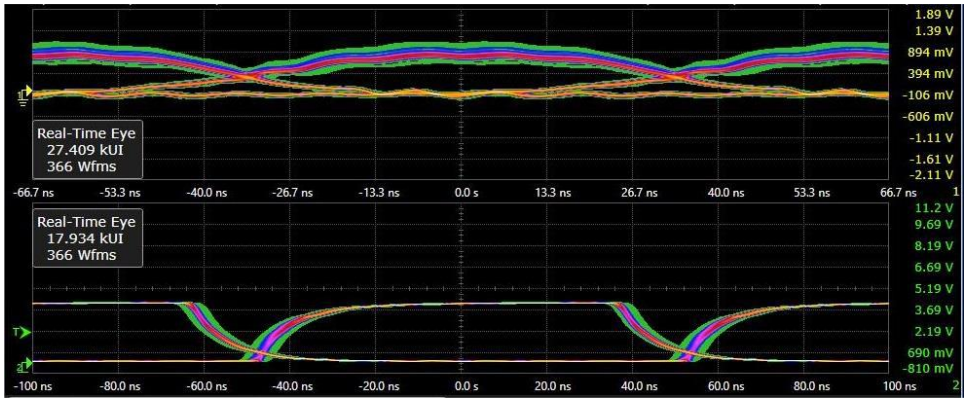

Fig. 4.56. Comparator & Amplified photodetector signal and corresponding their eye patterns for the visibility of 721 m using wavelength 1550 nm

Fig. 4.57, Fig. 4.58, Fig. 4.59, Fig. 4.60, and Fig. 4.61 show the comparator & Amplified photodetector signal and corresponding their eye patterns for the visibility of 1500 m using wavelength 532 nm, 638 nm, 808 nm, 980 nm, and 1550 nm respectively.

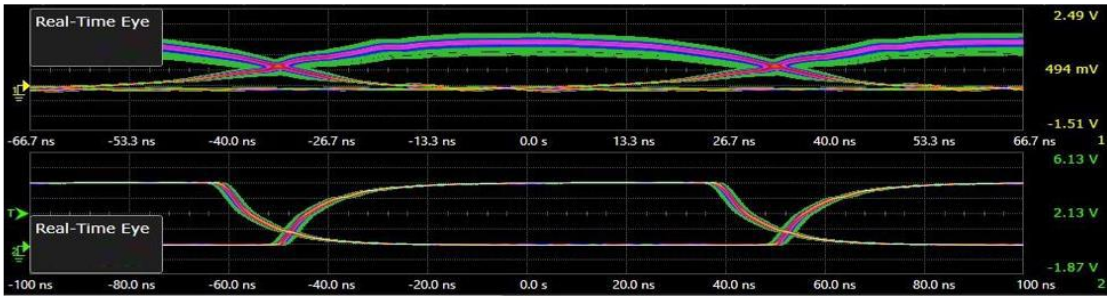

Fig. 4.57. Comparator & Amplified photodetector signal and corresponding their eye patterns for the visibility of 1500 m using wavelength 532 nm

The eye height of the amplified photodetector signal of 1550 nm is higher and 532 nm is lower for the same visibility condition scenario.

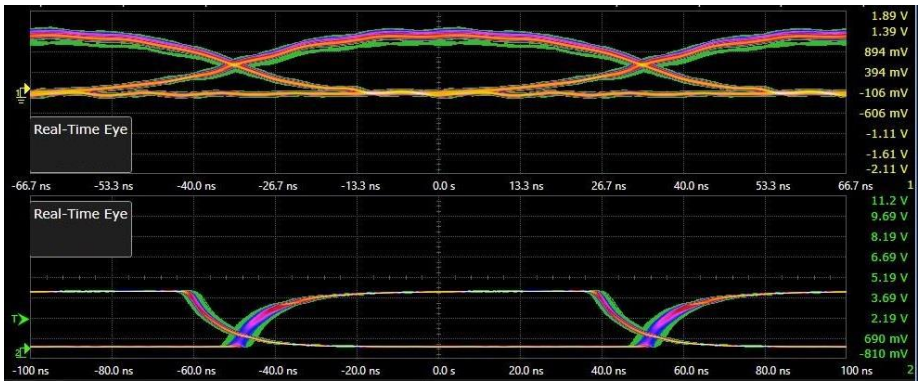

Fig. 4.58. Comparator & Amplified photodetector signal and corresponding their eye patterns for the visibility of 1500 m using wavelength 638 nm

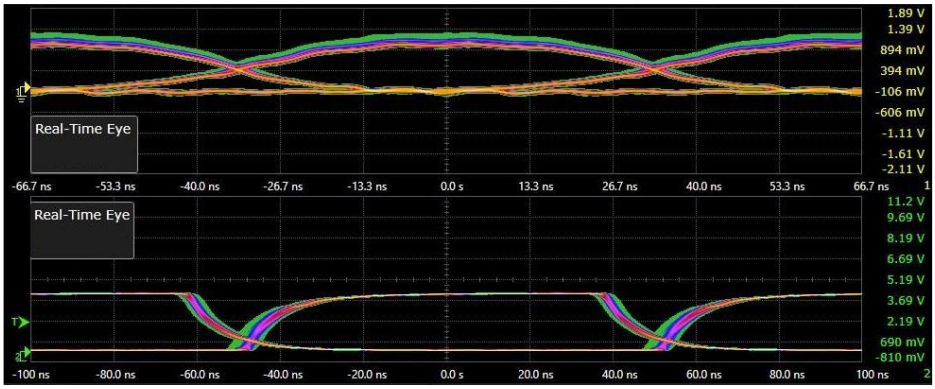

Fig. 4.59. Comparator & Amplified photodetector signal and corresponding their eye patterns for the visibility of 1500 m using wavelength 808 nm

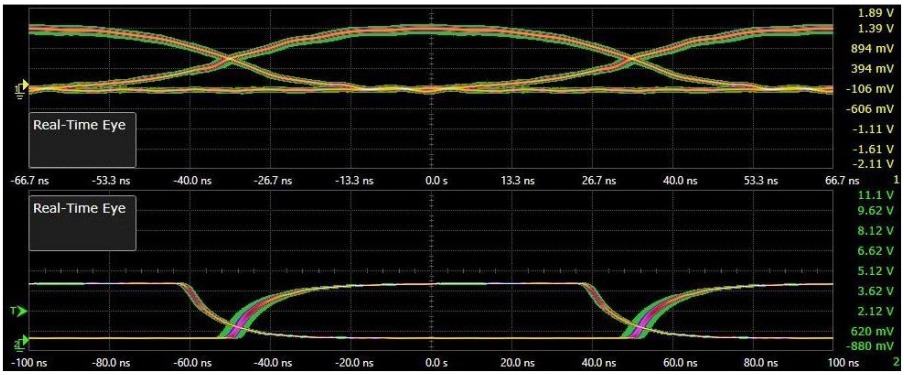

Fig. 4.60. Comparator & Amplified photodetector signal and corresponding their eye patterns for the visibility of 1500 m using wavelength 980 nm

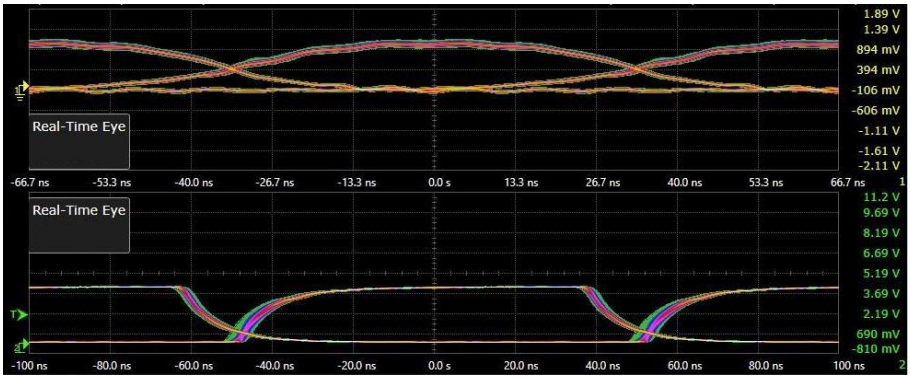

Fig. 4.61. Comparator & Amplified photodetector signal and corresponding their eye patterns for the visibility of 1500 m using wavelength 1550 nm

4.4.6. SNR & BER MEASUREMENT OF DIFFERENT VISIBILITY FOG

Table 4.19 shows the SNR (dB) values for different visibility (m) with different wavelengths. At very lower visibility conditions (190 m-445 m), the optical power attenuation is almost same for all the considered wavelengths, so the SNR values are almost same irrespective of considered wavelengths.

Table. 4.19. SNR (dB) values for different visibility (m) with different wavelengths

532 nm		**638 nm**		**808 nm**		**980 nm**		**1550 nm**	
Visibility (m)	**SNR (dB)**	**Visibility (m)**	**SNR (dB)**	**Visibility (m)**	**SNR (dB)**	**Visibility (m)**	**SNR (dB)**	**Visibility (m)**	**SNR (dB)**
190	2.5	190	2.51	190	2.53	190	2.536	190	2.538
312	4.2	312	4.2	312	4.211	312	4.216	312	4.28
445	6.84	445	6.843	445	6.844	445	6.845	445	6.849
522	7.89	522	7.96	522	8.05	522	8.21	522	8.894
618	9.06	618	9.36	618	10.71	618	11.01	618	11.94
721	11.15	721	11.67	721	12.84	721	13.28	721	14.05
1012	14.05	1012	14.46	1012	15.41	1012	15.96	1012	16.17
1500	17.89	1500	18.06	1500	18.84	1500	19.24	1500	20.02
2400	22.02	2400	22.35	2400	22.98	2400	23.23	2400	24.06
3012	24.96	3012	25.51	3012	26.65	3012	27.05	3012	27.88

At the moderate visibility condition (522 m – 1500 m) and higher visibility condition (2400 m – 3012 m), the optical power attenuation is not the same for all the considered wavelengths, so the SNR has been varied. As the lower wavelengths are more attenuated for the same visibility condition, therefore, lower wavelength exhibits poor SNR values (dB). Fig. 4.62 shows the SNR (dB) values for different visibility (m) ranges with different wavelengths.

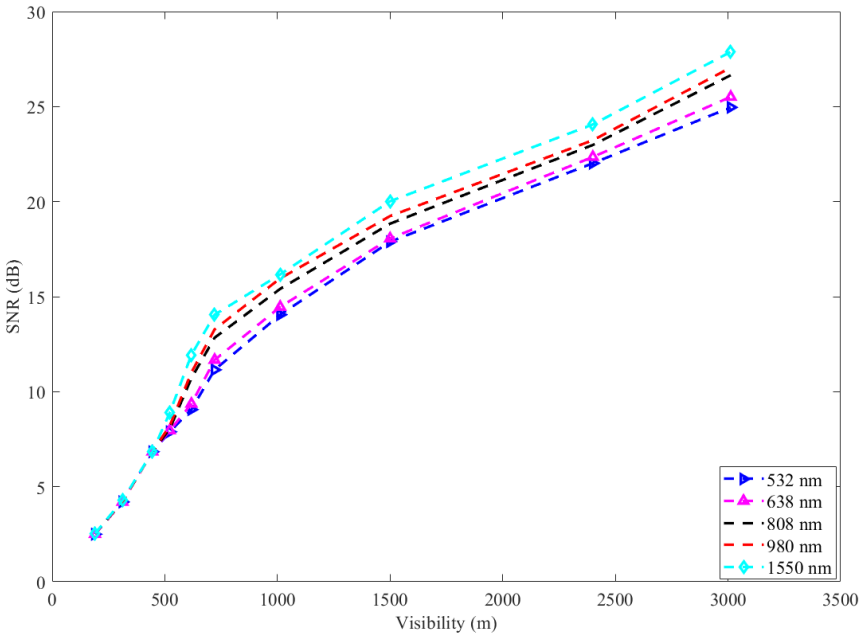

Fig. 4.62. SNR (dB) values for different visibility (m) ranges with different wavelengths

Similarly, Table 4.20 shows BER values for different visibility with different wavelengths condition. When the visibility is increased, the BER is also improved. This trend is observed for all the considered wavelengths.

Table. 4.20. BER values for different visibility (m) with different wavelengths

532 nm		**638 nm**		**808 nm**		**980 nm**		**1550 nm**	
Visibility (m)	**BER**	**Visibility (m)**	**BER**	**Visibility (m)**	**BER**	**Visibility (m)**	**BER**	**Visibility (m)**	**BER**
190	0.5055	190	0.50551	190	0.50421	190	0.5038	190	0.5037
312	0.4181	312	0.418	312	0.417	312	0.4173	312	0.4138
445	0.2725	445	0.272	445	0.2723	445	0.273	445	0.272
522	0.2156	522	0.211	522	0.2072	522	0.199	522	0.164
618	0.1565	618	0.142	618	0.0867	618	0.0761	618	0.0484
721	0.07152	721	0.0557	721	0.0185	721	0.0081	721	0.00218
1012	0.01185	1012	0.0083	1012	0.00325	1012	0.0017	1012	0.00131
1500	9.020×10^{-5}	1500	6.53×10^{-5}	1500	1.25×10^{-5}	1500	4.79×10^{-6}	1500	5.62×10^{-7}
2400	2.99×10^{-10}	2400	6.02×10^{-11}	2400	1.99×10^{-12}	2400	4.46×10^{-13}	2400	1.63×10^{-15}
3012	9.85×10^{-19}	3012	4.76×10^{-21}	3012	6.99×10^{-27}	3012	2.58×10^{-29}	3012	3.91×10^{-35}

Fig. 4.63 shows the BER values for different visibility (m) ranges with different wavelengths conditions.

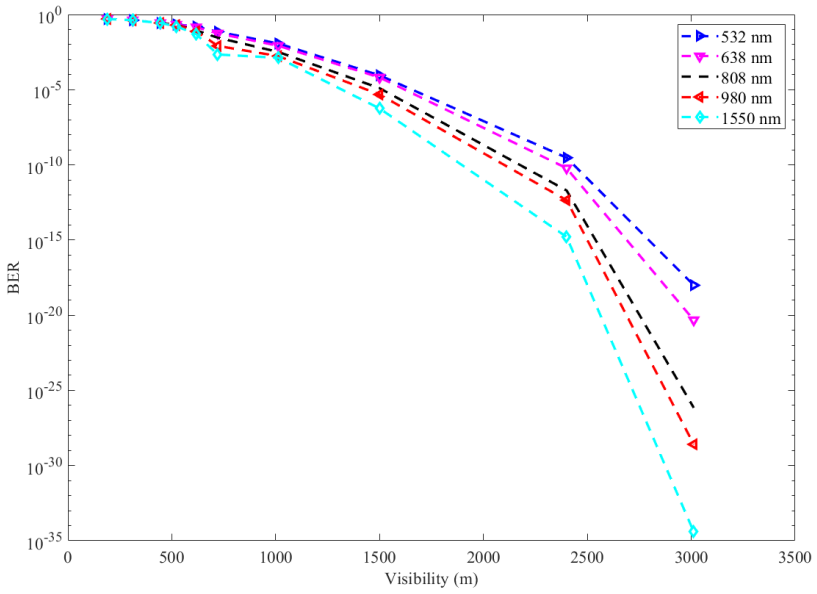

Fig. 4.63. BER values for different visibility (m) ranges with different wavelengths

As the lower visibility ranges, the SNR are almost same for all the wavelengths, the BER values are almost same for all the considered wavelengths. In the moderate and higher visibility condition, the 1550 nm provides lower BER than others wavelengths. Again, comparing between visible wavelengths that is 532 nm and 638 nm, 638 nm provides better results. Similarly, comparing between 808 nm and 980 nm, 980 nm provides better result. Moreover, among the considered wavelengths, 1550 nm provides superior results and 532 nm provides worse result for the same visibility condition scenario.

From the aforesaid experimental results and analysis, the permissible limit for the different wavelengths for the different atmospheric conditions for a particular BER are given in the below:

Table 4.21. Permissible limit of visibility, scintillation, and rain rates for the range of BER 10^{-6} for different wavelengths

532 nm		**638 nm**		**808 nm**		**980 nm**		**1550 nm**	
Visibility (m)	**BER**	**Visibility (m)**	**BER**	**Visibility (m)**	**BER**	**Visibility (m)**	**BER**	**Visibility (m)**	**BER**
1800	10^{-6}	1750	10^{-6}	1589	10^{-6}	1500	10^{-6}	1400	10^{-6}
Scintillation ($m^{-2/3}$)	**BER**	**Scintillation ($m^{-2/3}$)**	**BER**	**Scintillation ($m^{-2/3}$)**	**BER**	**Scintillation ($m^{-2/3}$)**	**BER**	**Scintillation ($m^{-2/3}$)**	**BER**
$2.5x10^{-15}$	10^{-6}	10^{-15}	10^{-6}	$8.5x10^{-14}$	10^{-6}	$6.5x10^{-14}$	10^{-6}	$2.0x10^{-14}$	10^{-6}

Rain Rates (mm/hr)	BER	Rain Rates (mm/hr)	BER	Rain Rates (mm/hr)	BER	Rain Rates (mm/hr)	BER	Rain Rates (mm/hr)	BER
66.67	10^{-6}	66.6	10^{-6}	66.54	10^{-6}	66.5	10^{-6}	66.46	10^{-6}

Table 4.21 shows the Permissible limit of visibility, scintillation, and rain rates for the range of BER 10^{-6} for different wavelengths. From the table, it has been shown that for maintaining the 10^{-6} BER values, 532 nm works upto 1800 m visibility, 638 nm works upto 1750 m visibility, 808 nm works upto 1589 m visibility, 980 nm works upto 1500 m visibility, and 1550 nm works upto 1400 m visibility respectively. Similarly, for scintillation condition scenario, 532 nm works upto $2.5x10^{-15}$ $m^{-2/3}$ scintillation range, 638 nm works upto 10^{-15} $m^{-2/3}$ scintillation range, 808 nm works upto $8.5x10^{-14}$ $m^{-2/3}$ scintillation range, 980 nm works upto $6.5x10^{-14}$ $m^{-2/3}$ scintillation range, and 1550 nm works upto $2.0x10^{-14}$ $m^{-2/3}$ scintillation range respectively for 10^{-6} BER. Finally, for rainy weather condition scenario, 532 nm works upto 66.67 mm/hr, 638 nm works upto 66.60 mm/hr, 808 nm works upto 66.54 mm/hr, 980 nm works upto 66.5 mm/hr, and 1550 nm works upto 66.67 mm/hr for the Bit Error Rate of 10^{-6}.

4.5. CONCLUSION

In this chapter, an exhaustive list of experimental findings is presented. The optical power attenuation of various wavelength laser sources over a given connection distance in various simulated atmospheric circumstances, such as fog, rain, and scintillation, was discussed in the first portion of this chapter. The atmospheric impact on various wavelengths of the FSO channel was illustrated in the second section of this chapter. These experimental evaluations have demonstrated that the rain effect is a wavelength independent phenomena, while the wavelength dependence of fog and scintillation. In all of the investigated simulated atmosphere hazardous scenarios, the 1550 nm offers better outcomes.

CHAPTER 5
IMPROVEMENT OF SYSTEM PERFORMANCE

5.1. INTRODUCTION

The received signal's quality is lowered by the atmospheric channel, which has a negative impact on the FSO system's BER performance. Various mitigating approaches are used to increase the FSO system's dependability in all-weather circumstances. Probable mitigation techniques are given in the Fig .5.1.

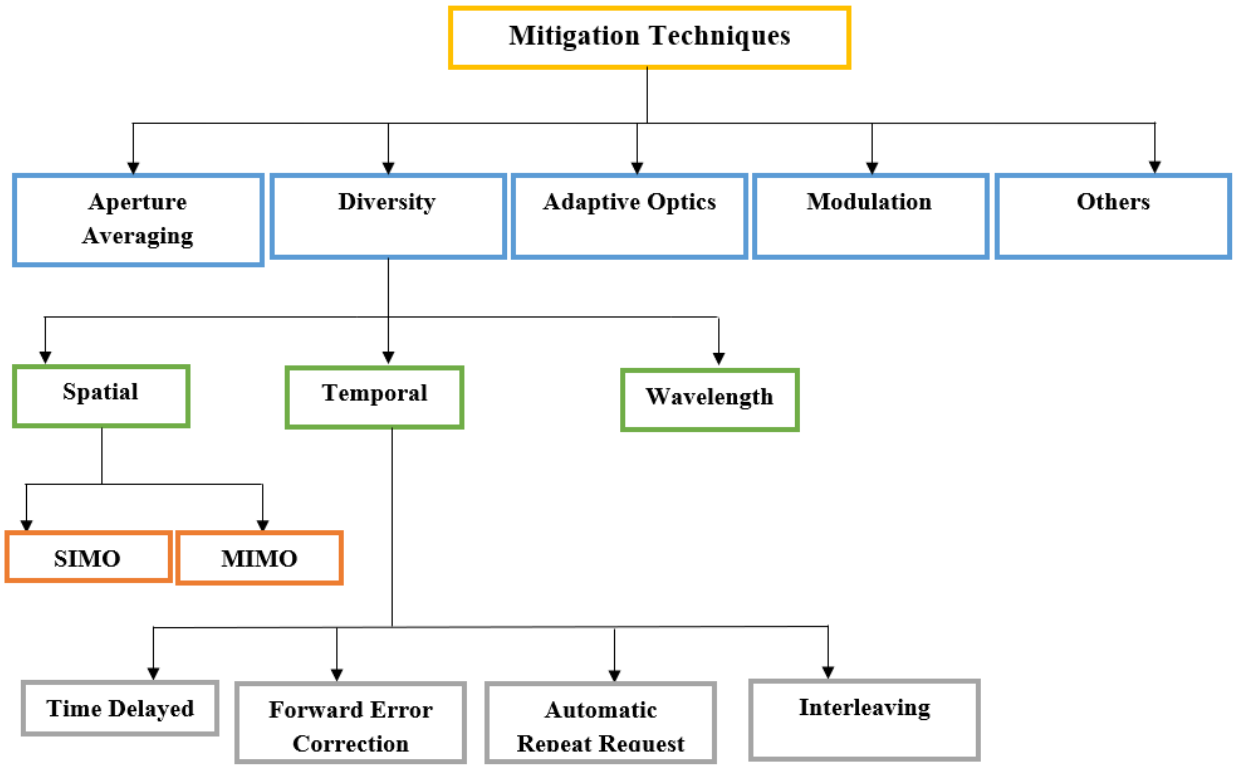

Fig. 5.1. Several methods for reducing air turbulence and hazards

5.1.1. APERTURE AVERAGING

By enlarging the receiver aperture, this approach serves to reduce the effects of air turbulence by averaging out the relatively quick oscillations brought on by small-size eddies and minimizing channel fading [96]. Aperture averaging factor, abbreviated as A, is the quantity that measures the amount of fading decrease caused by aperture averaging. The definition of the parameter A is the variance of the signal fluctuations from a receiver with a D_R diameter

aperture compared to a receiver with an infinitely tiny aperture that can be expressed as in equation 5.1. [97]

$$A = \frac{\sigma_I^2(D_R)}{\sigma_I^2(0)} \qquad 5.1.$$

5.1.2. DIVERSITY

The diversity approach may work on time, frequency, and space to reduce the impact of atmospheric turbulence. In this instance, an array of smaller receiver apertures is employed in place of a single big aperture to enable the transmission of numerous copies of the signal that are independently correlated in time, frequency, or location. This will enhance the system's BER performance and link availability [98].

Diversity gain is accomplished in receiver diversity (SIMO, single input multiple output) by averaging over various independent signal routes. Selective combining (SC), equal gain combining (EGC), and maximum ratio combining (MRC) are three methods that may be used to combine the signals at the receiver. Despite being easier than the other two, SC has a modest gain. The benefit from MRC is somewhat more than that from EGC, but at the sacrifice of complexity and expenditure. As a result of EGC's simplicity and equivalent speed, it is recommended over MRC for implementation [99].

If the beams are independent or uncorrelated, the FSO MIMO (multiple input multiple output) system functions well. The FSO system's performance will suffer otherwise. RF MIMO and optical MIMO systems perform almost equally well. The number of transmitting antennas improves the system's channel capacity practically linearly [100].

It has also been found that time diversity, with or without codes, can decrease channel fading in an FSO system. This kind of variety may be used with time-selective fading channels, which enable the transmission of repeating symbols over a range of coherence times. If the length of the data frame is longer than the channel coherence time, variety can be used via coding or interleaving. Convolutional codes are a viable option for minor atmospheric turbulence in the presence of temporal variety, whereas Turbo-codes offer a considerable coding advantage for high turbulence circumstances. For dependable data transfer, re-transmission protocols like automated repeat request (ARQ) are frequently employed in data communication. In this case, the communication is done via packets with specific frame lengths. The packet is retransmitted if, for whatever reason, the recipient does not acknowledge the transmitted packet within the anticipated time range. The packet is retransmitted if, for whatever reason, the recipient does

not acknowledge the transmitted packet within the anticipated time range. The cycle repeats until either the preset counter value is surpassed or the transmitter receives an affirmative response from the receiver. Due to the retransmission process, this type of stop, wait, and go-back-N ARQ technique causes a significant latency, high energy usage, and bandwidth penalties. Selective repetition another kind of ARQ is called SR-ARQ, which eliminates the requirement for individual receiver acknowledgments by sending data packets continuously from the transmitter to the receiver. The receiver will continue to accept and acknowledge the received frame [101] [102].

Wavelength is another important factor to reduce the turbulence and atmospheric effect on FSO system. Basically, IR is good choice compared to visible and UV. Again, MWIR is better choice than SWIR.

5.1.3. ADAPTIVE OPTICS

In order to convey an undistorted beam across the environment and reduce the impact of atmospheric turbulence, adaptive optics (AO) is utilized. The AO system essentially uses a closed loop control, where the beam is pre-corrected by adding the conjugate of air turbulence before it is sent into the atmosphere. The FSO system's performance can be enhanced by employing diversity or increasing transmit power. But AO have shown to be quite useful in order to achieve additional gains in SNR with a lower transmit power need. However, implementation of the AO method is very complex and very much costly compared to Aperture averaging and spatial diversity techniques [103][104].

5.1.4. MODULATION

The two primary criteria for choosing modulation methods in FSO communication are optical power and bandwidth efficiency. Optical power gain over OOK (On Off Keying) may be used to calculate optical power efficiency if both modulation methods have the same minimum link distance. For low data rates, power efficient modulation methods are easier to implement and very good at reducing the impact of turbulence. On the other side, bandwidth efficiency establishes the maximum amount of data for a specific modulation technique and a given link length. The FSO communication generally accepts a wide range of binary and multilevel modulation formats. The binary level format is the more popular of the two because to its ease of use and great power efficiency. OOK and PPM (Pulse Position Modulation) are the two most well-known binary modulation methods. For optimal performance, OOK modulation technique requires adaptive threshold under turbulent atmospheric circumstances. OOK modulation is

particularly widespread in FSO communication systems due to its ease of use, and it is typically used with IM/DD transmission and reception mechanisms. Intensity modulated signals' duty cycle selection will have an influence on system design factors including transmission bit rate and channel spacing. Effective pulse shaping at the transmitter is necessary to ensure transmission efficiency over a wide variety of duty cycles [105].

In the case of M-PPM (Multiple Pulse Position Modulation), each symbol interval is splitted into M time slots, some of which are filled with a non-zero optical pulse and some of which are left empty. The M-PPM system is frequently employed for long-distance or deep space communications because it has a high peak-to-average power ratio (PAPR), which boosts its average-power efficiency. Additionally, M-PPM does not need an adjustable threshold, in contrast to OOK. For systems with limited bandwidth, multi-level modulation techniques are chosen since the M-PPM scheme performs poorly at larger values of M [106].

The multi-level intensity modulation algorithms most frequently employed in this situation are pulse amplitude modulation (PAM) and quadrature amplitude modulation (QAM). The transmitted data might have various amplitude levels. The loss in power level is the cost of bandwidth efficiency, though. Therefore, these modulation techniques are not a wise choice for systems with restricted power or for very turbulent air conditions [107].

Another type of modulation is called optical sub-carrier intensity modulation (SIM), whereby a base-band signal modulates an electrical RF sub-carrier (which might be analogue or digital), which is then intensity-modulated by an optical carrier. Since the sub-carrier signal is sinusoidal, the optical signal is delivered without the sub-carrier signal's negative amplitude by adding a DC bias. Unlike the OOK approach, SIM does not call for adaptive threshold, and it is also more bandwidth-efficient than the PPM method [108].

5.1.5. OTHER TECHNIQUES

By utilizing various Forward Error Control (FEC) techniques, such as trellis-coded modulation (TCM), LDPC (Low Density Parity Check), Turbo, convolutional, and Reed-Solomon (RS) codes, error control coding further enhances the performance of the FSO link. FEC methods also slow down processing and reduce bandwidth efficiency [109].

Relay-aided transmission is an useful method for reducing turbulence's impact on FSO communication. It is a type of distributed spatial diversity that enables numerous terminals to share their resources through cooperative communication in order to build a distributed virtual antenna array. Instead of having numerous apertures at the transmitter or reception end, a single

antenna can provide a significant diversity gain in this situation. When relay transmission is used at a high SNR, where the received signal strength is strong enough to overcome signal-dependent shot noise and atmospheric fading, it offers a good performance benefit. In the absence of a high SNR, relays will only transmit noisy copies of the information they have already received. Relay transmission in the FSO system offers a considerable improvement over direct transmission in a turbulent air route due to the outage probability and ergodic capacity [110].

The primary cause of ambient noise is daytime solar radiation. The operational wavelength has a substantial influence on the background noise level throughout the day, with lower background noise at longer wavelengths. Spatial filters and an appropriate modulation method with a high peak-to-average power can assist to alleviate it. The Doppler-shifted laser line width, the number of temporal modes, and the angle of the signal's arrival are all significant design considerations. [111].

Atmospheric turbulence and weather conditions have a significant impact on the FSO communication's performance. As a result, the FSO system may have link failures or have subpar BER performance. Therefore, it makes sense to couple the FSO system with a more dependable RF system in order to increase the dependability and availability of the link. These systems, known as hybrid RF/FSO, may maintain high connection availability despite unfavourable weather conditions. Rain (because the carrier wavelength is similar to the size of a rain drop) and fog are the main causes of signal deterioration in RF transmission and FSO communication, respectively. Therefore, by employing when the FSO connection is down, the overall system availability may be enhanced by using a low data rate RF link as a backup. [112-116].

5.2. THEORETICAL APPROACH OF IMPROVEMENT OF SYSTEM PERFORMANCE

5.2.1. APERTURE AVERAGING WITH WAVELENGTH DIVERSITY TECHNIQUE

Different kinds of mitigation approaches have been covered in Section 5.1. The aperture averaging technique is the simplest and least complicated to execute of the aforementioned options, and no additional or external circuitry needs to be installed for its integration into the FSO system. There is no influence on bandwidth distortions when the transmitting frequency

from the transmitted side is received by the receiver. Therefore, this technique is chosen for this work.

With this technique (aperture averaging), wavelength diversity technique has been integrated. For the wavelength diversity technique, two wavelengths have been considered, one is 1550 nm and another one is 4000 nm. From the chapter 4, it has been shown that 1550 nm wavelength is worked well compared to other considered wavelengths like visible & NIR. The Mid Wave Infrared (MWIR) spectrum includes the 4000 nm wavelength, and utilization this of wavelength has various benefits. First of all, it has a higher atmospheric transmittance than other commonly and commercially used wavelengths like 785 nm, 808 nm, 850 nm, 980 nm, 1550 nm, etc. This allows these specific MWIR optical wavelength bands (3400nm-4100nm) to be used in a variety of weather conditions. Secondly, Laser beams in the visible to near-infrared (NIR) (400 nm-1400 nm) optical range penetrate through the lens and cornea of the human eye and can be focused on the retina, posing a risk to the retina. This is according to the International Electrotechnical Commission's (IEC) eye safety rating. The human eye's lens and cornea, however, absorb Short Wavelength Infrared (SWIR), mid-infrared, and far-infrared source beams, which is why these wavelengths do not concentrate on the retina. Therefore, compared to the visible and NIR, these optical bands function with lower danger to the retina [117].

It has been shown from Fig 5.2, in different atmospheric particles, aerosols, etc. situations, the transmittance performance of MWIR band (3500 nm- 4100 nm) is highest compared to other wavelengths. Another crucial point is that the penetration power in foggy weather conditions is significantly higher in the MWIR (3500 nm – 4100 nm) band compared to other wavelengths, and in the higher scintillation regime, the MWIR beam performs better than other commercially available Laser sources. [118-120].

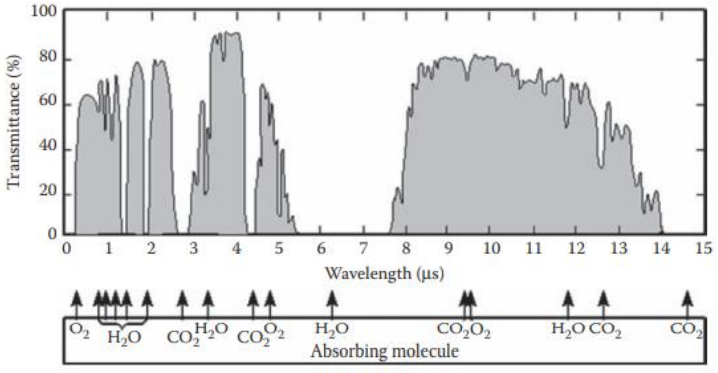

Fig 5.2. Atmospheric transmittance with different wavelength [121][122]

5.2.2 CHANNEL MODELLING

As the optical beam moves through the free space channel, air turbulence (ht) and atmospheric conditions (ha) reduce the signal intensity (h), which may be represented as $h = h_t h_a$ [123]. Based on their range of vision, different meteorological conditions, such as extremely clear air, clear air, light haze, dense haze, light fog, etc., may be characterized. The attenuation coefficient can be predicted using equation (5.2) below [124].

$$\sigma = \frac{17}{V}\left(\frac{\lambda}{550}\right)^{-q} \qquad (5.2)$$

Where V = Visibility (km), λ = Optical wavelength (km), q =Particle size distribution.

The values of q are predicted using the Kim's Model, under various visibility conditions, already discussed in Chapter 2.

The transmittance or extinction coefficient for a given link distance may be calculated using equation (5.3), sometimes referred to as the 'Beer-Lambert Law'.

$$h_a = e^{-\sigma L} \qquad (5.3)$$

Where, σ = Attenuation coefficient.

The attenuation coefficient (dB/km) for wavelengths of 1550 nm and 4000 nm under varied visibility circumstances is summarized in Table 5.1.

Table 5.1. For the wavelengths of 1550 nm and 4000 nm, there are various visibility and attenuation coefficients [121-122][125]

Different Weather Circumstances	Visibility Value (km)	Attenuation (dB/km) 1550 nm	Attenuation (dB/km) 4000 nm
Extreme Clear Weather	50	0.0648	0.0142
Clear Weather	20	0.22103	0.064448
Haze	6	0.73678	0.2148
Light Fog	2	4.2898	2.294

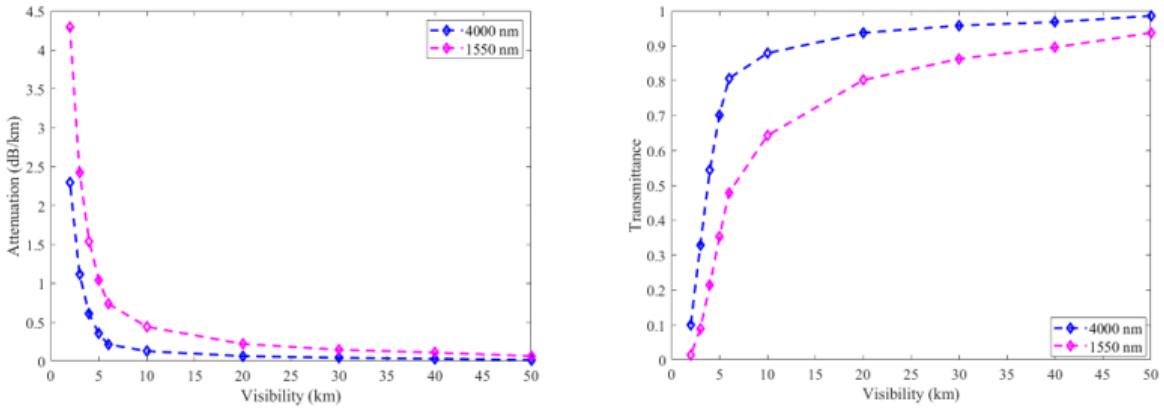

(a) (b)

Fig. 5.3. (a) Different visibility and corresponding attenuation coefficients (b) Transmittance for different visibility for 1550 nm and 4000 nm wavelength

The attenuation coefficients (dB/km) for different visibility situations are shown in Figure 5.3. (a), while Figure 5.3. (b) displays transmittance for various visibility conditions.

Figure 5.3. (a) shows that optical attenuation for both wavelengths is lowest in the lower visibility range. Compared to 1550 nm wavelength, 4000 nm wavelength exhibits reduced attenuation for the varied visibility conditions. Both wavelengths' transmittance increases with increasing visibility, however 4000 nm has a higher transmittance than 1550 nm. There have been observations of gamma-gamma, I-K, negative exponential, and log normal optical turbulence models, among others. For this work, the gamma-gamma model was taken into account since it can be easily calculated and is valid for a wide range of turbulence strengths, from strong to weak [126].

The intensity fluctuation probability density function (pdf) is represented by equation (5.4). f_{h_t} is modelled as a gamma-gamma distribution, which is applicable for all turbulence strengths [126][127].

$$f_{h_t}(h_t) = \frac{2(\Omega\beta)^{\frac{\Omega+\beta}{2}}}{\Gamma(\Omega)\Gamma(\beta)} h_a^{\frac{\Omega+\beta}{2}-1} K_{\Omega-\beta}\left(2\sqrt{\Omega\beta h_t}\right) \qquad (5.4)$$

Where, $K_{\alpha-\beta}(.)$ is the second order Bessel function, and the effective number of large and small scale turbulent eddies for a spherical wave is represented by Ω, β.

The pdf of a channel state under turbulence and different visibility circumstances may be expressed using equation (5.5) [126] [127].

$$f_h(h) = \left|\frac{d}{dh}\left(\frac{h}{h_a}\right)\right| f_{h_t}\left(\frac{h}{h_a}\right) \tag{5.5}$$

The Bessel function [126], which is given in equation (5.6), may be expressed using the Meijer-G function.

$$f_{h_t}(h_t) = \frac{(\Omega\beta)^{\Omega+\beta/2}}{\Gamma(\Omega)\Gamma(\beta)} h_t^{\frac{\Omega+\beta}{2}-1} G_{0,2}^{2,0}\left(\Omega\beta h_t \middle| \frac{\Omega-\beta}{2}, \frac{\Omega-\alpha}{2}\right) \tag{5.6}$$

Equations (5.5) and (5.6) are used to determine the pdf of the channel state as 5.7, [127-128]

$$f_h(h) = \frac{(\Omega\beta)^{\Omega+\beta/2}}{\Gamma(\Omega)\Gamma(\beta)} \frac{h^{\frac{\Omega+\beta}{2}-1}}{h_a^{\frac{\Omega+\beta}{2}}} G_{0,2}^{2,0}\left(\Omega\beta \frac{h}{h_a} \middle| \frac{\Omega-\beta}{2}, \frac{\Omega-\alpha}{2}\right) \tag{5.7}$$

5.2.3. BER PERFORMANCE FOR APERTURE AVERAGING SCHEME

By averaging the conditional error probability, Pe(h), throughout the probability density function of the random signal, fh(h), as shown in equation (5.8), one important performance measure known as Bit error rate (BER) might be obtained [128-130].

$$P_e = BER = \int_0^\infty P_e(h) f_h(h) dh \tag{5.8}$$

Where

$$P_e(h) = \frac{1}{2} erfc\left(\sqrt{\frac{SNR(h)}{2}}\right) \tag{5.9}$$

and equation (5.7) gives the value of $f_h(h)$. According to equation (5.9), the mean output SNR(h) related with probability function $P_e(h)$.

The complementary error function, erfc(.) in equation (5.9) is expressed in relation to the Meiger-G function as provided in equation (5.10) to calculate the BER value. [130],

$$P_e(h) = \frac{1}{2\sqrt{\pi}} G_{1,2}^{2,0}\left(\frac{\gamma h^2}{2} \middle| \begin{matrix} 1 \\ 0, \frac{1}{2} \end{matrix}\right) \tag{5.10}$$

The expression for BER is produced and shown in equation (5.11) by integrating equation (5.10) and substituting this adjusted value of $P_e(h)$ and the channel state pdf $f_h(h)$ from equation (5.7).[128]

$$BER = \frac{2^{\Omega+\beta}}{8\pi^{\frac{3}{2}}\Gamma(\Omega)\Gamma(\beta)} \times G_{5,2}^{2,4}\left(\frac{8\gamma h_a^2}{(\Omega\beta)^2} \middle| \begin{matrix} \frac{1-\Omega}{2}, 1-\frac{\Omega}{2}, \frac{1-\beta}{2}, 1-\frac{\beta}{2}, 1 \\ 0, \frac{1}{2} \end{matrix}\right) \tag{5.11}$$

The values of are obtained from equations (5.12) and (5.13) in order to calculate the BER of an aperture averaged link.

In order to determine the BER of an aperture averaged condition, the values of **Ω**, β are derived from equations (5.12) and (5.13).

$$\Omega = \left(\exp\left[\frac{0.49\beta_o^2}{\left(1 + 0.18d_1^2 + 0.56\beta_o^{\frac{12}{5}}\right)^{\left(\frac{7}{6}\right)}} \right] - 1 \right)^{-1} \qquad (5.12)$$

$$\beta = \left(\exp\left[\frac{0.51\beta_o^2 \left(1 + 0.69\beta_o^{\frac{12}{5}}\right)^{-\frac{5}{6}}}{1 + 0.9d_1^2 + 0.62d_1^2\beta_o^{\frac{12}{5}}} \right] - 1 \right)^{-1} \qquad (5.13)$$

Where, $\beta_o^2 = 0.5C_n^2k^{7/6}L^{11/6}$ is the spherical wave Rytov variance [126], C_n^2 the refractive index structure parameter ($m^{-2/3}$) and $d_1 = \sqrt{(\frac{kD^2}{4z})}$ is the circular aperture radius [125] [126], where D stands for the receiver's aperture diameter.

5.3. SIMULATION RESULTS

The FSO link range, which has been assessed to be 4 km, has been used for all analyses. The study's results evaluation has taken into account a number of values from the strong to weak refractive index structure parameter (c_n^2) regimes, including $0.5x10^{-13}$, $1.5x10^{-14}$, and $8.4x10^{-15}$ $m^{-2/3}$[126]. Consideration has been given to the two operating wavelengths of 1550 nm and 4000 nm. A maximum SNR of 90 dB has been considered for a 4 km link range. Under this SNR value, varying visibility, and various turbulence strength conditions, the BER performance has been evaluated for both wavelengths in the aperture averaging scheme and SIMO scheme. Similar to this, the BER performance evaluations are evaluated for various SNR values, under various turbulence regimes, and under various visibility conditions for various SIMO and aperture averaging schemes (the highest SNR value has been considered to be 90 dB for a 4 km connection range).

In this simulation, two types of simulations have been executed: one where only the impact of different turbulence strengths is taken into account (i.e., the impact of different meteorological conditions is ignored), and the other where both impacts—i.e., turbulence and different meteorological impacts—are taken into account.

5.3.1. APERTURE AVERAGING SCHEME WITH TURBULENCE ONLY

This section only studies various turbulence intensities; the influence of meteorological variables is not considered. By inserting the value $h_a^2 = 1$ into equation (5.11), the aforementioned condition is established, and the effects of the other visibility conditions are removed, leaving just the turbulence effect visible. The average SNR is used to display the BER value under the effect of various turbulence intensities and utilizing various aperture averaging technique. Different aperture diameters between 0.05 and 0.2 metres have been considered. An aperture size greater than 0.2 m is typically not taken into consideration since it increases background noise at the receiver side. The graphs in Fig. 5.4. (a), (b), and (c) illustrate the BER values vs. various SNRs for various apertures.

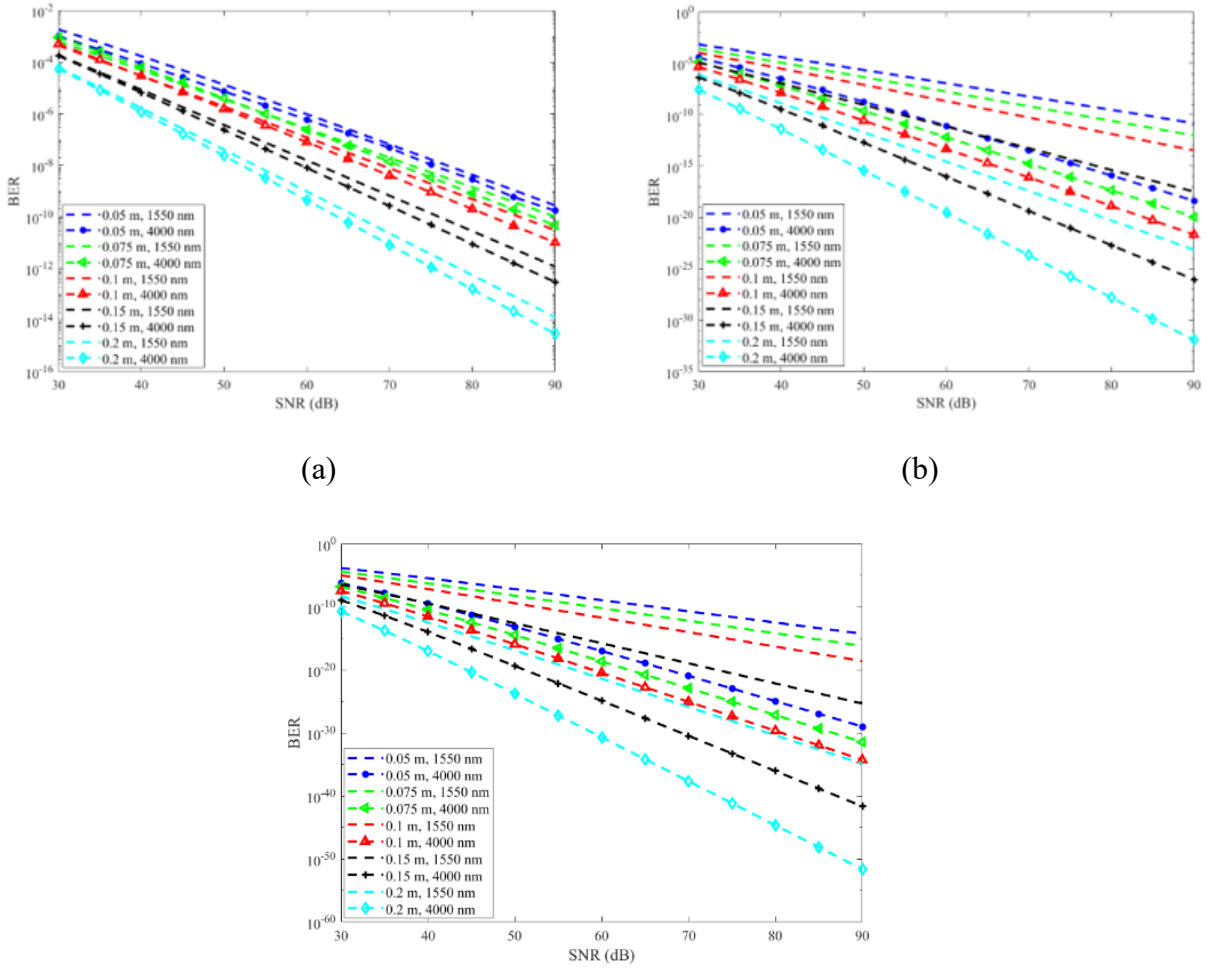

(a) (b)

(c)

Fig.5.4. Values of BER vs various SNR for various aperture averages at (a) strong turbulence ($C_n^2 = 0.5\text{x}10^{-13}$) , (b) moderate turbulence ($C_n^2 = 1.5\text{x}10^{-14}$) and (c) lower turbulence ($C_n^2 = 8.4\text{x}10^{-15}$) only

These graphs show that the BER increases for both wavelengths as turbulence strength rises from mild to strong. When the receiver aperture size is gradually increased, the value of BER is reduced for both wavelengths. When all other factors remain the same, the MWIR wavelength provides lower BER values than the SWIR wavelength for all turbulence regimes.

5.3.2. APERTURE AVERAGING UNDER VARIOUS TURBULENCE & VISIBILITY SITUATIONS

This section demonstrates how well the BER operates in a range of turbulence regimes, from high to low, under various visibility conditions, with varying SNR values for the two wavelengths. Aperture averaging techniques have been used to complete all of the analyses in this section. Fig. 5.5 (a), (b), (c), and (d) illustrate the varied BER values that correlate to different SNR values of higher turbulence regimes and different visibility conditions, such as extremely clear, clear, moderate haze, and dense haze, respectively.

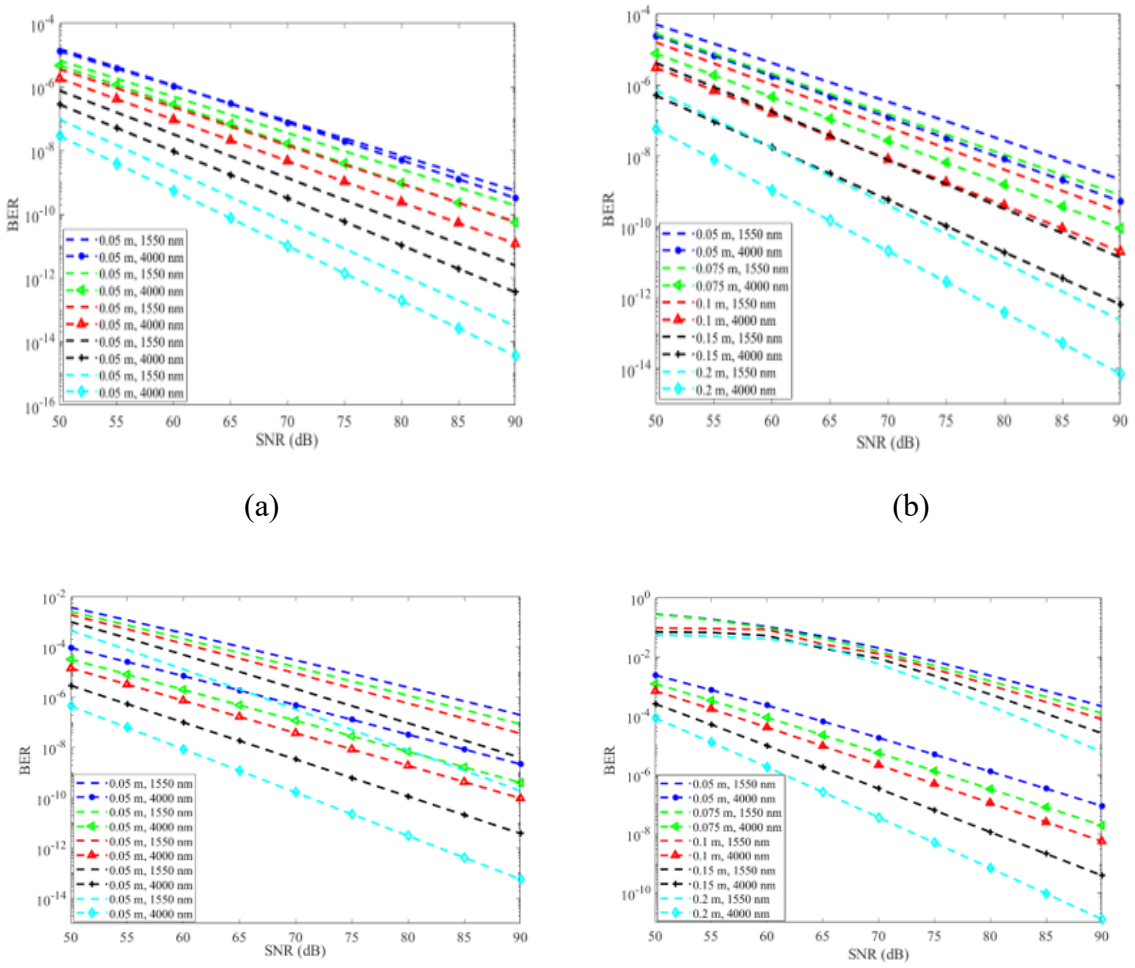

(a) (b)

(c) (d)

Fig.5.5. A variety of SNR vs. BER at increasing turbulence regimes (a) Extremely Clear weather (b) Clear Weather (c) Ligh Haze (d) Dense Haze conditions

In contrast to a scenario analysis using only scintillation, the SNR need in this case is larger. As in this case, the combined impact of the different visibility and scintillation has been considered. Similar to how the BER is depicted as a relationship of average SNR under the influence of different visibility circumstances, such as extremely clear visibility, clear visibility, light haze, and moderate haze in Figs. 5.6 (a), (b), (c), (d) & 5.7 (a), (b), (c), (d) for lower and moderate turbulence strength, respectively. The value of h_a, obtained from equation (5.3.) and calculated using Table 5.1, takes into consideration the influence of weather conditions. The presence of dense haze is seen to have the worst BER rating, followed by the presence of mild haze and clear skies.

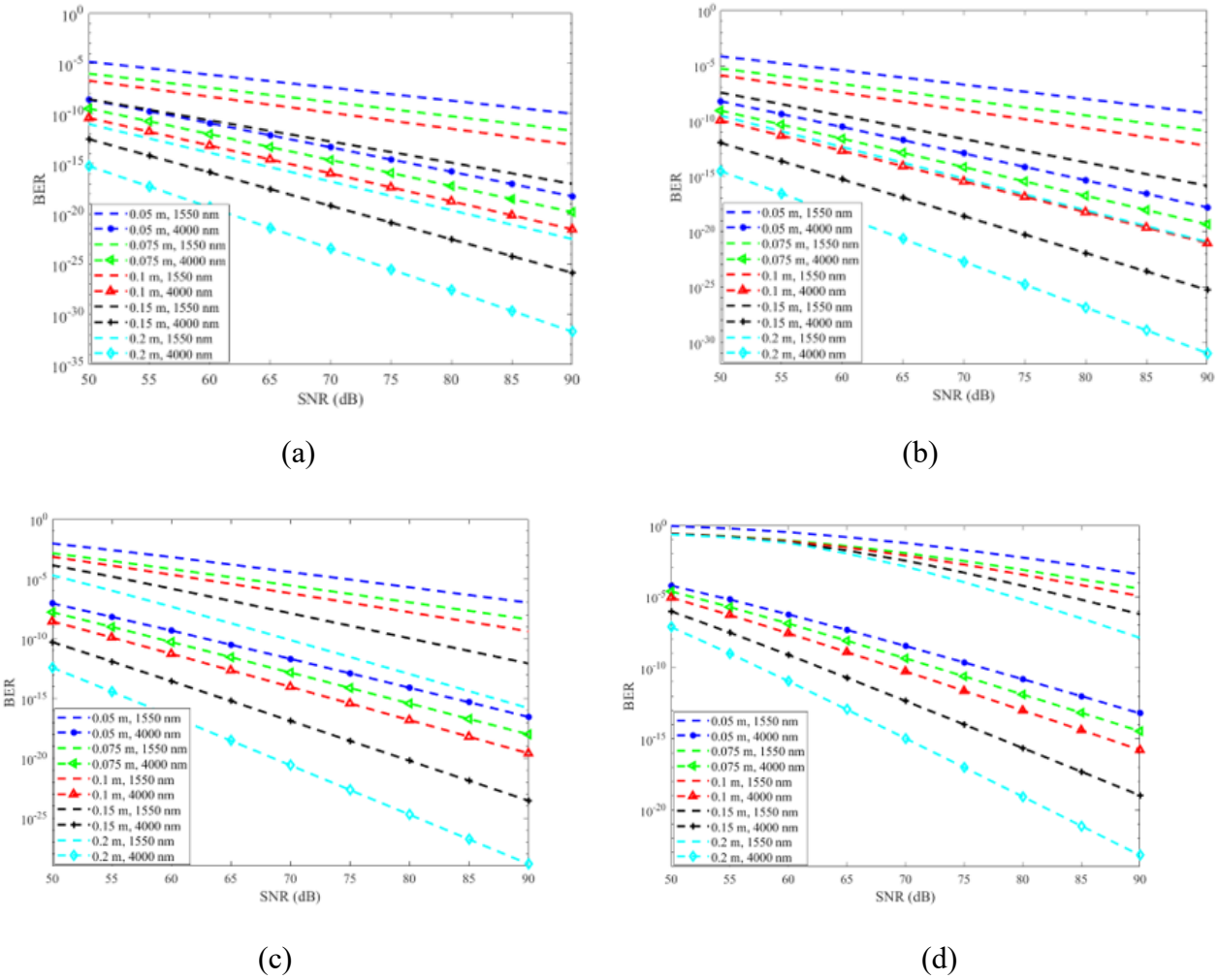

Fig.5.6. Various SNR vs BER at moderate turbulence regime (a) Extremely Clear weather (b) Clear Weather (c) Light Haze (d) Dense Haze conditions

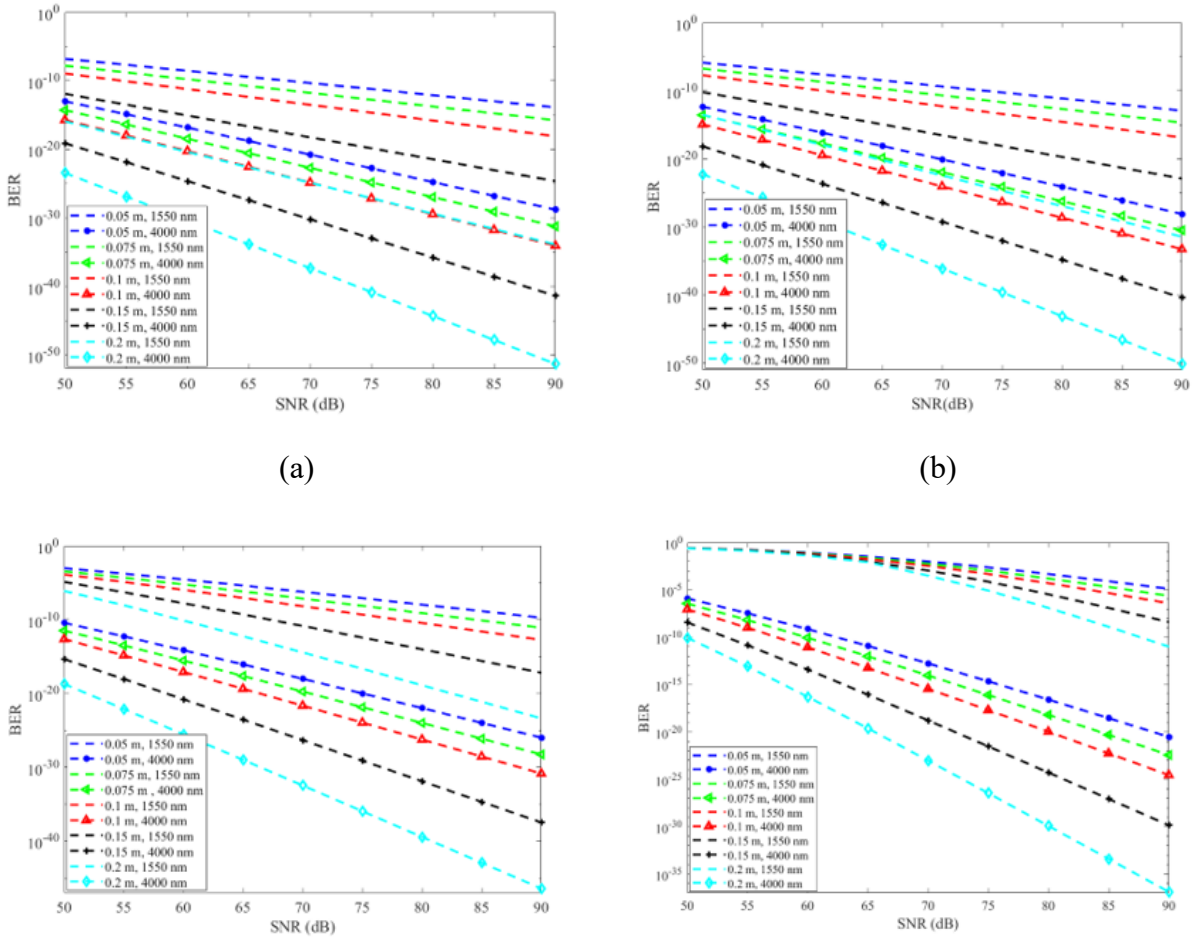

(a) (b)

(c) (d)

Fig.5.7. Various SNR vs BER at lower turbulence regime (a) Extremely Clear weather (b) Clear Weather (c) Light Haze (d) Dense Haze conditions

After comparing the outcomes utilizing the wavelength diversity method, it has been shown that in all turbulence regimes and climatic circumstances, MWIR wavelength outperforms SWIR wavelength.

Since light fog possesses a significant attenuation coefficient, it is impossible to use the SWIR wavelength for a 4-kilometer connection distance under these circumstances. A bigger aperture diameter (0.2 m) may be required for this weather. The aperture size has been a limiting issue in this range since the solar background noise is quite loud above this aperture size. Fog circumstances have a higher SNR need than other weather states due of the greater optical attenuation in this state of affairs. This is because the attenuation coefficient of the MWIR wavelength is smaller than that of the SWIR wavelength. To reflect the effects of light fog, the BER is displayed as a consequence of the average SNR in Fig. 5.8 (a).

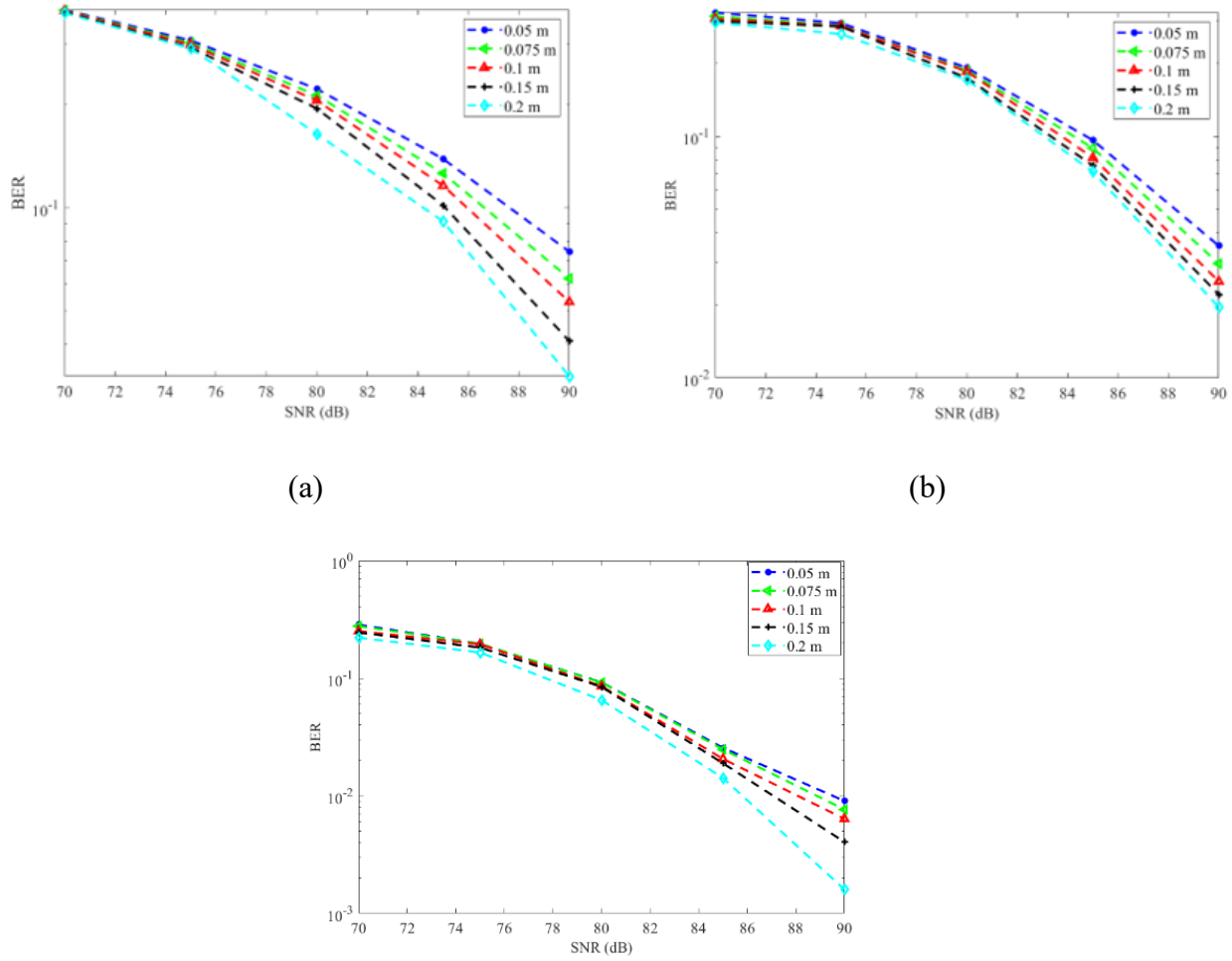

Fig.5.8. Various SNR vs BER at Light fog condition for MWIR wavelength (a) Strong (b) Moderate (c) Lower turbulence regime

These figures also demonstrate that, independent of visibility, the BER performance improves from strong to lower turbulence strength for the different SNR levels.

5.4. EXPERIMENTAL SIMULATION OF IMPROVEMENT FOR SYSTEM PERFORMANCE

5.4.1. EXPERIMENTATION ON APERTURE AVERAGING TECHNIQUE

In the previous chapter (Chapter 4), the whole experimentation has been shown without receiver optics, that is without lens (without aperture averaging technique). Another important point has been deduced from the previous chapter is that at the higher wavelength scenario, the optical power attenuation is less for scintillation, fog, etc. The 1550 nm Laser provides better results or better link performance compared to visible and other lower IR wavelengths compared to 1550 nm Laser. However, the system performance can be improved by the different techniques which is discussed at the introduction section of this chapter. From this

chapter & the 'Theoretical approach of improvement of system performance' section, it has been inferred that aperture averaging technique is better for improving the system performance at the diverse weather condition and different turbulence scenario. As this system is very cost effective, simple in implementation in the FSO system and no other external circuitry is used in this technique, so this technique is considered for the experimentation.

5.4.1.1. EXPERIMENTAL SETUP OF APERTURE AVERAGING (TRANSMITTER SIDE)

To see the system performance using the 'Aperture Averaging' into the existing FSO system, with different wavelengths LASER, a 10 cm. plano-convex lens is placed into the receiver side (at the front of the photodetector system). The transmitter section is remaining same as the previous arrangements. The link distance between transmitter and receiver also remained same that is 35 ft. The transmitter part of using different wavelengths LASER sources have been depicted in the Fig. 5.9.

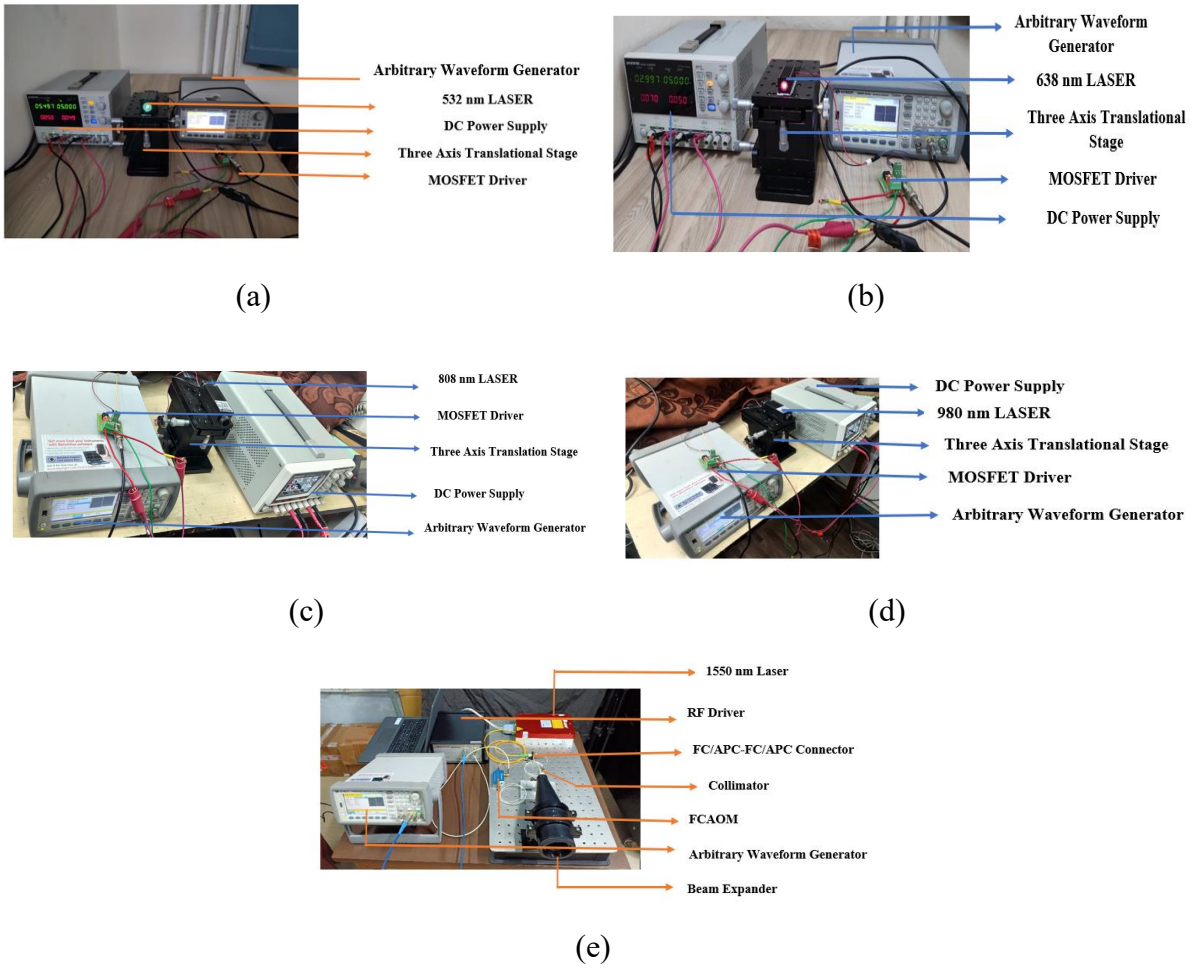

Fig. 5.9. Transmitter side using different wavelengths of Laser (a) 532 nm, (b) 638 nm, (c) 808 nm, (d) 980 nm, & (e) 1550 nm.

5.4.1.2. EXPERIMENTAL SETUP OF APERTURE AVERAGING (RECEIVER SIDE)

At the receiver side, a 10 cm. plano-convex lens has been used at the front of the photodetector system. Fig. 5.10 shows the aperture averaging scheme using different wavelengths Laser source and corresponding their Photodetector system.

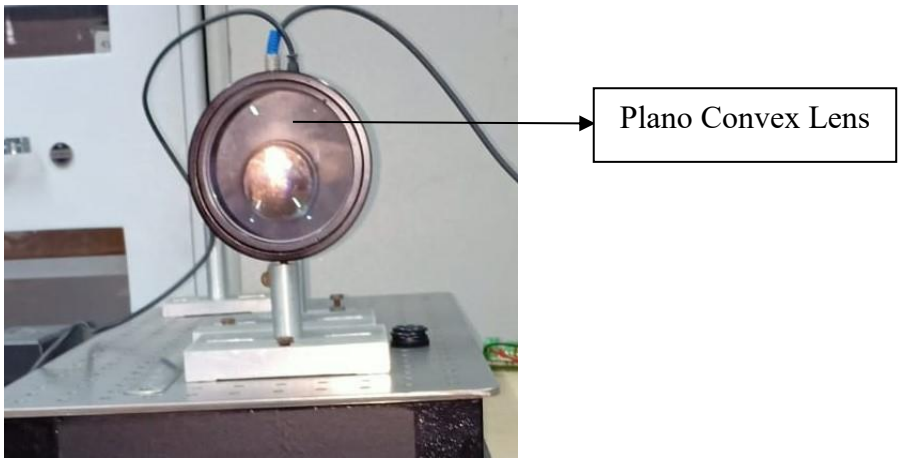

Fig. 5.10. Receiver side using aperture averaging technique (using plano-convex lens) for different wavelength lengths

5.4.2. PERFORMANCE ANALYSIS USING APERTURE AVERAGING SCHEME

5.4.2.1. EFFECT ON RISING AMBIENT TEMPERATURE (SCINTILLATION)

At the higher scintillation regime, that is $2.5x10^{-13}$ $m^{-2/3}$, the optical loss has been reduced from 1.14 dB to 0.73 dB after using aperture averaging technique for 532 nm Laser. Similarly, for 638 nm Laser the optical attenuation is reduced from 1.04 dB to 0.61 dB, for 808 nm Laser, the optical power attenuation reduced from 0.925 dB to 0.51 dB, for 980 nm Laser, the optical power attenuation has been reduced from 0.74 dB to 0.44 dB and finally, for 1550 nm, the optical power attenuation has been reduced from 0.66 dB to 0.38 dB respectively, for the higher scintillation regime.

Table 5.2. Measured values of optical power attenuation for different wavelengths and different scintillation ranges with aperture averaging scheme

532 nm		638 nm		808 nm		980 nm		1550 nm	
C_n^2 ($m^{-2/3}$)	Loss (dB)	C_n^2 ($m^{-2/3}$)	Loss (dB)	C_n^2 ($m^{-2/3}$)	Loss (dB)	C_n^2 ($m^{-2/3}$)	Loss (dB)	C_n^2 ($m^{-2/3}$)	Loss (dB)
$2.5x10^{-13}$	0.73	$2.5x10^{-13}$	0.61	$2.5x10^{-13}$	0.51	$2.5x10^{-13}$	0.44	$2.5x10^{-13}$	0.38
10^{-14}	0.16	10^{-14}	0.135	10^{-14}	0.114	10^{-14}	0.12	10^{-14}	0.072
$3.5x10^{-15}$	0.1	$3.5x10^{-15}$	0.11	$3.5x10^{-15}$	0.071	$3.5x10^{-15}$	0.055	$3.5x10^{-15}$	0.051
10^{-16}	0.02	10^{-16}	0.01	10^{-16}	0.011	10^{-16}	0.0102	10^{-16}	0.008

Table 5.2. depicts the measured values of optical power attenuation for different wavelengths and different scintillation ranges with aperture averaging scheme.

Fig. 5.11. shows that at different scintillation regimes (from high to low), the optical power attenuation has been reduced using different wavelengths using aperture averaging scheme. The same trend has been observed for aperture averaging similar to that of the without aperture averaging. At higher wavelength, the optical power attenuation is lower compared to lower wavelengths.

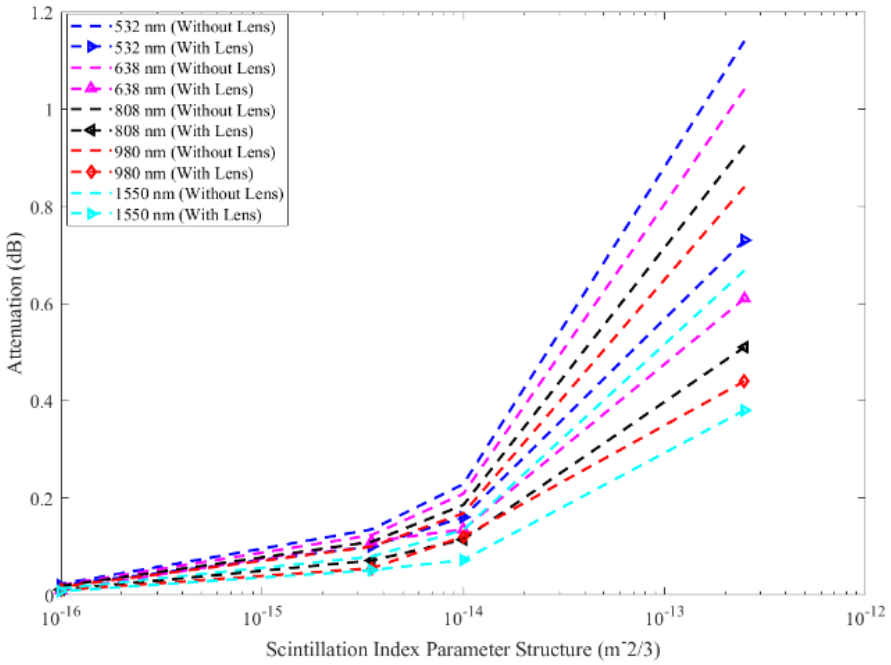

Fig. 5.11. Optical power attenuation (dB) due to different scintillation range ($m^{-2/3}$) using different wavelengths (With Aperture Averaging & Without Aperture Averaging schemes)

As the SNR is directly proportional to the received optical power, therefore, the SNR performance has been enhanced as the received optical power loss is reduced using aperture averaging technique.

Table. 5.3. SNR (dB) values for different scintillation range ($m^{-2/3}$) with different wavelengths with aperture averaging scheme

532 nm		638 nm		808 nm		980 nm		1550 nm	
C_n^2 ($m^{-2/3}$)	SNR (dB)	C_n^2 ($m^{-2/3}$)	SNR (dB)	C_n^2 ($m^{-2/3}$)	SNR (dB)	C_n^2 ($m^{-2/3}$)	SNR (dB)	C_n^2 ($m^{-2/3}$)	SNR (dB)
$2.5x10^{-13}$	11.24	**$2.5x10^{-13}$**	11.38	**$2.5x10^{-13}$**	12.10	**$2.5x10^{-13}$**	12.77	**$2.5x10^{-13}$**	13.44
10^{-14}	18.66	**10^{-14}**	18.94	**10^{-14}**	19.27	**10^{-14}**	19.85	**10^{-14}**	20.23
$3.5x10^{-15}$	22.45	**$3.5x10^{-15}$**	22.91	**$3.5x10^{-15}$**	23.25	**$3.5x10^{-15}$**	24.15	**$3.5x10^{-15}$**	24.25
10^{-16}	25.56	**10^{-16}**	26.13	**10^{-16}**	26.35	**10^{-16}**	27.19	**10^{-16}**	28.14

Table 5.3. depicts SNR (dB) values for different scintillation range ($m^{-2/3}$) with different wavelengths with aperture averaging scheme.

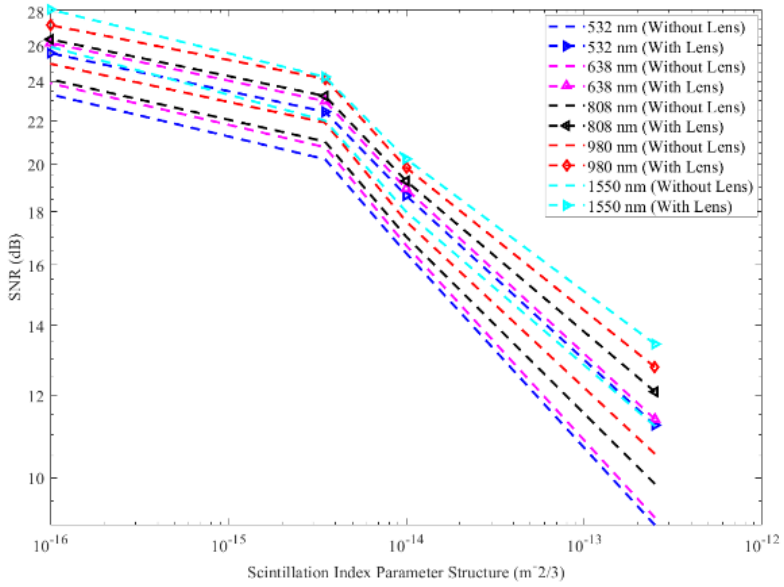

Fig. 5.12. SNR (dB) values for different scintillation ranges with different wavelengths (With Aperture Averaging & Without Aperture Averaging Scheme)

A greater SNR has been attained when the turbulence strength is smaller, but a lower SNR has been achieved when the turbulence strength is strong. The aperture averaging approach has been used to increase the SNR value, and it can be seen from the graph that for high to low turbulence strengths, the SNR has improved greatly (average SNR enhanced average 1.67

times than the without aperture averaging). Fig. 5.12. represents SNR (dB) values for different scintillation ranges with different wavelengths (With Aperture Averaging & Without Aperture Averaging Scheme)

Table. 5.4. BER values for different scintillation range ($m^{-2/3}$) with different wavelengths with aperture averaging scheme

532 nm		**638 nm**		**808 nm**		**980 nm**		**1550 nm**	
C_n^2 ($m^{-2/3}$)	**BER**	**C_n^2 ($m^{-2/3}$)**	**BER**	**C_n^2 ($m^{-2/3}$)**	**BER**	**C_n^2 ($m^{-2/3}$)**	**BER**	**C_n^2 ($m^{-2/3}$)**	**BER**
$2.5x10^{-13}$	0.0343	**$2.5x10^{-13}$**	0.032	**$2.5x10^{-13}$**	0.0222	**$2.5x10^{-13}$**	0.015	**$2.5x10^{-13}$**	0.0095
10^{-14}	$9.46x10^{-6}$	**10^{-14}**	$4.95x10^{-6}$	**10^{-14}**	$2.22x10^{-6}$	**10^{-14}**	$4.65x10^{-7}$	**10^{-14}**	$1.47x10^{-7}$
$3.5x10^{-15}$	$1.78x10^{-11}$	**$3.5x10^{-15}$**	$9.53x10^{-13}$	**$3.5x10^{-15}$**	$2x10^{-13}$	**$3.5x10^{-15}$**	$4.23x10^{-16}$	**$3.5x10^{-15}$**	$1.97x10^{-16}$
10^{-16}	$1.46x10^{-21}$	**10^{-16}**	$2.27x10^{-24}$	**10^{-16}**	$1.75x10^{-25}$	**10^{-16}**	$1.64x10^{-30}$	**10^{-16}**	$1.65x10^{-37}$

Table 5.4. shows BER values for different scintillation range ($m^{-2/3}$) with different wavelengths with aperture averaging scheme.

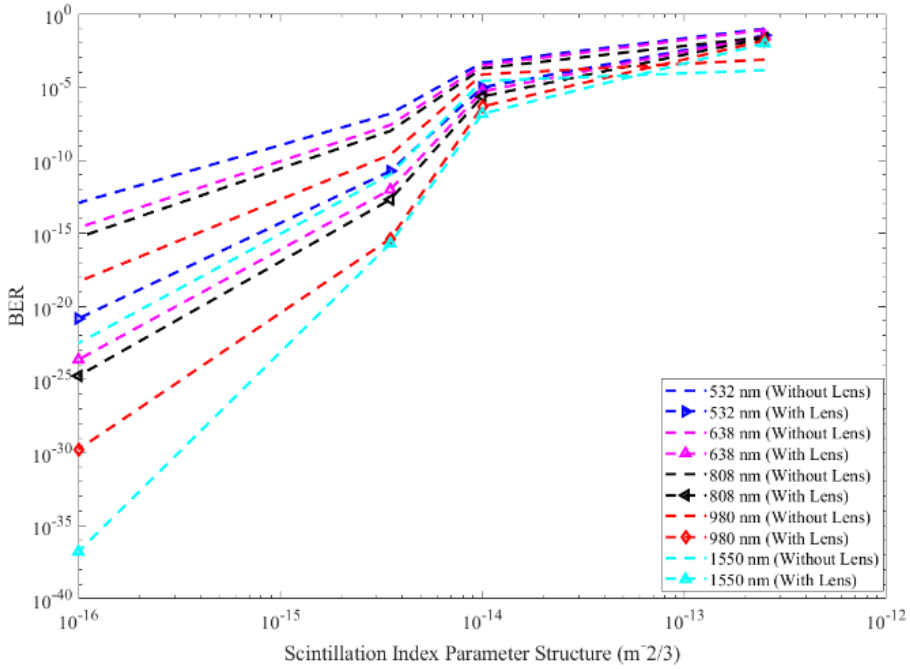

Fig. 5.13. BER values for different scintillation ranges with different wavelengths (With Aperture Averaging & Without Aperture Averaging Scheme)

Similar to this, Fig. 5.13 shows the measured BER for the various turbulence strengths, from low to extremely strong, both with and without aperture averaging. When using the aperture averaging approach, the BER performance is superior to when not using it.

5.4.2.2. EFFECT ON RAIN

From the previous chapter (Chapter 4), it has been shown that the optical power attenuation due to rain for different wavelengths Laser sources are almost same. Therefore, the optical power attenuation improvement using aperture averaging scheme is almost same for all the considered wavelengths like 532 nm, 638 nm, 808 nm, 980 nm, & 1550 nm. Table 5.5. shows the Optical power loss for different rain rates (mm/hr) using different wavelengths at link distance of 35 ft. for aperture averaging scheme.

Table 5.5. Optical power loss for different rain rates (mm/hr) using different wavelengths at link distance of 35 ft. for aperture averaging scheme

Rain Rates (mm/hr)	**Optical power loss for 532 nm (dB)**	**Optical power loss for 638 nm (dB)**	**Optical power loss for 808 nm (dB)**	**Optical power loss for 980 nm (dB)**	**Optical power loss for 1550 nm (dB)**
7	0.0647	0.0658	0.0644	0.0643	0.064
28	0.1547	0.1532	0.153	0.153	0.151
69	0.296	0.292	0.289	0.284	0.279
121	0.421	0.424	0.422	0.414	0.406
153	0.471	0.47	0.471	0.473	0.471
180	0.505	0.503	0.498	0.501	0.497

Table 5.5 shows that optical power loss for different rain rates (mm/hr) using different wavelengths at link distance of 35 ft. for aperture averaging scheme. Before using aperture averaging technique, the optical power attenuation due to different rain rates like 7 mm/hr, 28 mm/hr, 69 mm/hr, 121 mm/hr, 153 mm/hr, and 180 mm/hr are 0.097 dB, 0.2375 dB, 0.425 dB, 0.6112 dB, 0.709 dB & 0.791 dB respectively. As the optical power attenuation for different rain rates are not changed rapidly for different wavelengths, so in the different rain rates, the optical power attenuation is remaining same irrespective of wavelengths.

After using the aperture averaging technique into the system, the optical power attenuation has been improved. The optical power attenuation has been reduced to 0.064 dB, 0.154 dB, 0.296 dB, 0.421 dB, 0.471 dB & 0.505 dB respectively for the rain rate of 7 mm/hr, 28 mm/hr, 69 mm/hr, 121 mm/hr, 153 mm/hr & 180 mm/hr.

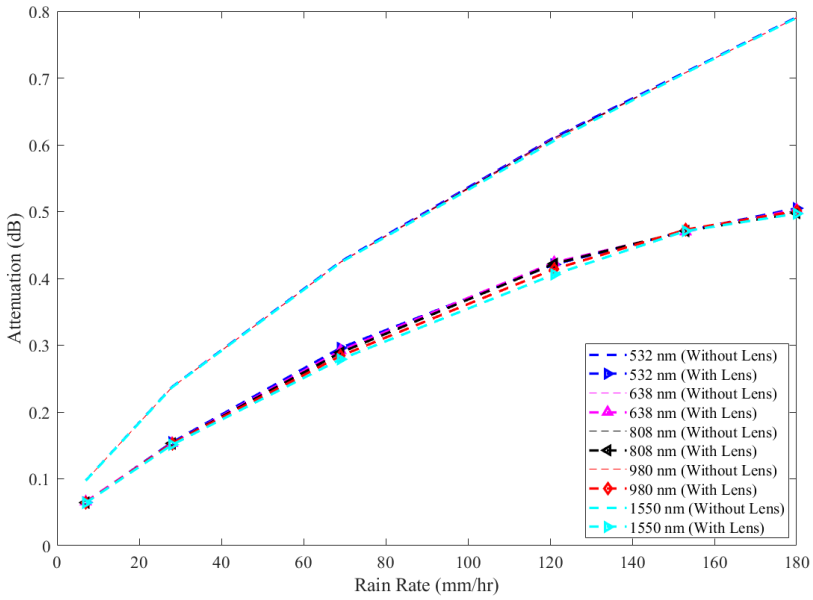

Fig. 5.14. Optical power attenuation (dB) due to different rain rates (mm/hr) using different wavelengths (With Aperture Averaging & Without Aperture Averaging schemes)

Fig. 5.14 shows the optical power attenuation (dB) due to different rain rates (mm/hr) using different wavelengths (With Aperture Averaging & Without Aperture Averaging schemes). From the figure, it has been shown that using aperture averaging, the optical power attenuation is low compared to without using aperture averaging system, irrespective of wavelengths.

Table. 5.6. SNR (dB) values for different rain rates (mm/hr) with different wavelengths with aperture averaging scheme

Rain Rates (mm/hr)	SNR for 532 nm (dB)	SNR for 638 nm (dB)	SNR for 808 nm (dB)	SNR for 980 nm (dB)	SNR for 1550 nm (dB)
7	24.23	24.23	24.27	24.27	24.62
28	22.45	22.45	22.52	22.52	22.79
69	19.53	19.53	19.64	19.64	19.85
121	15.65	15.64	15.75	15.756	16.21
153	14.53	14.52	14.62	14.627	14.74
180	11.02	11.01	11.05	11.053	11.53

Table. 5.6. shows the SNR (dB) values for different rain rates (mm/hr) with different wavelengths with aperture averaging scheme.

When the rain rate is lower, a higher SNR has been achieved whereas higher rain rate, lower SNR has been attained. Aperture averaging approach was used to increase SNR value, and it can be seen from the graph that SNR has greatly improved for high to low rain rates (average SNR enhanced 1.46 times than that of without aperture averaging).

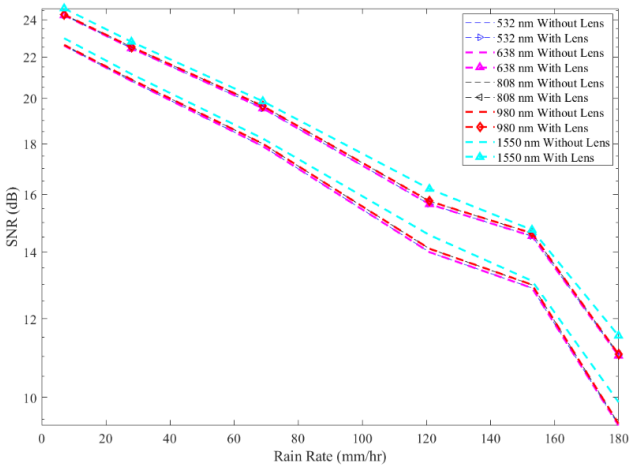

Fig.5.15. SNR (dB) values for different rain rates (mm/hr) with different wavelengths (With Aperture Averaging & Without Aperture Averaging Scheme)

Fig. 5.15. represents SNR (dB) values for different rain rates with different wavelengths (With Aperture Averaging & Without Aperture Averaging Scheme).

Table. 5.7. BER values for different rain rates (mm/hr) with different wavelengths with aperture averaging scheme

Rain Rates (mm/hr)	**BER for 532 nm**	**BER for 638 nm**	**BER for 808 nm**	**BER for 980 nm**	**BER for 1550 nm**
7	2.19×10^{-16}	2.18×10^{-16}	1.6×10^{-16}	1.6×10^{-16}	9.4×10^{-18}
28	1.776×10^{-11}	1.77×10^{-11}	1.23×10^{-11}	1.23×10^{-11}	2.87×10^{-12}
69	1.104×10^{-6}	1.104×10^{-6}	8.31×10^{-7}	8.31×10^{-7}	4.5×10^{-7}
121	0.00124	0.00124	0.00109	0.00109	0.000625
153	0.00391	0.00391	0.0036	0.0036	0.00321
180	0.0378	0.038	0.0373	0.037	0.02977

Table. 5.7. represents the BER values for different rain rates (mm/hr) with different wavelengths with aperture averaging scheme.

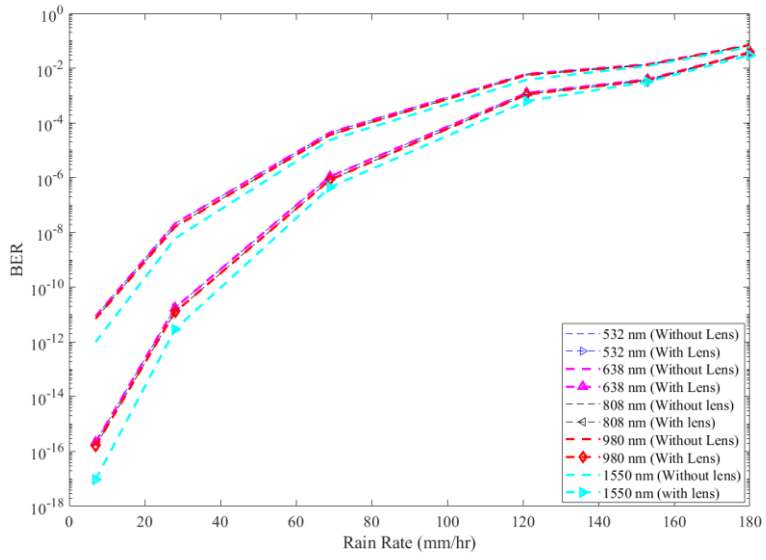

Fig. 5.16. BER values for different rain rates (mm/hr) with different wavelengths (With Aperture Averaging & Without Aperture Averaging Scheme)

Similar to this, Fig. 5.16 shows the measured BER for the various rain rates, from very light to heavy, both with and without aperture averaging. When using the aperture averaging approach, the BER performance is superior to when not using it.

5.4.2.3. EFFECT ON FOG

In the previous Chapter (i.e. Chapter 4), attenuation due to fog has been studied without aperture averaging technique. As the KIM model is used to measure the optical power attenuation due to fog, so upto 500 m visibility range, the optical power attenuation is same for all the considered wavelengths. After 500 m visibility range, the attenuation has been lower as the wavelength is increased. Without aperture averaging scheme, we have shown in Chapter 4, in Table 4.14.1 that 532 nm Laser provides optical power attenuation for the visibility range of 190 m, 312m , 445 m, 522 m, 618 m, 721 m, 1012 m, 1500 m, 2400 m & 3012 m of 1.073 dB, 0.654 dB, 0.46 db, 0.4 dB, 0.331 dB, 0.285 dB, 0.205 dB, 0.14 dB, 0.087 dB, 0.0696 dB respectively. This case is described here as an example.

Table. 5.8. Attenuation (dB) values for different visibility (m) with different wavelengths with aperture averaging scheme

532 nm		638 nm		808 nm		980 nm		1550 nm	
Visibility (m)	Attenuation (dB)	Visibility (m)	Attenuation (dB)	Visibility (m)	Attenuation (dB)	Visibility (m)	Attenuation (dB)	Visibility (m)	Attenuation (dB)
190	0.96	190	0.97	190	1.01	190	1.01	190	0.997
312	0.554	312	0.653	312	0.56	312	0.591	312	0.5947
445	0.41	445	0.45	445	0.41	445	0.421	445	0.4321
522	0.3	522	0.28	522	0.37	522	0.37	522	0.356
618	0.22	618	0.27	618	0.298	618	0.26	618	0.288
721	0.2	721	0.21	721	0.24	721	0.23	721	0.21
1012	0.16	1012	0.152	1012	0.153	1012	0.124	1012	0.1085
1500	0.12	1500	0.123	1500	0.092	1500	0.078	1500	0.0614
2400	0.07	2400	0.0621	2400	0.052	2400	0.045	2400	0.035
3012	0.06	3012	0.0378	3012	0.041	3012	0.033	3012	0.0185

Table 5.8 shows the attenuation (dB) values for different visibility (m) with different wavelengths with aperture averaging scheme. From the table 5.8, it is clear that, using aperture averaging scheme, the 532 nm laser provides attenuation 0.96 dB, 0.554 dB, 0.41 dB, 0.3 dB, 0.22 dB, 0.2 dB, 0.16 dB, 0.12 dB, 0.07 dB, & 0.06 dB for the visibility range of 190 m, 312m , 445 m, 522 m, 618 m, 721 m, 1012 m, 1500 m, 2400 m & 3012 m respectively.

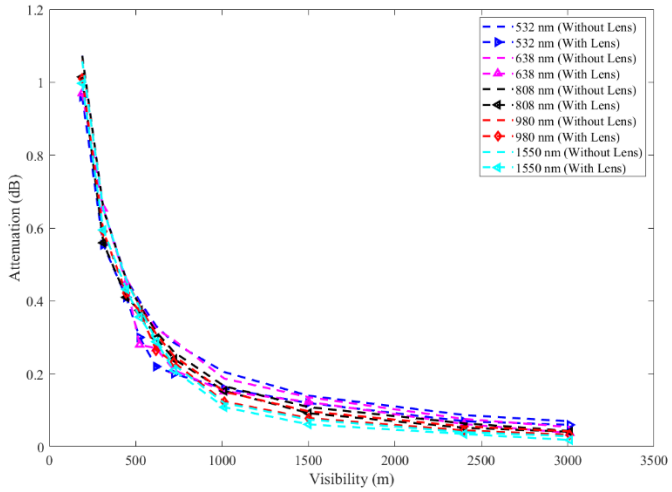

Fig. 5.17. Optical power attenuation (dB) due to different visibility (m) using different wavelengths (With Aperture Averaging & Without Aperture Averaging schemes)

Fig. 5.17 shows the optical power attenuation (dB) due to different visibility (m) using different wavelengths (With Aperture Averaging & Without Aperture Averaging schemes). From the graph, it has been shown that using aperture averaging scheme, the optical power attenuation is less (average optical power less attenuated 1.14 times than that of without aperture averaging) for all the considered wavelengths compared to without aperture averaging scheme.

Table 5.9 shows the SNR (dB) values for different visibility (m) with different wavelengths with aperture averaging scheme.

Table. 5.9. SNR (dB) values for different visibility (m) with different wavelengths with aperture averaging scheme

532 nm		**638 nm**		**808 nm**		**980 nm**		**1550 nm**	
Visibility (m)	**SNR (dB)**	**Visibility (m)**	**SNR (dB)**	**Visibility (m)**	**SNR (dB)**	**Visibility (m)**	**SNR (dB)**	**Visibility (m)**	**SNR (dB)**
190	2.91	190	2.92	190	2.94	190	2.95	190	2.95

312	4.61	312	4.61	312	4.62	312	4.63	312	4.69
445	7.25	445	7.26	445	7.26	445	7.26	445	7.26
522	8.30	522	8.37	522	8.46	522	8.62	522	9.31
618	9.47	618	9.77	618	11.12	618	11.42	618	12.35
721	11.56	721	12.08	721	13.25	721	13.69	721	14.46
1012	14.46	1012	14.87	1012	15.82	1012	16.37	1012	16.58
1500	18.3	1500	18.47	1500	19.25	1500	19.65	1500	20.43
2400	22.43	2400	22.76	2400	23.39	2400	23.64	2400	24.47
3012	25.37	3012	25.92	3012	27.06	3012	27.46	3012	28.29

When the visibility is higher, a higher SNR has been achieved whereas in lower visibility, lower SNR has been attained. The aperture averaging approach has been used to improve the SNR value, and it can be seen from the graph that SNR has greatly increased for high to poor visibility (average SNR enhanced average 1.10 times over the without aperture averaging).Fig. 5.18. represents SNR (dB) values for different rain rates with different wavelengths (With Aperture Averaging & Without Aperture Averaging Scheme).

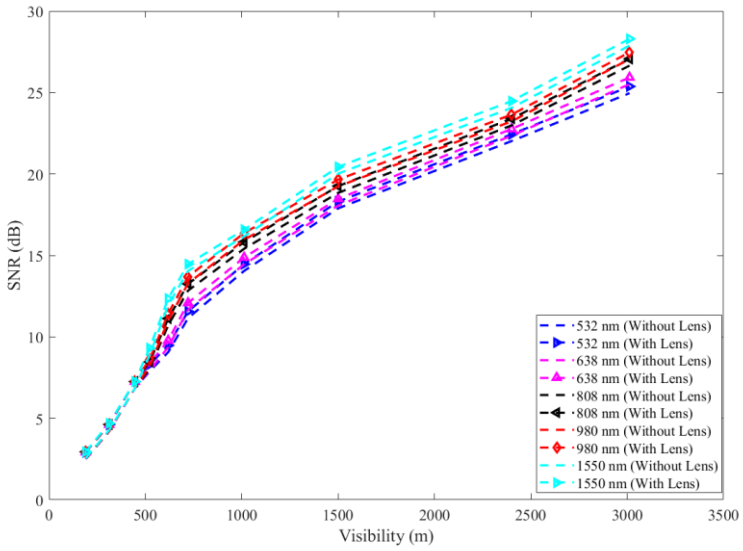

Fig.5.18. SNR (dB) values for different visibilities (m) with different wavelengths (With Aperture Averaging & Without Aperture Averaging Scheme)

Table. 5.10. represents the BER values for different rain rates (mm/hr) with different wavelengths with aperture averaging scheme.

Table. 5.10. BER values for different visibility (m) with different wavelengths with aperture averaging scheme

532 nm		638 nm		808 nm		980 nm		1550 nm	
Visibility (m)	**BER**	**Visibility (m)**	**BER**	**Visibility (m)**	**BER**	**Visibility (m)**	**BER**	**Visibility (m)**	**BER**
190	0.24	190	0.242	190	0.241	190	0.24	190	0.24
312	0.198	312	0.1978	312	0.1975	312	0.197	312	0.195
445	0.125	445	0.125	445	0.125	445	0.124	445	0.124
522	0.097	522	0.095	522	0.093	522	0.088	522	0.072
618	0.068	618	0.062	618	0.036	618	0.031	618	0.0192
721	0.0293	721	0.022	721	0.01	721	0.0078	721	0.00415
1012	0.0041	1012	0.0028	1012	0.001	1012	0.0005	1012	0.0003
1500	$2x10^{-5}$	1500	$1.4x10^{-5}$	1500	$2.3x10^{-6}$	1500	$8.04x10^{-7}$	1500	$7.67x10^{-8}$
2400	$1.96x10^{-11}$	2400	$3.38x10^{-12}$	2400	$7.98x10^{-14}$	2400	$1.54x10^{-14}$	2400	$3.25x10^{-17}$
3012	$9.48x10^{-21}$	3012	$2.7x10^{-23}$	3012	$1.05x10^{-29}$	3012	$2.21x10^{-32}$	3012	$8.89x10^{-39}$

Similar graphs have been shown in Fig. 5.19 for the measured BER for the various visibilities, from very low to very high, both without and with aperture averaging. When using the aperture averaging approach, the BER performance is superior to when not using it.

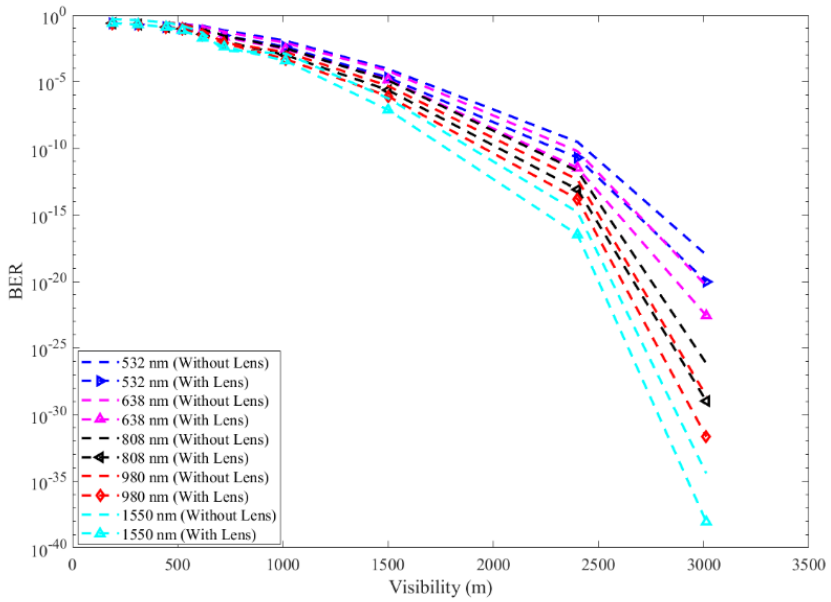

Fig. 5.19. BER values for different visibility (m) with different wavelengths (With Aperture Averaging & Without Aperture Averaging Scheme)

Table 5.11. Permissible limit of visibility, scintillation, and rain rates for the range of BER 10^{-6} for different wavelengths after using aperture averaging scheme

532 nm		**638 nm**		**808 nm**		**980 nm**		**1550 nm**	
Visibility (m)	**BER**	**Visibility (m)**	**BER**	**Visibility (m)**	**BER**	**Visibility (m)**	**BER**	**Visibility (m)**	**BER**
1650	10^{-6}	1575	10^{-6}	1212	10^{-6}	1110	10^{-6}	925	10^{-6}
Scintillation ($m^{-2/3}$)	**BER**	**Scintillation ($m^{-2/3}$)**	**BER**	**Scintillation ($m^{-2/3}$)**	**BER**	**Scintillation ($m^{-2/3}$)**	**BER**	**Scintillation ($m^{-2/3}$)**	**BER**
$5x10^{-14}$	10^{-6}	$2x10^{-14}$	10^{-6}	10^{-14}	10^{-6}	$6.5x10^{-13}$	10^{-6}	$3x10^{-13}$	10^{-6}
Rain Rates (mm/hr)	**BER**	**Rain Rates (mm/hr)**	**BER**	**Rain Rates (mm/hr)**	**BER**	**Rain Rates (mm/hr)**	**BER**	**Rain Rates (mm/hr)**	**BER**
69.5	10^{-6}	69.6	10^{-6}	70	10^{-6}	70.1	10^{-6}	70.4	10^{-6}

Table 5.11 shows the Permissible limit of visibility, scintillation, and rain rates for the range of BER 10^{-6} for different wavelengths with aperture averaging scheme. From the table, it has been shown that for maintaining the 10^{-6} BER values, 532 nm works upto 1650 m visibility, 638 nm works upto 1575 m visibility, 808 nm works upto 1212 m visibility, 980 nm works upto 1110 m visibility, and 1550 nm works upto 925 m visibility respectively. Similarly, for scintillation condition scenario, 532 nm works upto $5x10^{-14}$ $m^{-2/3}$ scintillation range, 638 nm works upto $2x10^{-14}$ $m^{-2/3}$ scintillation range, 808 nm works upto 10^{-14} $m^{-2/3}$ scintillation range, 980 nm works upto $6.5x10^{-13}$ $m^{-2/3}$ scintillation range, and 1550 nm works upto $3.0x10^{-13}$ $m^{-2/3}$ scintillation range respectively for 10^{-6} BER. Finally, for rainy weather condition scenario, 532 nm works upto 69.5 mm/hr, 638 nm works upto 69.60 mm/hr, 808 nm works upto 70 mm/hr, 980 nm works upto 70.10 mm/hr, and 1550 nm works upto 70.4 mm/hr for the Bit Error Rate of 10^{-6}.

5.5. CONCLUSION

The fundamental concept of system improvement under hazardous environmental circumstances is presented in this chapter. This chapter is divided into three sections: the first section discusses the fundamental methods for enhancing system performance; the second section offers a theoretical analysis of a wavelength diversity scheme using the MWIR (4000 nm) and SWIR (1550 nm) wavelengths in various scintillation and visibility conditions. This theoretical simulation has shown that MWIR performs better in lower visibility and higher scintillation environments, but SWIR does not operate in these circumstances.

The experimental evaluation of the mitigation of the atmospheric hazards has been described in the third section of this chapter. The system has incorporated aperture averaging approach that is also economically advantageous. These experimental findings demonstrate that all wavelengths under consideration get the same degree of attenuation, and that the aperture averaging method performs better in rainy conditions. Another interesting finding from these experimental results is that, when utilising an aperture averaging strategy, the average SNR in a scintillation situation was substantially higher than it was in a foggy and rainy weather circumstances.

CHAPTER 6
CONCLUSION & FUTURE SCOPE

6.1. CONCLUSION

Free Space Optics (FSO) communication system has a lot of benefits over currently used methods, including optical, radio, and microwave ones. The primary benefits of an FSO system are lower setup costs and setup times. With a few adjustments, optical equipment may be used in an FSO system. The benefits of FSO communication systems and their potential applications make them a popular technology, although the medium's attenuation like fog, rain, temperature, snow etc. have significant drawbacks. FSO systems have various issues, such as attenuation in the medium, which might impair transmission efficiency because there will be power loss, data loss, etc. In the present study, an FSO communication channel has been established utilizing a variety of laser sources, including near-infrared and visible wavelength lasers.

A 5 MHz FSO communication channel has been developed for this experimental investigation employing several laser sources at different wavelengths. In order to evaluate the reliability of these channels in varying atmospheric circumstances, many artificial environments, such as rain, fog, and scintillation chambers, have been developed. The optical power attenuation, real-time eye pattern, Bit error rate (BER), Signal to noise ratio (SNR), at the receiver side have all been used to evaluate the reliability of different wavelength optical communication channels. Lasers with wavelengths of 532 nm, 638 nm, 808 nm, 980 nm, and 1550 nm are taken into consideration for this work. The wavelengths of 532 nm, 638 nm, 808 nm, and 980 nm are Diode Pump Solid State (DPSS) lasers, whereas 1550 nm is a Fibre laser. These include visible wavelength Lasers at 532 nm and 650 nm, and near-infrared lasers at 808 nm, 980 nm, and 1550 nm.

The usage of DPSS lasers (532, 638, 808, and 980 nm) has a number of benefits since they are easily available on the market and are relatively less expensive than other laser types, such as fibre. DPSS lasers are employed for high-speed operations in the Megahertz (MHz) range because the modulated signal efficiently switches them on and off. A Fibre Coupled Acousto Optic Modulator (FCAOM) is used to modulate the laser beam for the continuous wave Fibre Laser (1550 nm).

Since the main objective is to find out how well the existing FSO channel operates in various atmospheric erosion scenarios, different artificial experimental setup was developed to investigate the established FSO communication channel. For this reason, different artificial environmental simulation chambers like fog, temperature, rain have been developed. Different rain rates were created in the artificial rain simulation set up, and these allowed us to understand how the created FSO channel behaves at various rain rates.

The experiment takes into account a minimum rain rate of 7 mm/hr and a maximum rain rate of 180 mm/hr. Regardless of wavelength, there is a greater optical power attenuation with higher rain rates. More optical power attenuation results in a decline in system performance metrics like SNR (dB) and BER. The models of optical power attenuation resulting from varying rainfall rates (mm/hr) were derived from several models established by scientists in different countries. The rain simulation used in this work was done in accordance with the various states in India, and the optical power attenuation differed from the attenuation models that were produced. Therefore, an optical power attenuation model has been developed based on the acquired experimental data.

For the temperature rising experiment, the scintillation value varies between 10^{-13} to 10^{-16} $m^{-2/3}$, where 10^{-16} $m^{-2/3}$ is the minimum value and 10^{-13} $m^{-2/3}$ is the maximum value of the scintillation. In this work, five different laser wavelengths were used: three near-infrared wavelengths (808 nm, 980 nm, and 1550 nm) and two visible wavelengths (532 nm and 650 nm). It has been found that the 638 nm wavelength laser outperforms the 532 nm wavelength laser in the visible wavelength scenario. The 1550 nm wavelength laser performs better than other NIR wavelength lasers that are taken into consideration. Furthermore, the 1550 nm laser performs better across the board in all scintillation regimes when compared to other wavelengths.

Similarly, an artificial nebulizer machine is utilized to create the foggy ambient scenario in the case of foggy weather. This machine uses an ultrasonic approach to break up the water droplets into very small particles like fog. Since the visibility meter was unavailable, the KIM model was used to calculate the optical power attenuation caused by fog. In this work, five different laser wavelengths also were used: three near-infrared wavelengths (808 nm, 980 nm, and 1550 nm) and two visible wavelengths (532 nm and 638 nm). Visibility has been rated as clean to extremely poor. When there is poor visibility, there is a greater attenuation of optical power, and 1550 nm outperforms other wavelengths in terms of performance. Nevertheless, regardless

of the wavelengths taken into consideration, the link is not functional in the case of extremely low visibility. Fog has thus been deduced to be the system's most hazardous component.

Wavelength diversity is an effective way to mitigate the atmospheric effect on the FSO link. To achieve this, higher wavelength like 1550 nm or higher than 1550 nm wavelengths may be used. For this system, many mitigation strategies have been implemented in order to reduce atmospheric hazards. The aperture averaging approach is the most economical, straightforward, and successful of them all. Regardless of wavelength, the system performance has increased in many atmospheric condition scenarios owing to the wavelength diversity with the aperture averaging approach used in this work. In contrast to other wavelengths, the aperture averaging approach at 1550 nm yields superior results under various simulated atmospheric conditions.

However, the wavelength selection point of view, the 1550 nm Wavelength provides better results compared to others considered wavelengths like Visible (532 nm, 638 nm) & IR (808 nm, 980 nm) in terms of optical power attenuation, SNR, BER, etc. From the cost-effective point of view, 980 nm provides better results compared to 808 nm, 638 nm & 532 nm.
The problem is identified as one of the challenging mode in data communication which is aimed to be used in satellite communication and 5G/6G communication. A novel method of environment simulation is carried out as part of the task. Also reestablished the suitability of 1550 nm wavelength to be the most appropriate frequency of operation. Besides that the communication link establishment and experimentation in different simulated atmospheric conditions, the aperture averaging technique also demonstrated for link performance improvement at different simulated atmospheric conditions. Finally, a theoretical approach has been given to link performance improvement using Mid Wave Infrared (MWIR) 4000 nm wavelength. From this approach, it has been revealed that 4000 nm LASER provides better results in bad weather (poor visibility) conditions compared with other considered wavelengths.

6.2. FUTURE SCOPE

The aforesaid developed FSO system can be upgraded as follows which are treated as a future scope of this study. The future scopes are follows:

(i) The system bandwidth frequency may be increased for greater than 5 MHz, using direct modulation technique or external modulation technique.

(ii) Dust is another important atmospheric anomaly, which can affect the system's performance. Therefore, the system performance may be evaluated in a dusty environment.

(iii) The system performance can be evaluated using a Mid-wavelength infrared (MWIR) band transmitter which has a wavelength bandwidth between (3600 nm and -4800 nm), & this system performance may be evaluated in different atmospheric conditions. Finally, the results may be compared with the obtained experimental results with the considered wavelengths. However, the MWIR wavelength Laser transmitter cost is very high and their corresponding optical accessories are very costly.

(iv) Different modulation technique apart from amplitude modulation (OOK), like Frequency Shift Keying, Phase shift Keying etc. may be used for evaluation the system performance in the different atmospheric conditions.

(v) The existing developed system has been tested for small distance (35 ft.). This developed system can be performed in longer distance (like 0.5 km). As a result, the optical beam is subjected to various impairments during propagation due to atmospheric turbulence, diffraction, scattering, and absorption. In bad weather and/or situations with a lot of turbulence, the FSO channel that is affected by these factors acts erratically and inconsistently. Techniques for spatial variety have been suggested as a way to provide redundancy while still improving the dependability of turbulent FSO channels. To create MIMO FSO systems with multiple parallel diversity routes via which multiple copies of data may be delivered at once, a number of transmit/receive apertures are used in conjunction with each other. Different diversity technique like SIMO, MIMO, aperture diversity, etc. is incorporated into the system to improve the signal fidelity of the system, it has been seen that theoretically, it works better than the SISO system.

(vi) The developed aforesaid system analysis has been done throughout PIN type Photodetector. The aforesaid system may be analysed using Avalanche avalanche-type (APD) photodetector.

(vii) This developed system can be established for long-distance (0.5 km) communication also, and as it is a line-of-sight technology, an auto-alignment technology should be developed for long-distance communication purposes.

If the aforesaid features will be developed and added into the existing developed system, the FSO Communication domain will now be moving in a new direction as a result.

REFERENCE

[1] Osseiran, A. Boccardi, F. Barun, V. Kusume, K. Marsch, P. Maternia, M. Queseth, O. Schellmann, M. Schotten, H. H. Tullberg, H. Uusitalo, M. Timus, B. Fallgren, M.: scenarios for 5G mobile and wireless communications: the vision of the METIS project. IEEE Commun. Mag. 52(5), 26-35 (2014) .

[2] Jungnickel, V. Manolakis, K. Zirwas, W. Panzner, B. Sternad, M. Svensson, T.: The role of small cells, coordinated multi-point and massive MIMO in 5G. IEEE Commun. Mag. 52(5), 44-21 (2014) .

[3] Rappaport, T.S. Sun, S. Mayzus, R. Zhao, H. Azar, Y. Wang, K. Wong, G.N. Schulz, J.K. Sammi, M. Guiterrez, F.: Millimeter wave mobile communications for 5G cellular: it will work. IEEE Access 1, 335-349 (2013).

[4] Etkin, R. Parekh, A. Tse, D.: Spectrum sharing for unlicensed bands. IEEE J. Sel. Areas Commun. 25(3), 517-528 (2007).

[5] Arnon, S. Barry, J.R. Karagiannidis, G.K. Schober, R.Uysal, M. (eds.): Advanced Optical Wireless Communication. Cambridge University Press (2012).

[6] Ghassemlooy, Z. Popoola, W.O. Rajbhandari, S.: Optical Wireless Communications – System and Channel Modelling with Matlab. CRC publish, USA (2012).

[7] Tsukamoto, K. Hashimoto, A. Aburakawa, Y. Matsumoto, M.: The case for free space. IEEE Microw. Mag. 10, 84-92 (2009).

[8] Arimoto, Y.: Compact free-space optical terminal for terminal for mulyi-gigabit signal transmissions with a single-mode fiber. In: Proceedings of SPIE, Free-Space Laser Communication Technologies, vol. XXI, pp. 719908(1)-(9) (2009).

[9] Nakajima, A. Sako, N. Kamemura, M. Wakayama, Y. Fukuzawa, A. Sugiyama, H. Okada, N.: A visible light communication experimental micro-satellite. In. Proceedings of the

International Conference on Space Optical Systems and Application (ICSOS) 2012, 12-1. Ajaccio, Corsica, France, October 9-12 2012.

[10] T. Tolker-Nielsen and G. Oppenhauser, “In-orbit test result of an operational intersatellite link between ARTEMIS and SPOT 4,” in Proc. SPIE, Free-Space Laser Commun. Technol. XIV, San Jose, CA, USA, Jan. 2002, vol. 4639, pp. 1–15.

[11] R. Lange, B. Smutny, B. Wandernoth, R. Czichy, and D. Giggenbach, “142 km, 5.625 Gb/s free-space optical link based on homodyne BPSK modulation,” in Proc. SPIE, Free-Space Laser Commun. Technol. XVIII, 2006, vol. 6105, p. 61050A.

[12] B. Smutnyet al., “5.6 Gbps optical intersatellite communication link,” in Proc. SPIE, Free-Space Laser Commun. Technol. XVIII, Feb. 2009, vol. 7199, p. 719 906.

[13] N. Karafolas and S. Baroni, “Optical satellite networks,” J. Lightw. Technol., vol. 18, no. 12, pp. 1792–1806, Dec. 2000.

[14] H. Hemmati, Deep Space Optical Communications. Hoboken, NJ, USA: Wiley-Interscience, 2006.

[15] C. Kachris and I. Tomkos, “A survey on optical interconnects for data centers,” IEEE Commun. Surveys Tuts., vol. 14, no. 4, pp. 1021–1036, Oct. 2012.

[16] M. Ijaz, Z. Ghassemlooy, J. Pesek, O. Fiser, H. L. Minh & E. Bentley “Modeling of Fog and Smoke Attenuation in Free Space Optical Communications Link under Controlled Laboratory Conditions”, Journal of Lightwave Technology, 2013.

[17] R. Ghalot, C. Madhu, G. Kaur, P. Singh, “Link Estimation of Different Indian Cities Under Fog Weather Conditions”, Wireless Personal Communications, 2019.

[18] A. Sharma, S. Kaur, “Performance evaluation and fog attenuation modelling of FSO link for hilly regions of India”, Optical and Quantum Electronics, vol.53, 2021.

[19] M. A. Esmail, H. Fathallah, M. S. Alouimi, Outdoor FSO Communication Under Fog: Attenuation Modeling and Performance Evaluation, IEEE Photonics Journal, 2016.

[20] J.L.Miller, “Principles of Infrared Technology: A practical guide to the State of the Art,” New York: Springer, 1994.

[21] T. Liu, J. Zhang, C. Zhu, Y. Lei, C.Sun, R. Zhang, “Investigation of the wavelength selection for the free space optical communication system,” 2018 Asia Communications and Photonics Conference (ACP), pp. 1-3, 2018

[22] J. Mikolajczyk, R. Weih, M. Motyka, “Optical wireless link operated at the wavelength of 4.0 μm with commercially available Interband Cascade Laser”, Sensors, 2021

[23] X. Pang, O. Ozolins, R. Schatz, J. Storck, A. Udalcovs, J.R. Navarro, A. Kakkar, G. Maisons, M. Carras, G. Jacobsen, S. Popov, S. Lourdudoss, “Gigabit free space multi level signal transmission with a mid-infrared quantum cascade laser operating at room temperature”, Optics Letters, vol.42, pp.3646-3649, 2017.

[24] S. A. Al-gailani, M. F. M. Salleh, A. A. Salem, R. Q. Shaddad, U. U. Sheikh, N. A. Algeelani, & T. A. Almohamad, “A Survey of Free Space Optics (FSO) Communication Systems, Links, and Networks”, IEEE Access, 2020.

[25] H. Singh, N. Mittal, “Performance analysis of free space optical communication system under rain weather conditions: a case study for inland and coastal locations of India”, Optical and Quantum Electronics, 2021

[26] A. B. Mohammad, “Optimization of FSO System in Tropical Weather using Multiple Beams”, Proc. Of 2014 IEEE 5th International Conference on Photonics (ICP), Kuala Lumpur, 2014.

[27] P. Singh, M. L. Singh, “Experimental determination and comparison of rain attenuation in free space optic link operating at 532 nm and 655 nm wavelength”, pp.4599-4602, Optik-International Journal for Light and Electron Optics, 2014.

[28] G. Soni, J. Kaur, “Performance evaluation of Free Space Optical link at 650 nm using red laser under rain conditions using experimental set up”, International conference on Control, Instrumentation, communication, and computational Technologies (ICCICCT), 2015.

[29] G.G. Soni, A. Tripathi, M. Shroti, K. Agarwal, “Experimental study of rain affected optical wireless link to investigate regression parameters for tropical Indian monsoon”, Optical and Quantum Electronics, 2023.

[30] H. Kaushal, V. Kumar, A. Dutta, H. Aennam, V.K. Jain, S. Kar, “Experimental study on beam wander under varying atmosphere turbulence conditions”, IEEE Photonics Technology Letters, 2011.

[31] W.O. Popoola, Z. Ghassemlooy, C.G. Lee, A.C. Boucouvalas, “Scintillation effect on intensity modulated laser communication systems-a laboratory demonstration”, Optics & Laser Technology, vol.42, pp.682-692, 2010.

[32] H. Le-Minh, Z. Ghassemlooy, M. Ijaz, S. Rajbhandari, O. Adebanjo, S. Ansari, E. Leitgeb, “Experimental study of Bit Error Rate of Free Space Optics Communications in Laboratoty controlled turbulence”, IEEE Globecom, 2010.

[33] M. I. PETKOVIC, G. T. DORDEVIC, D. N. Milic, “BER Performance of IM/DD FSO System with OOK using APD Receiver”, Serbian Journal of Electrical engineering, 2016.

[34] Y. Dikmelik, J. B. Khurgin, M. D. Escarra, P. Q. Liu, A.J. Hoffman, K. J. Franz, C. F. G. J. Fan & X. wang, “Intersubband absorption loss in high-performance mid-infrared quantum cascade lasers”, *Conference on Quantum electronics and Laser Science Conference,* Baltimore, MD, USA, 2009.

[35] M.Toyoshima, et al, “Assessment of eye hazard associated with an optical downlink in freespace laser communications,” Proc. SPIE, Free Space Laser Coom. Tech. XIII, vol. 4272, 2001

[36] O. Barder and C. Lui, “Laser safety and eye: Hidden hazards and practical pearls,” Tech. Report: American Academy of Dermatology, Lion Laser Skin Center, Vancouver and university of British Columbia, Vancouver, B.C., 1996

[37] “Surface Emitting Lasers Improve Communications using Vertical Cavity Surface Emitting Laser (VCSEL) Array,” NASA, https://ntts-prod.s3.amazonaws.com/t2p/prod/t2media/tops/pdf/TOP2-205.pdf

[38] A. Liu, P. Wolf, J.A. Lott, D. Bimberg, “Vertical-cavity surface-emitting lasers for data communication and sensing,” Photonics Research,Vol. 7, No. 2, 2019.

[39] Q.T. Nguyen, P. Besnard, L. Bramerie, A. Shen, “Using optical injection of Fabry-Perot lasers for high-speed access in optical telecommunications,” Proceedings of SPIE - The International Society for Optical Engineering, 7720, 2010.

[40] A. Vats, H. Kaushal, V.K.Jain, “Free space optical communication: laser sources, modulation schemes and detection technique, International Conference on Telecommunication and Networks (TEL-NET), 2013.

[41] R. Martini, E. A. Whittaker, “Quantum cascade laser-based free space optical communications,” Journal of optical and fiber communications report, 2008.

[42] M. Gutowska, D. Pierścińska, M. Nowakowski, K. Pierściński , D. Szabra , J. Mikołajczyk, J. Wojtas , & Z. Bielecki, “Transmitter with quantum cascade laser for free space optics communication system”, Bulletin of the polish academy of sciences, Vol. 59, No. 4, 2011.

[43] M. M. Islam, S. Ahmed, A. Islam, “Performance Analysis of 2.5 Gbps PIN and APD Photodiodes to Use in Free Space Optical Communication Link,” International Journal of Thin Films Science and Technology,Vol.8, no.2, pp.53-58, 2019

[44] THORLABS InGaAs Amplified Fixed Gain Detector User Guide, https://www.thorlabs.com/thorproduct.cfm?partnumber=PDA10CF

[45] H.Kaushal, V.K. Jain, S. Kar “Free-Space Optical Channel Models,” Chapter 2, Free Space Optical Communication, Optical Networks, Springer (India) Pvt. Ltd., 2017

[46] Laser beam expanders, Edmund optics, https://www.edmundoptics.com/knowledge-center/application-notes/lasers/beam-expanders/

[47] X. H. Huang, C.Y. Li, H.H. Lu, C.W. Su, Y.R. Wu, Z.H. Wang, Y.N. Chen, “WDM Free-Space Optical Communication System of High-Speed Hybrid Signals,” IEEE Photonics Journal, Vol. 10, No. 6, 2018

[48] A. G. Alkholidi & K. S. Altowij, “Free Space Optical Communications — Theory and Practices” Chapter 5, Contemporary Issues in Wireless Communications, 2014.

[49] H. Henniger and O. Wilfert, “An Introduction to Free Space Optical Communications”, Radio Engineering, vol.19, no. 2, June 2010.

[50] F. C. Bohren, D. R. Huffman, “Absorption and Scattering of Light by Small Particles”. Wiley, ISBN 0-471-29340-7, 1983

[51] C. David, “Inverse Acoustic and Electromagnetic Scattering Theory”, Springer, Rainer Press, ISBN 978-0-8194-1924-7, 1998.

[52] H. Manor and S. Arnon, “Performance of an optical wireless communication system as a function of wavelength,” Applied Optics, vol. 42, no. 21, pp. 4285–4294, 2003.

[53] N. Garg, V. Singh, “Free Space optical communication link using optical Mach-Zehnder modulator and analysis at different parameters”, ICICT, IEEE conference, pp 192-195, 2014.

[54] D.O. Caplan, M.L. Stevens, D.M. Boroson, & J.E. Kaufmann, "A multi-rate optical communications architecture with high sensitivity," in LEOS, 1999.

[55] M.L. Stevens, D.M. Boroson, & D.O. Caplan, "A novel variable-rate pulse-position modulation system with near quantum limited performance," in LEOS, 1999.

[56] D.O. Caplan & W.A. Atia, "A quantum-limited optically-matched communication link", Optical Fiber Conference (OFC), 2001.

[57] M.A. Khalighi, M .Uysal, "Survey on free space optical communication: a communication theory perspective", IEEE Commun. Surveys Tuts. 16, 2231–2258, 2014.

[58] M.A. Naboulsi, H. Sizun, F. Fornel, "Fog attenuation prediction for optical and infrared waves", Opt. Eng., 43, (2), pp. 319–329, 2004.

[59] J. Joss and E.G. Gori, "Shapes of raindrop size distributions," Journal of Applied Meteorology, vol. 17, no. 7, 1978.

[60] A. Z. Suriza, I. Md Raqul, A. K. Wajdi, and A. W. Naji, "Proposed parameters of specific rain attenuation prediction for free space optics link operating in tropical region," Journal of atmospheric and solar-terrestrial physics, vol. 94, pp. 93-99, March, 2013

[61] L.A.R. da Silva Mello, E. Costa, R. S. L. Souza, "Rain attenuation measurements at 15 and 18 GHz," Electronics Letters, vol. 38, pp. 197-198, 2002.

[62] A. K. Majumdar & J. C. Ricklin, "Free-Space Laser Communications: Principles and Advances", New York, USA: Springer-Verlag, 2010.

[63] S. G. Wilson, M.B. Pearce, C. Qianling, J.H. Leveque, "Free-space optical MIMO transmission with Q-ary PPM", IEEE Trans. Commun, 53, 1402–1412, 2005.

[64] E. Lee, V. Chan, "Optical communication over the clear turbulent atmospheric channel using diversity", IEEE J. Sel. Areas Commun., 22, 1896–1906, 2004.

[65] S. K. Mandal, B. Bera and G.G. Dutta, “Free Space Optical (FSO) Communication Link Design Under Adverse Weather Condition”, International Conference on Computer, Electrical & Communication Engineering (ICCECE), 2020.

[66] Uysal, M., Li, J., Yu, M.:‘Error rate performance analysis of coded free-spaceoptical links over gamma-gamma atmospheric turbulence channels”,IEEE Trans.Wirel. Commun., ,5, (6), pp. 1229–1233, 2006.

[67] V. W. S. Chan, “Free-space optical communications”, J. Lightw. Technol., vol. 24, no. 12, pp. 4750–4762, 2006.

[68] F. A. Wahab, T. K. Leong, H. Zulki_i, M. I. Ibrahim, M. A. B. Talib, N. A. Zamri, and O. K. Ibrahim, “Multiple transmitters & receivers for free space optical communication link performance analysis”, J. Telecommun. Electron. Comput. Eng., vol. 8, no. 5, pp. 29_32, 2016.

[69] A. Al-Kinani, C.-X. Wang, L. Zhou, and W. Zhang, “Optical wireless communication channel measurements and models”, IEEE Commun. Surveys Tuts., vol. 20, no. 3, pp. 1939_1962, 3rd Quart., 2018.

[70] I. K. Son and S. Mao, “Optical networks, digital communications and networks”, Tech. Rep., 2016.

[71] D.R. Kim, S.-H. Yang, H.-S. Kim, Y.-H. Son, and S.-K. Han, “Outdoor visible light communication for inter- vehicle communication using controller area network”, in Proc. 4th Int. Conf. Commun. Electron. (ICCE), pp. 31_34, 2012.

[72] A. K. Majumdar and J. C. Riclkin, *Free-Space Laser Communications: Principles And Advances*. New York, NY, USA: Springer-Verlag, 2007

[73] H. Yuksel, S. Milner, & C. C. Davis, “Aperture averaging for optimizing receiver design and system performance on free-space optical communication links,” J. Opt. Netw., vol. 4, no. 8, pp. 462–475, Aug. 2005.

[74] J. Mikoáajczyk, Z. Bielecki, M. Bugajski, J. Piotrowski, J. Wojtas, W. Gawron, D. Szabra, and A. Prokopiuk, ``Analysis of free-space optics development," *Metrol. Meas. Syst.*, vol. 24, no. 4, pp. 653_674, 2017.

[75] C. Z. Çil, Y. Baykal, H. T. Eyyubo˘glu, and Y. Cai, "Beam wander characteristics of cos and cosh-Gaussian beams," Appl. Phys. B, vol. 95, no. 4, pp. 763–771, Jun. 2009.

[76] Y. Ren, A. Dang, B. Luo, and H. Guo, "Capacities for long-distance freespace optical links under beam wander effects," IEEE Photon. Technol. Lett., vol. 22, no. 14, pp. 1069–1071, Jul. 2010.

[77] S. Arnon, "Effects of atmospheric turbulence and building sway on optical wireless communication systems," Opt. Lett., vol. 28, no. 2, pp. 129– 131, Jan. 2003.

[78] H. Willebrand and B. S. Ghuman, "Free Space Optics: Enabling Optical Connectivity in Today's Networks". Indianapolis, IN, USA: Sams, 2001.

[79] A. Harris, J. J. Sluss, H. H. Refai, and P. G. LoPresti, "Alignment and tracking of a free-space optical communications link to a UAV", in Proc. AIAA/IEEE Digit. Avion. Syst. Conf., vol. 1, pp. 1-9, 2005.

[80] A. Malik and P. Singh, "Free space optics: Current applications and future challenges", Int. J. Opt., vol. 2015, pp. 1-7, 2015.

[81] I. Kim, B. McArthur, and E. Korevaar, "Comparison of laser beam propagation at 785 nm and 1550 nm in fog and haze for optical wireless communications," in Proc. SPIE, Opt. Wireless Commun. III, Boston, MA, USA, vol. 4214, pp. 26–37, 2001.

[82] H. A. Fadhil, A. Amphawan, H. A. B. Shamsuddin et al., "Optimization of free space optics parameters: an optimum solution for bad weather conditions," Optik, vol. 124, no. 19, pp.3969–3973, 2013.

[83] L. C. Andrews and R. L. Phillips, Laser Beam Propagation Through Random Media, 2nd ed. Bellingham, WA, USA: SPIE, 2005.

[84] L. C. Andrews, R. L. Phillips, C. Y. Hopen, and M. A. Al-Habash, “Theory of optical scintillation,” J. Opt. Soc. Amer. A, Opt. Image Sci., vol. 16, no. 6, pp. 1417–1429, Jun. 1999.

[85] I. D. A. Singapore, ``A trial-based study of FreeSpace optics systems in Singapore," Info Commun. Develop. Authority Singapore (iDA), Singapore, Tech. Rep., 2002.

[86] P. W. Kruse, L. D. McGlauchlin, & R. B. McQuistan, “Elements of Infrared Technology: Generation, Transmission and Detection”, vol. 1. New York, NY, USA: Wiley, 1962.

[87] Propagation data required for the design of terrestrial free-space optical links ITU-R Recommendation, document ITU-R P.1817, 2012.

[88] M. A. Al-Habash, “Mathematical model for the irradiance probability density function of a laser beam propagating through turbulent media”, Opt. Eng., vol. 40, no. 8, p. 1554, Aug. 2001.

[89] X. Wu, P. Liu, and M. Matsumoto, “A study on atmospheric turbulence effects in full-optical free-space communication systems”, in Proc. Int. Conf. Comput. Intell. Softw. Eng., 2010.

[90] L. D. Emiliani, L. Luini, and C. Capsoni, “Extension of ITU-R method for conversion of rain rate statistics from various integration times to one minute”, Electron. Lett., vol. 44, no. 8, pp. 557_558, 2008.

[91] Specific Attenuation Model for Rain for Use in Prediction Methods, 1999

[92] S. Babani, Y. Abdulmalik, A. Abdul'aziz, A. Loko, and M. Gajibo, “Free space optical communication: The main challenges and its possible solution”, Int. J. Sci. Eng. Res., vol. 5, pp. 1-4, 2014.

[93] M. Uysal, J. Li, M. Yu, “Error rate performance analysis of coded free-spaceoptical links over gamma-gamma atmospheric turbulence channels”,IEEE Trans.Wirel. Commun., pp. 1229–1233, 2006.

[94] N.D. Chatzidiamantis, G.K. Karagiannidis, D.S. Michalopoulos, “On the distribution of the sum of gamma-gamma variates and application in MIMO optical wireless systems” Proc. IEEE Global Telecommunications Conf. (GLOBECOM), Hawaii, USA, 2009.

[95] M. A. Naboulsi, H. Sizun, F. Fornel, “Fog attenuation prediction for optical and infrared waves”, Opt. Eng., pp. 319–329, 2004.

[96] S. D. Lyke, D. G. Voelz, and M. C. Roggemann, “Probability density of aperture-averaged irradiance fluctuations for long range free space optical communication links,” Appl. Opt., vol. 48, no. 33, pp. 6511–6527, 2009

[97] L. M. Wasiczko and C. C. Davis, “Aperture averaging of optical scintillations in the atmosphere: Experimental results,” in *Proc. SPIE Atmospheric Propag. II*, vol. 5793, pp. 197–208, Orlando, FL, USA, 2005.

[98] C. Higgs, H. Barclay, D. Murphy, and C. A. Primmerman, “Multibeam illumination,” *Lincoln Lab. J.*, vol. 11, no. 1, pp. 8–22, 1998

[99] K. Li, J. Ma, A. Belmonte, L. Tan, and S. Yu, “Performance analysis of satellite-to-ground downlink optical communications with spatial diversity over Gamma–Gamma atmospheric turbulence,” *Opt. Eng.*, vol. 54, no. 12, pp. 1–9, 2015.

[100] F. Xu, M.-A. Khalighi, P. Causse, and S. Bourennane, “Performance of coded time-diversity free-space optical links,” in *Proc. IEEE 24th Biennial Symp. Commun.*, Kingston, ON, Canada, pp. 146–149, 2008.

[101] N. Letzepis and A. G. I. Fabregas, “Outage probability of the Gaussian MIMO free-space optical channel with PPM,” *IEEE Trans. Commun.*, vol. 57, no. 12, pp. 3682–3690, 2009

[102] M. Niu, “Coherent optical wireless communications over atmospheric turbulence channels,” Ph.D. dissertation, Dept. Elect. Comput. Eng., Univ. Brit. Columbia, Vancouver, BC, Canada, 2012.

[103] R K Tyson, “Bit-error rate for free space adaptive optics laser communications”, J. Opt. Soc. Amer. A Opt. Image Sci. Vis., vol. 19, 2002

[104] F. E. Zocchi, “A simple analytical model of adaptive optics for direct detection free-space optical communication,” *Opt. Commun.*, vol. 248, nos. 4–6, pp. 359–374, 2005

[105] A. Viswanath, V. K. Jain, and S. Kar, “Analysis of earth-to-satellite free-space optical link performance in the presence of turbulence, beam-wander induced pointing error and weather conditions for different intensity modulation schemes,” *IET Commun.*, vol. 9, no. 18, pp. 2253–2258, 2015

[106] A. Kumar and V. K. Jain, “Antenna aperture averaging with different modulation schemes for optical satellite communication links,” *J. Opt. Netw.*, vol. 6, no. 12, pp. 1323 1328, 2007

[107] A. Viswanath, H. Kaushal, V. K. Jain, and S. Kar, “Evaluation of performance of ground to satellite free space optical link under turbulence conditions for different intensity modulation schemes,” in *Proc. SPIE Free Space Laser Commun. Atmospheric Propag. (XXVI)*, vol. 8971, pp. 1–12, San Francisco, CA, USA, 2014.

[108] D. Zwillinger, “Differential PPM has a higher throughput than PPM for the band-limited and average-power- limited optical channel,” IEEE Trans. Inf. Theory, vol. 34, no. 5, pp. 1269–1273, 1988.

[109] M. Czaputa, T. Javornik, E. Leitgeb, G. Kandus, and Z. Ghassemlooy, “Investigation of punctured LDPC codes and time-diversity on free-space optical links,” in *Proc. Int. Conf. Telecommun.*, pp. 359–362, 2011.

[110] I. B. Djordjevic, “LDPC-coded MIMO optical communication over the atmospheric turbulence channel using Q-ary pulse-position modulation,” *Opt. Express*, vol. 16, no. 16, pp. 10026–10032, 2007

[111] N. Kumar, V. K. Jain, and S. Kar, “Evaluation of the performance of FSO system using OOK and M-PPM modulation schemes in intersatellite links with turbo codes,” in *Proc. IEEE Int. Conf. Elect. Commun. Comput. Technol.*, pp. 59–63, Viluppuram, India, 2011.

[112] A. Eslami, S. Vangala, and H. Pishro-Nik, “Hybrid channel codes for efficient FSO/RF communication systems,” *IEEE Trans. Commun.*, vol. 58, no. 10, pp. 2926–2938, Oct. 2010

[113] H.-J. Liu, “Overview of U.S. military airborne RF and FSO hybrid communication,” *Telecommun. Eng.*, vol. 54, no. 2, pp. 1711 1716, 2014.

[114] S. D. Milner and C. C. Davis, “Hybrid free space optical/RF networks for tactical operations,” in *Proc. Mil. Commun. Conf. (MILCOM)*, pp. 404–415, Monterey, CA, USA, 2004.

[115] H. Dahrouj, A. Douik, F. Rayal, T. Y. Al-Naffouri, and M.-S. Alouini,“Cost-effective hybrid RF/FSO backhaul solution for next generation wireless systems,” *IEEE Wireless Commun.*, vol. 22, no. 5, pp. 98–104, 2015

[116] H. Kaushal, G. Kaddoum, “Optical Communication in Space: Challenges and Mitigation Techniques”, IEEE communications surveys & tutorials, Vol. 19, No. 1, 2017

[117] J.L.Miller, “Principles of Infrared Technology: A practical guide to the State of the Art,” New York: Springer, 1994

[118] A. M Tabirian, D. P Stanley, D. E Roberts, A. B Thompson, “Atmospheric propagation of novel MWIR laser output for emerging free-space applications” Proceedings Atmospheric Propagation V, vol. 6951, p. 69510T, International Society for Optics and Photonics, 2008.

[119] J. Mikolajczyk, R. Weih, M. Motyka, “Optical wireless link operated at the wavelength of 4.0 μm with commercially available Interband Cascade Laser”, Sensors, 2021.

[120] Q. Hao, G. Zhu, S. Yang, K. Yang, T. Duan, X. Xie, K. Huang, H. Zeng, “Mid-infrared transmitter and receiver modules for free-space optical communication”, Applied Optics, 2017.

[121] T. Liu, J. Zhang, C. Zhu, Y. Lei, C.Sun, R. Zhang, “Investigation of the wavelength selection for the free space optical communication system,” 2018 Asia Communications and Photonics Conference (ACP), pp. 1-3, 2018.

[122] J. Mikolajczyk, “Comparison study of data link with medium wavelength infrared pulsed and CW quantum cascade lasers” Photonics, 2021

[123] A. A.Farid, S. Hranilovic, “Diversity gain and outage probability for MIMO free space optical links with misalignment”, IEEE Transaction Communication, vol. 60, no.2, pp.479-487, 2012.

[124] D. Sarkar, S. K. Metya, “Effects of atmospheric weather and turbulence in MSK based FSO communication system for last mile users,” Telecommunication Systems, 2019.

[125] P. Kaur, V.K, Jain, S. Kar, “Performance analysis of FSO array receivers in presence of atmospheric turbulence”, IEEE Photonics Technology Letters, vol.26, pp.1165-1168, 2014

[126] V. Srivastava, A. Mandloi, D. Patel, “Analysis of outage probability in wavelength diversity based FSO link under gamma-gamma fading with varying atmospheric attenuation”, Wireless Personal Communication, 2020.

[127] L.C. Andrews, R.L. Phillips, C.Y. Hopen, Laser beam scintillation with applications, Bellingham, Washington, SPIE Press, 2001

[128] A.P. Prudnikov, Y.A. Brychkov, O.I. Marichev, Integrals and series, Gordon and Breachscience publishers, 1986.

[129] B. Chen, Y. Chen, Z. Deng, “Recent advances in high-speed photodetectors for eSWIR/MWIR/LWIR applications”, Photonics, 2021

[130] V. Srivastava, A. Mandloi, D. Patel, “Analysis of outage probability in wavelength diversity based FSO link under gamma-gamma fading with varying atmospheric attenuation”, Wireless Personal Communication, 2020

REFERENCE

[1] Osseiran, A. Boccardi, F. Barun, V. Kusume, K. Marsch, P. Maternia, M. Queseth, O. Schellmann, M. Schotten, H. H. Tullberg, H. Uusitalo, M. Timus, B. Fallgren, M.: scenarios for 5G mobile and wireless communications: the vision of the METIS project. IEEE Commun. Mag. 52(5), 26-35 (2014) .

[2] Jungnickel, V. Manolakis, K. Zirwas, W. Panzner, B. Sternad, M. Svensson, T.: The role of small cells, coordinated multi-point and massive MIMO in 5G. IEEE Commun. Mag. 52(5), 44-21 (2014) .

[3] Rappaport, T.S. Sun, S. Mayzus, R. Zhao, H. Azar, Y. Wang, K. Wong, G.N. Schulz, J.K. Sammi, M. Guiterrez, F.: Millimeter wave mobile communications for 5G cellular: it will work. IEEE Access 1, 335-349 (2013).

[4] Etkin, R. Parekh, A. Tse, D.: Spectrum sharing for unlicensed bands. IEEE J. Sel. Areas Commun. 25(3), 517-528 (2007).

[5] Arnon, S. Barry, J.R. Karagiannidis, G.K. Schober, R.Uysal, M. (eds.): Advanced Optical Wireless Communication. Cambridge University Press (2012).

[6] Ghassemlooy, Z. Popoola, W.O. Rajbhandari, S.: Optical Wireless Communications – System and Channel Modelling with Matlab. CRC publish, USA (2012).

[7] Tsukamoto, K. Hashimoto, A. Aburakawa, Y. Matsumoto, M.: The case for free space. IEEE Microw. Mag. 10, 84-92 (2009).

[8] Arimoto, Y.: Compact free-space optical terminal for terminal for mulyi-gigabit signal transmissions with a single-mode fiber. In: Proceedings of SPIE, Free-Space Laser Communication Technologies, vol. XXI, pp. 719908(1)-(9) (2009).

[9] Nakajima, A. Sako, N. Kamemura, M. Wakayama, Y. Fukuzawa, A. Sugiyama, H. Okada, N.: A visible light communication experimental micro-satellite. In. Proceedings of the

International Conference on Space Optical Systems and Application (ICSOS) 2012, 12-1. Ajaccio, Corsica, France, October 9-12 2012.

[10] T. Tolker-Nielsen and G. Oppenhauser, “In-orbit test result of an operational intersatellite link between ARTEMIS and SPOT 4,” in Proc. SPIE, Free-Space Laser Commun. Technol. XIV, San Jose, CA, USA, Jan. 2002, vol. 4639, pp. 1–15.

[11] R. Lange, B. Smutny, B. Wandernoth, R. Czichy, and D. Giggenbach, “142 km, 5.625 Gb/s free-space optical link based on homodyne BPSK modulation,” in Proc. SPIE, Free-Space Laser Commun. Technol. XVIII, 2006, vol. 6105, p. 61050A.

[12] B. Smutnyet al., “5.6 Gbps optical intersatellite communication link,” in Proc. SPIE, Free-Space Laser Commun. Technol. XVIII, Feb. 2009, vol. 7199, p. 719 906.

[13] N. Karafolas and S. Baroni, “Optical satellite networks,” J. Lightw. Technol., vol. 18, no. 12, pp. 1792–1806, Dec. 2000.

[14] H. Hemmati, Deep Space Optical Communications. Hoboken, NJ, USA: Wiley-Interscience, 2006.

[15] C. Kachris and I. Tomkos, “A survey on optical interconnects for data centers,” IEEE Commun. Surveys Tuts., vol. 14, no. 4, pp. 1021–1036, Oct. 2012.

[16] M. Ijaz, Z. Ghassemlooy, J. Pesek, O. Fiser, H. L. Minh & E. Bentley “Modeling of Fog and Smoke Attenuation in Free Space Optical Communications Link under Controlled Laboratory Conditions”, Journal of Lightwave Technology, 2013.

[17] R. Ghalot, C. Madhu, G. Kaur, P. Singh, “Link Estimation of Different Indian Cities Under Fog Weather Conditions”, Wireless Personal Communications, 2019.

[18] A. Sharma, S. Kaur, “Performance evaluation and fog attenuation modelling of FSO link for hilly regions of India”, Optical and Quantum Electronics, vol.53, 2021.

[19] M. A. Esmail, H. Fathallah, M. S. Alouimi, Outdoor FSO Communication Under Fog: Attenuation Modeling and Performance Evaluation, IEEE Photonics Journal, 2016.

[20] J.L.Miller, “Principles of Infrared Technology: A practical guide to the State of the Art,” New York: Springer, 1994.

[21] T. Liu, J. Zhang, C. Zhu, Y. Lei, C.Sun, R. Zhang, “Investigation of the wavelength selection for the free space optical communication system,” 2018 Asia Communications and Photonics Conference (ACP), pp. 1-3, 2018

[22] J. Mikolajczyk, R. Weih, M. Motyka, “Optical wireless link operated at the wavelength of 4.0 μm with commercially available Interband Cascade Laser”, Sensors, 2021

[23] X. Pang, O. Ozolins, R. Schatz, J. Storck, A. Udalcovs, J.R. Navarro, A. Kakkar, G. Maisons, M. Carras, G. Jacobsen, S. Popov, S. Lourdudoss, “Gigabit free space multi level signal transmission with a mid-infrared quantum cascade laser operating at room temperature”, Optics Letters, vol.42, pp.3646-3649, 2017.

[24] S. A. Al-gailani, M. F. M. Salleh, A. A. Salem, R. Q. Shaddad, U. U. Sheikh, N. A. Algeelani, & T. A. Almohamad, “A Survey of Free Space Optics (FSO) Communication Systems, Links, and Networks”, IEEE Access, 2020.

[25] H. Singh, N. Mittal, “Performance analysis of free space optical communication system under rain weather conditions: a case study for inland and coastal locations of India”, Optical and Quantum Electronics, 2021

[26] A. B. Mohammad, “Optimization of FSO System in Tropical Weather using Multiple Beams”, Proc. Of 2014 IEEE 5th International Conference on Photonics (ICP), Kuala Lumpur, 2014.

[27] P. Singh, M. L. Singh, “Experimental determination and comparison of rain attenuation in free space optic link operating at 532 nm and 655 nm wavelength”, pp.4599-4602, Optik-International Journal for Light and Electron Optics, 2014.

[28] G. Soni, J. Kaur, “Performance evaluation of Free Space Optical link at 650 nm using red laser under rain conditions using experimental set up”, International conference on Control, Instrumentation, communication, and computational Technologies (ICCICCT), 2015.

[29] G.G. Soni, A. Tripathi, M. Shroti, K. Agarwal, “Experimental study of rain affected optical wireless link to investigate regression parameters for tropical Indian monsoon”, Optical and Quantum Electronics, 2023.

[30] H. Kaushal, V. Kumar, A. Dutta, H. Aennam, V.K. Jain, S. Kar, “Experimental study on beam wander under varying atmosphere turbulence conditions”, IEEE Photonics Technology Letters, 2011.

[31] W.O. Popoola, Z. Ghassemlooy, C.G. Lee, A.C. Boucouvalas, “Scintillation effect on intensity modulated laser communication systems-a laboratory demonstration”, Optics & Laser Technology, vol.42, pp.682-692, 2010.

[32] H. Le-Minh, Z. Ghassemlooy, M. Ijaz, S. Rajbhandari, O. Adebanjo, S. Ansari, E. Leitgeb, “Experimental study of Bit Error Rate of Free Space Optics Communications in Laboratoty controlled turbulence”, IEEE Globecom, 2010.

[33] M. I. PETKOVIC, G. T. DORDEVIC, D. N. Milic, “BER Performance of IM/DD FSO System with OOK using APD Receiver”, Serbian Journal of Electrical engineering, 2016.

[34] Y. Dikmelik, J. B. Khurgin, M. D. Escarra, P. Q. Liu, A.J. Hoffman, K. J. Franz, C. F. G. J. Fan & X. wang, “Intersubband absorption loss in high-performance mid-infrared quantum cascade lasers”, *Conference on Quantum electronics and Laser Science Conference,* Baltimore, MD, USA, 2009.

[35] M.Toyoshima, et al, “Assessment of eye hazard associated with an optical downlink in freespace laser communications,” Proc. SPIE, Free Space Laser Coom. Tech. XIII, vol. 4272, 2001

[36] O. Barder and C. Lui, “Laser safety and eye: Hidden hazards and practical pearls,” Tech. Report: American Academy of Dermatology, Lion Laser Skin Center, Vancouver and university of British Columbia, Vancouver, B.C., 1996

[37] “Surface Emitting Lasers Improve Communications using Vertical Cavity Surface Emitting Laser (VCSEL) Array,” NASA, https://ntts-prod.s3.amazonaws.com/t2p/prod/t2media/tops/pdf/TOP2-205.pdf

[38] A. Liu, P. Wolf, J.A. Lott, D. Bimberg, “Vertical-cavity surface-emitting lasers for data communication and sensing,” Photonics Research,Vol. 7, No. 2, 2019.

[39] Q.T. Nguyen, P. Besnard, L. Bramerie, A. Shen, “Using optical injection of Fabry-Perot lasers for high-speed access in optical telecommunications,” Proceedings of SPIE - The International Society for Optical Engineering, 7720, 2010.

[40] A. Vats, H. Kaushal, V.K.Jain, “Free space optical communication: laser sources, modulation schemes and detection technique, International Conference on Telecommunication and Networks (TEL-NET), 2013.

[41] R. Martini, E. A. Whittaker, “Quantum cascade laser-based free space optical communications,” Journal of optical and fiber communications report, 2008.

[42] M. Gutowska, D. Pierścińska, M. Nowakowski, K. Pierściński , D. Szabra , J. Mikołajczyk, J. Wojtas , & Z. Bielecki, “Transmitter with quantum cascade laser for free space optics communication system”, Bulletin of the polish academy of sciences, Vol. 59, No. 4, 2011.

[43] M. M. Islam, S. Ahmed, A. Islam, “Performance Analysis of 2.5 Gbps PIN and APD Photodiodes to Use in Free Space Optical Communication Link,” International Journal of Thin Films Science and Technology,Vol.8, no.2, pp.53-58, 2019

[44] THORLABS InGaAs Amplified Fixed Gain Detector User Guide, https://www.thorlabs.com/thorproduct.cfm?partnumber=PDA10CF

[45] H.Kaushal, V.K. Jain, S. Kar “Free-Space Optical Channel Models,” Chapter 2, Free Space Optical Communication, Optical Networks, Springer (India) Pvt. Ltd., 2017

[46] Laser beam expanders, Edmund optics, https://www.edmundoptics.com/knowledge-center/application-notes/lasers/beam-expanders/

[47] X. H. Huang, C.Y. Li, H.H. Lu, C.W. Su, Y.R. Wu, Z.H. Wang, Y.N. Chen, “WDM Free-Space Optical Communication System of High-Speed Hybrid Signals,” IEEE Photonics Journal, Vol. 10, No. 6, 2018

[48] A. G. Alkholidi & K. S. Altowij, “Free Space Optical Communications — Theory and Practices” Chapter 5, Contemporary Issues in Wireless Communications, 2014.

[49] H. Henniger and O. Wilfert, “An Introduction to Free Space Optical Communications”, Radio Engineering, vol.19, no. 2, June 2010.

[50] F. C. Bohren, D. R. Huffman, “Absorption and Scattering of Light by Small Particles”. Wiley, ISBN 0-471-29340-7, 1983

[51] C. David, “Inverse Acoustic and Electromagnetic Scattering Theory”, Springer, Rainer Press, ISBN 978-0-8194-1924-7, 1998.

[52] H. Manor and S. Arnon, “Performance of an optical wireless communication system as a function of wavelength,” Applied Optics, vol. 42, no. 21, pp. 4285–4294, 2003.

[53] N. Garg, V. Singh, “Free Space optical communication link using optical Mach-Zehnder modulator and analysis at different parameters”, ICICT, IEEE conference, pp 192-195, 2014.

[54] D.O. Caplan, M.L. Stevens, D.M. Boroson, & J.E. Kaufmann, "A multi-rate optical communications architecture with high sensitivity," in LEOS, 1999.

[55] M.L. Stevens, D.M. Boroson, & D.O. Caplan, "A novel variable-rate pulse-position modulation system with near quantum limited performance," in LEOS, 1999.

[56] D.O. Caplan & W.A. Atia, "A quantum-limited optically-matched communication link", Optical Fiber Conference (OFC), 2001.

[57] M.A. Khalighi, M .Uysal, "Survey on free space optical communication: a communication theory perspective", IEEE Commun. Surveys Tuts. 16, 2231–2258, 2014.

[58] M.A. Naboulsi, H. Sizun, F. Fornel, "Fog attenuation prediction for optical and infrared waves", Opt. Eng., 43, (2), pp. 319–329, 2004.

[59] J. Joss and E.G. Gori, "Shapes of raindrop size distributions," Journal of Applied Meteorology, vol. 17, no. 7, 1978.

[60] A. Z. Suriza, I. Md Raqul, A. K. Wajdi, and A. W. Naji, "Proposed parameters of specific rain attenuation prediction for free space optics link operating in tropical region," Journal of atmospheric and solar-terrestrial physics, vol. 94, pp. 93-99, March, 2013

[61] L.A.R. da Silva Mello, E. Costa, R. S. L. Souza, "Rain attenuation measurements at 15 and 18 GHz," Electronics Letters, vol. 38, pp. 197-198, 2002.

[62] A. K. Majumdar & J. C. Ricklin, "Free-Space Laser Communications: Principles and Advances", New York, USA: Springer-Verlag, 2010.

[63] S. G. Wilson, M.B. Pearce, C. Qianling, J.H. Leveque, "Free-space optical MIMO transmission with Q-ary PPM", IEEE Trans. Commun, 53, 1402–1412, 2005.

[64] E. Lee, V. Chan, "Optical communication over the clear turbulent atmospheric channel using diversity", IEEE J. Sel. Areas Commun., 22, 1896–1906, 2004.

[65] S. K. Mandal, B. Bera and G.G. Dutta, “Free Space Optical (FSO) Communication Link Design Under Adverse Weather Condition”, International Conference on Computer, Electrical & Communication Engineering (ICCECE), 2020.

[66] Uysal, M., Li, J., Yu, M.:‘Error rate performance analysis of coded free-spaceoptical links over gamma-gamma atmospheric turbulence channels”,IEEE Trans.Wirel. Commun., ,5, (6), pp. 1229–1233, 2006.

[67] V. W. S. Chan, “Free-space optical communications”, J. Lightw. Technol., vol. 24, no. 12, pp. 4750–4762, 2006.

[68] F. A. Wahab, T. K. Leong, H. Zulki_i, M. I. Ibrahim, M. A. B. Talib, N. A. Zamri, and O. K. Ibrahim, “Multiple transmitters & receivers for free space optical communication link performance analysis”, J. Telecommun. Electron. Comput. Eng., vol. 8, no. 5, pp. 29_32, 2016.

[69] A. Al-Kinani, C.-X. Wang, L. Zhou, and W. Zhang, “Optical wireless communication channel measurements and models”, IEEE Commun. Surveys Tuts., vol. 20, no. 3, pp. 1939_1962, 3rd Quart., 2018.

[70] I. K. Son and S. Mao, “Optical networks, digital communications and networks”, Tech. Rep., 2016.

[71] D.R. Kim, S.-H. Yang, H.-S. Kim, Y.-H. Son, and S.-K. Han, “Outdoor visible light communication for inter- vehicle communication using controller area network”, in Proc. 4th Int. Conf. Commun. Electron. (ICCE), pp. 31_34, 2012.

[72] A. K. Majumdar and J. C. Riclkin, *Free-Space Laser Communications: Principles And Advances*. New York, NY, USA: Springer-Verlag, 2007

[73] H. Yuksel, S. Milner, & C. C. Davis, “Aperture averaging for optimizing receiver design and system performance on free-space optical communication links,” J. Opt. Netw., vol. 4, no. 8, pp. 462–475, Aug. 2005.

[74] J. Mikoáajczyk, Z. Bielecki, M. Bugajski, J. Piotrowski, J. Wojtas, W. Gawron, D. Szabra, and A. Prokopiuk, ``Analysis of free-space optics development," *Metrol. Meas. Syst.*, vol. 24, no. 4, pp. 653_674, 2017.

[75] C. Z. Çil, Y. Baykal, H. T. Eyyuboˇglu, and Y. Cai, "Beam wander characteristics of cos and cosh-Gaussian beams," Appl. Phys. B, vol. 95, no. 4, pp. 763–771, Jun. 2009.

[76] Y. Ren, A. Dang, B. Luo, and H. Guo, "Capacities for long-distance freespace optical links under beam wander effects," IEEE Photon. Technol. Lett., vol. 22, no. 14, pp. 1069–1071, Jul. 2010.

[77] S. Arnon, "Effects of atmospheric turbulence and building sway on optical wireless communication systems," Opt. Lett., vol. 28, no. 2, pp. 129– 131, Jan. 2003.

[78] H. Willebrand and B. S. Ghuman, "Free Space Optics: Enabling Optical Connectivity in Today's Networks". Indianapolis, IN, USA: Sams, 2001.

[79] A. Harris, J. J. Sluss, H. H. Refai, and P. G. LoPresti, "Alignment and tracking of a free-space optical communications link to a UAV", in Proc. AIAA/IEEE Digit. Avion. Syst. Conf., vol. 1, pp. 1-9, 2005.

[80] A. Malik and P. Singh, "Free space optics: Current applications and future challenges", Int. J. Opt., vol. 2015, pp. 1-7, 2015.

[81] I. Kim, B. McArthur, and E. Korevaar, "Comparison of laser beam propagation at 785 nm and 1550 nm in fog and haze for optical wireless communications," in Proc. SPIE, Opt. Wireless Commun. III, Boston, MA, USA, vol. 4214, pp. 26–37, 2001.

[82] H. A. Fadhil, A. Amphawan, H. A. B. Shamsuddin et al., "Optimization of free space optics parameters: an optimum solution for bad weather conditions," Optik, vol. 124, no. 19, pp.3969–3973, 2013.

[83] L. C. Andrews and R. L. Phillips, Laser Beam Propagation Through Random Media, 2nd ed. Bellingham, WA, USA: SPIE, 2005.

[84] L. C. Andrews, R. L. Phillips, C. Y. Hopen, and M. A. Al-Habash, “Theory of optical scintillation,” J. Opt. Soc. Amer. A, Opt. Image Sci., vol. 16, no. 6, pp. 1417–1429, Jun. 1999.

[85] I. D. A. Singapore, ``A trial-based study of FreeSpace optics systems in Singapore," Info Commun. Develop. Authority Singapore (iDA), Singapore, Tech. Rep., 2002.

[86] P. W. Kruse, L. D. McGlauchlin, & R. B. McQuistan, “Elements of Infrared Technology: Generation, Transmission and Detection”, vol. 1. New York, NY, USA: Wiley, 1962.

[87] Propagation data required for the design of terrestrial free-space optical links ITU-R Recommendation, document ITU-R P.1817, 2012.

[88] M. A. Al-Habash, “Mathematical model for the irradiance probability density function of a laser beam propagating through turbulent media”, Opt. Eng., vol. 40, no. 8, p. 1554, Aug. 2001.

[89] X. Wu, P. Liu, and M. Matsumoto, “A study on atmospheric turbulence effects in full-optical free-space communication systems”, in Proc. Int. Conf. Comput. Intell. Softw. Eng., 2010.

[90] L. D. Emiliani, L. Luini, and C. Capsoni, “Extension of ITU-R method for conversion of rain rate statistics from various integration times to one minute”, Electron. Lett., vol. 44, no. 8, pp. 557_558, 2008.

[91] Specific Attenuation Model for Rain for Use in Prediction Methods, 1999

[92] S. Babani, Y. Abdulmalik, A. Abdul'aziz, A. Loko, and M. Gajibo, “Free space optical communication: The main challenges and its possible solution”, Int. J. Sci. Eng. Res., vol. 5, pp. 1-4, 2014.

[93] M. Uysal, J. Li, M. Yu, “Error rate performance analysis of coded free-spaceoptical links over gamma-gamma atmospheric turbulence channels”,IEEE Trans.Wirel. Commun., pp. 1229–1233, 2006.

[94] N.D. Chatzidiamantis, G.K. Karagiannidis, D.S. Michalopoulos, “On the distribution of the sum of gamma-gamma variates and application in MIMO optical wireless systems” Proc. IEEE Global Telecommunications Conf. (GLOBECOM), Hawaii, USA, 2009.

[95] M. A. Naboulsi, H. Sizun, F. Fornel, “Fog attenuation prediction for optical and infrared waves”, Opt. Eng., pp. 319–329, 2004.

[96] S. D. Lyke, D. G. Voelz, and M. C. Roggemann, “Probability density of aperture-averaged irradiance fluctuations for long range free space optical communication links,” Appl. Opt., vol. 48, no. 33, pp. 6511–6527, 2009

[97] L. M. Wasiczko and C. C. Davis, “Aperture averaging of optical scintillations in the atmosphere: Experimental results,” in *Proc. SPIE Atmospheric Propag. II*, vol. 5793, pp. 197–208, Orlando, FL, USA, 2005.

[98] C. Higgs, H. Barclay, D. Murphy, and C. A. Primmerman, “Multibeam illumination,” *Lincoln Lab. J.*, vol. 11, no. 1, pp. 8–22, 1998

[99] K. Li, J. Ma, A. Belmonte, L. Tan, and S. Yu, “Performance analysis of satellite-to-ground downlink optical communications with spatial diversity over Gamma–Gamma atmospheric turbulence,” *Opt. Eng.*, vol. 54, no. 12, pp. 1–9, 2015.

[100] F. Xu, M.-A. Khalighi, P. Causse, and S. Bourennane, “Performance of coded time-diversity free-space optical links,” in *Proc. IEEE 24th Biennial Symp. Commun.*, Kingston, ON, Canada, pp. 146–149, 2008.

[101] N. Letzepis and A. G. I. Fabregas, “Outage probability of the Gaussian MIMO free-space optical channel with PPM,” *IEEE Trans. Commun.*, vol. 57, no. 12, pp. 3682–3690, 2009

[102] M. Niu, “Coherent optical wireless communications over atmospheric turbulence channels,” Ph.D. dissertation, Dept. Elect. Comput. Eng., Univ. Brit. Columbia, Vancouver, BC, Canada, 2012.

[103] R K Tyson, “Bit-error rate for free space adaptive optics laser communications”, J. Opt. Soc. Amer. A Opt. Image Sci. Vis., vol. 19, 2002

[104] F. E. Zocchi, “A simple analytical model of adaptive optics for direct detection free-space optical communication,” *Opt. Commun.*, vol. 248, nos. 4–6, pp. 359–374, 2005

[105] A. Viswanath, V. K. Jain, and S. Kar, “Analysis of earth-to-satellite free-space optical link performance in the presence of turbulence, beam-wander induced pointing error and weather conditions for different intensity modulation schemes,” *IET Commun.*, vol. 9, no. 18, pp. 2253–2258, 2015

[106] A. Kumar and V. K. Jain, “Antenna aperture averaging with different modulation schemes for optical satellite communication links,” *J. Opt. Netw.*, vol. 6, no. 12, pp. 1323 1328, 2007

[107] A. Viswanath, H. Kaushal, V. K. Jain, and S. Kar, “Evaluation of performance of ground to satellite free space optical link under turbulence conditions for different intensity modulation schemes,” in *Proc. SPIE Free Space Laser Commun. Atmospheric Propag. (XXVI)*, vol. 8971, pp. 1–12, San Francisco, CA, USA, 2014.

[108] D. Zwillinger, “Differential PPM has a higher throughput than PPM for the band-limited and average-power- limited optical channel,” IEEE Trans. Inf. Theory, vol. 34, no. 5, pp. 1269–1273, 1988.

[109] M. Czaputa, T. Javornik, E. Leitgeb, G. Kandus, and Z. Ghassemlooy, “Investigation of punctured LDPC codes and time-diversity on free-space optical links,” in *Proc. Int. Conf. Telecommun.*, pp. 359–362, 2011.

[110] I. B. Djordjevic, “LDPC-coded MIMO optical communication over the atmospheric turbulence channel using Q-ary pulse-position modulation,” *Opt. Express*, vol. 16, no. 16, pp. 10026–10032, 2007

[111] N. Kumar, V. K. Jain, and S. Kar, “Evaluation of the performance of FSO system using OOK and M-PPM modulation schemes in intersatellite links with turbo codes,” in *Proc. IEEE Int. Conf. Elect. Commun. Comput. Technol.*, pp. 59–63, Viluppuram, India, 2011.

[112] A. Eslami, S. Vangala, and H. Pishro-Nik, “Hybrid channel codes for efficient FSO/RF communication systems,” *IEEE Trans. Commun.*, vol. 58, no. 10, pp. 2926–2938, Oct. 2010

[113] H.-J. Liu, “Overview of U.S. military airborne RF and FSO hybrid communication,” *Telecommun. Eng.*, vol. 54, no. 2, pp. 1711 1716, 2014.

[114] S. D. Milner and C. C. Davis, “Hybrid free space optical/RF networks for tactical operations,” in *Proc. Mil. Commun. Conf. (MILCOM)*, pp. 404–415, Monterey, CA, USA, 2004.

[115] H. Dahrouj, A. Douik, F. Rayal, T. Y. Al-Naffouri, and M.-S. Alouini,“Cost-effective hybrid RF/FSO backhaul solution for next generation wireless systems,” *IEEE Wireless Commun.*, vol. 22, no. 5, pp. 98–104, 2015

[116] H. Kaushal, G. Kaddoum, “Optical Communication in Space: Challenges and Mitigation Techniques”, IEEE communications surveys & tutorials, Vol. 19, No. 1, 2017

[117] J.L.Miller, “Principles of Infrared Technology: A practical guide to the State of the Art,” New York: Springer, 1994

[118] A. M Tabirian, D. P Stanley, D. E Roberts, A. B Thompson, “Atmospheric propagation of novel MWIR laser output for emerging free-space applications” Proceedings Atmospheric Propagation V, vol. 6951, p. 69510T, International Society for Optics and Photonics, 2008.

[119] J. Mikolajczyk, R. Weih, M. Motyka, “Optical wireless link operated at the wavelength of 4.0 μm with commercially available Interband Cascade Laser”, Sensors, 2021.

[120] Q. Hao, G. Zhu, S. Yang, K. Yang, T. Duan, X. Xie, K. Huang, H. Zeng, “Mid-infrared transmitter and receiver modules for free-space optical communication”, Applied Optics, 2017.

[121] T. Liu, J. Zhang, C. Zhu, Y. Lei, C.Sun, R. Zhang, “Investigation of the wavelength selection for the free space optical communication system,” 2018 Asia Communications and Photonics Conference (ACP), pp. 1-3, 2018.

[122] J. Mikolajczyk, “Comparison study of data link with medium wavelength infrared pulsed and CW quantum cascade lasers” Photonics, 2021

[123] A. A.Farid, S. Hranilovic, “Diversity gain and outage probability for MIMO free space optical links with misalignment”, IEEE Transaction Communication, vol. 60, no.2, pp.479-487, 2012.

[124] D. Sarkar, S. K. Metya, “Effects of atmospheric weather and turbulence in MSK based FSO communication system for last mile users,” Telecommunication Systems, 2019.

[125] P. Kaur, V.K, Jain, S. Kar, “Performance analysis of FSO array receivers in presence of atmospheric turbulence”, IEEE Photonics Technology Letters, vol.26, pp.1165-1168, 2014

[126] V. Srivastava, A. Mandloi, D. Patel, “Analysis of outage probability in wavelength diversity based FSO link under gamma-gamma fading with varying atmospheric attenuation”, Wireless Personal Communication, 2020.

[127] L.C. Andrews, R.L. Phillips, C.Y. Hopen, Laser beam scintillation with applications, Bellingham, Washington, SPIE Press, 2001

[128] A.P. Prudnikov, Y.A. Brychkov, O.I. Marichev, Integrals and series, Gordon and Breachscience publishers, 1986.

[129] B. Chen, Y. Chen, Z. Deng, “Recent advances in high-speed photodetectors for eSWIR/MWIR/LWIR applications”, Photonics, 2021

[130] V. Srivastava, A. Mandloi, D. Patel, “Analysis of outage probability in wavelength diversity based FSO link under gamma-gamma fading with varying atmospheric attenuation”, Wireless Personal Communication, 2020.

Shibabrata Mukherjee
02/01/2024